Mathematical and computer modelling of the enteric nervous system

Evan Alexander Thomas

Submitted in total fulfilment of the requirements
of the degree of Doctor of Philosophy

December 2001

Department of Physiology
University of Melbourne

Contents

Declaration

This is to certify that

(i) the thesis comprises only my original work,

(ii) due acknowledgement has been made in the text to all other material used,

(iii) the thesis is less than 100,000 words in length, exclusive of tables, maps, bibliographies and appendices.

Evan Thomas

Acknowledgements

I would like to acknowledge my supervisor, Dr Joel Bornstein, for suggesting the topic of this thesis and then giving me the freedom to explore the subject in my own way, while at the same time offering frequent physiological insight into curious results. I have been working for Joel more than just the duration of this thesis and I would like to thank him for the very substantial efforts he has made in keeping the modelling project supported. Finally, I am grateful to Joel for offering to supervise this PhD and encouraging me to pursue science at a higher level.

I would like to thank Drs Paul Bertrand and Wolf Kunze for teaching me enteric neurophysiology and for many fascinating and informative discussions. I am indebted to Dr Henrik Sjöval for helping me understand the mysteries of interdigestive motility, for forcing me to make the work physiologically relevant and for several beers. Paul Bertrand, Phil Davies, Henrik Sjöval and Tricia Wright all read versions of this thesis and their suggestions made it much better than it otherwise would have been.

On a personal level I would like to thank my wife Dorota for putting up with the stress and anxiety that I have brought home for the last few years and my daughter Katherine for all those hours that I didn't spend with her. I would especially like to thank my mother-in-law, Krystyna Galicka, for helping us while this thesis was being written. Without her help, it might never have been written. Finally, I would like to thank my parents for making me interested in science from a young age and giving me the discipline to follow it through.

Financial support was provided, in part, by Swedish Medical Research Council grant 8288. Use of computer facilities was provided by the Ormond Supercomputing

Facility, a joint venture between the University of Melbourne and the Royal Melbourne Institute of Technology. I am also grateful to Dr P. J. Johnson for allowing me the use of his unpublished data.

Abstract

The enteric nervous system (ENS) runs within the intestinal wall and is responsible for initiating and enacting several reflexes and motor patterns, including peristalsis and the complex interdigestive motor programs, known as migrating motor complexes (MMCs). The ENS consists of several neuron types including intrinsic sensory neurons, interneurons and motor neurons. A great deal is known about the anatomy, pharmacology and electrophysiology of the ENS, yet there is almost no understanding of how enteric neural circuits perform the functions that they do and how they switch from one function to another. The ENS contains intrinsic sensory neurons (ISNs) that connect to every neuron type in the ENS, including making recurrent connections amongst themselves. Thus, they are likely to play a key role, not just in sensory transduction, but in coordination of reflexes and motor patterns. This thesis has explored how these functions are performed by developing and analysing mathematical and computer models of the network of ISNs.

ISNs interact with each via slow excitatory post-synaptic potentials (EPSPs). Experimentally, slow EPSPs require several presynaptic stimuli to evoke, last several seconds to several minutes, the onset can be delayed by several hundred milliseconds and the membrane potential response sums nonlinearly in the inputs. Slow EPSPs are thus qualitatively different from fast, directly ligand gated EPSPs usually included in network models. Therefore the first part of this work was to develop a mathematical model of slow synaptic transmission in the ENS. The model was based on an abstraction of the processes of activation, inactivation and summation of a cAMP, protein kinase A (PKA)-dependent second messenger cascade. The model describes the activation of receptors, G-proteins and production of cAMP as the first

stage and uses first order, non-rate limited kinetics. The second stage corresponds to the release of active, PKA catalytic sub-unit and can use first or higher order kinetics. The third stage represents simple phosphorylation of ion channels and is limited by the number of channels available. The decay of each stage is based on first order, mass action kinetics. These equations and some variations were solved numerically and values of the parameters were determined by fitting to a variety of experimental data from myenteric neurons of the guinea-pig ileum.

In the absence of activity dependent mechanisms to reduce firing (generically termed inhibition), recurrent excitatory networks are inherently bistable and cannot meaningfully encode input signals. In many recurrent circuits, inhibition is provided by a specialised subpopulation of inhibitory interneurons, but in the ENS this type of interneuron is absent and another form of inhibition must be present. Inhibition in this recurrent network may come either from long after-hyperpolarising potentials (AHPs) characteristic of the action potentials in these neurons or from inhibitory synaptic potentials (IPSPs) arising from the same terminals that produce slow EPSPs (inhibitory cotransmission). These possibilities were examined using mathematical analysis based on the Wilson-Cowan model and biologically realistic network simulations. Mathematical analysis of steady states showed that, under appropriate conditions, both types of inhibition can provide robust regulation of firing, allowing the networks to encode input signals. Provided the residual AHP is larger than a small threshold, networks with AHPs will always provide graded responses to input. As with networks containing inhibitory interneurons, responses in networks with inhibitory cotransmission can be more complex, however, under physiologically realistic conditions these networks also provide graded responses to

input. Numerical simulations were performed using large networks with anatomically realistic numbers of neurons and connections and using realistic models for metabotropic transmission and suppression of the AHP. In the presence of constant exogenous input, parameters controlling the sizes and durations of inhibitory and excitatory events were varied, confirming the analytical results for static stimuli. Periodic forcing, using sinusoidally varying stimuli, was used to probe for oscillations or other complex behaviours, but none were found. In addition, simulation revealed that neurons in networks with inhibitory cotransmission fired in erratic bursts, a phenomenon observed in extracellular recordings of neurons in unparalysed tissue. It is concluded that either AHPs or inhibitory cotransmission can allow recurrent networks of ISNs to encode the magnitude of an ongoing sensory input in a biological useful way.

Short term activity dependent synaptic depression was also examined as a possible source of inhibition in the ISN network. Synaptic plasticity is common in the nervous system and has been implicated in signal transduction and motor pattern generation. There is some evidence for presynaptic auto-inhibition at enteric synapses and many receptors desensitise. Inhibition through synaptic depression is unlike the previous forms of inhibition in that it turns on more slowly and thus acts as delayed negative feedback. This creates the possibility for more complex dynamics, including spontaneous oscillations, oscillations driven under a variety of conditions and possibly chaotic dynamics. When spatially extended networks were considered, propagating regions of localised activity, or waves, were discovered. These waves propagate at propagate at speeds in the range of millimetres per second, reminiscent of MMC phase III contractions, region of strong contractile activity that

propagates from the stomach to the ileum. Furthermore, due to the anal bias of ISN projections, these waves have a propensity to propagate anally, as does the observed MMC. The speed of the wave is graded with synaptic strength, the duration of the wave is graded with slow EPSP duration and the spacing between waves is graded with the synaptic recovery time. Passage of a wave depresses synapses and as the network recovers excitability between waves it may be subject to spontaneous local activity reminiscent of MMC phase II activity. These results suggested that the interdigestive motor program is coordinated by the ISNs of the intestine and that the time keeper is within the synapses connecting ISNs to each other. This leads to a number of experimentally testable predictions.

Drugs

Name	Abbreviation	action
Acetylcholine	ACh	excitatory neurotransmitter acting via nicotinic or muscarinic receptors
Strychnine		inhibitory glycine receptor antagonist its function in gut is unclear
Hexamethonium		nicotinic receptor antagonist
Xylocaine		Na^+ channel blocker and local anaesthetic
Nitric oxide	NO	inhibitory neuromuscular transmitter
Motilin		amino acid implicated in the induction of phase III MMC
Tetrodotoxin	TTX	Na^+ channel blocker (blocks nerve action)
Atropine		muscarinic receptor antagonist
Hyoscine		muscarinic receptor antagonist
Nicardipine		Ca^{++} channel blocker (paralyses smooth muscle)
nitric oxide synthase	NOS	enzyme producing of NO from amino acid L-arginine
Apamin		small conductance K^+ channel blocker
Somatostatin	SOM	a putative enteric neurotransmitter
Serotonin, 5-hydroxytryptamine	5-HT	neurotransmitter
Dimethylphenlpiperazinium	DMPP	nicotinic receptor agonist
Choline acetyltransferase	ChAT	enzyme producing ACh
Vasoctive intestinal peptide	VIP	excitatory neurotransmitter to muscle
ω-conotoxin-MVIIC		blocks N-type Ca^{++} channels
ω-conotoxin-GVIA		blocks high voltage activated Ca^{++} channels
ryanodine		blocks Ca^{++} channel in intracellular structures
isoprenaline		β-adrenergic receptor agonist which relaxes smooth muscle

Major drugs referred in the text, their abbreviations and actions. The order corresponds roughly to the order of appearance in the text.

Preface

Some of this work has been published or submitted as full papers. Electrophysiology for chapter 3 was carried out by Dr Paul Bertrand.

Papers

P. P. Bertrand, E. A. Thomas, W. A. A. Kunze, and J. C. Bornstein. A simple mathematical model of second messenger mediated slow excitatory post-synaptic potentials. *J. Comput. Neurosci.*, 8(2):127–142, 2000.

E. A. Thomas, P. P. Bertrand and J. C. Bornstein. A computer simulation of recurrent, excitatory networks of sensory neurons of the gut in guinea-pig. *Neurosci. Lett.*, 287(2):137–140, 2000.

E. A. Thomas and J. C. Bornstein. Novel aspects of recurrent networks with metabotropic transmission. *submitted.*, 2001.

Chapter 1

Introduction

1.1 Mathematical modelling of biological systems

> The need for modeling in neuroscience is particularly intense because what most neuroscientists ultimately want to know about the brain *is* the model — that is, the laws governing the brain's information processing functions.
>
> Bartlett W. Mel.

Why model gastro-intestinal reflexes? The gut is a major organ system in nearly all multi-celled animals. It takes raw material from the environment and applies complex mechanical and chemical processing to it to extract the energy and substances that are required to maintain life. It usually does this robustly over the life of the animal, coping with any number of mechanical or chemical insults. There is a great deal of descriptive knowledge which explains which components of the gut are involved in different aspects of these processes. These can range from macroscopic components through the cellular level to the molecular. Yet despite this knowledge it is not possible to answer (or even ask) many basic questions about gut reflexes

such as peristalsis, the pattern of muscle contraction and relaxation believed to propel the contents along the intestine. The descriptive model of the peristaltic reflex is based on the "law of the intestine" [Bayliss and Starling, 1899] and basic anatomical and electrophysiological observations. In can be stated:

> The bolus generates a response locally in the sensory neurons which transmit to orally and anally projecting interneurons. These, in turn, transmit to inhibitory motor neurons in the anal direction and excitatory motor neurons in the oral direction. A contraction is generated behind the bolus and a relaxation in front. Thus, the bolus is propelled down the intestine.

There are any number of quantative questions (how soon? how fast? how long?) that cannot be addressed with this kind of descriptive model. But the more interesting questions are: what are the components of the system that determine the quantative properties? What determines how far a bolus will move, how fast, etc? What components of the system are involved in any particular reflex and why? How are reflexes switched on and off? How and where are reflexes modulated? These questions are difficult to answer using a reductionist experimental approach. Somehow the data that have been gathered from diverse experiments need to be put together again in some way so that the interactions between parts of the system can be understood. This is what mathematical modelling aims to do.

Broadly speaking, a model is an abstract construct consisting of a number of assumptions (axioms or facts) and an inference process that allows these facts to be combined into new knowledge. A model should be able to do two things. It

should show the self consistency and completeness of the underlying assumptions or highlight where experimental data or knowledge are missing. Secondly, it should be possible to infer knowledge not explicitly encoded in the assumptions. It should explain known observations and data and, most importantly, it should make predictions about the outcomes of novel experiments. The strengths of a model depend on the veracity of the assumptions and rigour of the methods used to make inferences from these assumptions. Mathematical models are those in which the assumptions are expressed as axioms or equations and the inference is that of mathematical analysis. The assumptions of a mathematical model are as questionable as those of any model, but stating them in the rigorous language of mathematics frequently reveals weaknesses and inconsistencies. The advantage of mathematical models is that now the tools of mathematics can be brought to bear to perform inference on the assumptions. Furthermore, correct reasoning leads to unassailable conclusions. Computer models are mathematical models which use a subset of mathematical reasoning (numerical methods and other algorithms) and in which the mechanics of this reasoning are performed by a machine.

The biological sciences lag behind the physical sciences in the degree to which mathematical models are constructed and used. In fact, the exercise of mathematical modelling is far from established practice in many branches of biology. In neuroscience many modelling studies are now published in mainstream journals, but the community still feels the need for specialised journals and special issues of mainstream journals (for example the November 2000 issue of Nature Neuroscience). The main reason for this is the profound complexity of biological systems. Simplifying assumptions are essential to construct mathematical models. If these models are

to be useful the simplifications must be experimentally realistic. This complexity also makes it hard to get the quantitative data necessary for model construction. Experiments on tissue are also fraught with difficulties of knowing which parts of the system are "under control" and which parts are being manipulated by the experimenter. Even when these difficulties are overcome it is frequently possible to obtain only qualitative data or incomplete quantitative data. (Of course, this is partly because modelling is uncommon so it is frequently not considered worthwhile to obtain quantitative data, or the wrong data are measured.)

The gut is a highly complex organ, involving many cell types, displaying a large array of mechanical and chemical behaviours. Each component (however the system is broken down) has complex, nonlinear interactions with several other components, on time scales ranging from milliseconds to hours. A full mathematical model of something even as seemingly simple as perstalsis is still a long way off. It is still only possible to model a small number of interactions at one time and at only one or two length and time scales. The strongest result of this thesis is the nature of networks of sensory neurons. The major components in these models are the after-hyperpolarising potential (or some other current that behaves in a "similar" way, explained fully below), synaptic currents and network architecture. Hopefully, I have shown how these interact to provide some "biologically useful" functions. The techniques used are mathematical analysis and simulation of large networks. The former is powerful for drawing qualitative conclusions about a system and the conditions under which they will be true, but at the cost of strong simplifying assumptions. The latter allows significantly more complex models to be examined but only in the "vicinity" of the numerical parameters used in the actual runs.

1.2 Basic description of gut reflexes

Man's interest in his guts presumably goes back as far as his interest in anything else, but for the purposes of this review I will start with the classical observations of peristalsis and segmentation of Bayliss and Starling and of Cannon. Careful experimental dissection of the peristaltic reflex is still an ongoing area of research.

The major structures in the gastro-intestinal tract are: mouth, esophagus, stomach, duodenum, jejunum, ileum, cecum, ascending colon, transverse colon, descending colon, Sigmoid colon, rectum and anus. The intestinal wall consists of several layers, including the mucosa and several muscle and nerve plexuses, which is illustrated in figure 1.1, adapted from Furness and Costa [1980].

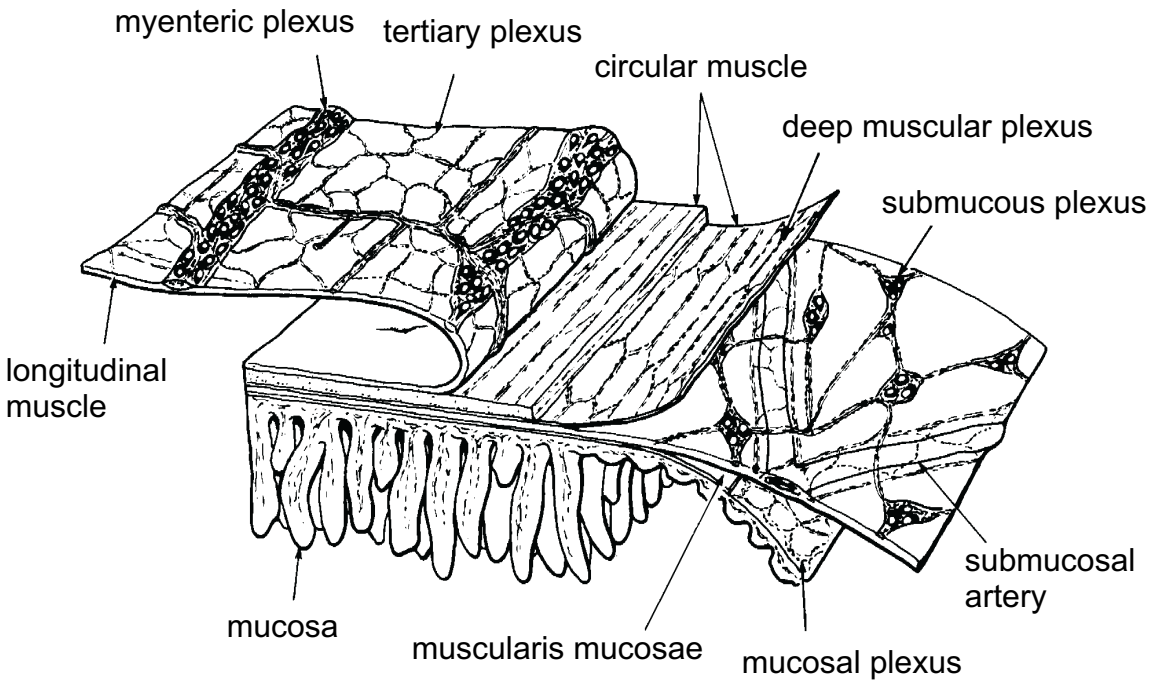

Figure 1.1: Diagrammatic representation of the basic anatomy of the small intestine of the guinea-pig. Adapted from Furness and Costa [1980]

Perstalsis and segmentation

Perhaps the earliest reliable observation of peristalsis in natural conditions is that of Cannon [1898]. His method was to use Röntgen rays (X-rays in current jargon) to observe disgestion of a meal containing bismuth subnitrate, a substance opaque to X-rays. The movements of the intestine were observed as shadows on a fluorescent screen. The meal was fed to conscious, undistressed cats and its progress in the stomach and entry into the duodenum observed. He was able to observe rings or waves of contraction moving over the lower part of the stomach from the antrum to the pyloric sphincter. These peristaltic contractions occurred regularly over many hours and, normally, more than one would be in progress at any one time. Some contractions resulted in food being squirted into the duodenum. The purpose of these contractions, as well as moving the contents into the duodenum, was to mix the contents with gastric juices that are secreted in the lower part of the stomach. The relative quiescence of the fundus (upper part of the stomach) allowed this food to be acted on by salivary peptides before the next stage of processing.

Bayliss and Starling [1899] coined the term "law of the intestine" as follows

> ... excitation at any point of the gut excites contraction above, and inhibition below.

They arrived at this conclusion from studying the small intestine of dogs. Fasted dogs were anesthetized with morphine and ACE (not defined), the abdominal cavity opened and the intestine removed and allowed to float in a saline bath. The intestine was disconnected from central nerves. As well as observing spontaneous peristaltic contractions, they were able to readily elicit peristalsis by inserting a bo-

lus into the opened intestine. To study the reflex in a more controlled manner they introduced a balloon into the intestine. By inflating the balloon they observed a ring of contraction in the oral direction and apparent relaxation anal to the balloon. Several peristaltic contractions could be invoked closely together. The ring of oral contraction showed a visible progagation delay as it expanded or moved in the oral direction and similarly the anal relaxation also showed a finite propagation speed, the descending inhibition travelled faster and farther. A descending relaxation is not seen by all authors [Alvarez and Starkweather, 1919, Bolzer, 1949, Spencer et al., 1999], although Spencer et al. [1999] point out that inhibition may serve to grade the strength of the early part of the contraction. Bayliss and Starling [1899] observed multiple peristaltic waves move over a single stimulus, so they did not state that peristalsis requires the stimulus to move. This point has sometimes been forgotten (for example Brookes et al. [1999]). They blocked peristalsis with cocaine, nicotine or muscarine (which were considered sufficient to block nerve activity at that time). They concluded that peristalsis was nerve mediated and that the nerves were intrinsic to the intestine. This observation has only recently been conclusively confirmed [Furness et al., 1995a].

As well as peristalsis they observed "pendular" movements of the intestine. These are waves of weak contraction that moved over large distances and appeared to be in the longitudinal muscle layer only. They had a frequency of approximately 0.2Hz, which is close to the slow wave frequency (an electrical rhythm in the muscle which generates contractions under some circumstances [Makhlouf, 1999]). They persisted when nerve toxins were applied and so were concluded to be myogenic in origin. In general, these pendular movements have not received much attention, in part

because they are not observed *in vitro*. Their physiological role is unknown.

Although Bayliss and Starling [1899] believed that intestinal reflexes were mediated by an intrinsic nervous system this view was not universally adopted. Alvarez and Starkweather [1919] held the view that a propagating contraction was the result of "conduction" along a "metabolic gradient" running down from the duodenum to the ileum. This gradient apparently resided in the smooth muscle. Inference in this model is based on an analogy with a frictive potential slope — a signal will propagate further and faster down the gradient. They used a variety of stimuli including pinching, cutting, electric shocks and balloon distensions and were only able to observe descending inhibition when using balloon distension. They noted that the "myenteric reflex was rarely observed" and concluded, in the absence of an effect by strychnine, that the myenteric plexus is "without synapses or reflex arcs". However, Alvarez and Bennett [1931] later reported a role for myenteric nerves in response to certain (unclear) electrical stimulus protocols and appeared to attribute their role to the "finer coordination" of peristalsis. These workers were early, and influential proponents, of the myogenic origin of intestinal reflexes.

Hukuhara et al. [1960] studied the nature of the intrinsic reflex illicited by different sensory modalities, specifically mechanical and chemical stimulation of the mucosa and stretch of the smooth muscle. The preparations used in these experiments were decerebrated and anesthesised dogs, cats and rabbits in which a loop of small intestine was externalised and extrinsically denervated by severing the mesentery. The mucosa was exposed to allow application of stimuli and stripped away in parts to allow stretch stimuli to be applied to the muscle without interference from mucosal stimuli. All mucosal stimuli illicited a strong polarised reflex — relaxation

anally and increased contractions orally. Furthermore, this was blocked by intravenous administration of hexamethonium, indicating a reflex arc with at least one synapse. Transecting the muscle layers blocked propagation of the reflex indicating the propagation occured in the myenteric plexus. Stimulation of the muscle, either mechanically or by application of drugs, produced a different response. In this case, inhibition was seen in both directions with the inhibition being greater on the anal side. Hukuhara et al. [1960] seemed to consider the mucosal response the primary or main reflex. In other experiments based on fluid transport through a excised and denervated section of dog jejenum, it was shown that chemical stimuli controlled the response [Hukuhara et al., 1959]. An HCl perfusate caused a stronger response than NaCl and blocking mucosal response with xylocaine (a local anaesthetic that acts by blocking Na^+ channels) reduced the response from control.

When a meal first enters the small intestine it undergoes a rhythmic mixing and kneading process known as segmentation. The first observation of segmentation seems to be that of Cannon [1902]. After exiting the stomach the meal spread out through several coils in the duodenum. After a short period of time, and possibly triggered by the entry of bile and pancreatic juices into the duodenum, regular contractions started. They were spaced and timed such that alternate sections of the intestine contract and relaxed together and adjacent sections contract and relaxed alternately. This action is universally assumed to break up the food, mix it with intestinal secretions and bring it into contact with the absorbing mucosa, as well as slowly propelling the contents anally. Cannon [1902] also pointed out that this helps the venous blood circulation and circulation of lymph within the intestinal wall. The food is generally maintained in the same position, but every few minutes

segmentation pauses and the content is moved a short distance by peristaltic like contractions. Cannon [1902] made distinction between these short, slow peristaltic movements and longer and faster movements. The latter were observed less frequently in the small intestine, but may have occured when the contents were moved from the duodenum into the jejunum. Cannon [1902] was not able to observe segmentation in externalised intestine as it was disrupted by anaesthesia. He thought segmentation may have been similar to the pendular movements, however pendular movements were described as "slight" waves travelling in the anal direction which is incompatible with a mixing process.

When the content moved into the lower intestine, below the ileocaecal valve, motor patterns changed somewhat. Initially the content was maintained in the ascending colon and caecum by "anti-peristaltic" waves. It was kept in this position for some time. As new content enters the ascending colon from above, the content in the lower intestine is moved forward by strong contractions. Shortly afterwards, it is moved back the colon again by further anti-peristaltic contractions. This is obviously quite a complex reflex or motor pattern. When content builds up in the transverse colon, peristaltic contractions move it into the descending colon.

Since it was quickly established that the intestine can perform peristalsis in the absence of extrinsic innervation, it was natural to develop an *in vitro* preparation which allows better measurements to be made and gives more control over the environment. One of the main preparations has been the Trendelenburg preparation [Kosterlitz and Lees, 1964, Tonini et al., 1981, Waterman et al., 1992, Bülbring et al., 1958]. This consists of several centimeters of intestine mounted horizontally in an organ bath with tight intraluminal catheters inserted in each end. Pressure can be

both controlled and measured by allowing fluid to flow into the intestine. When this is done slowly the intestine initially distends — longitudinal muscle contracts [Kosterlitz and Lees, 1964] and circular muscle relaxes [Waterman and Costa, 1994]. This is known as the preparatory phase. Once a threshold is reached, a ring of contraction forms in the circular muscle, near the oral end of the preparation, and this ring moves anally expelling the contents as it does so. This is known as the emptying phase. Fluid outflow can be measured and either isotonic or isometric measurements of longitudinal muscle contraction can be taken. This preparation presumably represents the real physiology quite closely since the content of the small intestine is quite liquid.

The reflexes are triggered by increasing tension or circumference of the intestinal wall, rather than pressure, since placing a sleeve around the intestine blocks the reflex [Kosterlitz and Lees, 1964]. The emptying phase starts at the oral end of the preparation because of the reduced descending inhibition in this region [Waterman et al., 1994b]. Destroying the myenteric plexus over a small length in the middle of the preparation moves the site of initiation to just anal of the lesion. The initial accommodation, or preparatory, phase is mediated by inhibitory motor neurons [Waterman et al., 1994b]. If the nitric oxide component of inhibitory transmission to the muscle (see section 1.6) is blocked then accommodation is reduced, the threshold is reduced, but the emptying phase is unaffected [Waterman and Costa, 1994]. If the apamin sensitive component of inhibitory transmission to the muscle (see section 1.6) is blocked then contractions of the circular muscle occur in an apparently random manner along the length of the intestine. These results indicated that there are two roles for inhibitory motor neurons in peristalsis. This first is to mediate the initial

accommodation as fluid enters the intestine. The second is essential for proper coordination of the contraction that travels anally. The emptying phase of the reflex is blocked by hexamethonium [Kosterlitz and Lees, 1964]. By preventing the intestine from expanding with the use of variable length sleeves Waterman et al. [1994b] argued that initiation of the emptying phase of peristalsis is the result of the net balance of excitation originating from ascending pathways and inhibition originating from descending pathways.

Interdigestive motor patterns of the small intestine

Slowly moving regions of strong contractile activity, or migrating motor complexes, have been observed in the small bowels of man and dog since the twenties and thirties [Castleton, 1934]. However, Szurszewski [1969] appears to have been the first to recognise both their spatial extent and temporal characteristics, in particular that they occur cyclically. For these experiments, electrodes were implanted at approximately regular distances along the intestine of dogs, from the duodenum to the terminal ileum. Observations were usually made after the animal had fasted for 21 hours since migrating complexes were not seen in animals that had not been fasted. It was observed that a long region of "diffuse and random action potentials" organised into a region of intense action potential activity that then started to migrate anally. Most travelled the entire length of the small bowel and the remainder fizzled out after travelling more than 75% of the length. When one complex terminated in the ileum another would start in the duodenum. The propagation speed of the complex started at 3.5–6.2cm/min at the duodenum and decreased gradually to 1.2–1.9cm/min when they terminated in the ileum. The length of the complex in the

duodenum was 25.0–36.5cm at the start and 6.0–12.0cm at the end. The duration of an episode was roughly constant over the length of its travel at 4.8–7.0 minutes. In guinea-pig propagation speed varies from 17.5 cm/min in the duodenum to 4.1 cm/min in the ileum [Galligan et al., 1985]. Phase III like are events are also seen in rabbit [Ruckebusch et al., 1985], cat [Vos, 1993], kangaroo and wallaby [Richardson and Wyburn, 1983], pig [Rayner et al., 1981] and sheep [Ruckebusch and Bueno, 1977].

The pattern defined above is now referred to as phase III of the interdigestive migrating motor complex (MMC). It is now known to be part of a cycle with 4 phases [Code and Marlett, 1975]. Phase I is characterised by near quiescence. Phase II has intermittent, apparently random, peristaltic contractions, which are weaker than the phase III contractions. Phase III is as described above. Phase IV is a period of phase II like activity following phase III and may be brief or absent. In humans, the individual contractions within phase III move faster than the complex itself [Summers et al., 1983]. The modern definition of MMC phase III is that these contractions must occur at the slow wave frequency [Sarna, 1985, Husebye, 1999]. The duration of the complete cycle is 90–240 minutes in humans [Kellow et al., 1986] and 90–144 minutes in dogs [Code and Marlett, 1975]. Guinea-pigs show a similar pattern, except that the initiation of a phase III in the duodenum occurs quite some time after the termination of the preceding phase III in the ileum [Galligan et al., 1985, 1986]. In this species the MMC is not abolished by feeding, which produces an increase in the duration of the cycle by increasing the duration of phase II. Table 1.1 summarises some basic properties of the interdigestive for man, dog and guinea-pig.

The modulator that drives the cycle remains unidentified. Motilin was, and is,

Parameter	species	region	value	source
phase I duration	man	–	23 min	Kellow et al. [1986]
phase II duration	man	all	70 min	Kellow et al. [1986]
phase III duration	man	duodenum	11.7 min	Kellow et al. [1986]
phase III duration	man	jejunum	10.7 min	Kellow et al. [1986]
phase III duration	man	ileum	8.9 min	Kellow et al. [1986]
phase III speed	man	jejunum (near duodenum)	4.3 cm/min	Kellow et al. [1986]
phase III speed	man	terminal ileum	0.6 cm/min	Kellow et al. [1986]
phase I duration	dog	all	31–48 min	Code and Marlett [1975]
phase II duration	dog	all	26–62 min	Code and Marlett [1975]
phase III duration	dog	stomach	12 min	Code and Marlett [1975]
phase III duration	dog	duodenum	7.8 min	Code and Marlett [1975]
phase III duration	dog	jejunum	6.0 min	Code and Marlett [1975]
phase III duration	dog	ileum	5.5 min	Code and Marlett [1975]
phase III speed	dog	near pylorus	5.7–11.7 cm/min	Code and Marlett [1975] Szurszewski [1969]
phase III speed	dog	distal ileum	0.9–2.5 cm/min	Code and Marlett [1975]
phase I duration	guinea-pig	all	10–12 min	Galligan et al. [1985]
phase II duration	guinea-pig	all	70 min	Galligan et al. [1985]
phase III duration	guinea-pig	duodenum	2.7 min	Galligan et al. [1985]
phase III duration	guinea-pig	jejunum	3.9 min	Galligan et al. [1985]
phase III duration	guinea-pig	ileum	3.9 min	Galligan et al. [1985]
phase III speed	guinea-pig	duodenum	17.5 cm/min	Galligan et al. [1985]
phase III speed	guinea-pig	jejunum	7.3 cm/min	Galligan et al. [1985]
phase III speed	guinea-pig	ileum	4.1 cm/min	Galligan et al. [1985]

Table 1.1: Properties of the MMC for various regions and species.

considered a strong candidate. Motilin levels in the blood are elevated during MMCs [You et al., 1980] and administration of synthetic motilin can cause a premature MMC phase III [Itoh et al., 1978, Vantrappen et al., 1979] However, more detailed studies in dogs have shown that the motilin peak occurs after the start of phase III in the antrum [Sarna et al., 1983], indicating that elevated motilin levels may be caused by MMC contractions, rather than being the cause. Furthermore, other substances can induce premature MMC phase III [Sarna et al., 1983] and any number of other peptides and neurotransmitters are elevated during MMC phase III [Husebye, 1999]. Nevertheless, in humans, the motilin peak always procedes MMC phase III [Bormans et al., 1987].

Locally the MMC is controlled by the enteric nervous system, but is modulated by extrinsic nerves. Itoh et al. [1981] installed force transducers in dog jejunem. After control recordings were taken, a 40cm segment of jejunem was extrinsically denervated and animals allowed several weeks to recover. No significant differences were found in the motor patterns after denervation. Feeding disrupted the MMC in the same way in both denervated and control animals. In some animals a Thiry loop was created from the denervated section. This involves removing a section of intestine and rejoining the main part of the intestine. The excised section retains its blood supply and force transducers. The MMC migrated along the rejoined intestine with the same speed. This indicates that the MMC is driven by a signal that travels along the intestine as opposed to being coordinated by some higher mechanism. The isolated loop also continued to show MMC like behaviour. However, both the duration and frequency of the MMC like episodes was increased and speed of propagation was decreased. These contractions were also interrupted by feeding.

However, in a similar experiment phase III episodes were not disrupted by feeding in either an auto-transplanted segment or loop of jejunoileum [Sarr and Kelly, 1981]. In the latter experiments the blood vessels supplying the transplanted regions were sectioned and reanastomosised, whereas in Itoh et al. [1981] extrinsic denervation was only performed by dissecting tissue away from blood vessels.

In another elegant experiment twelve electrodes were installed along the small intestine of dogs [Sarna et al., 1983]. After control records were taken, the intestine was transected in three places and rejoined. Independent MMCs, displaying all four phases, appeared in each segment and cycled independently. The duration of the cycle was longest in the first segment where it was slightly longer than control, but not significantly. The cycle duration in the second segment was significantly different from both control and the first transected segment. The duration then increased in the third and fourth segments, until it was, again, not significantly different from control. After 45–60 days MMCs started to propagate across transections and MMC propagation was fully recovered by 98–108 days.

In another experiment electrodes were implanted in dogs [Sarna et al., 1981]. In addition intra-arterial cannulas were installed and externalized, allowing perfusion of drugs into 3–5cm lengths of intestine. Drugs tested were tetrodotoxin (TTX), atropine and hexamethonium. When atropine was perfused just before the arrival of a phase III event, the phase III did not appear in the perfused region or in the regions more anal to the perfused region. When atropine was perfused after a phase III event had passed the electrode, local slow wave activity was blocked but propagation continued anally. The results of hexamethonium infusion were similar. In addition, hexamethonium was perfused while a phase III event was about half

through the perfusion area. The event was immediately blocked at the perfusion site, but continued to propagate. Infusion of TTX caused vomiting within 80–270 s. As with the other drugs, when TTX was infused before the arrival of a phase III event propagation was halted at the infusion site. Unlike the hexamethonium and atropine, a new phase III was initiated distal to the infusion site in 10 of 14 trials. The new phase III event started 130–880 s after the expected time of arrival of the initial phase III.

Blocking inhibitory neuro-muscular transmission with nitric oxide inhibitors disrupts MMC cycling [Sarna et al., 1993]. Infusion of L-NAME or L-NNA into the carotid artery of fasted dogs generated an immediate MMC cycle. Subsequent cycling was significantly faster for several days after that because of a decrease in the duration of phase II. The duration and propagation speed of phase III contractions was not significantly altered. Inhibition of NOS also significantly reduced the period of postprandial disruption to MMC cycling.

These studies show that the MMC cycle is coordinated and initiated in the enteric nervous system. Specifically, it is not initiated or coordinated by extrinsic innervation [Itoh et al., 1981]. Furthermore, when sections of the myenteric plexus are isolated from each other, each section continues cycling on its own [Sarna et al., 1983]. In the intact intestine, initiation at any point normally occurs because of a signal that propagates in the anal direction, within the intestinal wall [Sarna et al., 1981]. This signal can be disrupted by blocking muscarinic transmission to the muscle or by blocking nicotinic transmission within the ganglia [Sarna et al., 1981]. Furthermore, decreasing inhibitory transmission to the muscle seems to increase the signal in that MMC cycle time is reduced [Sarna et al., 1993], presumably because

contractions are more likely or stronger. These data imply that feedback from muscle contraction is an essential element of the system. One model proposed for propagation is that local contraction excites mechanoreceptors slightly more distally which, in turn, excites local circuits [Sarna et al., 1981].

1.3 Electrophysiological analysis of reflexes

Bayliss and Starling [1899] hypothesised that, not only was peristalsis intrinsic to the intestine, but it was neurally mediated. They deduced that it was independent of the central nervous system by showing that the reflex remained after sectioning of the splanchnic and vagus nerves. Intraveneous administration of nicotine or application of cocaine directly to the intestine blocked contractions and so it was concluded that a nervous mechanism was involved. Of course, physiological knowledge has increased and it is now known that this evidence was not conclusive. This issue has since been laid to rest by showing that reflexes are neurally mediated because they are abolished by TTX [Smith et al., 1990, Barthó et al., 1989]. The possibility of an axon reflex from extrinsic innervation [Grider and Jin, 1994] has been eliminated by demonstrating that reflexes continue even in tissue chronically denervated of extrinsic inputs [Furness et al., 1995a], at least in guinea-pig.

The investigation of enteric reflexes at the cellular level began with Hirst and McKirdy [1974], Hirst et al. [1975]. The preparation consisted of a segment of ileum with a flap opened at either the oral or anal end. The flap was pinned down, allowing impalement of neurons or muscle with microelectrodes. Stimuli were either electrical or from a balloon inserted in the intact end and distended. Because balloon distension evokes peristaltic like contractions *in vivo* [Bayliss and Starling, 1899], intracellular recordings made in this preparation will represent the cellular membrane potential correlates of motility reflexes. Recordings were made in the circular muscle. A hyperpolarising potential, called an inhibitory junction potential (IJP), was readily seen in the anal circular muscle in response to both electrical stimulation and

distension. This is the electrical correlate of relaxation. When atropine was absent from the bath depolarising potentials, called excitatory junction potentials (EJPs), were also seen in both in the circular muscle and in the longitudinal muscle, with that in the circular muscle following the IJP. This was presumed to be the electrical equivalent of the peristaltic wave — an inhibition followed by a contraction that propagates down the gut. Bayliss and Starling [1899], in their observations, always saw a muscle relaxation as the first component of the peristaltic wave, followed by a contraction. This descending excitation seen in muscle responses does not seem to have been observed by later authors (e. g. [Smith and Furness, 1988]) and its nature and role remain unresolved. In addition to muscle responses, many neurons impaled on the anal side of the stimulus responded with bursts of fast excitatory post-synaptic potentials (EPSPs), occasionally summing to fire action potentials [Hirst and McKirdy, 1974, Hirst et al., 1975]. In some cases, neurons were spontaneously active. In the oral pathway, only a few neurons responded to stimuli, with very brief bursts, and no spontaneous activity was observed.

Although an intralumenal balloon mimics a physiological stimulus, it excites two modalities — mucosal distortion and distension of the intestinal wall. Stimulation of these modalities separately has been shown to generate a reflex [Hukuhara et al., 1958, 1960]. A series of electrophysiological studies were undertaken to analyse the temporal and spatial interaction between mucosal and/or distension stimuli [Bornstein et al., 1991a, Smith et al., 1992, 1990, Smith and Furness, 1988, Smith et al., 1991, Yuan et al., 1992, 1991]. The basic preparation in most of these studies consisted of a section of opened guinea-pig ileum, pinned flat, with the mucosa facing upwards or downwards depending on the type of stimuli to be applied. The tissue

was paralysed with drugs, usually nicardipine which blocks L-type Ca^{++} channels on the muscle preventing contraction, or sometimes hyoscine, to block the muscarinic component of excitatory transmission to the muscle. Distension was applied by inflating balloons underneath the tissue without compressing the mucosa. Mechanical distortion of the mucosa can be applied as stroking with a brush or compression with a sponge block. The latter method has the advantage that the intensity of the stimulus can be quantified in terms of how far the sponge is advanced into the mucosa. Recordings were made from the smooth muscle or from myenteric neurons, oral or anal to the stimulus.

The first electrophysiological study to look specificially at mucosal stimulation was that of Smith and Furness [1988] (using a tube preparation with both ends opened and pinned flat allowing stimulation of the mucosa). The mucosa was stroked with a mechanically operated brush and recordings made from the circular muscle. Cholinergic transmission to the muscle was blocked by hyoscine. It was found that mucosal distortion elicited a polarised reflex — IJPs were observed in the anal direction and EJPs in the oral direction. There was no sign of the descending excitation seen previously [Hirst et al., 1975]. When multiple stimuli were applied more frequently than every 6 s, EJPs displayed depression [Smith and Furness, 1988]. At high frequency ($>$ 1 Hz), EJPs overlapped and the resulting response was greater because of summation. As stroking continued the response died away. The anal IJP increased in both peak and duration with successive stimuli, initially, but rundown was observed after repeated stroking [Smith et al., 1991]. Similar results were found by using compression from a mechanically operated sponge block rather than a brush stroke [Yuan et al., 1991]. In this later study, junction potential

amplitude was found to be graded with the degree of advancement of the sponge. Yuan et al. [1992] showed that the response to the second of two compressions was reduced by about 30% when the inter-stimulus interval was 2 s, in both pathways. Responses in a small number of neurons to multiple high frequency bursts of strokes have also been recorded [Bornstein et al., 1991a]. In both pathways the number of fast EPSPs in response to subsequent stimuli decreased, with the decrease occurring more slowly in the descending pathway.

By filling neurons with dye, or another marker which can then be revealed immunohistochemically, it is possible to correlate a neuron's response during a reflex with its morphology and projections [Bornstein et al., 1991a, Smith et al., 1992] (P. D. Thornton & J. C. Bornstein, in press). The morphology of these neurons was either Dogiel type I (see section 1.4) or other morphologies with a single axon exiting the cell body and several dendrites. Some neurons had long projections that ran longitudinally along the gut in either the oral or anal directions and which responded to stimuli located in the opposite direction to their projections. Another group had projection patterns, or expansion bulbs, that indicated that they probably ramified in one of the muscle layers and hence were probably motor neurons. A final large group projected a fairly short distance longitudinally (∼1mm) and a longer distance circumferentially (∼3–3.5mm). Most of these did not respond to stimuli and for those that did the longitudinal projection did not necessarily predict the pathway. These projection patterns are consistent with these neurons being circular muscle motor neurons [Smith et al., 1988, Brookes et al., 1991b] (see section 1.4).

Smith et al. [1990] used the flat preparation to study the effect of distension without mucosal distortion. Again, polarised electrical responses were found in the

muscle, IJPs oral and EJPs anal. Both EJPs and IJPs increased in amplitude and duration as the duration of the distension was increased. Although, responses were graded they were quite complex and seemed to be the sum of several components. Oral responses to moderate distension were blocked by hyoscine and a small IJP revealed. Increasing the distension restored the EJP, which was then blocked by the addition of a substance P receptor antagonist. To locate the stretch sensor, experiments were performed with mucosa, submucosa, deep muscular plexus and circular muscle removed. The response remained, indicating that the sensor is either in the myenteric plexus or the longitudinal muscle. This also showed that nerve impulses were carried in the myenteric plexus. Recordings from neurons during distension showed that most interneurons and motor neurons, and no sensory neurons, responded with a burst of fast EPSPs [Smith et al., 1992]. The neurons were filled with dye and their projections analysed.

Most interneurons responded to stimuli predicted by their projections, and a small number responded to stimuli coming from the opposite direction, implying some cross talk between orally and anally projecting interneurons. Many longitudinal muscle motor neurons and a few circular muscle motor neurons responded to stimuli from either direction. Fast EPSP bursts were erratic in both duration and latency, however the duration of bursts in the descending pathway was significantly longer than those in the ascending pathway.

Repeated distensions have also been applied systematically. Yuan et al. [1992] found that the second junction potential response to maximal stimuli applied 2 s apart was reduced by 90% in the oral pathway and 70% in the anal pathway. There was also a large reduction in the responses to test distensions at 30mm when the

conditioning response was given at 15mm. However, the changes in response were not as large as those seen when the test and conditioning responses were at the same site, implying that at least some depression occurs in the sensory neurons or at the output synapses of the sensory neurons. Neurons in both pathways also exhibited strong depression in response to multiple stimuli separated by less than 2 min [Smith et al., 1992]. Consistent with muscle recordings, this depression was stronger in the ascending pathway.

Because mucosal distortion and distension occur together under physiological conditions it is particularly interesting to know how these modalities interact. There is strong evidence that the different modalities originate in different populations of sensory neurons [Smith et al., 1991]. Junction potentials in response to mucosal stimulation remained undiminished even when the response to repeated descending stimuli at the same site had been abolished. When the response to mucosal stimuli had been depressed to almost zero the response to distension was enhanced. Neurons in the submucous plexus displayed immunoreactivity for an activity dependent dye after mucosal mechanical stimulation [Kirchgessner et al., 1992]. However, in this experiment the only blocker of synaptic transmission present was hexamethonium, and so the possibility that these neurons were synaptically driven cannot be eliminated. On the other hand, stretch sensitive neurons [Kunze et al., 1999, 1998, 2000] and chemosensitive neurons [Kunze et al., 1995, Bertrand et al., 1997a] are located in the myenteric plexus.

1.4 Micro-analysis of nerve circuits

Obviously, any attempt to understand how enteric nerve circuits control motility or secretion requires a knowledge of the "wiring diagram". That is, what components are in the circuit and how are they connected together. A number of techniques are used, but perhaps the key insight to elucidating the enteric nerve circuits is the observation that neurons fall into a number of mutually exclusive classes based on the presence of certain chemicals, so called chemical coding [Furness et al., 1995b]. Most of these chemicals are either known or putative neurotransmitters, such as serotonin or somatostatin, or are involved in their synthesis, for example, choline acetyltransferase or nitric oxide synthase. In the case of motor neurons, this allows predictions to be made about their function. In some cases, the function of the markers is not known; for example the calcium binding proteins, calbindin and calretinin, are found in specific subclasses of enteric neurons. Many years of careful immunohistochemical studies have shown that these classes also correlate with projection and connection patterns, morphology and, to a large extent, their electrophysiology. The different projection classes imply different functional classes, specificially sensory neuron, ascending and descending interneurons and motor neurons. The data reviewed below are for the guinea-pig ileum, the most thoroughly studied species and region.

Morphology of cell bodies

The initial observations of Dogiel [1899], using methylene blue staining, were that there are three morphological classes of neurons and these observations have only recently been surpassed by more modern work (for example Furness et al. [1988a],

Hodgkiss and Lees [1983], Bornstein et al. [1984a], Katayama et al. [1986]). Dogiel type I neurons have broad flat dendrites, termed lamellar, and a single process [Dogiel, 1899]. Axon processes project in all directions, but mostly in the circumferential direction, and entered the muscle leading to the conclusion that they were motor neurons. A later study, using intracellular injection of the dye Lucifer yellow, was not able to observe the processes entering the muscle, presumably because the dye failed to follow the processes sufficiently far [Furness et al., 1988a]. More recently, intracellular injection of either biocytin or neurobiotin has allowed this deficiency to be overcome [Bornstein et al., 1991a, Smith et al., 1992]. Dogiel type II neuron bodies have been described as "angular, star or spindle" shaped when visualized by methyline blue or smooth [Hodgkiss and Lees, 1983, Furness et al., 1988a] when visualized using intracellular dye and by later observers. Their characteristic feature is that they have several long processes [Furness and Costa, 1987, Furness et al., 1988a]. Intracellular dye studies have also defined body shapes with many filamentous processes, or dendrites, and small smooth cell bodies [Furness et al., 1988a]. The small neurons may have been Dogiel III neurons, however this last class was not very well defined [Furness et al., 1988a]. Not all neuron morphologies can be readily classified or matched to functional class.

Sensory neurons

Dogiel speculated that type II neurons are sensory neurons because of their projections to the mucosa [Furness et al., 1988a]. Neurons with the electrophysiological category of AH (see section 1.5) have been proposed to be sensory because they appeared to lack synaptic input [Hirst et al., 1974]. It is now known that AH neu-

rons, morphological type II neurons [Iyer et al., 1988, Bornstein et al., 1984a] and primary sensory neurons [Kunze et al., 1995, Bertrand et al., 1997a] are the same thing. Sensory neurons project mainly in the circumferential direction, 1.5–2.5mm on average [Bornstein et al., 1991b], and up to 7mm [Stebbing and Bornstein, 1996]. They also project 0.3mm orally and 0.4mm anally; that is, there is a slight bias of the projections in the anal direction [Furness et al., 1990, Bornstein et al., 1991b]. This is also born out by retrograde labeling studies (for example Song et al. [1997]). The majority, 80–90%, of Dogiel type II neurons are reactive to the Ca^{++} binding protein calbindin and only Dogiel type II neurons in the ileum are positive to calbindin [Furness et al., 1988b] (although only 8% of Dogiel type II neurons are positive in the guinea-pig colon [Lomax and Furness, 2000].) Calbindin positive synapses are found on neurons of all morphologies [Pompolo and Furness, 1988], including other Dogiel type II neurons. About 10% of Dogiel type II neurons have long anal projections, up to 110mm, that originate from a single process [Brookes et al., 1995]. It is not known if the long anal or short circumferential projections make connections to the same classes of neurons. Divided organ bath studies indicate that these long projections play a role in reflexes [Johnson et al., 1998]. Projections of calbindin positive neurons in the myenteric plexus also traverse the circular muscle and enter the submucous plexus and villi of the mucosa [Furness et al., 1990]. Sensory neurons make up about 30% of the population of enteric neurons [Costa et al., 1996].

Interneurons

There are several classes of interneurons in the myenteric plexus. The technique of choice for analyzing their projections is retrograde labelling [Brookes and Costa,

1990, Song et al., 1992]. A small section of circular muscle or mucosa is removed from a strip of guinea-pig ileum to reveal the myenteric plexus or submucous plexus respectively. A crystal of the lipophilic, fluorescent dye DiI is placed onto the plexus. The tissue is typically kept in organotypic culture for 3–4 days. The dye travels retrogradely along the processes and into the soma. The tissue can be processed for the immunoreactivity of interest and the morphology and projections of the neurons can be visualised. This techniques allows projections to be quantitively analysed, which is difficult to do with other techniques.

Somatostatin immunoreactive interneurons

There are two classes of neurons containing somatostatin (SOM), descending interneurons and secretomotor neurons [Song et al., 1995], both of which are also immunoreactive for acetyltransferase [Costa et al., 1996]. The reported percentage of SOM positive interneurons in the myenteric plexus varies — 2.6% [Portbury et al., 1995], 4% [Costa et al., 1996], 9.3% [Song et al., 1997]. Their morphology is "ovoid ... with a single axon and several filamentous dendrites" [Song et al., 1997], that is they have filamentous morphology [Costa et al., 1996]. They make close contacts and synapses with SOM immunopositive targets, as determined by both confocal and electron microscopy [Portbury et al., 1995, Song et al., 1997, Pompolo and Furness, 1998]. Their processes run up to 60–70mm in the anal direction [Song et al., 1997, Meedeniya et al., 1998] and the distribution of distances of cell bodies from the site of the dye crystal implies that the distribution of process lengths is broad rather than clustered [Song et al., 1997].

Nitric oxide synthase immunoreactive interneurons

There are 3 classes of neuron immunopositive for nitric oxide synthase (NOS) – two classes of inhibitory circular muscle motor neuron and one of descending interneuron [Costa et al., 1996]. Most NOS neurons have lamellar dendrites and a single process characteristic of Dogiel type I neurons [Costa et al., 1992]. No retrograde labelling studies have been done on these interneurons but studies in which the myenteric plexus is lesioned revealed that they project predominantly in the anal direction with average projection lengths of 5–10mm [Costa et al., 1992]. They make up 5% of the total population of myenteric neurons [Costa et al., 1996]. Two types of vesicle containing apposition are presumed to be functional, *close contacts* which are contacts within 50nm and *synapses* which are closer appositions with thickened pre and post synaptic membranes [Young and Furness, 1995]. NOS reactive cell bodies all have close appositions of both types with other NOS reactive boutons [Young et al., 1995, Mann et al., 1997]. It is usual to interpret these data to mean that NOS interneurons make contacts with both NOS motor neurons and other NOS interneurons. Thus, NOS descending interneurons also form chains. Thus, interconnected networks of NOS and SOM descending interneurons form an inhomogeneous feedforward network [Mann et al., 1997]. This was shown using double and triple labelling and observing appositions using confocal microscopy. The confocal microscope has resolution of around 300nm, which, while significantly better than conventional microscopy, is not sufficient by itself to determine if appositions are within 50nm, the usual requirement for apposition to presumed functional [Young and Furness, 1995]. However, where there are dense baskets of fibres surrounding a cell, it is likely that

there are appositions within the "functional range" [Llewellyn-Smith et al., 1988].

Serotonin immunoreactive descending interneurons

The third class of descending interneurons are immunopositive for serotonin and acetyltransferase and make up 2% of enteric neurons [Costa et al., 1996]. Ultrastructural studies have been performed by making serial sections (90nm) of a single ganglion labelled for serotonin and viewing with both light and electron microscopy [Young and Furness, 1995]. Appositions were found with large serotonin containing vesicles and were made with both Dogiel type I and type II neurons. In the case of the latter, these were few and of the close contact type rather than being proper synapses. Where the target neurons were also immunocytochemically labelled, it was found that targets include other serotonin positive neurons, and that serotonin positive neurons had thick baskets of positive processes surrounding them. Thus, these neurons also form chains. Most of the neurons positive for NOS received only a small number of serotonin positive appositions. Inhibitory motor neurons are NOS immunoreactive, so this implies that serotonin neurons do not directly activate them, although serotonin neurons might form intermediate parts of the pathway.

Projections of neurons labeled for SOM and serotonin have been analysed using retrograde labelling [Meedeniya et al., 1998]. Neurons that are serotonin positive and SOM negative have projections up to 60 mm anal, but a small number had short anal projections. Neurons with serotonin and SOM positive labeling had similar projections and together they made up 9% of the population of labelled neurons. Neurons with serotonin negative and SOM positive labelling made up 20% of the labelled population and also had long anal projections.

Ascending interneurons

There is a single class of orally projecting interneuron [Brookes et al., 1997], which is immunoreactive to calretinin, choline acetyltransferase, enkephalin, neurofilament protein triplet and substance P [Brookes et al., 1991a] (another class of calretinin positive neuron projects to the longitudinal muscle [Costa et al., 1996] (see below)). These interneurons make up about 4–5% of the population of myenteric neurons [Costa et al., 1996, Brookes et al., 1991a]. Retrograde labelling shows that they project up to 14mm orally, with most projecting more than 4mm [Brookes et al., 1997]. Ultrastructural and immunocytochemical studies have shown that calretinin neurons make many synaptic connections to other positive neurons [Pompolo and Furness, 1995, 1993]. Thus, as with descending interneurons, ascending interneurons form chains. Applying DMPP (a nicotinic receptor agonist) to a single ganglion induced a burst of fast EPSPs in an impaled orally directed interneuron located oral to the site of application, showing that these interneurons do indeed form functional synapses with other oral interneurons [Brookes et al., 1997]. Interestingly, 36% of ascending interneurons receive inputs from a descending interneurons [Pompolo and Furness, 1995].

Muscle motor neurons

Six classes of motor neurons that innervate the smooth muscle were identified by Costa et al. [1996]. These are two short projection and one long projection classes of excitatory circular muscle motor neuron projecting in the oral direction, a short and a long class of inhibitory circular muscle motor neurons projecting in the anal

direction and excitatory longitudinal muscle motor neurons. In addition, there are longitudinal muscle motor neurons that contain NOS and so may be inhibitory [Williamson et al., 1996]. Other motor neurons of the gut are secretomotor and vasodilator neurons, which are found predominantly in the submucous plexus [Furness, 2000], and are not considered further here.

In addition to retrograde labelling, the techniques for analysing muscle motor neurons have included immunohistochemical and ultrastructural studies [Llewellyn-Smith et al., 1988] to determine neuronal inputs to the motor neurons. Projection patterns of processes within the muscle have been determined electrophysiologically [Smith et al., 1988, Bornstein et al., 1986]. With this technique, synaptic transmission onto motor neurons is blocked and transmural electric shocks applied to the preparation. The smooth muscle is impaled longitudinally or circumferentially at various distances from the site of stimulation and IJPs or EJPs recorded in the muscle.

Excitatory circular muscle motor neurons

Excitatory transmission to the circular smooth muscle is predominantly mediated by acetylcholine [Hirst et al., 1975, Bauer and Kuriyama, 1982] with a component mediated by tachykinins [Franco et al., 1979, Taylor and Bywater, 1986]. Thus, by applying hexamethonium and hyoscine to the bath, cholinergic transmission to the motor neurons is blocked. Because a residual excitatory transmission onto the muscle is present, the upper bounds on the projection distances of non-cholinergic excitatory motor neurons can be mapped [Smith et al., 1988]. (A confounding issue with this study is that trains of stimuli were used, which can potentially generate

slow EPSPs in the motor neurons.) In the presence of hexamethonium, projections of the motor neurons travel about half way around the circumference (5–10mm). Removal of the myenteric plexus and applying electrical stimuli to excite neuron processes lead to the conclusion that they project about 3–4mm in the myenteric plexus before descending into the circular muscle. Most longitudinal projections are less than 3mm, however some ran more than 10mm in the oral direction and seem to have collaterals along their entire length. Retrograde tracing studies identified three ChAT positive classes of orally projecting motor neurons [Brookes et al., 1991b]. These included two classes positive for substance-P, one with short projections and one with long. The third class is not immunoreactive for substance-P and has local projections. This is consistent with (and extends) the electrophysiological study of Smith et al. [1988]. The proportion of long projection neurons is 7% of all enteric neurons and short projection neurons make up 5% [Costa et al., 1996].

Inhibitory circular muscle motor neurons

Similar electrophysiological techniques were used to analyse projections of inhibitory motor neurons [Bornstein et al., 1986]; however, in these experiments only a single stimulus pulse was used minimising the potential confounding effects of slow EPSPs. In all cases IJPs were maximal at 1 mm from the electrode, the closest recording point. As the recording electrode moved circumferentially away from the stimulating electrode, the maximum IJP amplitude declined approximately linearly. The slope of the decline was 5.5%/mm for control, about 7%/mm in hexamethonium, and 10%/mm in preparations from which the myenteric plexus had been removed. This implies that motor neurons project about 11 mm in the circumferential direction,

but only a short distance is travelled within the myenteric plexus before the processes enter the muscle itself. In the longitudinal direction, IJP amplitudes declined faster than linearly (the magnitude of the derivative increased), but could be detected as far as 30mm in the anal direction. Addition of hexamethonium to the bath caused only a small, but statistically significant, decrease in the amplitude of IJPs recorded 1 mm from the stimulus. In islands created by two circumferential lesions of the myenteric plexus, IJPs returned to over 50% of control within 2mm of the lesions indicating that the majority of neurons have longitudinal projections of less than 2mm. Retrograde labelling supported these observation by identifying two classes of noncholinergic muscle motor neurons based on projection lengths [Brookes et al., 1991b]. These neurons were immunopositive for vasoactive intestinal polypeptide and NOS. They project anally up to 40 mm. There was an absence of cell bodies close to the location of the dye crystal indicating that they must run some distance before entering the muscle. The proportions of short and long projecting neurons in the myenteric plexus are 12% and 5% respectively [Costa et al., 1996].

Longitudinal muscle motor neurons

There are several types of longitudinal muscle motor neuron based on immunohistochemical classifications and pharmacology [Ambache and Freeman, 1968, Brookes et al., 1992, Williamson et al., 1996, Yunker and Galligan, 1998]. Retrograde labelling showed that the vast majority of these neurons are cholinergic and half of those also contain substance-P [Brookes et al., 1992]. In addition, there are some NOS positive fibres in the longitudinal muscle [Williamson et al., 1996]. These results are consistent with pharmacological studies — there is exitatory transmission

that is blocked by atropine [Hirst et al., 1975], there is an antropine resistant excitatory transmission [Ambache and Freeman, 1968] and there is an inhibitory transmission [Yunker and Galligan, 1998]. Based on projection patters, there is only one class of longitudinal muscle motor neuron [Brookes et al., 1991a]. These projections have no bias in either the longitudinal or circumferential directions. Most projections were within 2–3mm in either direction. This is consistent with anterograde labelling studies [Furness et al., 2000b].

Many longitudinal muscle motor neurons are immunopositive for calretinin [Brookes et al., 1991a] and this fact has been combined with ultrastructural studies to determine the input to these neurons [Pompolo and Furness, 1993]. These neurons receive inputs from other calretinin positive neurons (ascending interneurons), calbindin positive neurons (sensory neurons) [Pompolo and Furness, 1988] and other sources. Since the intestine was not extrinsically dennervated, it cannot be excluded that these other inputs were extrinsic. If they were not extrinsic then presumably they were descending interneurons, but it is not possible to conclude which subtype. Reflex studies also show that longitudinal muscle motor neurons receive synaptic input from the descending pathway in response to both mucosal and compression stimuli [Bornstein et al., 1991a, Smith et al., 1992].

1.5 Electrophysiology of enteric neurons

... detailed information on the electrical and synaptic behaviour of enteric neurons ... will be basic to understanding the physiology of nervous control of digestive function in both the normal and disordered states.

Starodub and Wood [2000].

This section summarises the literature describing the voltage and Ca^{++} dependent conductances of enteric neurons and their action potential firing patterns. Membrane potential changes due to synaptic transmission are covered in section 1.6.

Early data on the electrophysiology of the ENS was obtained using extracellular recording techniques. Although the exact waveforms of extracellularly recorded spikes seem to fall into distinct classes [Wood, 1989] the information obtained in this way is limited. On the other hand, the preparations do not have to be paralysed to the extent required for intracellular recordings and this has led to observations of firing patterns that have not been seen using intracellular techniques [Wood, 1970, 1989, Athey et al., 1981, Wood, 1975, Ohkawa and Prosser, 1972].

The first report in English of recordings of single unit activity from enteric neurons was by Wood [1970]. A section of cat jejunum was opened up and pinned out. In some cases, the longitudinal muscle was removed to expose the myenteric plexus and in others the electrode was driven through the serosa and longitudinal muscle. Several types of firing pattern were observed. Some units fired single spikes randomly and at low frequency. Mechano-sensitive units responded to mechanical inputs, such as local deformations caused by moving the recording electrode, with either bursts of activity that ceased before the stimulus ceased (phasic firing) or fired thoughout the stimulus (tonic firing). Finally, some units fired in erratic bursts. The erratic bursts appeared to be uncorrelated with mechanical activity or electrical activity in the smooth muscle. A later study further classified the erratic bursters as fast or slow depending the spike rate within a burst [Ohkawa and Prosser, 1972]. Burst firing

is seen occasionally in Dogiel type II neurons using intracellular recording [Kunze et al., 1997, 1999], when the myenteric plexus was being driven by sensory input. Kunze et al. [1997] impaled neurons that were close to a region of intact mucosa which was shown to be providing input to the myenteric plexus. Impaled neurons either received direct sensory input or as second order neurons. Kunze et al. [1999] impaled neurons that were receiving mechanical inputs from the muscle. In other words, the bursting seen in intracellular studies is because the neurons are being driven by exogeneous inputs. Strangely, this bursting behaviour has never been systematically followed up, however modelling studies reported in chapter 5 predict erratic bursting in networks of AH neurons.

Intracellular recordings from enteric neurons presented a technical challenge because of the continual movement of the muscle and susceptibility of electrodes and neurons to damage because of this. The first intracellular recordings of enteric neuron activity were made by Hirst et al. [1972] who overcame this difficulty by applying isoprenaline to the tissue bath. (Isoprenaline acts on β-adrenoceptors to stimulate the production of cAMP, which is part of the second messenger pathway needed for muscle relaxation. However, cAMP is now known to be part of the pathway mediating slow synaptic transmission in enteric neurons [Nemeth et al., 1986], so the use of isoprenaline may have effected the results.) The first full published account of intracellular recordings from myenteric neurons was that of Nishi and North [1973]. The preparation consisted of longitudinal muscle strips with myenteric plexus still attached. The tissue was not paralysed, but a single ganglion was prevented from moving by pins. These authors classified the neurons into two categories based on membrane properties and whether the neurons fired many action potentials (tonic

firing) or a single action potential (phasic firing) in response to a depolarising current. They observed a large (15mV), slow (5–20 s) after-hyperpolarising potential (AHP) and determined that it was probably a Ca^{++} dependent K^+ conductance increase. They also noted that some neurons received (fast) synaptic inputs in response to electrical stimuli applied to the preparation either circumferentially or longitudinally displaced from the recording site.

Hirst et al. [1974] did not see the same division in membrane properties or firing patterns. However, they observed that the long AHP potential and fast synaptic inputs were mutually exclusive and suggested the nomenclature AH and S neuron respectively. This is the predominant electrophysiological classification today. AH neurons have been identified to be morphologically of the class Dogiel II [Iyer et al., 1988] and functionally as intrinsic primary afferent neurons [Kunze et al., 1995].

Electrophysiology of intrinsic sensory neurons

AH neurons expresses a large variety of voltage and Ca^{++} dependent conductances. As with other neurons the upstroke of the action potential is carried largely by Na^+. However, the presence of TTX or absence of Na^+ in the extracellular medium does not abolish the action potential, but it does significantly increase the threshold for AP activation [Hirst and Spence, 1973, North, 1973, Hirst et al., 1974]. The Na^+ current has been studied in cultured rat myenteric neurons [Franklin and Willard, 1993]. Even though the authors state that enteric neurons remain differentiated in culture, data were not reported separately for AH and S neurons. The Na^+ current rapidly activates and inactivates. Onset is around -60mV and peak current is achieved around -15 mV. Its activation was negligible at -100 mV and the current

fully inactivated at -20 mV. Activation and inactivation time constants were similar and varied from about 2 ms at -40 mV to about 0.8 mV at 40 mV. Whole cell conductances increased dramatically, the longer the neuron was in culture so it is not clear what the whole conductance would be *in vivo*. All Na^{+} currents were blocked by TTX.

Several Ca^{++} currents are observed in AH neurons. Rapidly activating conductances are part of the action potential. The Ca^{++} component makes the action potential in AH neurons unusually wide, with a half width of 2.5 ms, and gives it a characteristic hump on the falling phase [Iyer et al., 1988, Kunze et al., 1994]. The hump is significantly, but not completely, blocked by ω-conotoxin-GVIA [Furness et al., 1998, Vogalis et al., 2001], indicating that N-type calcium channels are involved. When this is further dissected into high or low voltage activated currents it appears that the high voltage activated currents are completely blocked by ω-conotoxin-MVIIC, but low voltage activated currents are not [Starodub and Wood, 1999]. The ω-conotoxin-MVIIC block was more complete than that of ω-conotoxin-GVIA, indicating that P or Q type channels might also be present. The cultured neurons also expressed two fast Ca^{++} channels, one of which was blocked by ω-conotoxin-GVIA and one of which was blocked by dihydropyridine nitrendipine, an L-type channel blocker [Franklin and Willard, 1993]. Furthermore, these two currents had slightly different kinetics. Both cultured neurons and those freshly dissociated from adult rats showed channels with both kinetics. L-type channels have also been shown to exist in more intact preparations of the guinea-pig ileum [Reis et al., 2000], however, this study was concerned with transmitter release so these channels may exist on the processes rather than on the cell body. Neverthe-

less, two kinetic studies agree qualitatively about the properties of the fast Ca^{++} channels [Franklin and Willard, 1993, Hirst et al., 1985a]. The Ca^{++} current starts to activate at around -20 mV and reaches its peak in about 10–20 ms. Inactivation starts at about -120 mV and reaches 100% at 0 mV. Replacing Ca^{++} with Ba^{++} as the charge carrier reveals that inactivation is made up of two components with decay time constants of 2.5 s and 70 ms at -20 mV and 20 ms and 1 s at 30 mV, respectively. The rate of inactivation of the slow component decreased with decreasing Ca^{++} concentration or with replacement of Ca^{++} by Ba^{++}. This indicates that Ca^{++} entering the cell is directly or indirectly causing the slow inactivation. These data imply that the Ca^{++} conductance is partially inactivated at rest.

Calcium entering the cell during the action potential also binds to a K^+ channel which mediates the famous long AHP seen in these neurons. The AHP starts about 70 ms after the action potential, lasts 2–30 s and hyperpolarises the cell by 6–20 mV [Hirst et al., 1974, 1985b]. This causes a profound decrease in cell excitability both by the action of hyperpolarisation and because of the large shunt introduced by the open conductance. Removal of extracellular Ca^{++} reduces or abolishes the AHP [Morita et al., 1982a, North, 1973, Hillsley et al., 2000]. Simultaneous measurements of the intracellular Ca^{++} concentration, using the fluorescent intracellular dye bis-fura-2, and membrane potential indicate that the Ca^{++} concentration is elevated during the AHP and this elevation closely follows the membrane potential time course [Tatsumi et al., 1988] or perhaps lags slightly behind [Hillsley et al., 2000]. The amplitude of the response is reduced by about 60% in the presence of ryanodine [Hillsley et al., 2000, Vogalis et al., 2001]. (Ryanodine prevents release of Ca^{++} from intracellular stores, preventing its release into the cytosol). This indicates that Ca^{++}

induced Ca^{++} release is largely responsible for the elevated Ca^{++} during the AHP. The fact that the response is not completely blocked by ryanodine indicates that the origin of the elevated Ca^{++} is not critical, in contrast to some other neurons [Davies et al., 1996]. Reports differ as to the degree of linearity in the summation of the AHP with multiple action potentials. According to Hillsley et al. [2000], the resting intracellular Ca^{++} concentration was around 203 nM and each action potential increased the peak linearly by about 47 nM, up to the maximum of 15 action potentials tested. The duration of the Ca^{++} transient was also linear in the number of action potentials. The change in peak membrane potential and AHP duration were linear in the peak and duration of the Ca^{++} transient and hence in the number of action potentials. On the other hand, Morita et al. [1982a] found that the peak hyperpolarisation and conductance summed linearly for only a small numbers of action potentials and summed less than linearly for larger numbers of action potentials. This seems to be at least partly due to the fact that the AHPs in Morita et al. [1982a] are larger than those in Hillsley et al. [2000] which might have been due to the use of nicardipine in the latter study. When the intracellular Ca^{++} was reduced, it was anecdotally observed that the AH neurons were electrophysiologically similar to S neurons [Wood et al., 1979, Hillsley et al., 2000].

The channel underlying the AHP conductance might be a small conductance channel. Analysis of noise in current traces can be used to make an estimate of the numbers of channels involved, their individual conductances and open times. This leads to an estimates of a conductance around 10 pS [Vogalis et al., 2001]. No estimate of the statistical power of the calculation was given. This is in contradiction to pharmacological evidence that the AHP is blocked by charybdotoxin and iberiotoxin,

and not by apamin [Kunze et al., 1994]. Charybdotoxin blocks large conductance channels and some intermediate conductance channels, iberiotoxin blocks large conductance channels [Castle et al., 1989, Marty, 1989, Haylett and Jenkisnon, 1990]. Apamin selectively blocks small conductance channels [Brewster and Strong, 1992]. The conductance carrying the AHP is also not voltage dependent [Hirst et al., 1985b, Morita et al., 1982a], unlike most large conductance channels [Sah and Davies, 2000].

AH neurons seem to have 3 rapid onset outward currents that contribute to the repolarisation of the action potential and the early AHP following the action potential.

- an A-type current (I_A) that is blocked by 4-aminopyridine (4-AP) and Ba^{++}, but not tetraethylammonium (TEA) [Hirst et al., 1985b, Zholos et al., 1999, Starodub and Wood, 2000]

- a TEA and 4-AP sensitive delayed rectifier like current [Hirst et al., 1985b, Zholos et al., 1999]

- a TEA insensitive hyperpolarisation activated inward rectifier [Hirst et al., 1985b, Zholos et al., 1999]

I_A has been fully characterized by Starodub and Wood [2000] in neurons cultured from adult guinea-pig small intestine, using perforated patch clamp. Neurons were classified according to their immunoreactivity to calbindin. Biophysical properties were uniform across both groups, except for maximum current densities which were about 23 pA/pF uniformly within the calbindin negative group and either low (around 9 pA/pF) or high (around 25 pA/pF) within the calbindin positive group. The activation and inactivation curves were well described by Boltzmann curves

$(1/(1 + \exp((V - V_{1/2})/k)))$, where $V_{1/2}$ is the voltage of (in)activation and k is the reciprocal of the slope at that point. The values of these parameters for the activation curve are $V_{1/2} = -7$mV and $k = 15$mV and for the inactivation curve these are $V_{1/2} = -87$mV and $k = -11.5$mV. The time courses of activation and inactivation were well described by exponentials, the time constants of which had voltage dependences of $\exp(0.77 - V/36.8)$ and $\exp(3.38 - V/45.2)$ (using units of mV and ms). The current showed a voltage dependent block by 4-AP.

The inward rectifier and delayed rectifier were also studied in cultured guinea-pig small intestine AH neurons [Zholos et al., 1999]. The inwardly rectifying current activated around -70 mV and had a time constant of activation that varied from about 180 ms at -130 mV to about 800 ms at -80 mV. The delayed rectifier current starts to activate around -20 mV and shows no appreciable inactivation during 2.5 ms current pulses. The time constant of activation was well described by $76.5 \exp((V + 10)/17)$ and the degree of activation was described by a Boltzmann curve with half activation potential of 7.1 mV and slope factor of 11.3 mV.

Three other currents have been identified that are less well characterised. The first is a rapid Ca^{++} induced inward current blocked by niflumic acid identified in guinea-pig duodenum [Vogalis et al., 2001]. It is voltage independent and has a reversal around -35 mV. These two properties indicate that it is probably a Cl^- current. There is a rapid outward current invoked after the action potential that is reduced by low concentrations of TEA, also in guinea-pig duodenum [Vogalis et al., 2000]. This indicates that it is probably a large conductance Ca^{++} dependent K^+ channel. Single channel patch clamp studies have identified a large conductance, voltage and Ca^{++} dependent channel that activates quickly (10s of milliseconds)

and does not inactivate (W. A. Kunze and E. A. Thomas, unpublished data). Interestingly, this channel also responds to mechanical deformation [Kunze et al., 2000]. Finally, there is a hyperpolarisation activated non-specific cation current [Galligan et al., 1990] (I_h). This starts to activate around -50 mV and has a time constant on the order of 80 ms. The current reverses around -43 mV and is carried by, at least, K^+ and Na^+. It is active during the AHP.

Resting membrane potential of AH neurons is around -60 mV, low compared to other enteric neurons [Hirst et al., 1985a, Kunze et al., 1994, Vogalis et al., 2001]. The resting conductance seems to be made up in part of $g_{K_{Ca}}$ since agents that block the AHP directly also increase membrane resistance and increase (i.e. depolarise) resting potential [Kunze et al., 1994].

Firing properties of S neurons

AH neurons, in most preparations, are highly phasic due to the AHP, low resting membrane potential and low input resistance. They will typically fire only a small number of action potentials in response to a moderate depolarising current injection, before the onset of the AHP inhibits further firing [Nishi and North, 1973]. S neurons on the other can fire phasically or tonically [Bornstein et al., 1994]. In a recent study, it was found that about 50% of S neurons within 600 μm of intact mucosa fired tonically [Kunze et al., 1997]. On the other hand, the vast majority of neurons 600 μm or more away from the mucosa fired phasically. If the mucosa was dissected away and replaced then, again, the vast majority of neurons fired phasically. Phasic neurons possessed a rapidly activating, non-inactivating outward current which seemed to be responsible for quenching firing. When TTX was added

to the bath, tonic neurons, in which the current was absent, developed the current. AH neurons within 600 μm of intact mucosa were observed to be spontaneously active so the conclusion drawn was that sensory input from the mucosa drove slow excitatory synaptic potentials in S neurons, which in turn inhibited the current that caused them to fire phasically.

The idea that the location of cells within a myenteric ganglion is not random has received anecdotal support in the past [Meedeniya et al., 1998]. For example, it has been suggested that mechano-sensitive neurons are located on the outside of ganglia in order to make better contact with connective tissue [Wood, 1970]. Calretinin immunoreactive neurons are preferentially located on the edges of the ganglia and in the *micro-ganglia* at the intersections of internodal strands [Brookes et al., 1991a]. More recently, S neurons near the edge of ganglia, and in micro-ganglia located at the intersection of internodal strands, were systematically impaled [Smith et al., 1999]. It was found that 80% of this subpopulation fired tonically. As a control, neurons in the centre of the ganglia were also impaled and these were predominantly phasic. Interestingly, the neurons on the outside of the ganglia represented only some of the functional classes of S neurons, specifically longitudinal muscle motor neurons, circular muscle motor neurons and ascending interneurons. Electrophysiologically, the tonic neurons were further classifiable on the presence of an after-depolarising or after-hyperpolarising potential. The AHPs in tonic S neurons were studied separately at around the same time (by the same authors) [Shuttleworth and Smith, 1999]. The technique used was simultaneous measurement of intracellular Ca^{++} concentration using fluorescent dye and microelectrode voltage recording. Bursts of action potentials (mean number 7.3), induced by current injection, elicited an

AHP lasting from 0.8–7.7 s with an amplitude of 6.2 mV. This was accompanied by a transient rise in intracellular Ca^{++} that followed the action potential. As with the long AHP in AH neurons, the transient was slightly briefer than the AHP. Occasionally transients were discernible following single action potentials. The Ca^{++} transients were significantly, but not completely, blocked by ω-conotoxin-GVIA. In some neurons, the AHP was blocked by apamin [Smith et al., 1999], suggesting small conductance K^+ channels are involved. The putative role of this AHP is to regulate excitability, however it was so small that neurons were able to fire at high frequency throughout current injections as long as 500 ms. The afterdepolarisation occurred in the minority of tonic S neurons and lasted around 170 ms [Smith et al., 1999]. The reversal potential was between -35 and -45 mV, suggesting a Cl^-conductance. In some neurons an initial after-depolarisation gave way to an AHP.

The upstroke of the action potential in S neurons is carried by TTX sensitive Na^+ channels [Hirst et al., 1974]. Nothing appears to be known about the fast repolarising currents involved in the action potential. An A-type K^+ current is definitely present in cultured S neurons [Starodub and Wood, 2000]. Phasic S neurons, or S neurons that are phasic due to lack of synaptic input, also express a rapid delayed rectifier, which is presumed to be the cause of the phasic firing [Kunze et al., 1997]. This has an onset of around 7ms and is blocked by TEA. The same study also reports a slower outward current with an onset of tens of milliseconds.

Some work has been done on the electrophysiological properties of specific classes of S neurons. In organ culture, SOM positive neurons supposedly have lower resting membrane potentials (-52 mV), but is not clear what these data have been compared to [Song et al., 1997]. They fired phasically, except for very large current injections.

They displayed a small AHP, an A-type current and an I_h. An earlier study did not find an I_h in S neurons [Galligan et al., 1990]. Ascending interneurons, also in organ culture, have a similar resting membrane potential to SOM neurons, displayed an A-type current and no small AHP or I_h [Brookes et al., 1997].

1.6 Synaptic transmission

One of the major goals of neuroscience is to identify all the transmitters and receptors in the nervous system. From this point of view, study of the enteric nervous system is particularly exciting because of the large number of identified transmitters and the fact that many neurons contain more than one [Furness et al., 1995b]. Since the topic of this thesis is dynamical models for networks, this section will concentrate on the dynamics of synaptic transmission rather than the pharamcology. Of course, given the complex nature of synaptic transmission in the enteric nervous system, pharmacological techniques are essential in unravelling the synaptic dynamics. There have been very few studies specifically addressing this issue, so this section will focus on studies that bear indirectly on this.

Fast excitatory transmission

Fast synaptic transmission occurs when the release of transmitter from a presynaptic terminal leads to a change in the postsynaptic membrane potentials lasting a few tens of milliseconds. Fast EPSPs have been observed in the ENS from the earliest intracellular recordings [Hirst et al., 1974, Nishi and North, 1973]. They are seen in response to electrical stimulation [Hirst et al., 1974, Nishi and North, 1973], mucosal

compression [Bornstein et al., 1991a], distension [Hirst et al., 1975, Smith et al., 1992] and in response to application of chemical stimuli [Kunze et al., 1995, Bertrand et al., 1997a]. They vary in amplitude from 1 mV [Bornstein et al., 1991a] to 25 mV [Nishi and North, 1973] and reverse at around 0 mV [Galligan et al., 2000]. Event durations were 30-50 ms. Synaptic potentials are blocked in low Ca^{++} solutions [Nishi and North, 1973]. In response to repetitive stimulation, fast EPSPs display significant "run down" for frequencies greater than about 0.1 Hz [Nishi and North, 1973]. For example, the amplitude of the 11^{th} response to a 40 Hz stimulus was only 30% of the first. This appears to be due to inhibition at muscarinic receptors on the presynaptic membrane [Morita et al., 1982b].

In the ascending pathway, fast EPSPs are solely mediated by acetylcholine acting at nicotinic receptors [Lepard and Galligan, 1999, Johnson et al., 1999]. The conductance appears to be a non-specific cation conductance [Trouslard et al., 1993, Galligan and Bertrand, 1994]. Fast EPSPs in some neurons of the descending pathway are partially blocked by suramin and PPADS [Galligan and Bertrand, 1994, Johnson et al., 1999, Lepard and Galligan, 1999]. The receptor appears to be $P2X_2$ [Zhou and Galligan, 1996]. These channels are also nonspecific cation channels [Fieber and Adams, 1991, Barajas-Lopez et al., 1994, Surprenant et al., 1995, Evans et al., 1996]. Some 11% of myenteric neurons have fast EPSPs that are partially mediated by serotonin acting at 5-HT_3 receptors [Galligan et al., 2000]. Serotonin receptor channels reverse around 0 mV and also appear to be nonspecific cation ion channels [Derkach et al., 1989].

Fast EPSPs are mediated by directly gating the ion channels that generate the membrane potential change. This accounts for their short latency and suggests a

simple model in which multiple events sum linearly at the membrane conductance level, until the amount of the post synaptic receptor starts to saturate.

Slow excitatory transmission

In the ENS, slow EPSPs are qualitatively different from fast EPSPs in that they last from seconds [Morita and North, 1985] to hours Clerc et al. [1999]. They appear to be important in both ascending and descending pathways [Johnson et al., 1998].

Experimentally, slow EPSPs are evoked by 1 to 40 Hz trains of electrical pulses delivered to internodal strands. For increasing numbers of presynaptic stimuli at a fixed frequency or for a fixed number of stimuli at increasing frequencies, the amplitude of the slow EPSP will initially increase, but eventually reach a plateau, typically resulting in a 10–20 mV depolarisation [Morita and North, 1985]. Under these same conditions, the duration of the slow EPSP will continue to increase [Clerc et al., 1999]. Slow EPSPs can also be illicited by chemical stimuli applied to the mucosa [Bertrand et al., 1997b, 2000a]. In this case, AH neurons are also being excited by other AH neurons in the vicinity. The slow EPSP always significantly outlasts the stimulus period.

The depolarisation associated with the slow EPSPs in sensory neurons is primarily due to closure of resting potassium conductances (g_K and $g_{K,Ca^{++}}$) [Akasu and Tokimasa, 1989, Bertrand and Galligan, 1994] and with opening of a Cl^- conductance [Bertrand and Galligan, 1994]. There is strong evidence that slow EPSPs are mediated by the mobilization of intracellular second messengers, which ultimately cause the observed changes in membrane conductances. Application of tachykinins, such as substance P, mimics the slow EPSP [Katayama and North, 1978, Morita and

Katayama, 1992, Galligan et al., 1987] and has been shown to cause accumulation of cyclic 3', 5' adenosine monophosphate (cAMP) [Baidan et al., 1992]. Activators of adenylate cyclase, such as forskolin, also cause slow EPSP-like membrane depolarisations [Nemeth et al., 1986, Bertrand and Galligan, 1995]. The receptors mediating the slow EPSP and the tachykinin responses are coupled through a pertussis toxin-insensitive G-protein [Bertrand and Galligan, 1995]. The end point appears to be inhibition of g_K via a phosphorylation event [Bertrand and Galligan, 1995, Pan et al., 1997].

Alternative pathways and interactions between G-proteins and second messengers are also supported by the data. For example, slow EPSPs are mediated through NK1 and NK3 receptors [Bertrand and Galligan, 1995, Johnson et al., 1998]. The NK3 pathway is mediated by pertussis toxin insensitive G-proteins [Bertrand and Galligan, 1995] which cause formation of IP3 and diacylglycerol which activate protein kinase C which in turn phosphorylates K^+ channels [Guard et al., 1988].

Slow inhibitory transmission

Inhibitory postsynaptic potentials (IPSPs) are observed in the submucous plexus [Surprenant and North, 1988, Mihara et al., 1991] and in myenteric sensory neurons [Johnson et al., 1980, Christofi and Wood, 1993] (P. J. Johnson & J. C. Bornstein, unpublished). IPSPs in the myenteric plexus typically require repetitive nerve stimulation to be evoked [Christofi and Wood, 1993, Johnson et al., 1980] and have long durations (2–17 s (Johnson & Bornstein, unpublished)), like the G-protein coupled, second messenger mediated slow EPSPs in the submucous and myenteric plexus and the slow IPSPs in the submucous plexus. In standard preparations they are

less common than slow EPSPs, however they may be masked by slow EPSPs or membrane noise. The source of the myenteric IPSPs is unknown. However, most enteric neurons are accounted for and there is no known class of neuron that makes connections with sensory neurons [Costa et al., 1996] other than other sensory neurons [Pompolo and Furness, 1988]. Thus, it seems likely that inhibitory transmission occurs as some form of cotransmission with excitatory transmission from the sensory neurons. (See also chapter 5.)

Synaptic plasticity

Receptors mediating fast transmission desensitise [Galligan et al., 2000]. Nicotinic acetylcholine receptors in the ENS desensitises in less than 0.3 s to high concentrations of acetylcholine [Galligan et al., 2000], the P2X receptor desensitises in 7 s [Zhou and Galligan, 1996] and the 5-HT receptor desensitises in 2 s [Zhou and Galligan, 1999]. NK1 receptors internalise after 20 mins exposure to substance P at concentrations higher than 10^{-11} M [Southwell et al., 1998]. There is evidence that endocytosis occurs under physiological conditions in rat myenteric neurons [Mann et al., 1999], but it is not known how quickly it occurs or recovers. Presynaptic inhibition mediated by muscarinic receptors occurs at terminals releasing acetylcholine [Morita et al., 1982b, North et al., 1985], and this mechanism may also inhibit slow EPSP. Again, no quantitative data have been reported.

Metabotropic transmission

Metabotropic receptors for various neurotransmitters are also widely distributed throughout the central nervous system (CNS), but what roles they perform and

how they do this is only just starting to be explored [Batchelor and Garthwaite, 1997]. G-protein coupled, second messenger mediated postsynaptic potentials share several characteristics including slow onset (hundreds of milliseconds to seconds), long duration and a non-linear relationship between number of presynaptic nerve impulses and the size of the response. In the central nervous system, the best studied of these slow synaptic potentials are the slow IPSPs mediated by $GABA_B$ receptors [Mott and Lewis, 1994]. 5-HT_1 and 5-HT_2 receptors are located in many brain regions [Barnes and Sharp, 1999], have been implicated in mood disorders [Sargent et al., 2000] and act through protein signalling pathways [Berg et al., 1998, Tournois et al., 1998, Barnes and Sharp, 1999]. When acting on postsynaptic 5-HT_2A receptors they cause neurons to depolarise [Barnes and Sharp, 1999]. Metabotropic glutamate receptors in the CNS mediate EPSPs [Batchelor et al., 1994, Batchelor and Garthwaite, 1997, Shen and Johnson, 1997, Miniaci et al., 2001] and IPSPs [Fiorillo and Williams, 1998], although their function is only just starting to be explored [Batchelor and Garthwaite, 1997]. Tachykinins and their receptors are also located in the CNS [Bolam and Smith, 1990, Saria, 1999] and also seem to have a role in mood disorder [Saria, 1999]. Virtually no studies have been done to understand how excitatory metabotropic transmission effects the networks in which it is expressed.

Neuromuscular transmission

Ultrastructural studies show that the circular and longitudinal muscle are richly innervated [Gabella, 1972, Klemm, 1995]. In the circular muscle, nerve fibres are distributed in an approximately 2:1 ratio between the deep muscular plexus (see figure 1.1) and the rest of the tissue. In both layers, fibres have frequent varicosities

that make close appositions to muscle cells. These are presumed to be the sites of neuromuscular transmission [Gabella, 1972, Klemm, 1995].

Acetylcholine acting through muscarinic receptors is a major excitatory pathway in the circular muscle [Kosterlitz and Lees, 1964, Hirst et al., 1975]. Muscle strips devoid of the myenteric and submucous plexus contract in the presence of ACh [Kosterlitz and Lees, 1964]. EJPs in the descending pathway are blocked by atropine [Hirst et al., 1975]. In the presence of hyoscine, EJPs can still be evoked in the ascending pathway by physiological [Smith et al., 1990, Smith and Furness, 1988] or electrical stimuli [Bywater et al., 1981]. The transmitter of the hyoscine resistant component of excitation appears to be substance P [Taylor and Bywater, 1986, Costa et al., 1985, Barthó and Holzer, 1985] or a similar peptide [Furness et al., 1995b]. Substance P contracts circular muscle strips in the presence of TTX [Costa et al., 1985] and the substance P antagonist, [D-Arg1,D-Pro2,D-Trp7-9,Leu11]-substance P, reduced the size of the atropine resistant EJP [Taylor and Bywater, 1986]. These facts are consistent with the presence of NK1 receptors on the circular muscle [Southwell and Furness, 2001] and immunoreactivity of excitatory circular muscle motor neurons for substance P [Costa et al., 1996].

Inhibition of the muscle is more complicated. There is a fast and slow component of the IJP that are separated by their sensitivity to the small K^+ channel blocker apamin [He and Goyal, 1993, Costa et al., 1986]. Apamin appears to block the component of the IJP mediated by ATP. Pharmacology indicates that nitric oxide (NO) is also an inhibitory transmitter [Shuttleworth and Sanders, 1996, Shuttleworth et al., 1991, He and Goyal, 1993]. This is also supported by the immunohistochemistry, because a population of motor neurons are immunoreactive to NOS [Costa

et al., 1996]. Specialised cells, known as Interstitial cells of Cajal, seem to act as intermediaries in neuromuscular transmission, by reacting to NO or and releasing NO in turn [Publicover et al., 1993, Shuttleworth and Sanders, 1996]. Other likely inhibitory neurotransmitters are vasoactive intestinal peptide [Crist et al., 1992, He and Goyal, 1993] and pituitary adenylyl cyclase activating peptide [McConalogue et al., 1995].

1.7 Dynamical systems and neural networks

Neural network theory can be explored at a number of levels. A recent issue of Nature Neuroscience (November 2000, supplement to volume 3) used the term "computational approach". This is perhaps deliberately vague; does it just mean "using a computer" or does it mean explaining how a biological system works in terms of a theory of computation? The former meaning implies a tool or technique. Of course, the computer is an indispensable tool for handling large amounts of data and performing the almost infinite number of calculations required for model simulation. However, it is the knowledge and assumptions that have gone into constructing the computer programs that are the "science". The idea of neural networks as computers seems to have come from the original work in neural network theory [Rummelhart and McClelland, 1986] which, in turn, sprang from artificial intelligence research. Computational theories of cognitive functions have been very successful, for example in understanding movement [Wolpert and Ghahramani, 2000] or language processing [Pinker, 1995]. For lower level systems, or for explanations at the biophysical level, the term "computational" seems to be inappropriate. Instead, I prefer to emphasise

neurons and neural networks as objects governed by dynamical laws dictated by the laws of physics.

A note on the generation of figures Figures in this section were adapted from other authors as noted. The original equations were used but, in some cases, parameters had to guessed. Data were regenerated directly in Matlab (The Mathworks, Natick, MA, USA) or using the "dfield" ODE toolbox for Matlab (http://math.rice.edu/∼dfield/) and plotted in Origin (OriginLab Corporation, Northampton, MA, USA).

Overview of dynamical systems

This section provides a brief overview of dynamical systems concepts and terminology. For more detail consult any text book on dynamical systems, for example Wiggins [1990] or Khalil [1996].

A dynamical system consists of a vector of variables, x, known as *state variables*, which locate a point in an abstract space, known as *state space* or *phase space*. If the state vector is known at a particular time, t_0, then a rule (or equation) enables its position to be determined at all times afterwards (and before). For example, consider an object in orbit around the sun. Unpowered objects (such as planets) move in a plane, that is two dimensional space, and in this case there are four state variables, two describing the position in two dimensional space and two describing the object's velocity. (Phase space is not the physical space in which the object moves.) The representation of the state vector is not unique. In the planet example Cartesian coordinates, (x, y), or polar coordinates, (r, θ), can be used. Even the dimension of the state space need not be unique, for example, the z coordinate

could be included, although trivially $z(t) = 0$. (The requirement that the laws of physics be independent of the coordinate system used to describe them places strong constraints on the forms those laws can take [Einstein, 1996] [1].)

A dynamical system will often have one or more inputs, $u(t)$, and one or more parameters, α (u or α may be vectors representing several quantities). Returning to the celestial dynamics example, if the object has a rocket engine then the force applied by the rocket will be a time dependent input, $u(t)$. In addition the rocket's mass will vary with time as fuel burns and so the mass will also become a state variable. Finally, the modeler may include several parameters controlling the rocket's performance in the model.

A system may be linear in either the input or the state variables. If the system is linear in the input then if $x_1(t)$ is the solution for input $u_1(t)$ and similarly $x_2(t)$ is the solution for input $u_2(t)$ then the solution for input $a_1u_1(t) + a_2u_2(t)$ is $a_1x_1(t) + a_2x_2(t)$ for any constants a_1 and a_2. Analogue filters are frequently used in electrophysiology to remove high frequency components from a signal before it is digitized. Ideally, the filter should be linear in the input, if the input voltage doubles the output voltage should double. The filter is an example of a dynamical system. The input is the signal to be filtered and the output is the voltage across a component of the circuit. The other state variables include voltages across other components, the charge in capacitors, etc. A system is linear in the state variables if, for solutions $x_{\{1,2\}}(t)$ for initial conditions $x_{\{1,2\}}(0)$, $a_1x_1(t) + a_2x_2(t)$ is the solution for initial conditions $a_1x_1(0) + a_2x_2(0)$.

A common subset of dynamical systems are described by ordinary differential

[1] Gratuitous Einstein reference

equations (ODE)

$$\dot{x} = f(x, u(t); \alpha)$$

where $\dot{x}$ is the derivative with respect to time of the state variables. If f does not depend on u then the system is *autonomous*. The discussion in this section uses ODEs as examples, but the concepts apply more generally.

Very often the modeller is interested in the behaviour of the system as $t \to \infty$, that is the long term behaviour of the system. Will the system approach a stationary solution, will it oscillate, will it be chaotic? An *equilibrium* solution is one in which the system does not change, that is $\dot{x} = 0$ and these are found by solving $f(x; \alpha) = 0$ (for simplicity only autonomous systems are considered here). An equilibrium can be *stable* or *unstable*. If the equilibrium is stable then, when the solution is perturbed, $x \to x + \delta x$, by *any* small amount it returns to the equilibrium point. If the solution moves away from the equilibrium point for some perturbation then it is unstable. (More detail on the classification of equilibria is provided below.) For example, a rigid pendulum with friction has a stable and an unstable equilibrium. The unstable equilibrium is the point in which the pendulum points straight up. Any perturbation to the system causes the pendulum to fall to one side. On the other hand the equilibrium with the pendulum pointing straight down is stable. After a perturbation friction will eventually cause the pendulum to return to rest. Unstable equilibria are not achievable for real systems because there will always be perturbations.

The system may have *periodic orbits*. In this case $x(t) = x(t + T)$ for all t and some $T > 0$. Periodic orbits may be stable or unstable in a manner analogous to equilibria. Stability applies not only to perturbations in the solution, but also in

the parameters. Returning to the pendulum example, but without friction there are an infinite number of periodic solutions — the pendulum will keep returning to whichever point it is released at. In reality, the friction is never zero and so none of the periodic solutions are stable. It is a characteristic of linear systems that they do not have stable periodic solutions. If the system is two dimensional then the only solutions possible are stable equilibria, solutions that go to infinity and periodic solutions. In more than two dimensions, a solution may wander in a complex manner through phase space. These solutions may be chaotic, which means (amongst other things) they are extremely sensitive to the initial conditions, small changes in the initial conditions lead to large changes at later times.

The behaviour of solutions may vary qualitatively depending on where in phase space the system starts. Consider again an unpowered object moving in the vicinity of the earth. If the energy is not too low and not too high, the object will be trapped in a periodic, elliptic orbit around the earth. These solutions are not stable (in the sense defined above), but they have the property that any small perturbation results in another, similar periodic solution. If the energy is high the object will fly off in a hyperbolic trajectory. If the energy is too low, or the orbit too eccentric, the orbit will take the object into the atmosphere where friction will remove energy from the object eventually causing it to spiral into the atmosphere. In this example there are three qualitatively different regions of phase space, the region of stable orbits, the region of unbounded hyperbolic trajectories and the region of orbits that spiral into the earth. A solution starting in one region will stay in that region, for ever. For example, an object in a elliptic orbit will never move to a hyperbolic escape trajectory.

An n dimensional linear system has the form

$$\dot{x} = A\,x$$

where A is an $n \times n$ constant matrix and $x \in \mathbb{R}^n$. The equilibrium is at $x = 0$ (more generally there might be a subspace which satisfies $Ax = 0$, but that can be ignored for this discussion). The properties of the equilibrium are entirely determined by the eigenvalues of A. If all the real parts of the eigenvalues are negative then the equilibrium is stable. If any eigenvalues have positive real parts then the equilibrium is unstable. If there are purely imaginary eigenvalues then cyclic solutions exist. More generally, a nonlinear system may have several equilibria. If we consider an autonomous system ($u = 0$) with an equilibrium at $x = 0$, then in many cases the stability properties of the nonlinear system can be deduced by linearizing the system at the equilibrium

$$\dot{x} = J|_0\ x$$

where $J_{ij} = \partial f_i/\partial x_j$ is the Jacobian, a matrix of the derivative of each component of f with respect to each component of x and then evaluated at the equilibrium point. If the eigenvalues of J all have nonzero real parts, then stability of the nonlinear system is that of the linear system. If any of the eigenvalues of the linearized system are pure imaginary then the linearized system does not predict the behaviour of the nonlinear system.

Typically, the eigenvalues depend on the parameters of the system. It can happen that as a parameter changes a pair of complex eigenvalues changes from having a negative real parts to having positive real parts, thus passing though a point in which the reals parts are zero and the eigenvalues are purely imaginary. Thus, by changing

the parameter a stable equilibrium can become unstable. When stability is lost in this way a periodic orbit is created (which may or may not be stable) with a nonzero frequency. Thus, not only does the stability of the equilibrium change qualitatively but new dynamics are created. This qualitative change in dynamics as a parameter is varied is known as a *bifurcation*. The complete classification of bifurcations is a large and active area of research. The type of bifurcation just described is a *Hopf bifurcation*, that is an equilibrium switches stability and a periodic orbit emerges. The most famous Hopf bifurcation in neuroscience is the action potential threshold in the squid giant axon [Hodgkin and Huxley, 1952]. In this case, the bifurcation parameter is the amount of injected current. As the amount of current increases from zero the membrane has a single stable equilibrium. However, when the amount of current exceeds a threshold the stability of the equilibrium is suddenly lost and a periodic solution is born — repetitive action potential firing.

Theory of spiking

Rinzel and Ermentrout [1998] are the authors of an influential paper describing easily applied, yet powerful, techniques for qualitative analysis of low dimensional dynamical systems, either neurons or networks. As an example they use a simplified version of the equations of Morris and Lecar [1981], which are a simplified model of membrane potential oscillations in barnacle muscle. The model is

$$C\frac{dV}{dt} = -I_{ion}(V,w) + I(t) \tag{1.1}$$

$$\frac{dw}{dt} = \frac{w_\infty(V) - w}{\tau(V)} \tag{1.2}$$

$$I_{ion} = \bar{g}_{\mathrm{Ca}}\, m_\infty(V)\,(V - V_{\mathrm{Ca}}) + \bar{g}_{\mathrm{K}}\, w\,(V - V_{\mathrm{K}}) + \bar{g}_{\mathrm{leak}}\,(V - V_{\mathrm{leak}}) \tag{1.3}$$

where $\bar{g}_{\mathrm{Ca}}$, $\bar{g}_{\mathrm{K}}$ and $\bar{g}_{\mathrm{leak}}$ are the maximum conductances for Ca^{++}, K^{+} and leak respectively. There are two voltage dependent gating variables w and m. The kinetics of m are described by an equation similar to that of w, but they are very rapid so it can be assumed that m is always in equilibrium and the approximation $m = m_\infty(V)$ can be made. The voltage dependence of w comes through the voltage dependent quantities $\tau(V)$ and $w_\infty(V)$. These quantities can be understood through an imaginary voltage clamp experiment. If the voltage is stepped to V then $w \to w_\infty(V)$ exponentially with a time constant $\tau(V)$. This is a two dimensional problem because there are two state variables, V and w.

The state with $V = V_r = -60$ mV and $w = w_r$ nearly zero is the only equilibrium in this system in the absence of applied current ($I = 0$). If the initial voltage starts with some value $V_0 > V_r$ then $V(t)$ may spike, followed by an undershoot and then return to rest. In the phase plane (V–w plane) the trajectory will start out with $w = w_r$ at its rest value and the trajectory will move toward the global stable point. The *nullclines* are two curves in phase space which are the solutions of either $dw/dt = 0$ or $dV/dt = 0$, referred to as the w or V nullclines, respectively. When a trajectory crosses, say the V nullcline, because $dV/dt = 0$ it does so parallel to the w axis. These observations are illustrated in figure (1.2), adapted from Rinzel and Ermentrout [1998], which shows nullclines and two sample trajectories. The trajectories are plots of solutions that move in the V-w plane, that is $(V(t), w(t))$, with the direction of motion indicated by an arrow. The trajectories show imaginary voltage clamp like-experiments where the system is stepped from the stable point (at the intersection of the nullclines) to point near $V = -5$ or $V = -10$. For the lower starting voltage the returns rapidly back to the equilibrium, but for the higher

starting voltage the voltage initially increase before returning to the stable point. The latter behaviour is an action potential.

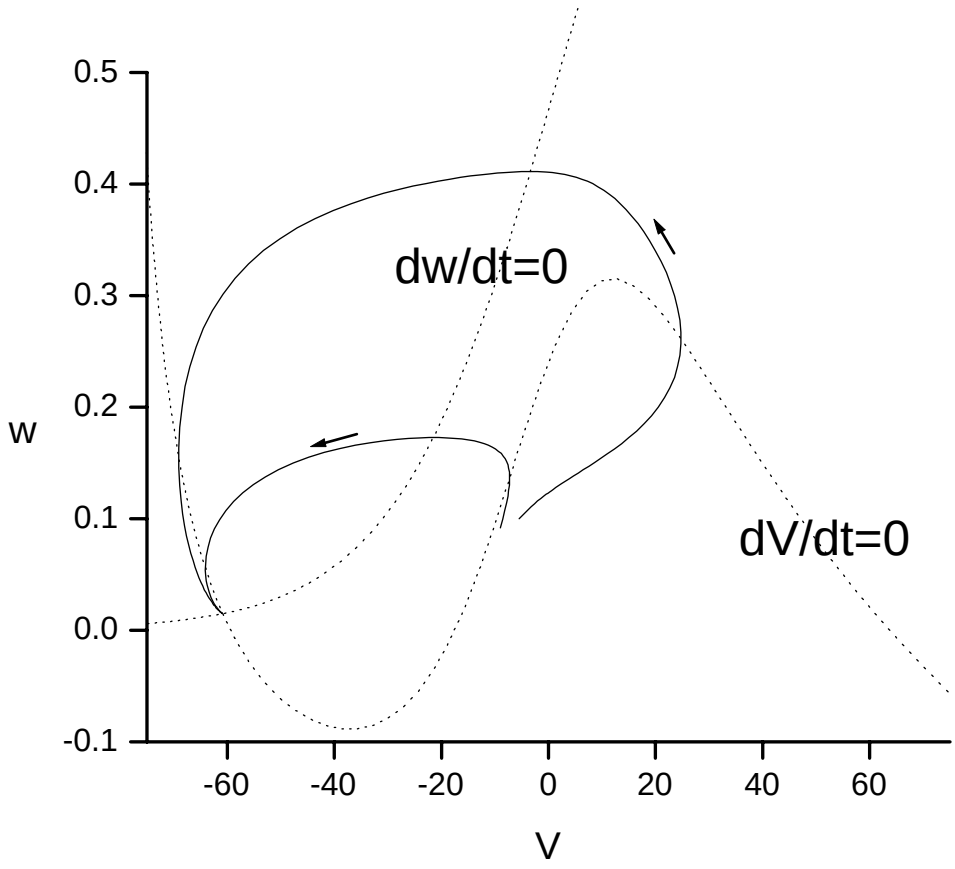

Figure 1.2: Nullclines for the Morris-Lecar model are plotted as dotted lines. A subthreshold and a superthreshold solution are plotted as solid lines. Adapted from figure 7.1 in Rinzel and Ermentrout [1998].

The following analysis is slightly expanded from Rinzel and Ermentrout [1998]. Oscillations can arise out of the stable point as a parameter of the model (I) changes. As mentioned above the stability of an equilibrium is determined by the eigenvalues of the Jacobian evaluated at the equilibrium point. The eigenvalue problem is

written

$$x = V - V_r \tag{1.4}$$

$$y = w - w_0 \tag{1.5}$$

$$\frac{d}{dt}\begin{bmatrix} x \\ \\ y \end{bmatrix} = J\begin{bmatrix} x \\ \\ y \end{bmatrix} \tag{1.6}$$

$$J = \begin{bmatrix} -\frac{\partial I_{ion}}{\partial V} & -\frac{\partial I_{ion}}{\partial w} \\ \\ \frac{1}{\tau}\frac{dw_\infty}{dV} & -\frac{1}{\tau} \end{bmatrix} \tag{1.7}$$

When $I = 0$ the eigenvalues of J at the equilibrium point are real and negative, indicating that the equilibrium is stable. As I increases a point comes when the stability of the equilibrium disappears. This can happen as soon as one of the eigenvalues (written λ_1 and λ_2), acquires a positive real part, which can occur if $\lambda_1 > 0$ and $\lambda_2 < 0$ and both eigenvalues are real. However, if it happens that the steady state V-I curve is monotonic then the real parts of the eigenvalues vanish. This is stated without proof in Rinzel and Ermentrout [1998], however the following argument works. Let

$$J = \begin{bmatrix} a & b \\ \\ c & d \end{bmatrix}$$

then the eigenvalues are

$$\lambda = \frac{1}{2}(a+d) \pm \sqrt{\frac{1}{4}(a+d)^2 - (ad - bc)}$$

For there to be one positive and one negative eigenvalue $ad - bc < 0$. This reduces to

$$\frac{\partial I}{\partial V} < -\frac{\partial I}{\partial w}\frac{dw_\infty}{dV}$$

Firstly, $dw_\infty/dV > 0$ because the steady state activation, $dw_\infty(V)$ is monotonic in V. Next, the left hand side of the inequality is positive because it is evaluated at

the point $I_{ion}(w, V) = I$ which is on the steady state I-V curve (since $dV/dt = 0$). The steady state I-V is monotonic, by the assumption above. Similarly, $\partial I/\partial w$ is also positive. Thus, the inequality cannot hold and stability must be lost as the real parts of the eigenvalues vanish. As discussed above, this is a Hopf bifurcation, which in this case creates a stable periodic solution (as opposed to an unstable periodic solution). It occurs when $\mathrm{re}(\lambda) > 0$, thus $a + d > 0$ or

$$-\frac{1}{C}\frac{\partial I_{ion}(V, w)}{\partial V} > \frac{1}{\tau} \tag{1.8}$$

The partial derivative is negative since it is the slope of the steady state V-I curve (not the I-V curve). (This condition is not properly stated in Rinzel and Ermentrout [1998]). The left hand side of the condition is the membrane time constant when the membrane is depolarised by imposed steady current and voltage dependent conductances have activated. An interpretation of this condition is as follows. The membrane time constant is now faster than the recovery time of the activation variable, w. Any depolarising fluctuations will allow the membrane to react faster than the repolarising K^+ current can activate. This causes further activation of the Ca^{++} current and positive feedback drives the membrane to depolarise. Ultimately the Ca^{++} driving force decreases and the K^+ driving force and conductance increase and the membrane repolarises, giving rise to the well known cycle of action potential firing. This example is a simplified version of the barnacle muscle fibre, however it applies more generally to any excitable membrane that fires repetitive action potentials when excited, including those of neurons.

An interesting feature of the Hopf bifurcation is that once oscillations emerge they do so with a finite frequency, which is approximately equal to $\mathrm{im}(\lambda)$. As steady

current is increased, a range of small frequencies are observed until a new regime is encountered in which stability returns. The classic Hodgkin-Huxley equations describing the action potential in the squid giant axon is a four dimensional system (membrane potential, K^+ activation, Na^+ activation and Na^+ inactivation), but the onset of firing is also a Hopf bifurcation. The classic equations produce very little gradation in firing frequency. The Hodgkin-Huxley limit cycle also disappears when the injected current is large enough, however the mechanism is different from that of the Morris-Lecar model discussed above. The mechanism in the Hodgkin-Huxley case is called Na^+ inactivation.

Many neurons burst, that is they show a cycle that consists of a period of spiking followed by a period of slow membrane potential change without spikes. This is not possible with a two dimensional model because it would mean that the trajectory must spiral between a loop state for the spiking phase and a fixed, or nearly fixed, point for the quiescent period. This is not possible without the trajectory crossing itself. (Trajectories cannot cross since this violates the uniqueness of solutions. If the state is at a point where trajectories cross which path does the system take?) Rinzel and Ermentrout [1998] discuss two conditions which together can lead to bursting. The first is that the steady state V-I curve is S-shaped. This means that for some values of I the dV/dt nullcline has three intersections with the dw/dt nullcline. In this case a stable periodic solution, around the high voltage part of the V-I curve, coexists with a stable equilibrium on the lower part, the middle solution is unstable. As the current is moved slowly back and forth across this region a hysteresis loop is formed in which the system jumps from the steady equilibrium to the limit cycle and back. The second condition is slow negative feedback to act

as the slowly moving source of current. The authors suggest a Ca^{++} activated K^+ current

$$\begin{aligned} I_{\mathrm{K\,Ca}} &= g_{\mathrm{K\,Ca}}\, z\, (V - V_{\mathrm{K}}) \\ z &= \frac{\mathrm{Ca}^p}{1 + \mathrm{Ca}^p} \\ \frac{d\mathrm{Ca}}{dt} &= -\alpha I_{\mathrm{K\,Ca}} - \beta \mathrm{Ca} \end{aligned}$$

In words, as the neuron depolarises, Ca^{++} accumulates in the cell over the course of several action potentials during the spiking phase which, in turn, activates $g_{\mathrm{K\,Ca}}$ which repolarises the cell until it jumps to the low voltage equilibrium. At this point the intracellular Ca^{++} concentration drops, $g_{\mathrm{K\,Ca}}$ closes and the cell depolarises again.

This illustrates a "divide and conquer" approach to analysing higher dimensional systems. If the dynamics of some state variables are slow compared to others then the fast subsystem can then be analysed, treating the slow variables as constants. The slow subsystem can then be analysed by considering an average of the fast subsystem over one period. In the example above, because the $g_{\mathrm{K\,Ca}}$-Ca^{++} dynamics are slow the system has been analysed as quasi-two dimensional system consisting of the Ca^{++} and K^+ dynamics slowly modulated by the $g_{\mathrm{K\,Ca}}$ current. This technique is not valid when the all time scales of the system are roughly similar.

Theory of recurrent networks with inhibition

Neurons, of course, are nearly always elements in networks and it is not possible to predict network behaviour from single neuron behaviour, since networks also incude synaptic dynamics which in turn depend on neuron behaviour and network

connections. There are many ongoing problems in central and peripheral neurophysiology that relate to the basic dynamics of recurrent networks and that have been addressed by modelling studies. These questions are ideally suited to theoretical analysis because they involve emergent properties of large networks that are impossible to deduce using existing experimental technology. Furthermore, because they involve large scale behaviour of the network, it seems unlikely they depend on the details of every neuron. (This is not to say that neuron or synaptic dynamics are simple or trivial.)

Some of these questions are:

- Why do neurons in the central nervous system (CNS) neurons fire at comparatively low rates (1–5 Hz) [Latham et al., 2000a]? CNS neurons can fire at rates 1 or 2 orders of magnitude faster than this and networks have strong recurrent excitation and so should be readily driven into high firing rate states. Even with the presence of inhibitory interneurons a wide range of firing rates might be expected, yet they are not often observed.

- Many networks show various forms of rhythmic behaviour. These include simple oscillations [Latham et al., 2000a, Wilson and Cowan, 1972] and episodic bursting [Latham et al., 2000a, O'Donovan, 1999, Tabak et al., 2000]. Are these patterns driven by neurons that display similar patterns or do they emerge from the network [Marder and Calabrese, 1996]?

- How do networks switch between different firing patterns [Latham et al., 2000a, Wilson and Cowan, 1972]?

Mean firing rate or "mass action" models are based on the idea that network

dynamics are sufficiently captured by the average spike firing rate, which is then modelled as a single variable for each subpopulation of neurons. Obviously, these models do not address such quantities as multiunit codes, higher order moments of spike statistics (for example the variance) or cross correlations. However, they have the advantage of being significantly simpler than models where neurons are individually modelled. In addition, it is necessary to make simplifying assumptions so that complex terms can be neglected or linearised. The arguments for neglecting terms are usually that something has a smaller or shorter time or length scale than the scale that the modeller is interested in. When linearising a term, the argument is that the linear term is qualitatively similar to the nonlinear term in the physiological range the modeller is interested in. The purpose of these simplifications is to make the model amenable to analytic techniques so that powerful conclusions can be drawn about the qualitative dynamics of which a system is capable, and about the relationship between parameters that create these dynamics. This provides strong intuitive insight into how the system behaves.

Mean firing rate models go back at least as far as Beurle [1956], who considered a model of uniformly interconnected excitatory cells. He (she?) considered activity, including propagating waves, in this network and showed amongst other things that recurrent networks with only excitatory interconnections have two stable firing states, a quiescent state and maximally firing state. Because the network does not return from the maximally firing state, it is not biologically useful. However, with the inclusion of inhibition in these models this problem was resolved [Griffith, 1963]. The first mean firing rate model to specifically study the effects of a separate population of inhibitory interneurons was probably that of Wilson and Cowan [1972].

In this model, a population of neurons is assumed to have a random distribution of firing thresholds. Neurons above threshold fire and are then refractory for a period r. There is also a spatially uniform distribution of synaptic inputs and propagation delays are ignored. The model then describes the average firing pattern within the separate subpopulations of inhibitory or excitatory neurons. (This can be generalised to any number of neuron subpopulations.)

Two dynamical variables are used, $E(t)$ for the proportion of excitatory cells firing at time t and similarly $I(t)$ for the proportion of inhibitory cells firing at t. The value of these variables at time $t + \tau$ is equal to the number of cells of each type that are not refractory and which receive super-threshold excitation during this period. If the (absolute) refractory period is r, then the number of cells which are absolutely refractory at time t is

$$\int_{t-r}^{t} E(t')\,dt'$$

and so the proportion of sensitive cells is

$$1 - \int_{t-r}^{t} E(t')\,dt'. \tag{1.9}$$

There is a similar expression for the inhibitory population.

The function which gives the proportion of the excitatory population that receives threshold activation is $S_e(x)$, where x is the average membrane potential (more below). S_e is monotonic because it is a cumulative distribution over synaptic input and threshold variations, thus it is monotonic because it is the integral of a positive function. This also means that it has zero slope at either ends of its range, because the underlying density function is zero at either end of the range. Because $S_e(x)$ is monotonic and has a zero slope at either end of its range it is sigmoidal.

There is an analogous function, $S_i(x)$, with similar properties, for the inhibitory population.

The level of excitation is derived as follows. Inputs are assumed to sum linearly at the level of the membrane potential and $E(t)$ is assumed to change slowly compared to individual synaptic events. The averaged total membrane potential response in the excitatory subpopulation is

$$x(t) = c_1 E(t) - c_2 I(t) + P(t) \tag{1.10}$$

where P is exogeneous, excitatory, input and the constants c_1 and c_2 represent the average strength of synaptic inputs from each population. Assuming that the firing threshold in equation (1.9) is independent of the excitation a cell receives, then the number of cells that fire in the next instant is the proportion of cells that are sensitive multiplied by the number of cells that receive sufficient synaptic input

$$E(t+\tau) = \left[1 - \int_{t-r}^{t} E(t')\, dt'\right]\ S_e(x) \tag{1.11}$$

with x defined in Eq. (1.10). There is a similar equation for the inhibition, I.

Assuming the time scale of the refractory period is small compared to the time scales of interest the following substitution is a good approximation

$$\int_{t-r}^{t} E(t')\, dt' \to rE(t). \tag{1.12}$$

Expanding $E(t+\tau)$ as a Taylor series and dropping higher order terms gives

$$E(t+\tau) \approx E(t) + \tau \frac{dE}{dt}.$$

The full equations can be reduced to the following equations

$$\tau_e \frac{dE}{dt} = -E + (1 - rE)\, S_e(c_1 E - c_2 I + P(t)) \tag{1.13}$$

$$\tau_i \frac{dI}{dt} = -I + (1 - rI)\, S_i(c_3 E - c_4 I + Q(t)). \tag{1.14}$$

This is a 2 dimensional, nonlinear ODE and is amenable to standard techniques of analysis.

Since, by definition, equilibria do not change with time the location of equilibria occur when $dE/dt = 0$ and $dI/dt = 0$. In absence of exogeneous input ($P = 0$, $Q = 0$)

$$c_2 I = c_1 E - S_e^{-1}(\frac{E}{1 - rE}) \tag{1.15}$$

$$c_3 E = c_4 I + S_i^{-1}(\frac{I}{1 - rI}) \tag{1.16}$$

where S^{-1} denotes the inverse function. These equations describe the nullclines in the I–E plane (phase space). The equilibria occur at the intesections of these curves, that is, where both derivatives are zero. A sigmoid is monotonically increasing so its inverse is also monotonically increasing. Thus, the nullcline given by equation (1.16) is monotonically increasing in I ($rI \leq 1$, from the definition of the refractory period). On the other hand, because of the negative sign, the E nullcline, equation (1.15), need not be monotonic. The inverse sigmoid will approach 0 or ∞ very rapidly as E approaches 0 or 1, therefore the E nullcline does same, however it need not be monotonic in the middle of the range. This can create a "Z" shaped curve which can be intersected by the I nullcline an odd number of times. This is illustrated in figure (1.3), adapted from Wilson and Cowan [1972]. There is always an intersection (and hence equilibrium) at $E = 0$ and $I = 0$, however the presence of more equilibria leads to interesting behaviour. A sufficient condition on the model parameters can be derived to ensure that the E nullcline is "Z" shaped, which amounts to the requirement that the variance in the excitatory input into each neuron must not exceed a simple monotonic function of the mean.

This condition only guarantees that the nullcline is "Z" shaped, not that there are 3 intersections. If the inputs, P and Q, take on constant non-zero values then the $dE/dt = 0$ nullcline can be moved parallel to the I axis and the $dI/dt = 0$ nullcline can be moved parallel to the E axis, so in this way multiple intersections can be created. In figure (1.3) stable points are marked (+) and unstable (-).

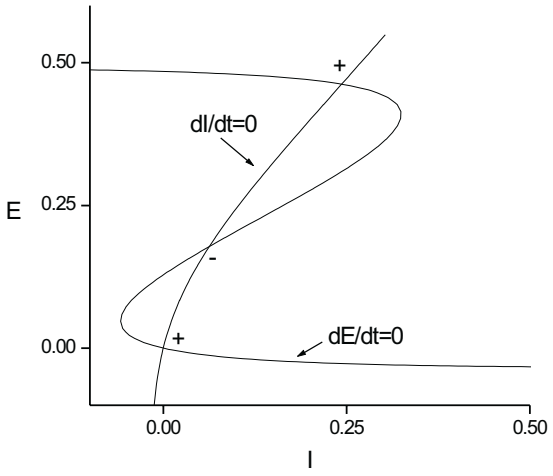

Figure 1.3: Nullclines for equations (1.15, 1.16), adapted from figure 4 in Wilson and Cowan [1972].

Hysteresis can occur as follows. If a P or Q input cycles slowly then stable equilibrium points can be created or destroyed forcing the system to move between different stable firing states. After the input has done a complete cycle the system may be in a different state to the one it started in. Hysteresis may be a form of switch, changing the network from one mode of operation to another.

If the slope of the I nullcline is shallower than the slope of the E nullcline then exogenous inputs can be chosen so that there is only one equilibrium. Periodic solutions can come into existence, via a Hopf bifurcation, if the parameters are such that some of the equilibria are not stable. This case is illustrated in figure

(1.4), adapted from Wilson and Cowan [1972] figure 11. By analysing the system, linearised around the equilibrium point, it is possible to derive conditions on the parameters that lead to periodic solutions. (Only periodic and stable solutions exist in a bounded two dimensional system.) As with hysteresis, the existence and nature of the limit cycle can be controlled by the inputs into the excitatory and inhibitory populations (P and Q). There is a threshold which P must exceed before periodic solutions exist, but the frequency is graded in P once the threshold is exceeded. With the nullclines in this configuration hysteresis and cyclic solutions cannot both exist for the same inputs.

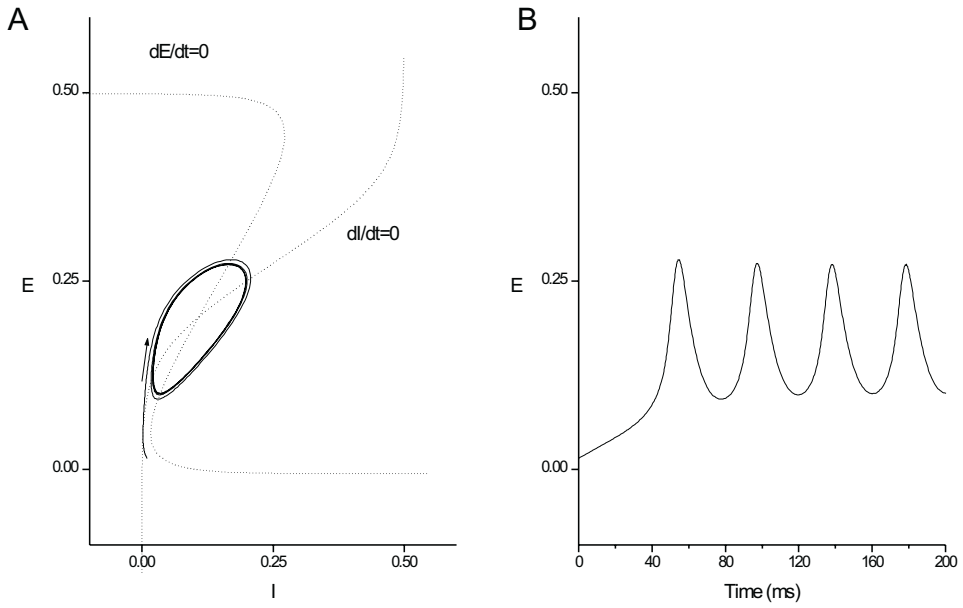

Figure 1.4: *A.* Nullclines and a trajectory, plotted in phase space, for equations (1.15, 1.16). *B.* $E(t)$ for the limit cycle shown in panel A. Adapted from figure 11 in Wilson and Cowan [1972].

This model has been reviewed in some detail to illustrate three points. Firstly,

it demonstrates the power of these sorts of models. They make strong explanations and predictions about qualitative behaviour of large networks that are simply not possible from "descriptive" models. Secondly, with this sort of study, more than with an experimental or numerical study, the mathematical argument is the result. A final point is that the Wilson-Cowan model has served as the basis for a number of other studies.

Latham et al. [2000a] used the Wilson-Cowan model as a starting point to address two questions. Firstly, given the strong recurrent excitation that exists in CNS networks, why are observed firing rates so low, 1–5Hz, compared to the hundreds of Hz which is the maximum firing rate for most central neurons? In particular, they tested the hypothesis that low firing rates may, paradoxically, be due to the presence of a percentage of endogenously active excitatory neurons. The second problem they addressed is how oscillations arise and how are they switched on and off. This study extended that of Wilson and Cowan [1972] by including firing adaptation.

Latham et al. [2000a] used these equations (in the notation of Wilson and Cowan [1972])

$$\tau_E \frac{dE}{dt} = -E + \Theta_e(E, I) \tag{1.17}$$

$$\tau_I \frac{dI}{dt} = -I + \Theta_i(E, I) \tag{1.18}$$

where

$$\Theta_e(E, I) = S_e((c_1 E + c_2 I + P - G_e)/(1 + I)) \tag{1.19}$$

$$\Theta_i(E, I) = S_i((c_3 E + c_4 I + P - G_i)/(1 + I)). \tag{1.20}$$

Here, P is external excitatory input and the refractory period has been assumed to be small, so terms involving r can be ignored.

The inhibitory feedback is different from that of Wilson and Cowan [1972] in that gain is controlled by the inclusion of *divisive inhibition* (the $1 + I$ term) [Nelson, 1994, Carandini and Heeger, 1994]. (Divisive inhibition is the idea that inhibition at the neural level can be achieved by increasing synaptic conductance without changing membrane potential. This can be achieved by a combination of excitatory and inhibitory input such that the net driving force of the conductance change is the near the resting membane potential. The effect, mathematically, is to divide normal excitatory inputs by the amount of divisive inhibition.) The $G_{\{E,I\}}$ terms control adaptation as follows

$$\tau_A \frac{dG_e}{dt} = \delta G\, E - G_e \tag{1.21}$$

$$\tau_A \frac{dG_i}{dt} = \delta G\, I - G_i \tag{1.22}$$

where δG is a constant. The interpretation of these equations is that the adaptation will move toward the value δGE at a rate determined by the time constant τ_A.

This time constant of the adaptation is long, hundreds of milliseconds or more. The time constants of equations (1.17) are determined by the neuron membrane time constants and so are of the order of a few milliseconds. This means the system can be "decomposed" into fast and slow susbsytems using the method proposed by Rinzel and Ermentrout [1998] (see above). To begin the E, I subsystem was considered on its own with $G_{\{E,I\}} = 0$. The next step was to determine the equilibria which occur when $dE/dt = 0$ and $dI/dt = 0$. Because Latham et al. [2000a] were interested in low firing rate states and because they wished to test the role of having a percentage of endogenously active neurons they paid more attention to the details of the gain functions, $\Theta_{\{e,i\}}$, at low firing rates. At high firing rates, the gain is independent

of neuron resting properties. At low firing rates, Latham et al. [2000a] recognised three regimes for excitatory gain function, Θ_e, depending on how close neurons were to firing. These are illustrated in figure (1.5), panel A. In regime 1, if all neurons are more than one EPSP from threshold the initial slope of the gain function is zero. The smallest firing rates are not sufficient to produce action potentials in the target neurons, hence the gain is zero. The gain function has a classic sigmoid shape, starting off with zero slope, then curving upwards and finally leveling off. This means that the nullcline

$$0 = \Theta_e(E, 0) - E \tag{1.23}$$

has three solutions. Small initial firing will die away and the network will return to the quiescent state. In regime 2 the gain function has a different shape because all neurons are within 1 EPSP of threshold. In this case, a single action potential will cause firing in all target neurons which in turn will lead to more firing and so on. Thus, in the absence of inhibition, the network has only the quiescent state and the maximal firing rate state as stable equilibria. In regime 3 the gain function is different again because some neurons are endogenously active. In this case, positive feedback always drives the network to the maximum firing rate state.

The inhibitory nullcline at $E = 0$ is

$$I = \Theta_i(I, 0).$$

In regimes 1 and 2 the inhibitory gain function is identically zero, since more inhibitory firing cannot increase firing beyond zero. In regime 3, because neurons are firing without input, $\Theta_i(0, 0) > 0$, and so the I nullcline starts at a non zero value of I and decreases to zero as I increases.

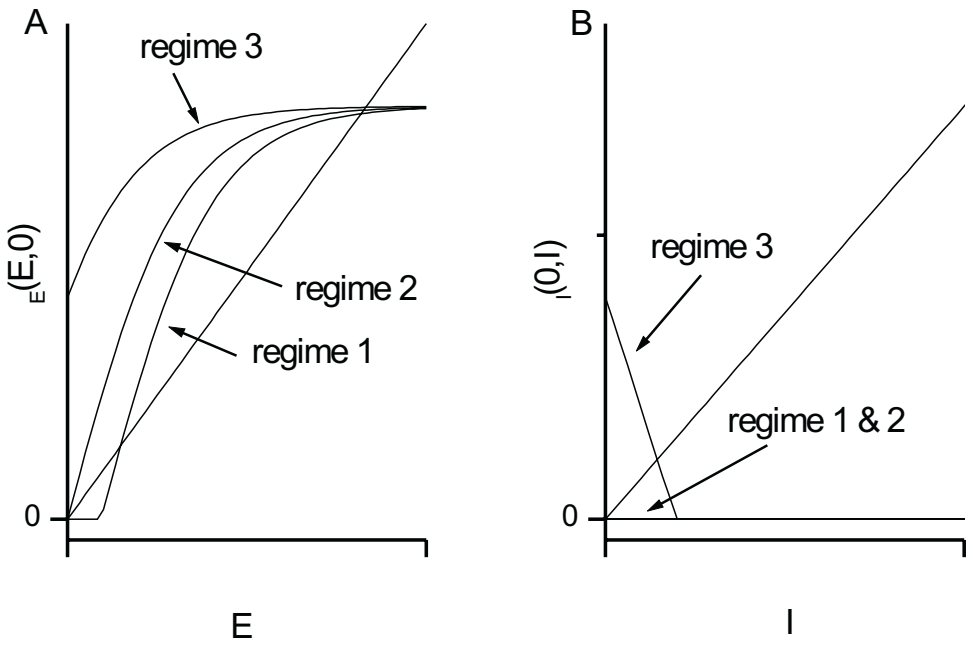

Figure 1.5: *A.* The excitatory gain function $\Theta_e(E, 0)$ plotted against E for the three network regimes discussed in the text. *B.* The inhibitory gain function, for the same regimes, $\Theta_i(E, 0)$ plotted against I. Adapted from figure 2 in Latham et al. [2000a].

As I increases the $\Theta_e(E, I)$ curve moves to the right and down, because there is less and less firing as the inhibition increases. Conversely, as E increases the $\Theta_i(E, I)$ curve moves upwards and to the right, because Θ_i is an increasing function of excititory firing. This allows the nullclines to be mapped out in the (E, I) plane by tracing the points of solution of equations (1.23) and (1.7) onto the (E, I) plane. As in Wilson and Cowan [1972] (figure 1.3), regime 1 has three equilibria, a stable equilibrium at zero firing, an stable equibilbrium at high firing (the authors term this a *metastable*, by which they apparently mean that the region of attraction around this point is small) and an unstable intermediate state. The last state acts as a threshold between the two stable states. The key point is that there is no stable state at low, but nonzero, firing, corresponding to spontaneous firing at low rates seen in the CNS. It is possible to "tweak" the nullcline to move the metastable state down to a lower firing rate. However, the location of this state is very sensitive to the precise shape of the curve which means that small changes in parameters can move the location dramatically. In regime 2 there is a low firing rate, metastable state. This state is also not robust because it requires the majority of neurons to be within one EPSP of threshold. EPSPs in the CNS are small, about 1 mV, and it is unrealistic to expect that a large number of neurons in the network can maintain their membrane potentials within 1 mV of threshold. Furthermore, the quiescent state is still present and perturbations that cause a drop in network firing can switch the network into the quiescent state. In regime 3 the quiescent state does not exist, because of the endogenous activity. Furthermore, the nullclines can be shaped so that there is no state at high firing. This leaves a single equilibrium at low firing.

Having shown a condition for the existence of an equilibrium, it is also neces-

sary to show that the equilibrium is stable. Stability amounts to conditions on the sensitivity of the gain functions to changes in firing. The inhibitory input into the inhibitory neuron population must increase quickly with increased inhibitory firing. Similarly, excitatory input into the excitatory population must increase quickly with excitatory firing. These conditions ensure that the network can react to perturbations in firing and restore the equilibrium state. If these conditions are not met then the equilibrium is unstable and this produces oscillations.

Neuron firing is always more complex than the simple on or off firing of the previous models — sustained firing leads to adaptation. If the adaptation time constant τ_A is long compared to the time constants of the firing rate changes τ_E and τ_I (and if it were not it would not be called adaptation), then the divide and conquer analysis of [Rinzel and Ermentrout, 1998] can be applied (see section 1.7). The nullclines are moved slowly by the adaptation variables and the firing rate closely tracks the stable points as they move about the phase plane. If the effect of adaptation is small, then movement of the stable point will be slight and the system will move to an intermediate equilibrium. On the other hand, small, smooth movements of the nullclines may lead to the disappearance of stable points in some regions of the phase plane and the appearance of new stable points elsewhere. Firing increases as the stable point moves in phase space, then the high firing rate stable point suddenly disappears and a zero firing rate stable point appears and system firing rate crashes to zero. Adaptation wears off and the zero firing rate state loses stability and firing increases again. In this case, the system is oscillating. The authors classify this kind of oscillation as bursting. This is because the creation and destruction of equilibria make this kind of oscillation qualitatively different from

oscillations which occur around an unstable equilibrium.

This kind of analysis allows very strong conclusions to be drawn from the assumptions, but assumptions are often made for the sake of the mathematics. To test weaker assumptions numerical simulation is the essential next step. Latham et al. [2000a] use a simple voltage dependent model of the action potential and stereotyped conductance time courses for the post spike fast and slow hyperpolarising currents (see Chapter 2 for more details of stereotyped conductance time course models). A constant depolarising current can be applied to control the fraction of endogenously active neurons. Post synaptic currents are also modelled as stereotyped time course conductance changes, with the conductances of multiple synaptic events summing linearly. The synaptic currents are weighted by a synaptic strength for the connection from the source neuron to the target neuron. Two connection models were studied. The first was a uniform connection model in which the probability of connection was independent of the distance between neurons. In the second model, a local connection model, neurons were in a 2D plane and the connection probability had a Gaussian profile in the distance between the 2 neurons. (It was found that the connection model made no difference to the results.) Propagation delays were ignored, presumably to keep the study as simple as possible. Networks contained about 10,000 neurons.

By varying the distribution of applied current, the authors were able to reproduce the three excitability regimes: 1) all neurons more than 1 EPSP away from threshold 2) some neurons within 1 EPSP of threshold and 3) some neurons endogenously active. The network simulations fulfilled the analytic model predictions. Networks were quiescent in regime 1 or had metastable states. The region of param-

eter space that supported the metastable states was small. Random fluctuations in firing rate drove the networks out of the region of attraction around the metastable state and they returned to the quiescent state. When endogeneously active neurons were present, the network was able to maintain a long term stable state with spike frequencies starting at around 0.15 Hz. Increasing the number of endogenously active neurons caused a graded increase in the stable firing rate. With the presence of spike firing adaptation, the lifetimes of the metastable states dropped. Bursting states came into existence when endogeneously active neurons were present. These states survived longer as the proportion of endogeneously active neurons increased, but disappeared as the proportion crossed a high threshold.

This is a particularly interesting study because the predictions were tested experimentally [Latham et al., 2000b]. Mouse spinal cord neurons were grown in culture and activity measured with, and without, blockers of synaptic transmission. The antagonist/receptor combinations were AP5/NMDA, CNQX/AMPA, mecamylamine/nicotinic, atropine/muscarinic, bicuculline/$GABA_A$ and strychnine/glycine. In the absence of blockers neurons fired either in bursts or indefinitely at low rates. By controlling the culture medium Latham et al. [2000b] were able to control whether the network was silent, whether it burst rythmically or whether it fired steadily at a low rate. Blockers were added to the bath and the number of neurons active in the absence of synaptic input determined. These were the endogenously active neurons. It was found that the transition from quiescence to bursting was at around 3.3-5% endogeneously active neurons. The endogenously active neurons burst in the presence of transmission blockers. The proportion of endogeneously active neurons at the transition from bursting to steady firing was not determined, but networks with

low steady firing rates had 30% endogenously active neurons.

Homogeneous recurrent networks

Many recurrent neural networks lack specialised inhibitory interneurons. An important class of these networks occurs during development, when the classical inhibitory neurotransmitters (GABA and glycine) are excitatory because of the differences in Cl^- driving potential compared to the fully developed environment [Sernagor et al., 1995]. Thus, these network have strong recurrent excitation, with no obvious source of inhibition. A number of these networks display spontaneous activity. The most extensively studied are those in the spinal cord [O'Donovan et al., 1998], retina [Feller et al., 1997, 1996] and hippocampus [Traub et al., 1994]. These networks are spontaneously active in periodic bursts, organised over large areas (several segments in spinal cord) [O'Donovan, 1999]. The neurons themselves do not burst, or oscillate spontaneously [O'Donovan et al., 1998]. Application of blockers of synaptic transmission causes an immediate quenching of activity, but bursting recovers after around 80 minutes [Chub and Donovan, 1998]. In the interburst intervals, the networks are refractory to external stimuli and immediately following an active period neurons are hyperpolarised and have weaker responses to synaptic transmission [Fedirchuk et al., 1999]. Within each burst, activity shows rapid oscillatory behaviour.

Recent papers give a simple analysis of these networks [Donovan et al., 1998, Tabak et al., 2000], which in turns follows from the theoretical work of Senn et al. [1996]. The authors use an elegant mean firing rate model, based on similar assumptions to the Wilson-Cowan model. In this case, there is a single population of

excitatory neurons, which transmit to each other by excitatory postsynaptic potentials. Hence

$$\tau_E \frac{dE}{dt} = S(n\,E) - E \tag{1.24}$$

where the notation conventions are from Wilson and Cowan [1972], rather than Tabak et al. [2000]. The *connectivity parameter*, n, controls the coupling between firing and synaptic response. The physiological meaning of this quantity is that it is a combination of the size of synaptic responses and network connectivity. For moderate to large n, the system shows bistability, as discussed above. When n is very large the unstable intermediate state disappears and the zero firing rate state becomes unstable, any noise or spontaneous firing in the system will send it over the edge into the high firing rate state. For small n, only the zero firing rate state satisfies $E = S(n\,E)$. Thus, changing n causes qualitative changes to the system behaviour.

Activity dependent synaptic depression means that the connectivity will change in response to the average firing rate. By analogy with other systems where depression has been shown to generate rhythmic or oscillatory behaviour [Feller et al., 1997, 1996, Traub et al., 1994], depression was also included in this model. The equations describing a homogeneous, recurrent, excitatory network with synaptic depression are

$$\tau_E \frac{dE}{dt} = S(n\,d\,E) - E \tag{1.25}$$

$$\tau_d \frac{dd}{dt} = D(E) - d \tag{1.26}$$

where d models the synaptic depression and varies between 0 and 1. The function D is a decreasing sigmoid, that is $D \to 0$ as $E \to 1$ (the maximum firing rate)

and $D \to 1$ as $E \to 0$. At zero firing the synaptic strength returns to full strength $d = 1$ with a time constant τ_d and full firing drives the synaptic strength to zero at the same rate. This provides negative feedback in the system. For most parameter values, the nullclines will have a single intersection, giving a single stable point. If feedback is very rapid, it will be able to follow the firing rate closely and the system will simply move to a lower firing rate equilibrium. If the depression does not react too quickly, then the depression and the firing rate will chase each other's tails and the system will oscillate. This occurs via a Hopf bifurcation at the equilibrium which in turn can be used to determine a relationship between the parameters of the model.

An important parameter in the model is the point of half activation of the sigmoid response function, θ. This parameter can be interpreted as the average action potential threshold. The corresponding slope of the sigmoid is an inverse measure of the variance of the threshold distribution. The steeper the slope the less the variance. This can be understood by considering injecting current uniformly into the population of neurons. If the slope is infinite then all neurons fire as the current exceeds θ. If the slope is very shallow the number of neurons that fire increases slowly as the size of the current injection increases, because of the large variation in the threshold within the population. The existence of periodic solutions depends on θ and the period of the oscillations varies by a factor of roughly 2 as θ varies from about 0.18–0.21. These oscillations are the rapid oscillations in firing seen within each episode of activity.

Tabak et al. [2000] compare two mechanisms to explain the interepisode interval. After an episode, the membrane potential of neurons is hyperpolarised and slowly

recovers before the next episode. In addition, synaptic potentials are also strongly depressed and recover with a time course of around a minute. In light of the first observation the authors allow θ to now depend on the level of activity

$$\tau_\theta \frac{d\theta}{dt} = \Theta(E) - \theta \tag{1.27}$$

where is Θ is an increasing sigmoid of E. The rate at which θ changes with time is much slower than E and d, so $\tau_\theta \gg \tau_E, \tau_d$. Because of this condition the system can be analysed as a quasi two dimensional system [Rinzel and Ermentrout, 1998], with properties of the system determined at each point in time by the E–d equations. Consider a system that is initially quiescent. The threshold, θ, is sufficiently large that there are too few active neurons to drive the system into the high firing rate state. In this case the $E = 0$ point is stable. However, as θ moves slowly toward $\Theta(0)$ with a time constant τ_θ, the system becomes more excitable. Eventually, θ will be small enough that some neurons will become spontaneously active or external noise will bump the system into the oscillatory state. The θ subsystem, because of its slow reaction time, sees the value of E averaged over a time scale of order τ_θ. This causes a slow increase in θ, until excibility is lost and the oscillations disappear again. (Interestingly, this makes the oscillations robust, despite the relative sensitivity on θ, because the system will "seek out" the oscillatory state.)

The second mechanism to explain episodic activity is a second synaptic depression, but on a slower time scale

$$\tau_E \frac{dE}{dt} = S(n\, r\, d\, E) - E \tag{1.28}$$

$$\tau_s \frac{dr}{dt} = R(E) - r \tag{1.29}$$

with d described by equation (1.26). Again $\tau_s \gg \tau_E, \tau_d$. This model also produces

episodic bursting in a similar manner to the θ model. However, they can be distinguished by how they depend on other parameters in the model, in particular the connectivity, n. In the θ model, greater connectivity means that the network can stay firing for high values of θ (larger action potential thresholds). However, the value of θ at which the network starts firing is not changed. Thus, the burst duration increases because of the increased range of θ. The interburst duration increases because the range over which θ must decay has increased. On the other hand, the effect of changing n on the r model is to change the slow r subsystem, rather than the fast E–d subsystem. This can been seen by rescaling $r \to \bar{r}/n$. Equation (1.28) becomes

$$\tau_E \frac{dE}{dt} = S(\bar{r}\, d\, E) - E \tag{1.30}$$

$$\tau_s \frac{d\bar{r}}{dt} = n\, R(E) - \bar{r} \tag{1.31}$$

with the d subsystem remaining unchanged. It is now evident that by increasing n the derivative $d\bar{r}/dt$ increases and so the $\bar{r}$ subsystem moves faster than before, moving the E–d subsystem more quickly into and out of the oscillatory state. Thus active episodes and inter-episode intervals are decreased. This is the opposite effect of changing n in the θ model and is experimentally testable.

To test these predictions, and determine the better model, experiments were done. The preparation was isolated chick embryonic spinal cord and electrical recordings were made from the ventral or muscle nerves. The connectivity parameter was manipulated by adding the NMDA receptor antagonist APV to the bath. This caused an increase in interepisode duration, thus indicating that the r model better explains the data. This was a simple model, but with powerful explanatory

abilities. Furthermore, the model made a predication that was far from obvious, a prediction that would not be possible without mathematical analysis.

Modelling intestinal function

The only group, other than our laboratory, that has attempted a systematic program of modelling to explain intestinal behaviour is that of Miftkahov and colleagues [Miftakhov et al., 1999b,a, Miftakhov and Wingate, 1996, Miftakhov and Abdusheva, 1996a,b, Miftakhov et al., 1996, Miftakhov and Wingate, 1995b,a, 1994c,a,b, 1993]. Unlike the models reviewed in this chapter, their aim has been to build models from the "bottom up" using as much biophysical detail as possible. Their complexity means that mathematical analysis in not possible, so they were solved numerically and small regions of the parameter space were examined. The authors concentrate mainly on synaptic tranmission from transmitter release to currents generated in the postsynaptic membrane. Unfortunately, because of the limited data currently available for much of ENS biophysics the insight provided by the models and comparison with experiment is limited. The work is also marred by serious physical and physiological errors. For example, EPSPs are calculated to have an absolute value of 87mV, well above the observed driving force and IPSPs are calculated to hyperpolarise membrane potential to -70mV below resting membrane potential. Miftakhov et al. [1999a] suggested that slow waves are the result of a feedback loop between mechano-sensitive neurons, motor neurons and motor contraction despite the overwhelming evidence that they are generated by the interstitial cells of Cajal [Sanders et al., 2000].

1.8 Aims of this thesis

The aim of this thesis is to take the initial step in determining the role of the instrinsic sensory neurons of the myentric plexus in motility and other reflexes, and understanding how they perform this role. The most significant aspects of intrinsic sensory neurons are: they are a major class of neuron within the ENS (they make up 30% of the population of myenteric neurons [Costa et al., 1996]); they connect to every other neuron type in the myenteric plexus [Pompolo and Furness, 1988]; they transmit to each other by slow EPSPs [Kunze et al., 1993, Clerc et al., 1999]; they project predominantly circumferentially and reciprocally [Bornstein et al., 1991b]. The sensory neurons undoubtably play a crucial role in intrinsic reflexes for a number of reasons. Since they are the first point of entry into the myenteric plexus the way they transduce stimuli determines how the rest of the system can respond to those stimuli. As well as connecting to interneurons, they also connect to motor neurons and can therefore mediate monosynaptic local reflexes. But perhaps the most interesting aspect of these sensory neurons is that also connect to each other locally to form a recurrent network. This gives these networks the ability to store and manipulate information about local conditions in the "reverberatory" activity within the network, and this opens up many possibilities for what they can do. For example, the network can alter the output of a stimulus based on the history of previous stimuli. Feedforward networks can do this to a certain extent, for example by membrane changes or changes in synaptic efficacy, but the existence of recurrent connections means that neurons can coordinate their activity in a less haphazard way than isolated neurons. Because sensory neurons connect to all other neuron types

they are in a position to play a coordinating role in motor patterns and reflexes. If this is to be effective in a large network then neurons must coordinate their firing and this implies synaptic transmission. The final possibility suggested by connections is transmission of activity over long distances.

This thesis must necessarily be concerned with the fundamental nature of the dynamics of sensory neuron networks. Therefore, first step is to construct a realistic model of synaptic transmission between sensory neurons. Synaptic transmission between sensory neurons is mediated by G-protein coupled second messenger cascades which ultimately change membrane conductance [Bertrand et al., 2000b]. This is qualitatively different from postsynaptic effects that are the result of direct ligand gating of ion channels. From the point of view of constructing a model, the important difference between slow and fast transmission is that nonlinear summation of inputs cannot be ignored [Morita and North, 1985]. Construction and interpretation of a model of slow synaptic transmission is the goal of chapter 3.

The next question is how is stability maintained in a recurrent network with strong excitation? Run away positive feedback will make the network likely to fire out of control. Yet, to be biologically useful firing must be controlled — therefore there must some form of inhibition. The remainder of the thesis examines three candidates for inhibition. The first candidate is the AHP, which is a very large current in neurons at rest and so must play a role in the control of firing, at least when the network starts at rest. During a slow EPSP the AHP is suppressed, but not completely abolished. This leads to the hypothesis that it can control firing in networks even when slow EPSPs are active. The second inhibitory candidate is IPSPs, which are observed in intrinsic sensory neurons, but are not well characterised.

The hypothesis tested is whether they can stabilise networks when evoked from the same terminals that evoke slow EPSPs. This is important because it can lead to an understanding of why both excitatory and inhibitory transmitters may be in the same terminals in other parts of the nervous system.

The third candidate for inhibition is activity dependent synaptic depression. The evidence for this short of synaptic plasticity is indirect and no quantitative data have been reported, however many synapses show plasticity, including those in the ENS. Synaptic depression differs from the two previous forms of inhibition in that it turns on only after firing and so is a form of delayed negative feedback. Delayed negative feedback introduces complex dynamics such as oscillations and propagating waves in spatially extended networks. The nature of the projections of sensory neurons are such that propagation within the sensory neuron network is orders of magnitude slower than propagation through the interneuron network. Thus, these waves are unlikely to be involved peristalsis, but identification with the slow moving wave front of MMC phase III is natural. This is explored in chapter 6 and 7.

The thesis ends, as all theses must, with a discussion of the larger implications and both experimental and theoretical work that follow on from this.

Chapter 2

Methods for computer simulations

2.1 Introduction

The two main techniques used in this study were mathematical analysis and numerical simulation. The nature of mathematical analysis is such that it should be presented as part of the argument. Numerical simulation, on the other hand, has a great deal of unedifying detail that only needs to be correct to be part of the argument and can be presented separately. This section presents details of the numerical simulation software and is in two parts. The main part presents the details of the underlying models of the neuron, synaptic transmission and connections. The second part gives some of the implementation details and discusses some of the practical issues in large scale simulation.

2.2 Simulation models

All network simulations were done with a purpose written simulation program called "Plexus". The initial versions of Plexus were written by Hugh Kelly [Bornstein et al.,

1997], however since 1996 development has been done by the author. Of course, the software is only one possible implementation of a number of mathematical submodels and algorithms that are designed to describe the underlying physiology of the gut at some appropriate level of detail. Because the aim is to understand macroscopic reflexes in terms of the underlying nerve circuits, the main submodels used in Plexus are: the model of spike generation; synaptic transmission and postsynaptic integration; and the models that describe how neurons are connected together.

The neuron model

The neuron model of spiking used in Plexus is closely related to the "leaky integrate and fire" model [Gabbiani and Koch, 1998]. Prior to firing, the equation describing the membrane potential is given by following equation

$$\tau_m \frac{dE_m}{dt} = I(t) - E_m \tag{2.1}$$

where E_m is the membrane potential and $I(t)$ is input current (normalised by the resting membrane conductance) with $E_m = 0$ initially. The quantity τ_m is the membrane time constant, which characterises how quickly the neuron reacts or "integrates" its inputs. The term E_m on the right hand side means that the neuron "forgets" its input exponentially with time constant τ_m, hence it is "leaky". Once the membrane potential crosses a threshold, the neuron is deemed to have emitted a spike, or "fired". In the classical implementation, the neuron potential then resets to rest. It is also possible that an absolute refractory period is imposed, in which the neuron may not fire another action potential no matter what the voltage.

The model implemented in Plexus has some refinements to the classic "leaky

integrate and fire" model. Firstly, rather than a simple current term, $I(t)$, current is modelled by the membrane equivalent circuit

$$I(t) = \sum_i g_i(t)(E_m - V_i) \tag{2.2}$$

where the sum is over conductance types, g_i is the conductance of the i^{th} type, normalised by the resting conductance, and V_i is the driving potential of that type. This scheme allows interaction of conductances, either by shunting or by enhancing the effect of one conductance when another closes. The main advantage is that it allows the detailed neuron model to be constructed directly from physiological data with the result that properties like resting membrane conductance and resting potential can be readily verified. As will be discussed in more detail below, it also allows for a more realistic post synaptic potential model.

As with the classic "leaky integrate and fire" model the user must specify the action potential threshold. In Plexus, rather than simply reset the membrane potential after the nominal spike emission, the action potential is simulated. This is done by starting stereotyped Na^+ and K^+ conductances with time courses given by (relative to $t = 0$)

$$\begin{aligned} g_{\text{Na}}(t) &= \begin{cases} \bar{g}_{\text{Na}}\,(E_m - V_{\text{Na}}) & t <= T_{\text{Na}} \\ 0 & t > T_{\text{Na}} \end{cases} \\ g_{\text{K}}(t) &= \bar{g}_{\text{K}}\,(t/k_{\text{K}})\,\exp(1 - (t/k_{\text{K}}))\,(E_m - V_{\text{K}}) \end{aligned}$$

In words, these are a pulse of depolarizing Na^+ conductance of duration T_{Na} and an alpha function shaped repolarizing K^+ conductance with time constant k_{K}. An absolute refractory period (usually 10ms) is imposed following the action potential. Normally, the K^+ current is set to outlast the Na^+ current and the absolute

refractory period, and so creates a relative refractory period.

This model of the action potential has some advantages over the standard "leaky integrate and fire" spike model. The first, is the natural implementation of a relative refractory period which, in turn, controls spiking frequency. Interestingly, the relative refractory period is the major determinant in the emergence of cooperative network bursting in feedforward networks [Bornstein et al., 1997, Thomas et al., 1999]. The other main advantage of this action potential model is aesthetic. Membrane voltage traces are much easier for electrophysiologists to interpret if spikes are readily identifiable as such.

The long after-hyperpolarisation of enteric sensory neurons is modelled in a similar way. Following a delay of t_{delay} after an action potential, a stereotyped conductance time course of the following form is started

$$g_{\text{Ca}}(t) = \bar{g}_{\text{Ca}}\ (t/k_{\text{AHP}}) \exp(1 - (t/k_{\text{AHP}})). \tag{2.3}$$

Here $\bar{g}_{\text{Ca}}$ is the maximum conductance opened and k_{AHP} is a parameter with the dimensions of time that controls the duration of the AHP. The time delay models the delay observed in the onset of the AHP following an action potential [Hirst et al., 1985b]. The delay to onset and the long duration of the AHP mean that it is possible for another action potential to be triggered either before the AHP starts or before the AHP has died away completely. In any case, the total conductance is the sum of the conductances from each AHP.

Slow synaptic transmission ultimately acts by closing the same group of channels that are opened to generate the AHP. Extensions to the AHP model that reproduce this interaction are presented in chapter 4.

Physiologically, sensory input enters the AH/sensory neuron as depolarising generator potentials on sensory terminal where they trigger action potentials. These action potentials propagate along the processes to the soma. Initially, they are seen in the soma as proximal process potentials (PPPs) [Wood, 1989] (also called initial segment potentials or neurite spikes). If they depolarise the membrane sufficiently, they generate a somatic spike. If the membrane is hyperpolarised (for example by current injection) so that they do not reach threshold, they appear as brief (20ms) depolarising potentials and lack any hyperpolarising potential or undershoot. These were modelled in a similar way to action potentials, using stereotyped time course conductance changes, except that they were smaller and did not hyperpolarise the membrane potential. In this study, each PPP was large enough to induce an action potential in a neuron at rest.

Network generation

The aim in developing Plexus was to model anatomically realistic networks on macroscopic scales. This means that the networks have thousands of neurons or more and it is not practical to construct networks of this size by hand. Therefore, Plexus has the ability to construct networks. Initially, it was thought that the anatomy was extremely important for the behaviour of these circuits [Furness et al., 1996], and so the anatomical models available in Plexus are highly detailed and give the user a great deal of control of how the network is constructed [Bornstein et al., 1997].

Neurons are placed within the simulated piece of gut as follows. The user specifies:

- a number of classes of neuron, for example "AH neuron", "ascending interneuron", etc.
- The longitudinal and circumferential dimensions of the network.
- The density of neurons.
- The distribution of the number and type of cells within the ganglia. This can be almost completely arbitrary.

The program:

- places ganglia on a rectangular grid, whose longitudinal spacing is specified by the user. The circumferential spacing then follows from this and the neuron density.
- randomly alters positions of ganglia in the circumferential and longitudinal directions according to a user specified Gaussian distribution, in order to mimic the natural pattern of the ganglionated Plexus.

The network connections are formed by generating synapses from a class of source neurons onto a class of targets. A number of contacts from a source neuron onto its targets are made in a rectangular *region of contact*. This is specified in terms of its longitudinal and circumferential dimensions and its longitudinal position relative to the source neuron. The software allows both the number of contacts within the region of contact and the dimensions and relative position of the region of contact to be randomly distributed according to a user specified Gaussian distribution. The software also allows the distribution within the region of contact to be specified, however for all the networks within this study the distribution was uniform.

Each synapse has a *synaptic strength*, s_i, associated with it, which is a constant (except in chapters 6 and 7) representing the amount of transmitter released in a single synaptic event. The meaning of the synaptic strength is defined in equations (2.5) and (2.6) below. The synaptic strengths are also drawn from a user specified random distribution, which can be either flat or Gaussian.

Processes run between neurons within the internodal strands which roughly line up on a rectangular grid. Neurons within a ganglion are assumed to have the same position. Thus the distance between two neurons is calculated using the "Manhattan metric" based on the locations of the ganglia, that is

$$d = |x_1 - x_2| + |y_1 - y_2| \tag{2.4}$$

where (x_1, y_1) and (x_2, y_2) are locations of the ganglia. When a neuron fires an action potential the delay before the synapse is activated depends on the distance and the axonal propagation speed. The propagation speeds are also drawn from a user specified distribution for each cell type.

The detailed definition of the network can be stored in files for later use. These files are human readable ASCII which allows network generation to checked and makes the files portable across multiple operating environments. This allows repeated runs on the same network or systematic variation of a particular parameter while keeping the exact network connections constant.

Synaptic transmission

The two most important models of synaptic transmission in Plexus are those of fast and slow synaptic transmission. The fast transmission model is designed to

represent directly ligand gated channels. The conductance for a single event has a stereotyped time course given by

$$g_{\text{fast}}(t) = s_i \, \bar{g}_{\text{fast}} \, (t/k_{\text{fast}}) \, \exp(1 - (t/k_{\text{fast}})) \tag{2.5}$$

where $\bar{g}_{\text{fast}}$ is the maximum conductance of a single event and k_{fast} is a constant with the dimensions of time that controls the duration of the event. The quantity s_i is the synaptic strength of the i^{th} synapse. The key assumption is that the conductance from multiple events is the sum of the conductances from individual events.

Slow transmission is more complicated because it is not possible to assume that the response from multiple synaptic events sums linearly at the conductance level. The equations describing slow transmission are

$$\begin{aligned} \frac{du}{dt} &= \alpha \sum_i s_i \delta(t - t_i) - \beta_1 u \\ \frac{dv}{dt} &= u^2 - \beta_2 v \\ \frac{dp}{dt} &= v(1 - p) - \beta_3 p \\ g_{\text{fast}}(t) &= \bar{g}_{\text{slow}} \, p(t) \end{aligned} \tag{2.6}$$

where $\delta(t)$ is the Dirac delta function (which describes an idealised pulse), t_i are the times of the synaptic events and s_i are synaptic strengths of the synapses producing those events [Bertrand et al., 2000b]. The physical interpretation of these equations is the creation of a diffusible second messenger (step 1) which disassociates the catalytic subunit from protein kinase A (step 2), which in turn phosphorylates calcium activated potassium channels (step 3). The parameter α determines the strength of the response in that increasing α shortens the rise time and increases the duration of the slow EPSP. The parameters α and $\beta_{1,2,3}$ are the decay rates of the three stages and were determined by fitting the model to experimental data, however α

was varied around the experimentally determined value as part of the study.

The derivation of the slow transmission model is described in detail in chapter 3. A model of the interaction between slow transmission and the AHP is presented in chapter 4. A model of activity dependent dependent changes to synaptic strength is discussed in chapter 6.

Stimulus models

Plexus provides two mechanisms for applying stimulus protocols to the networks. The first is a built in mechanism for applying stimuli with simple predetermined time courses. The experimenter specifies

- A rectangular region of the network.
- The type of neuron to receive the stimulus.
- For constant stimuli a percentage, ρ, which determines the intensity of the stimulus.
- A event to impose on stimulated neurons.

The stimulus algorithm then works as follows. At each time step of the simulation ρ neurons of the specified type are selected randomly from the specified rectangular region. The user specified event is then imposed on the selected neurons. In all experiments reported here, the event was the proximal process potential described above.

In principle, more complex stimuli can be constructed from primitives of the sort described above, or generated by another program. However, in some experiments,

it is desirable to have the stimulus depend on the output of the model. Specifically, for the experiments in chapters 6 and 7 it was necessary to model the effect of feedback from the muscle. To facilitate this, Plexus can read stimulus primitives from an external source as the simulation proceeds. Feedback is then implemented by another simple program that reads the output as the main simulator as it runs. It then generates stimulus primitives which it writes back to Plexus at run time.

2.3 Output

The two types of output used in this study are membrane potential data and action potential counts. Plexus captures the membrane potential for user specified neurons at each time step. In principle, it is possible to capture this data for all neurons, but in practice this consumes too much disk space. Network activity is also captured as action potential counts which are binned both spatially along the longitudinal direction and temporally to give a space and time representation of network activity.

Parameter details

The networks studied were all models of the subcircuit consisting of only the intrinsic sensory neurons of the guinea-pig ileum. This section details the definition of the "base network" used in this study. A large number of parameters were varied as part of the study and these are noted in the relevant sections of the text.

The smallest networks used were 5×5mm and contained about 1000 neurons. These were large enough to avoid size dependent artifacts. The dimensions and position of the region of contacts are chosen from normal distributions with the fol-

lowing parameters (mean $\pm$ standard deviation): 5.0 ± 2.3mm in the circumferential direction and 0.7 ± 0.8mm in the longitudinal direction and the centre of the region was located 0.3 ± 0.8mm in the anal direction from the cell body. This pattern mimics that seen in the myenteric plexus of the guinea-pig ileum [Bornstein et al., 1991b].

Other parameter values used in the numerical simulations are given in Table 2.1. Conductance changes are rarely reported directly, so they were calculated to give the appropriate membrane potential changes. Conductances are relative to resting membrane conductances.

Parameter	Value
τ_m	9ms
$\bar{g}_{\text{leak}}$	0.625
V_{leak}	-41.7mV
$\bar{g}_{\text{Na}}$	6
V_{Na}	55mV
T_{Na}	2ms
V_{K}	-90mV
k_{K}	5ms
$\bar{g}_{\text{KCa}}$	13.2
E_{AP}	-45mV
r_{basal}	0.045
r_{Ca}	0.25
α	1.6e-4ms^{-1}
β_1	5.6e-4ms^{-1}
β_2	6.4e-4ms^{-1}
β_3	3.8e-4ms^{-1}
mean(S_i)	1.0
std(S_i)	0.25
t_{delay}	70ms
mean(k_{AHP})	0.7s
std(k_{AHP})	0.2s
$\bar{g}_{\text{IPSP}}$	0.13, 0.26, 0.52, 1.0, 2.1, 4.2

Table 2.1: Parameter values used in network simulations.

2.4 Implementation details

Plexus is written in the C programming language. Operating system dependent API calls are kept to an absolute minimum making it easy to port to a variety of operating system. The interface to Plexus is through text files containing Plexus definitions coded in "Plexus definition language". The definition language includes variables and expressions. Plexus commands can be passed on the command line and this, in conjunction with use of appropriate variables, allows automation of large numbers of runs (see next section). There are two scanners and two parsers, one for the main Plexus language and one that reads stimulus primitives during the simulation proper. The scanners are generated with the "flex" scanner generator tool (flex is a lex compatible scanner generator, however, Plexus uses some flex extensions that are not backward compatible to lex type scanner generators). This tool is freely available under the GNU Public License. The parsers can be generated by any yacc compatible parser generator. Thus, Plexus can run on any operating system that supports the standard C library and on which flex and a yacc compatible parser generator are supported. (Some features may not be available on all operating systems.) Plexus has been compiled and run on SunOS, Solaris, Linux, Dec OSF and Windows.

Each neuron in the network is described by small system of ordinary differential equations, with one state variable for the membrane potential and three for each type of slow synaptic transmission defined. The numerical integration method used is Euler forward which is stable in the physiological range of parameters and sufficiently accurate given the nature of the model.

2.5 Parameter space searching

It is nearly always necessary to explore model behaviour over a range of values for one or more parameters. In some cases there will be small regions of parameter space in which network behaviour changes qualitatively (that is at a bifurcation) and so parameter values need to be finely spaced. There is a combinatorial explosion as the number of parameters increases and as the spacing of parameter values decreases. This presents two issues, managing the large number of individual runs involved and the CPU time required. A substantial fraction of the compute resources used in this work were provided by the Ormond High Performance Computer Facility, a joint venture between RMIT and Melbourne University. The particular facility used in the later part of this study was a "farm" of 16 Digital 600au workstations. In addition a dual processor Intel PC running linux was available. The Intel processors and the Dec processors were approximately the same speed.

Managing the large number of runs over this heterogeneous network was done using a simple batch queueing system written by the author. Servers ran on each of the target processors and communicated with a central controller. Commands were issued to the controller which in turn passed them on to a server when it became available. In some cases 200 or more jobs were need for one parameter space search. These commands were generated by other scripts. A single run might take between 3 and 48 hours. A batch run over 18 processors can take from a few hours to several days.

Chapter 3

A model of second messenger mediated slow excitatory post-synaptic potentials

3.1 Introduction

The very first intracellular recordings of enteric neurons identified a class of neuron in which synaptic events appeared to be absent [Nishi and North, 1973, Hirst et al., 1974]. This lead to the suggestion that this class of neuron represented the intrinsic sensory neurons. It is a historical curiosity that these neurons do actually receive synaptic inputs [Wood and Mayer, 1978] and they are also sensory neurons [Kunze et al., 1995, Bertrand et al., 1998, Kunze et al., 1998]. There are some reports that they do have fast excitatory postsynaptic potential (EPSP) like depolarisations in response to exogeneously applied agonists [Mawe et al., 1986], but most investigators do not see fast EPSPs under physiological conditions. Slow EPSPs, on the

other hand, are readily seen in sensory neurons [Johnson et al., 1980, Morita and North, 1985, Kunze et al., 1993]. Slow transmission has been directly confirmed as occurring between sensory neurons [Kunze et al., 1993]. The distinguishing feature of slow transmission is the duration of the membrane response which significantly outlasts the stimulus and can last from several seconds [Morita and North, 1985] to hours [Clerc et al., 1999] in guinea-pig ileum. Slow EPSPs change membrane potential predominantly by closing a K^+ conductance, and also in some cases, by opening a Cl^- conductance [Bertrand and Galligan, 1994]. There has been only one experimental study of the input/output properties of slow EPSPs [Morita and North, 1985]. It showed that, in response to fixed frequency electrical stimulation to internodal strands, the amplitude and duration of the depolarisation are less than linear in the number of pulses for large numbers of pulses, although the output might be more than linear for small numbers of pulses [Bornstein et al., 1984b].

The key features of slow EPSPs — long duration and nonlinear summation — present an immediate problem of how they should be modelled. The usual model of synaptic transmission is to initiate a stereotyped time course conductance change in the postsynaptic membrane for each event, with conductance of multiple events being the sum of the conductance from the individual events [Bornstein et al., 1997, Thomas et al., 1999]. Simply increasing the duration of a linearly summed conductance event will not work, because the event significantly outlasts the stimulus so that even a low input rate will mean that multiple events will be active concurrently. These events will sum linearly at the level of conductance and they will be rate limited at the level of the membrane potential as the membrane potential approaches the driving potential of the synaptic conductance. This is unrealistic for at least

three reasons. Firstly, this will lead to very large membrane conductances which will shunt other membrane effects. Secondly, the resulting depolarisation will be much larger than the observed depolarisation. Thirdly, slow EPSPs are mainly mediated by a reduction in conductance. It is therefore necessary to develop a more plausible model of slow EPSPs.

The first aim of this study was to produce a robust deterministic model of the activation, inactivation and summation of second messenger mediated slow EPSPs in enteric neurons. The second aim was to ensure that the resulting model is simple enough to be incorporated into a network simulation of tens of thousands of neurons. To achieve the former aim, a system of equations was derived based as closely as possible on the physical processes underlying generation of the slow EPSP. To meet the latter aim, the equations were simplified as follows. First, the simplest kinetics which produced a realistic output were used [Destexhe et al., 1994]. Second, all diffusion was ignored. Finally, multiple, short time scale events, on the order of 100 times faster than the output of the model, were collapsed into single events [Destexhe et al., 1994, Lamb, 1996]. Unfortunately, many of the biochemical processes that underlie the generation of slow EPSPs in enteric neurons are only known in general, thus a model of the slow EPSP would have many unknown parameters and weak predictive powers. However, by constructing a model which encapsulates the current knowledge of the system and simplifies it, a smaller number of parameters can be generated. These parameters can then be set by comparing the output of the model to experimental data. From the system identification point of view, this might be considered a "gray box" model [Ljung, 1999]. The model structure is inspired by physical insight, however it still has many unknowns that can only be filled in with

experimental data.

Historical background

The initial motivation for this study was to improve an existing model of the slow EPSP used in a large scale computer simulation of the ENS in the guinea-pig small intestine [Bornstein et al., 1997]. Myenteric neurons, which are primarily responsible for the movements of the intestine such as the complex motor behaviours that occur during peristalsis [Furness and Costa, 1987], were studied. The interactions between sensory neurons and higher order neurons are known to be, at least in part, via slow EPSPs [Kunze et al., 1998]. These events are well characterised in terms of the neural input required to generate them and their importance in reflexes is well documented, although not fully understood [Kunze and Furness, 1999]. In the Bornstein et al. [1997] study, slow synaptic input drove an internal stage, representing a concentration of a diffusible, second messenger-like substance. Once the internal stage exceeded a given threshold, the conductance change underlying the slow EPSP was triggered. The value of the internal stage followed a fixed time course for each synaptic event and was summed linearly for multiple events. The conductance change on the other hand was an "all or nothing" response in that it was independent of the exact nature of the input and further input events did not sum. These simulations demonstrated that transmission via slow EPSPs could explain the latencies of reflex responses evoked by physiological stimuli. The simulation also predicted that transmission of this sort would produce a high degree of temporal correlation in firing between neurons well away from the stimulus area [Bornstein et al., 1997, Thomas et al., 1999]. However, this correlation might be ex-

plained by the lack of graded responses in both the onset and amplitude of the slow EPSP. In order to test further whether correlated output is a real network property, a more physiologically realistic model of the slow EPSP was required.

The slow EPSP in myenteric neurons

Several slow EPSPs evoked in a single myenteric neuron are shown in Figure 3.1. The slow EPSP in panel *A* was evoked by a 1 second, 20 Hz train of stimuli to the presynaptic nerve fibres. In general, slow EPSPs in myenteric neurons can be evoked by brief trains of 1 to 40 Hz stimulation (as in Figure 3.1*C–D*), have a long latency ($>$ 100 ms) and long duration (seconds to minutes) [Morita and North, 1985]. For increasing numbers of presynaptic stimuli at a fixed frequency or for a fixed number of stimuli at increasing frequencies, the amplitude of the slow EPSP will initially increase, but eventually reaches a plateau, typically resulting in a 10–20mV depolarisation [Morita and North, 1985]. Under these same conditions, the duration of the slow EPSP will continue to increase [Clerc et al., 1999]. The slow EPSP always significantly outlasts the stimulus period.

The depolarisation associated with the slow EPSP is primarily due to closure of resting potassium conductances (g_K and $g_{K,Ca^{++}}$) [Akasu and Tokimasa, 1989, Bertrand and Galligan, 1994]. There is strong evidence that slow EPSPs are mediated by the mobilisation of intracellular second messengers which, ultimately, cause the observed changes in membrane conductances. Tachykinins, such as substance P, mimic the slow EPSP [Katayama and North, 1978, Morita and Katayama, 1992, Galligan et al., 1987] and have been shown to cause accumulation of cyclic 3', 5' adenosine monophosphate (cAMP) [Baidan et al., 1992]. Activators of adeny-

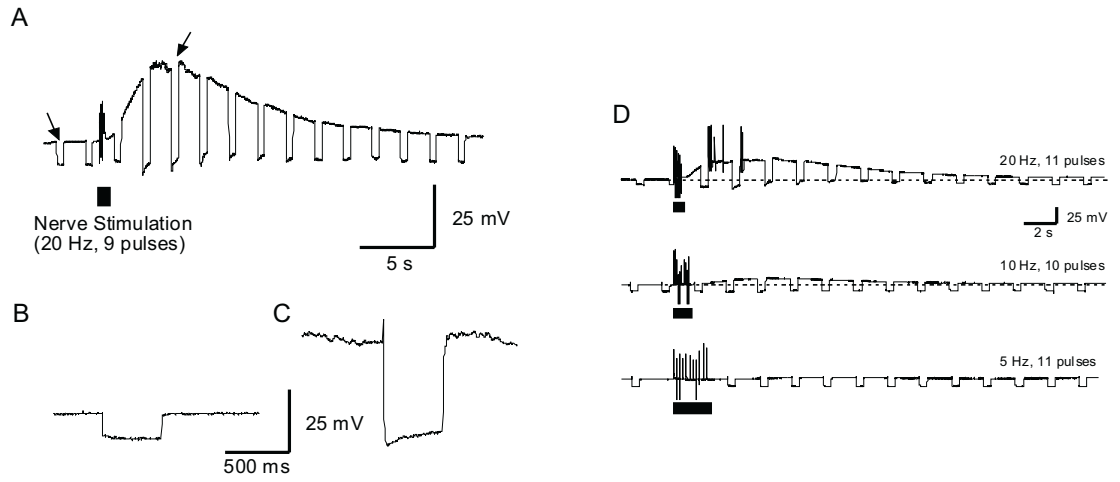

Figure 3.1: This figure shows a voltage trace of a slow EPSP obtained from an intracellular voltage recording from a myenteric neuron. *A*. The complete time course of the slow EPSP is shown. The downward deflections in the voltage trace are due to hyperpolarising current pulses passed through the recording electrode every 2 seconds in order to measure the input resistance of the cell before and during the slow EPSP. Stimulation of the presynaptic nerve fibers are indicated by the solid bar, note the stimulus artifacts. The arrows indicate the positions from which the enlarged traces in *B*. and *C*. were taken. *B*. The voltage deflection in response to a -100 pA current pulse before initiation of the slow EPSP. The small voltage deflection shows that the resistance is low. *C*. An identical hyperpolarising current pulse given near the peak response of the slow EPSP. The resistance is high; this coupled with the large depolarisation indicates that a potassium conductance has decreased. Note, the sag seen in the voltage deflection is due to an I_H. *D*. Slow EPSPs elicited by 10 or 11 pulse stimuli at 5, 10 and 20 Hz in the same neuron, the dashed line indicates the position of the resting membrane potential (approximately -70 mV). As the stimulus frequency is increased from 10 to 20 Hz, there is large increase in amplitude of slow EPSP. The upward deflections at the peak of the 20 Hz slow EPSP are truncated action potentials. Compared to other neurons, this neuron required higher stimulus intensities to evoke a slow EPSP (see Figure 3.7).

late cyclase, such as forskolin, also cause slow EPSP-like membrane depolarisations [Nemeth et al., 1986, Bertrand and Galligan, 1995]. The receptors mediating the slow EPSP and the tachykinin responses are coupled through a pertussis toxin-insensitive G-protein [Bertrand and Galligan, 1995]. The end point appears to be inhibition of g_K via a phosphorylation event [Bertrand and Galligan, 1995, Pan et al., 1997]. Alternative pathways and/or interactions between G-proteins and second messengers are also supported by some of these data [Bertrand and Galligan, 1995, Ross, 1989, Clapham and Neer, 1997, Guard et al., 1988]. For example the NK3 tachykinin receptor, which mediates some slow EPSPs in myenteric neurons [Alex et al., 2001], appears to couple to the inositol trisphosphate pathway [Guard et al., 1988]. These pathways are less well described in myenteric neurons and so have not been modelled here.

3.2 Methods

The model

The major components of the pathway that was modeled are illustrated in Figure 3.2. After activation of the receptor, there are three distinct stages that can be identified: the first stage, depicted on the left (Figure 3.2, stage 1) starts with the activated G-protein coupled receptor, and ends with the production of the second messenger, cAMP. The second stage, in the middle, relates only to the activation of protein kinase A, while the final stage, on the right, relates to the phosphorylation and closure of a potassium channel.

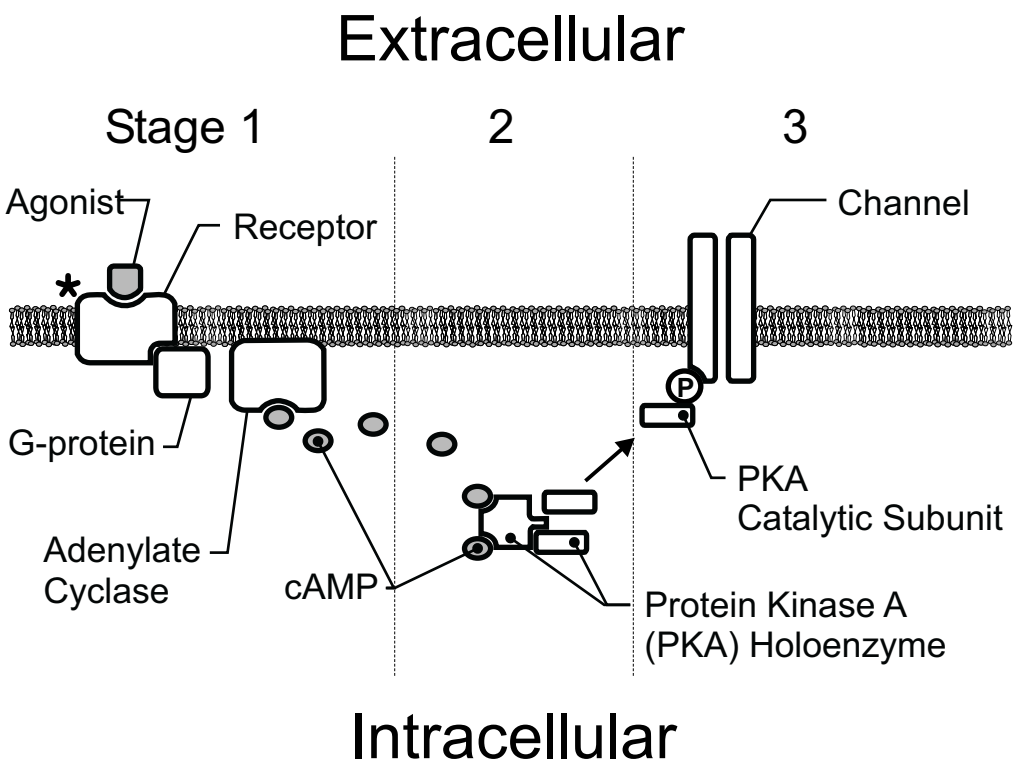

Figure 3.2: A schematic of the major steps involved in the cAMP second messenger system believed to be responsible for the slow EPSP in myenteric neurons. Stage 1 (panel 1). Agonist binds to the receptor and activates it (denoted by the *). The activated receptor then activates membrane bound G-proteins which dissociate and activate adenylate cyclase which then catalyses the production of cAMP. Stage 2 (panel 2). Several molecules of cAMP bind to the protein kinase A (PKA) holoenzyme which releases two catalytic subunits. Stage 3 (panel 3). The catalytic subunits phosphorylate channels (indicated by the P) and decreases their probability of opening.

The model input

The release of transmitter from the presynaptic nerve terminal, its diffusion across the synaptic cleft and its binding to the receptor are not modeled *per se*, but are described by the function, $L(t)$. When the input is individual synaptic events, the amount of time that the agonist is present and bound to receptor is very small compared to the time course of the slow EPSP so the shape of $L(t)$ does not matter and can be approximated as a series of Dirac delta functions [Bennett and Gibson, 1995, Destexhe and Sejnowski, 1995]. For example, for a series of action potentials occurring at times $\{t_i\}$

$$L(t) = \sum_i \rho_i \delta(t - t_i) \tag{3.1}$$

where ρ_i would represent relative synaptic strengths, absolute synaptic strength can be scaled into the final parameter α, see below.

First Stage

The first stage of the model describes the linear production and removal of cAMP (Figure 3.2, stage 1). The slow rate of production and removal of cAMP dominates the kinetics of this stage, thus the early reactions in the cascade are not included. Reactions involving cAMP typically last many seconds [Buxbaum and Dudai, 1989, Hille, 1992, Hempel et al., 1996] while those involving activation of G-proteins often only last tens to hundreds of milliseconds [Lamb, 1996, Torre et al., 1995]. The receptor activates the G-protein which can inactivate quickly. Both the receptor and the G-protein were assumed to inactivate independently of other substances and with first order kinetics. The rate of production of cAMP is proportional to the amount

of active adenylate cyclase, which in turn, is proportional to the amount of activated G-protein. Thus, the linear rate of activation of receptor leads directly to the linear rate of cAMP production. As with diffusion of transmitter, the diffusion of cAMP is not modeled. The cAMP is removed by the actions of a cAMP phosphodiesterase (PDE). It was assumed that the rate of removal of cAMP is proportional to the amount of cAMP present (see — Discussion). This leads to the equation

$$\frac{dD}{dt} = \alpha_1 L(t) - \beta_1 D \tag{3.2}$$

where D is the amount of diffusible second messenger (i.e., cAMP), $L(t)$ is the amount of agonist, α_1 is the rate constant for production of D and β_1 is the rate constant for the removal of D.

Second Stage

The second stage of the model covers events following the production of cAMP through to the activation of protein kinase A (PKA) (Figure 3.2, stage 2). The PKA holoenzyme is composed of two tightly bound regulatory subunits and two catalytic subunits. In this instance, second order kinetics were assumed as an approximation of the interactions of two molecules of cAMP with each of the two regulatory subunits [Buxbaum and Dudai, 1989] (see Model Variations, below). Furthermore, the amount of cAMP is assumed to be small compared to the amount of PKA and so the reaction is not limited by the amount of PKA. Thus, the rate of accumulation of the disassociated catalytic subunit is proportional to the square of the amount of second messenger. The catalytic subunits rebind with PKA independently and hence their rate of removal is assumed to be proportional to the amount of catalytic

subunit present (see — Discussion). This leads to

$$\frac{dC}{dt} = \alpha_2 D^2 - \beta_2 C \tag{3.3}$$

where C is the amount of catalytic subunit (the second stage reactant), α_2 is the rate constant for the production of the catalytic subunit and β_2 is the rate constant for the removal of C.

Third Stage

The final stage of the model describes phosphorylation of potassium channels (Figure 3.2, stage 3). A simplification was made by assuming that the channel has only one phosphorylation site and that phosphorylation causes a direct transition from an open conducting state, to a closed non-conducting state (see — Discussion). The rate of phosphorylation is proportional to both the amount of catalytic subunit and to the amount of unphosphorylated channel. Thus the reaction is rate limited by the number of channels available. The rate of dephosphorylation of the channel protein (which is carried out by protein phosphatases) is assumed to be proportional to the number of phosphorylated channels. Any variation in the activity of protein phosphatases has not been modelled as a part of this system. This gives

$$\frac{dP}{dt} = -\alpha_3 CP + \beta_3(1 - P) \tag{3.4}$$

where P is the relative amount of unphosphorylated channel, α_3 is the forward rate constant and β_3 is the rate constant at which channels return to the unphosphorylated state. The total conductance is simply the product of the maximum conductance and the relative amount of open channel.

If the total conductance change is small compared to the total membrane conductance, and there are no other active conductance changes, then the relative voltage change, r, will be equal to $1 - P$. In general, the conductance change is large compared to the passive membrane resistance (see Figure 3.1) so $r < 1 - P$. But as the slow EPSP evolves, voltage dependent conductances increase and other non-cAMP pathways also increase conductances [Bertrand and Galligan, 1994], which serve to increase the estimate for r. Thus, in what follows $r = 1 - P$. This produces better fits to electrophysiologically recorded data than calculating r assuming no other conductance changes.

Although the model has three forward rate constants, $\alpha_{\{1,2,3\}}$, the third stage, $P(t)$, depends only on the combination $\alpha_1\sqrt{\alpha_2\alpha_3}$. Furthermore, only the third stage will be fitted to data so redundant parameters can be eliminated. Therefore, the following substitutions were made

$$\begin{aligned} C &\rightarrow \frac{C}{\alpha_3} \\ D &\rightarrow \frac{D}{\sqrt{\alpha_2\alpha_3}} \\ \alpha_1 &\rightarrow \frac{\alpha}{\sqrt{\alpha_2\alpha_3}} \end{aligned} \tag{3.5}$$

to remove α_2 and α_3. This leaves four independent parameters — α, β_1, β_2 and β_3. The first parameter can be thought of as a coupling constant, gain or amplification factor. The three remaining parameters determine the rate of decay of the three stages. If no substance is present in the proceeding stages then the i^{th} stage will decay with a halflife given by $\ln(2)/\beta_i$. When no agonist is present there is one equilibrium, which is stable, at $D = 0$, $C = 0$, $P = 1$ representing no substance in the first two stages and the channel protein completely unphosphorylated. The

relationships between time courses of the three stages are illustrated in Figure 3.3; the seed parameter, 0.1, was used.

Properties of the model

For illustrative purposes two special cases of $L(t)$ are considered. The first is a brief high frequency input, where the duration of the input can be considered small. In this case

$$L(t) = A\,\delta(t) \tag{3.6}$$

where A is a measure of the strength of the stimulus. To simplify, only the case $\beta_1 = \beta_2 = \beta_3 \equiv \beta$ is considered. The constants $\beta_{1,2,3}$ have been assumed to be of similar magnitude so this special case will be qualitatively similar to the more general case. The solution is

$$D(t) = \alpha A \exp(-\beta t) \tag{3.7}$$

$$C(t) = \alpha A t \exp(-\beta t) \tag{3.8}$$

$$1 - P(t) = \int_0^t \exp(\int_0^s (\beta + C(u))du)ds \tag{3.9}$$

The last equation can simplified by converting time to units of $1/\beta$ and absorbing constants into A. This gives the expression

$$1 - P(t) = \frac{1}{f(t)} \int_0^t C(s) f(s) ds$$

where $C(t) = At\exp(-t)$ after rescaling and

$$f(t) = \exp(\int_0^t 1 + C(s)ds)$$

This equation was solved numerically and the qualitative stimulus response curve is plotted in figure 3.4, panel A and the time to peak and time to half decay are

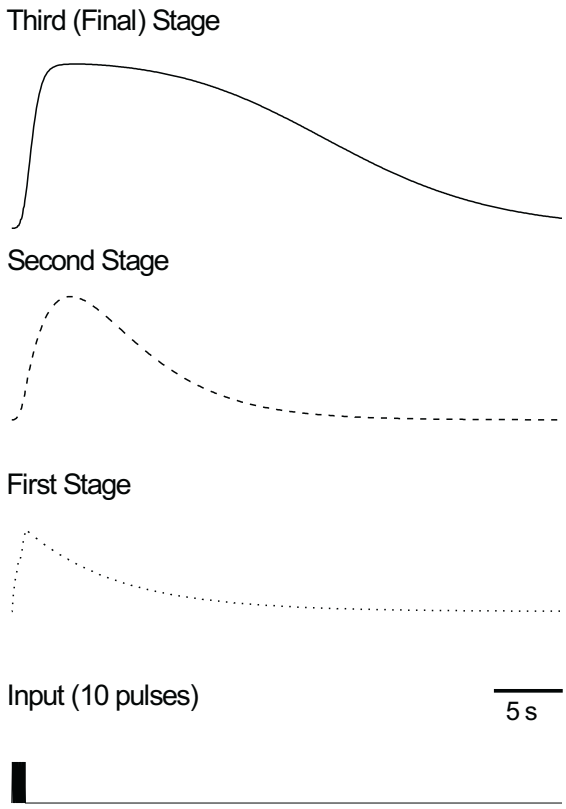

Figure 3.3: The relationship of the time dependent change of the three stages of the model. The model input (bottom trace) is a train of 10 pulses at 10 Hz. The different stages are scaled arbitrarily. The third, and final, stage (top trace) represents the closure of potassium channels and is comparable to the waveform of the slow EPSP. The intermediate traces represent the time courses of the internal stages of the model (stages 1 and 2), which were not directly compared to experimental data. All parameters used to generate these data were at the seed values of 0.1.

plotted in panel B.

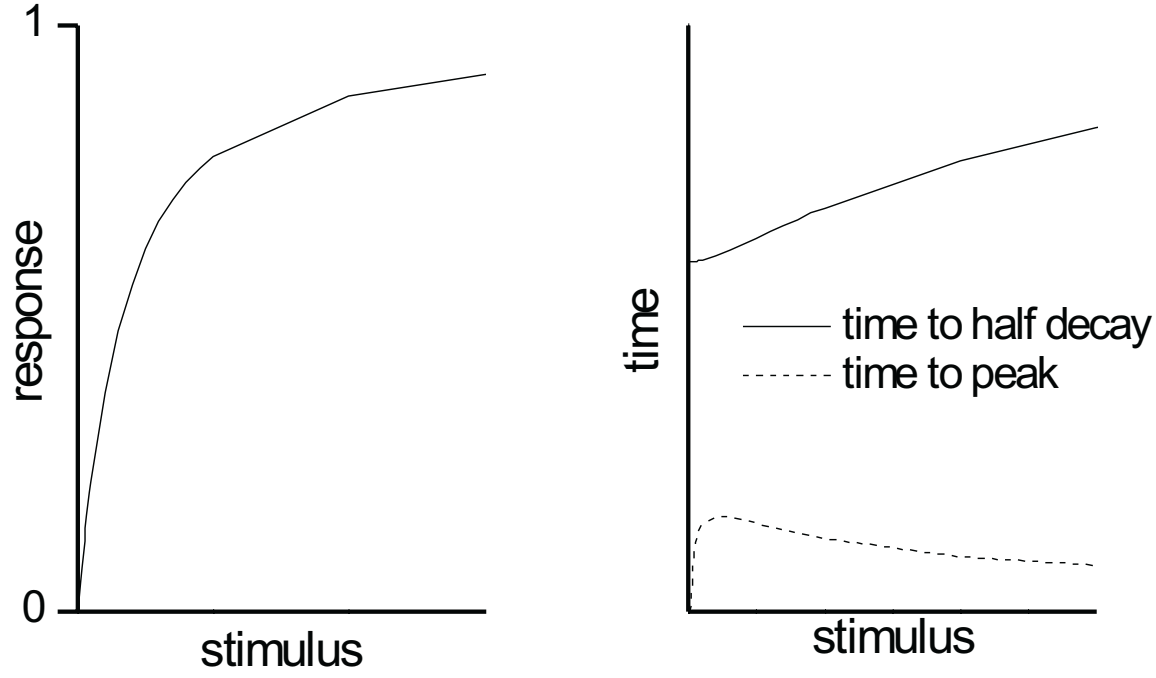

Figure 3.4: *A.* This is the qualitative stimulus response curve for the slow EPSP model, where the stimulus is a very brief pulse train and the response is relative to the maximum response. *B.* The time to peak and the time to half decay (in units of $1/\beta$ are plotted as a function of the stimulus strength. The time peak rises very quickly initially and so appears to start at a non zero value.

The second special case is response to constant input after the system has come to equilibrium. Now $L(t)$ can be approximated as

$$L(t) = A \tag{3.10}$$

where, again, A is a measure of the strength of the input. Ignoring the initial

transient period, as $t \rightarrow \infty$, the derivatives approach zero and the solution is

$$D = \frac{\alpha A}{\beta_1} \tag{3.11}$$

$$C = \frac{1}{\beta_2}(\frac{\alpha A}{\beta_1})^2 \tag{3.12}$$

$$1 - P = \frac{A^2}{A^2 + K} \tag{3.13}$$

where $K = (\beta_1^2 \beta_2 \beta_3)/\alpha$. Thus the steady state response shows a Michaelis-Menton like stimulus response curve.

3.3 Results

Model output

The equations (3.2, 3.3 and 3.4) derived above consist of three stages, with second order kinetics in the second stage and first order kinetics in the others (3 stage/2$^{\text{nd}}$ order). The output of these equations was characterized using values for the parameters obtained by fitting an experimental dataset (see below - Morita and North [1985]). In figure 3.5, various patterns of fixed frequency or number of synaptic inputs are shown. Figure 3.5A shows a family of simulated slow EPSPs produced by fixed duration stimuli, but with varying numbers of pulses while in B, the simulated slow EPSPs are produced in response to varying durations of the train of stimuli, but with the number of pulses held constant. Figure 3.5C show stimulus response curves with the peak amplitude of the simulated slow EPSP plotted versus the number of pulses for a range of frequencies.

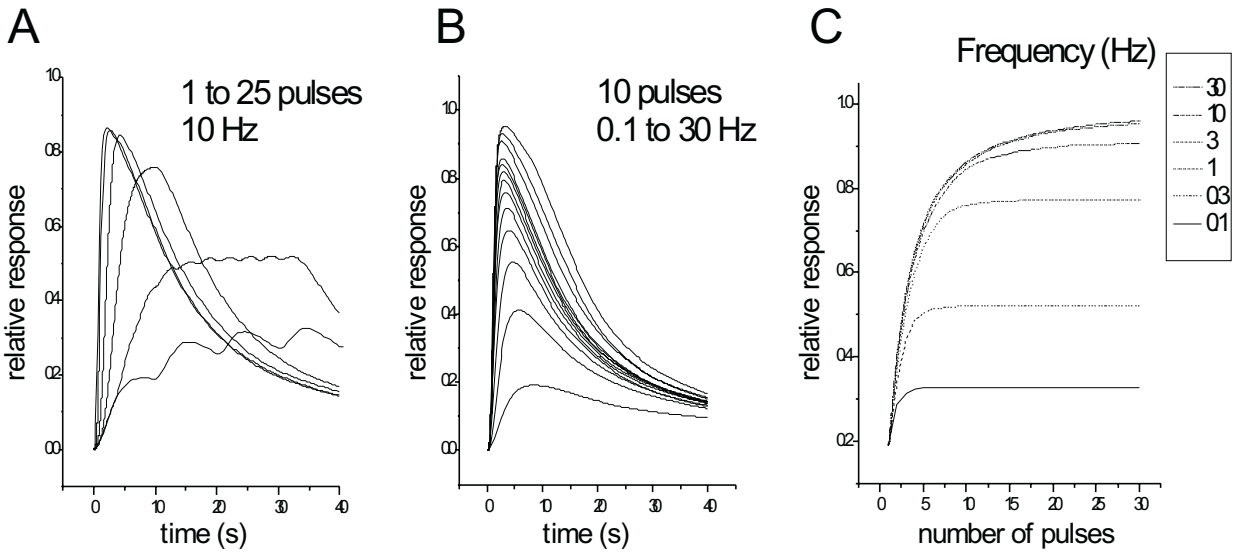

Figure 3.5: Waveforms generated by the model for a variety of inputs all with a fixed duration of 3 seconds. *A*. Each waveform is a full time course response for a fixed frequency of 10 Hz and a variable number of pulses. The peak duration increases as a function of the number of pulses. The sequence illustrated is from 1 to 10 Hz, and then 15, 20 and 25 Hz. *B*. Each curve is a full time course response for a fixed number of pulses (10) with different frequencies. The sequence illustrated is from 0.1 to 30 Hz in half log steps. The curve for 0.1Hz has been truncated at the fourth pulse. *C*. Composite graph showing how the peak response changes as a function of the number of pulses (on the abscissa) and the frequency (different lines). Frequencies from 0.1 to 30 Hz and from 1 to 30 pulses are illustrated. The dotted line indicates the position into which data represented in panel A and B were incorporated. The parameters used to illustrate this figure are from a 3 stage, 2^{nd} order model, fit to the Morita and North [1985] data; $\alpha = 0.30\text{s}^{-1}$, $\beta_1 = 0.51\text{s}^{-1}$, $\beta_2 = 0.73\text{s}^{-1}$ and $\beta_3 = 0.18\text{s}^{-1}$. These data also appear in Table 3.1.

	3/1 TR	3/1 MN	3/2 TR	3/2 MN
α	0.28	0.11	0.22	0.30
β_1	0.37	0.54	0.41	0.51
β_2	0.28	0.47	0.27	0.73
β_3	0.13	0.24	0.12	0.18

Table 3.1: The final parameters (α, $\beta_{\{1,2,3\}}$) in s^{-1}, for the Morita and North [1985] data (MN) and for the average trace data (TR) for the three stage model with either first (3/1) or second (3/2) order kinetics in the second stage. Parameters for TR are averages from 7 neurons.

Comparison to experimental data

The ability of the model to reproduce experimental data from two independent datasets was examined. The first was from Morita and North [1985] and consisted of peak relative response and time to half decay data for a variety of fixed frequency inputs in myenteric S neurons. The second dataset was generated for this study, by Dr Paul Bertrand, and consisted of the complete time courses of slow EPSPs from 7 myenteric S neurons.

Methods

For both datasets the input, $L(t)$, was approximated using Equation (3.1) with $\rho_i = 1$. The first differential equation was solved analytically and the remaining stages solved using the fourth order Runge-Kutta method with adaptive time step [Press et al., 1992]. Fitting parameters to data required minimisation of an error term (see

below), these minimisations were performed using Powell's algorithm [Press et al., 1992]. All fitting parameters were seeded at a value of 0.1; values of greater then 1 seemed to cause the fitting session to become unstable, with all parameters increasing indefinitely. In general, the solution to Equations (3.2) – (3.4) involves complex combinations of exponential terms for which the three time constants need to be determined. This is a difficult problem [Acton, 1970], which is characterized by being computationally expensive to solve, and by generating a wide range of parameters that fit the data almost as well. Codes were written in the C programming language. Data for Figures 3.3 and 3.5 were generated using the Linux version of Octave 2.0.5, which uses the LSODE package for differential equation integration. Octave is freely available from the internet at `http://www.che.wisc.edu/octave/`.

For the peak relative response and time to half decay from Morita and North [1985], the error term was calculated as follows: for each observation (i.e. for a given stimulus) in the experimental dataset, Equations (3.2) – (3.4) were solved (as in figure 3.5) and the relative peak response and time to half decay were extracted (as in figure 3.6). The error, as a function of the parameter set (α, β_1, β_2, β_3), was then calculated as

$$E(\alpha,\beta_1,\beta_2,\beta_3) = \sum_i \left(\frac{\tau_i - \tau(s_i,\alpha,\beta_1,\beta_2,\beta_3)}{\tau_i}\right)^2 + \sum_i \left(\frac{r_i - r(s_i,\alpha,\beta_1,\beta_2,\beta_3)}{r_i}\right)^2 \quad (3.14)$$

where s_i represents the i^{th} stimulus, τ_i and r_i represent the observed times to half decay and peak responses and $\tau()$ and $r()$ represent the model predictions for a particular parameter set. Since the two error terms are normalised, they give approximately equal contribution to the error. This summed value represents the

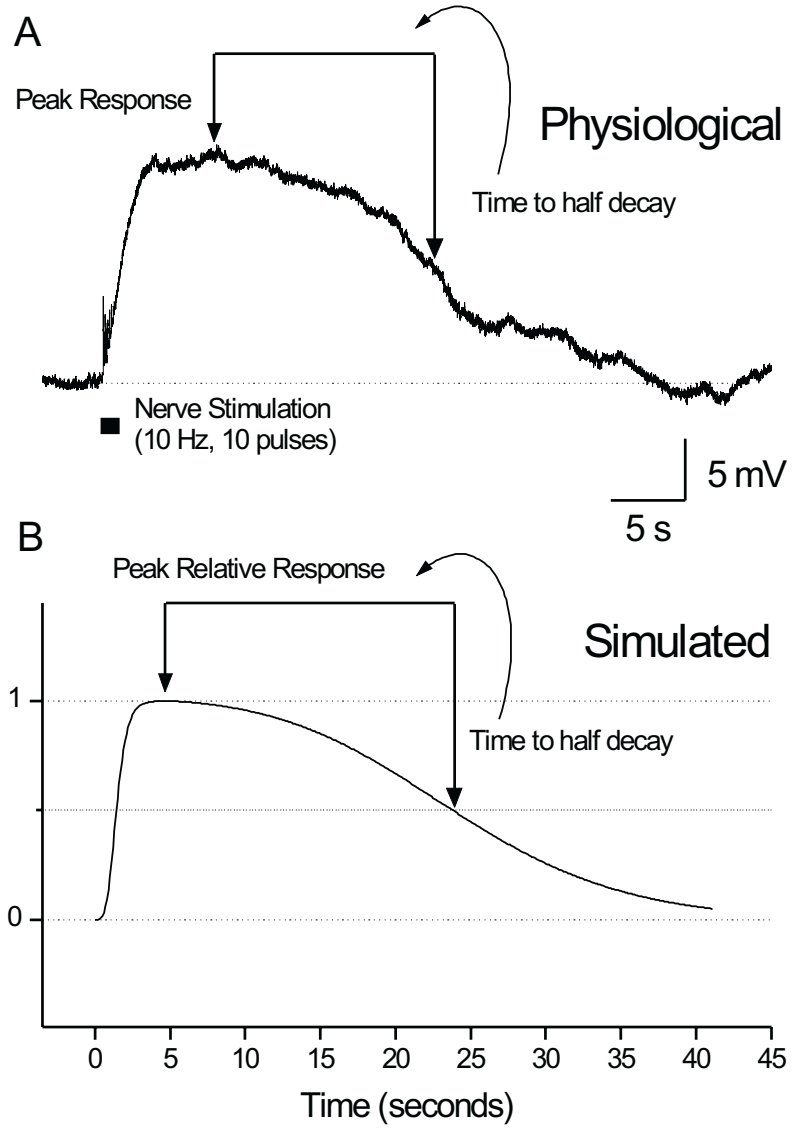

Figure 3.6: Features of the slow EPSP that were fitted by the model. *A*. A voltage trace from a myenteric neuron showing a slow EPSP evoked by stimulation presynaptic nerve fibers (at the bar), note the stimulus artifacts in the voltage trace. The peak amplitude and time to half-decay (as measured from the peak) of the slow EPSP are marked by the arrows. *B*. Simulated slow EPSP with the peak amplitude and time to half-decay marked by the arrows. The parameters derived for this fit for a 3 stage, 2^{nd} order model were $\alpha = 0.17\text{s}^{-1}$, $\beta_1 = 0.19\text{s}^{-1}$, $\beta_2 = 0.38\text{s}^{-1}$ and $\beta_3 = 0.21\text{s}^{-1}$. These data are part of the average data in Table 3.1. Interestingly, 2 other slow EPSPs from this cell were fit by very similar parameters.

"goodness of fit" for the current values of the parameters.

The individual trace data from 7 neurons were defined by a sequence of n experimental points, $\{t_i, V_i\}$. The error, as a function of the parameter set (α, β_1, β_2, β_3), was then calculated as

$$E(\alpha, \beta_1, \beta_2, \beta_3) = \sum_i (\frac{V_i}{V_{\max}} - r(t_i, \alpha, \beta_1, \beta_2, \beta_3))^2 \tag{3.15}$$

where $V_{\max} = \max V_i$ and $r()$ is the model prediction for a given time and parameter set.

Fitting the peak response and half life dataset

The data of Morita and North [1985] represents the most thorough investigation into the input/output relationship for slow EPSPs in the ENS. Their protocol consisted of evoking slow EPSPs with a constant frequency stimuli in the range of 1 to 30 Hz with a train duration of 3 seconds. Stimulus pulse duration and voltage were held constant. Figure 3.6 shows how the maximum amplitude and the time to half decay are defined. In general, slow EPSPs can show significant variation from cell to cell and this is particularly apparent in the time to half decay data from Morita and North [1985].

The results of simultaneously fitting both the time to half decay and relative peak response data to a 3 stage, 2^{nd} order model are shown in Figure 3.7 (also, see below - Model Variations). The parameter values found for the curves shown are $\alpha = 0.30\text{s}^{-1}$, $\beta_1 = 0.51\text{s}^{-1}$, $\beta_2 = 0.73\text{s}^{-1}$ and $\beta_3 = 0.18\text{s}^{-1}$; these data also appear in Table 3.1. The last three parameters are the decay constants for the three stages. The fact that they are all within an order of magnitude of each other indicates that

the kinetics of at least three stages seem to be important in determining the overall properties of the system. The first parameter, α, is an amalgam of many physical parameters and so does not have a direct interpretation; it is proportional to the time the agonist spends bound to the receptor, to a term involving the forward rate constants for each of the three stages and to the amount of agonist released at each connection.

Fitting full time course data

The equations were also fitted to a second set of data, a limited number of slow EPSPs from 7 myenteric S neurons whose stimulus parameters and time courses were determined experimentally for this study (see Bertrand and Galligan [1994] for details of electrophysiology). In each case, the stimulus was a 1 second train of identical pulses applied to an inter-nodal nerve strand at 10 Hz. These slow EPSPs showed a 2 to 3 fold variation in time to half decay, with a much smaller variation in peak amplitude and in the time to peak. Fitting was carried out as follows. Because the recorded waveforms included membrane events, such as action potentials, fast EPSPs and responses to current injections, a small number of points (13 to 25), including a point at or near the peak response, were manually extracted from each trace at times when no obscuring event occurred. To allow calculation of error terms, these data were then converted to relative responses and normalized to 1. The fitting was then carried out as described in the methods section.

Figure 3.8 shows an example of two slow EPSPs, each of which has been fitted by the model (including those from - Model Variations), and the parameters used. In general, the 3 stage, 2^{nd} order model can be well fitted to the decay phase of

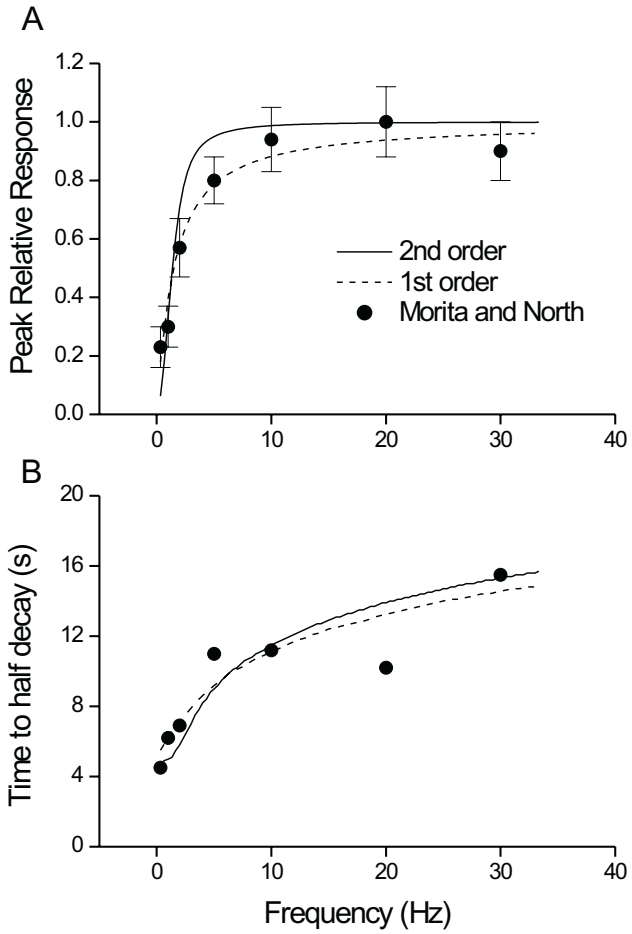

Figure 3.7: Real data were used to calibrate the internal parameters. Data from studies by Morita and North [1985] (shown in the filled circles) consisted of the peak response and time to half decay of the slow EPSP for a range of stimulus frequencies. These data were fit using a least squares, error minimisation method. Best fits using first and second order kinetics in the second stage are shown (with the dashed and solid lines respectively). In both graphs the abscissa is the frequency for a 3 second stimulus pulse. *A*. Peak relative amplitude. Both models fit these data well, but the 3 stage, 2^{nd} order model showed a tendency to saturate more quickly. *B*. Time to half-decay (seconds). Both models fit these data well.

the recorded waveform. This is not surprising as the decay phase in the model is largely controlled by three rate constants, $\beta_{\{1,2,3\}}$. The model is not always able to match the time to peak of the waveform, or the rate of rise. This is because the rising phase is controlled by a single rate constant, α, which also controls how much second messenger is generated in the first stage and hence the peak response. The parameters for all of the traces averaged together can be found in Table 3.1 (including those from section 3.3), while parameters for the individual traces are in Table 3.2. Interestingly, the final parameters for the 3 stage, 2^{nd} order model on the Morita and North [1985] dataset and for the full time course dataset are very similar, with a substantial difference only in the value of β_2.

	α	β_1	β_2	β_3
1	0.15	0.14	0.28	0.18
2	0.16	0.26	0.26	0.05
3	0.46	0.55	0.36	0.18
4	0.08	0.12	0.21	0.10
5	0.19	0.22	0.24	0.10
6	0.17	0.19	0.38	0.21
7	0.31	1.38	0.18	0.04
mean	0.22	0.41	0.27	0.12
STD	0.13	0.45	0.07	0.07

Table 3.2: The final parameters (α, $\beta_{\{1,2,3\}}$) in s^{-1}, for individual trace data (TR) for a three stage model with second (3/2) order kinetics in the second stage. The means and standard deviations (STD) for each parameter are listed at the bottom.

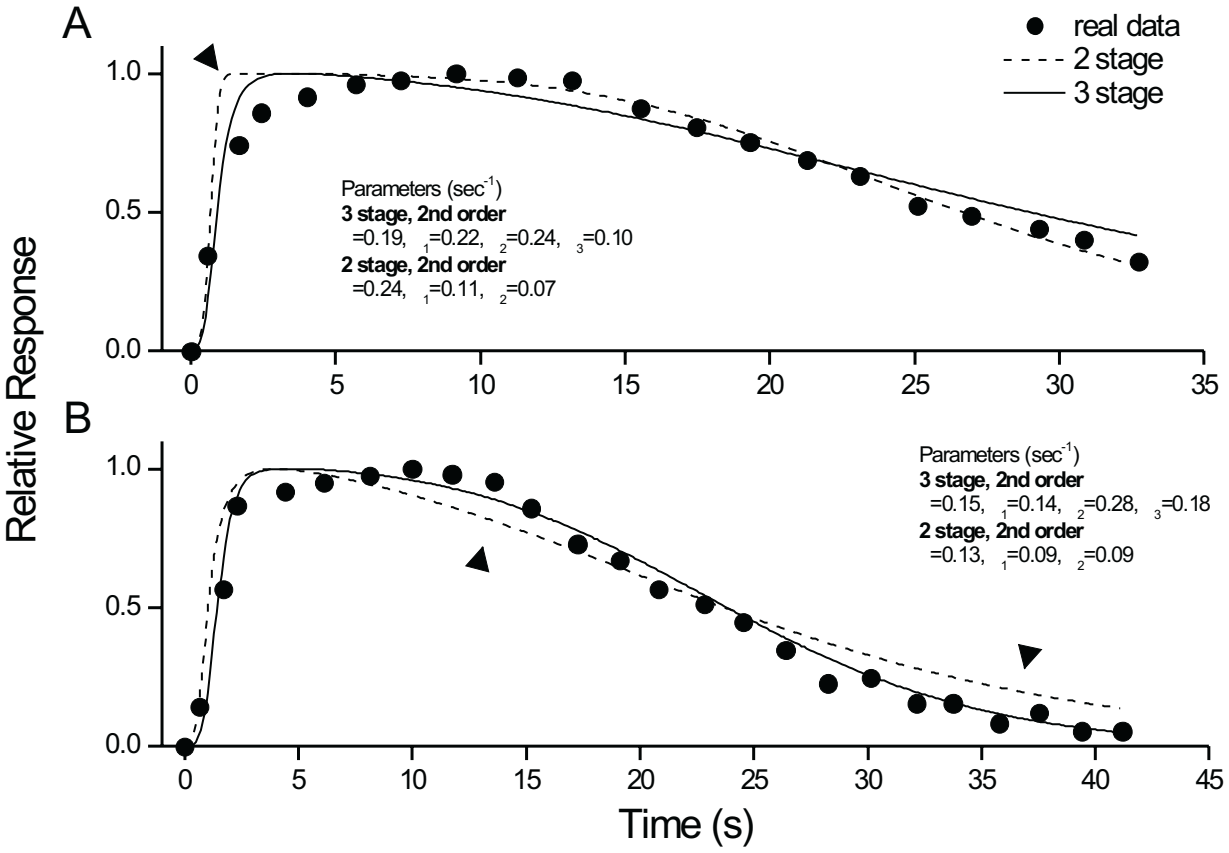

Figure 3.8: Graphs showing the output of the model fitted to two slow EPSPs from different enteric neurons; 7 neurons were fitted in all. Output from a two stage model, Equation 3.16 is shown in the dashed line, and the three stage model, equations 3.2–3.4 is shown in the solid line. The experimental data are shown as the filled circles. Only a small number of points from the recorded waveforms were used in the fitting process. The parameters derived for each fit are shown near the trace, these data are part of Tables 1, 2 and 3. *A*. In some cases the two stage model rose unnaturally quickly (arrow), apparently in an effort to match the decay phase of the recorded waveform. The three stage model was more constrained, and thus fit the rise and the decay reasonably well. *B*. Even when the rising phase of the 2 stage model fit as well as the 3 stage model, the decay phase was often poorly fit (arrows). Similar differences between the models were seen in the fits of the other 5 neurons. Adapted from Bertrand et al. [2000b].

Model variations

In the second stage of the model (which is described by Equation (3.3)), 2^{nd} order kinetics are used because two to four molecules of cAMP must bind simultaneously to the PKA regulatory subunits before the catalytic subunits are released [Builder et al., 1980, Buxbaum and Dudai, 1989]. The importance of this decision was determined by comparing a 3 stage, 1^{st} order model to the results obtained with the 3 stage, 2^{nd} order model (above). When fitted to individual waveforms from the full trace dataset, either model fit the data equally well (not shown). However, it might be expected that the order of the kinetics will be important in determining the stimulus response relationships. Figure 3.7 shows the comparison of 1^{st} and 2^{nd} order kinetics in the second stage. Figure 3.7*A* shows that the first order kinetics are able to fit the data better, especially for stimuli of intermediate strength, while the second order kinetics appear to have a larger range to the peak response. Figure 3.7*B* shows that both 1^{st} and 2^{nd} order kinetics are able to fit the time to half decay data equally well. The final parameters (shown in Table 3.1) for each model are also quite similar, with the largest differences in the values of α and β_2, as would be expected.

In writing down Equations (3.2) – (3.4) many assumptions were made about which reactions could be treated as single steps. Equations with more than three stages were not considered as this would introduce extra parameters. More parameters should make fitting the experimental data easier, but the model might then become too dependent on the data and thus have weaker predictive powers. A one stage system was also rejected immediately because in this case the agonist must

interact with the channel through a number of very rapid intermediate steps and, as soon as the agonist is no longer present, channels will start to re-open; i.e., the system would have no "memory". This is not compatible with the basic experimental observation that the peak response occurs well after the stimulus has ceased. A multi-stage system, on the other hand, "remembers" the stimulus as non-equilibrium concentrations of intermediate reaction products.

A two stage system, analogous to Equations (3.2) – (3.4), is

$$\begin{aligned} \frac{dD}{dt} &= \alpha_1 L(t) - \beta_1 D \\ \frac{dP}{dt} &= -\alpha_2 D^2 P + \beta_2 (1 - P) \end{aligned} \tag{3.16}$$

Note, this two stage model still incorporates the second order assumption (see above); a 2 stage, 1st order model was run (see Table 3.3) but qualitatively was not able to fit any of the datasets (not shown). In general, the 2 stage, 2nd order model was able to fit the peak response and half life data as well as the 3 stage, 2nd order model (not shown), but was less able to fit some of the individual trace data. Figure 3.8 shows two examples where the 2 stage, 2nd order model differed from the 3 stage, 2nd order model. The 2 stage model may rise too quickly (Figure 3.8*A*) or overshoot on the decay phase (Figure 3.8*B*). Alternately, the 3 stage, 2nd order model may also have trouble with the complex decay phase (Figure 3.8*A*).

	2/1 TR	2/1 MN	2/2 TR	2/2 MN
α	0.14	0.18	0.14	0.34
β_1	0.19	0.34	0.10	0.29
β_2	0.07	0.23	0.08	0.20

Table 3.3: The final parameters (α, $\beta_{\{1,2\}}$) in s^{-1}, as in Table 3.1, for the two stage model with either first (2/1) or second (2/2) order kinetics in the second stage. Parameters for TR are averages from 7 neurons.

Slow EPSPs with long latencies

The second messenger model described in section (3.2) predicts slow EPSP conductance changes with essentially no delay, however, in some electrophysiological experiments the latency to an apparent membrane potential change can be up to 12 s. An example is shown in figure 3.9 in which a slow EPSP evoked in an AH neuron, by a 1 second 20 Hz train of stimuli to the presynaptic nerve fibres. Once the membrane does start to depolarise it does so rapidly and this is not compatible with the slow onset mechanism described above or with a presynaptic mechanism, such as delayed transmitter release. No studies have been performed to determine whether the delay varies, but it seems reasonable to assume that the delay depends inversely on the stimulus. For example, with fixed frequency stimuli, the greater the number of pulses or the higher the frequency the shorter the delay. The model of section (3.2) assumed a single phosphorylation site on the channel. This model can be extended by assuming there are two sites and that the first has a much higher affinity than the second and that the channel only closes when both sites are phosphorylated. Intuitively, it would be expected that catalytic subunit will preferentially phosphorylate the first site initially and leave the second unbound. Once the first sites on all channels are bound, the second sites start to bind. It is only at this point that is there any response in the membrane. Continuing with the verbal argument, this explains the stimulus threshold anecdotally reported for some enteric neurons — small inputs are not sufficient to complete the first round of phosphorylation.

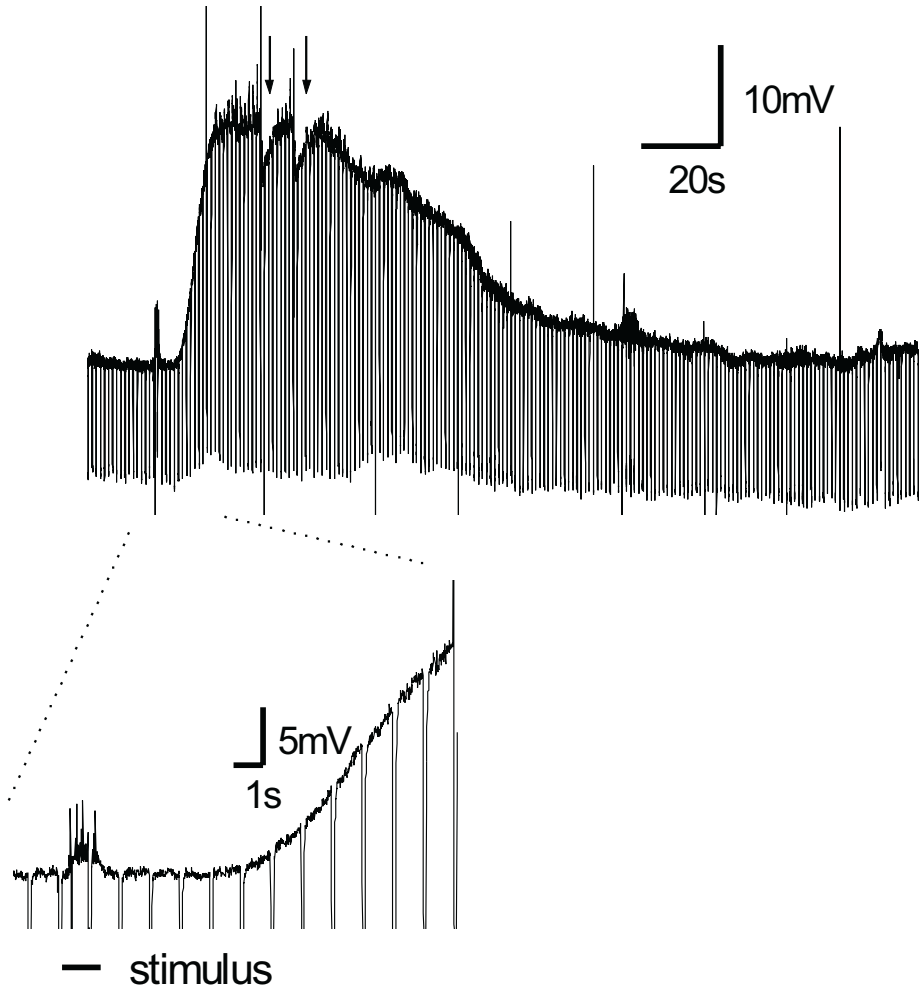

Figure 3.9: This figure shows a voltage trace of a slow EPSP obtained from an intracellular voltage recording from a myenteric AH neuron. The inset shows the same data, but at higher scale, for the period shortly before the stimulus until some time after the membrane start to depolarise. Hyperpolarising current pulses are visible as large, brief downward deflections in the trace. These illustrate the change in input resistance during the slow EPSP. Hyperpolarising deflections at the peak of the slow EPSP, indicated by the arrow, are after hyperpolarising potentials following action potentials triggered by the slow EPSP. There is a delay of 4.5 s until the response in the membrane potential. Data provided by P. J. Johnson.

To examine this more rigorously consider the following reactions

$$\mathrm{M} + \mathrm{P}_0 \xrightarrow{k} \mathrm{P}_1 \tag{3.17}$$

$$\mathrm{M} + \mathrm{P}_1 \xrightarrow{1} \mathrm{P}_2 \tag{3.18}$$

where P_i is the channel with i sites bound, M is the messenger and $k \gg 1$ is rate of the first phosphorylation compared to the second. Based on mass action kinetics and assuming conservation of mass ($P_0 + P_1 + P_2 = 1$) this leads to

$$\frac{dP_1}{dt} = kMP_0 = kM(1 - P_1 - P_2) \tag{3.19}$$

$$\frac{dP_2}{dt} = MP_1 \tag{3.20}$$

$$\frac{dM}{dt} = -kM(1 - P_1 - P_2) - MP_1 + u(t) \tag{3.21}$$

where $u(t)$ is the input or stimulus. To illustrate how this works choose

$$k = 1000$$

$$u(t) = AH(t - 2)$$

where A is a constant and H is the Heaviside function defined as $H(t) = 0$ for $t < 0$ and $H(t) = 1$ for $t \geq 0$. This value of k means that the affinity for binding to the first site is 1000 times greater than for the second. The stimulus is a brief pulse of strength A. Figure 3.10 panel A shows a time course for P_2 for the case $A = 1$. There is a clear, prolonged delay before the onset of the visible response. Panel B shows a stimulus response curve. Again, this agrees with the expectation that there is a threshold before a response is seen.

This qualitative 2 phosphorylation site model accounts for delay and threshold seen in some slow EPSP responses. It now needs to be incorporated into a full slow EPSP model that maintains the requirements of simplicity and the minimum

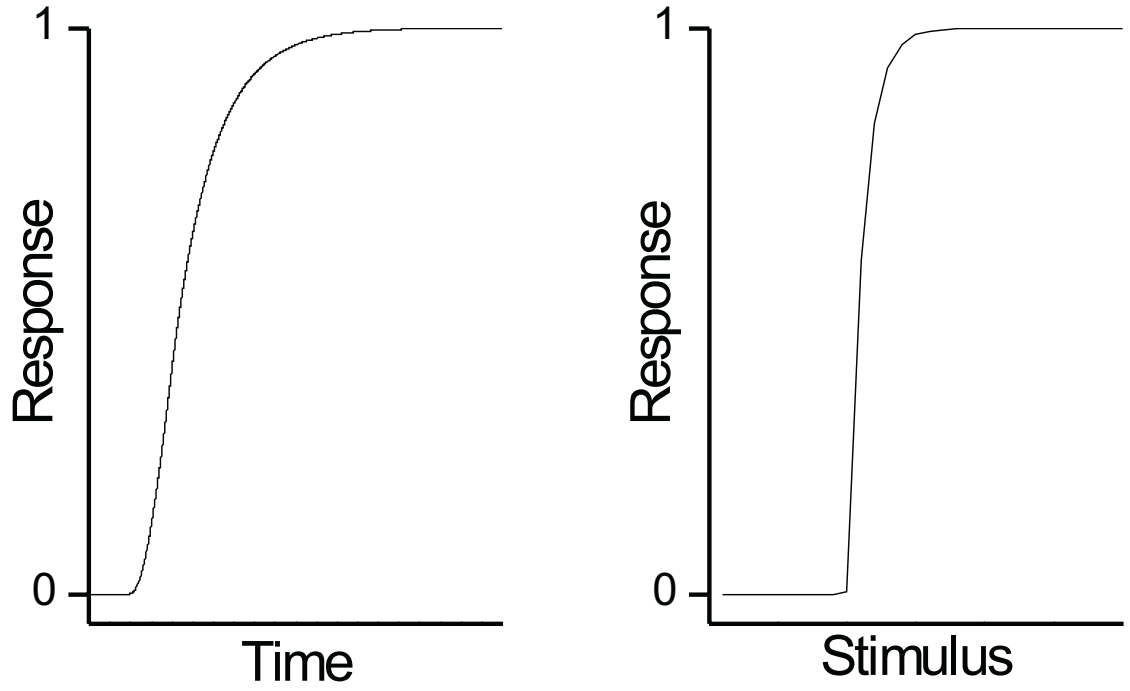

Figure 3.10: *A)* This is a simulated membrane potential response time course, elicited by a brief stimulus, for the qualitative model described by equations (3.19). There is a noticeable delay before the response is visible as a change in the membrane potential. *B)* This is a plot of the maximum membrane potential change against duration of the stimulus, for the same model. There is threshold in stimulus duration before a response is seen. Units are arbitrary in both graphs.

number of parameters. In order to perform an initial analysis a three stage model is considered, analogous to the one above

$$\frac{dD}{dt} = \alpha L(t) - \beta_1 D \tag{3.22}$$

$$\frac{dC}{dt} = D - \beta_2 C \tag{3.23}$$

$$\frac{dP}{dt} = -H(C - C_T)(C - C_T)P + \beta_3(1 - P) \tag{3.24}$$

where H is the Heaviside function, as above. The Heaviside function arises because there is effectively a threshold, C_T, in the level of C required before the second site starts to phosphorylate. The quantity P is now the amount of channel with exactly one site bound. Once the second site starts phosphorylating it does so at a rate proportional to $(C - C_T)(1 - P)$. The loss of C and the unbinding of the first site have been effectively collapsed into a single step.

An interesting question is how does the delay depend on the input and the model parameters? Consider a simple input $L(t) = A\delta(t)$, which is a brief input, of strength A at $t = 0$. To simplify further, take $\beta_1 = \beta_2 \equiv \beta$. The solution of the second stage is

$$C(t) = \alpha A t \exp(-\beta t). \tag{3.25}$$

The delay, t_T, is the time until $C(t_T) = C_T$. $C(t)$ is an alpha function that rises from zero, reaches a peak and decays back to zero. The larger A is the faster $C(t)$ rises and the sooner it reaches C_T and so the delay is shorter when A is larger. The maximum delay occurs when $C(t)$ only just reaches C_T. The peak value is $\alpha A/\mathrm{e}\beta$ which occurs at $t = 1/\beta$. Thus, the maximum delay is

$$t_T = \tau / ln(2) \tag{3.26}$$

where τ is the halflife of the D and C stages. This initially counter-intuitive result states that the longer the halflives of the first two stages, the greater the maximum delay. However, the interpretation is that the slower the decay of the early stages the longer the messenger is available to perform the first round of phosphorylations. The maximum delay does not depend on C_T.

Figure 3.11 shows membrane potential responses plotted against time for 3-6 synaptic events delivered at 10Hz. The model fulfils the qualities discussed above. The maximum response of the model appears to be graded only over a very small range of inputs. The parameters used to generate this figure were chosen for illustrative purposes and may not represent time courses of real slow EPSPs.

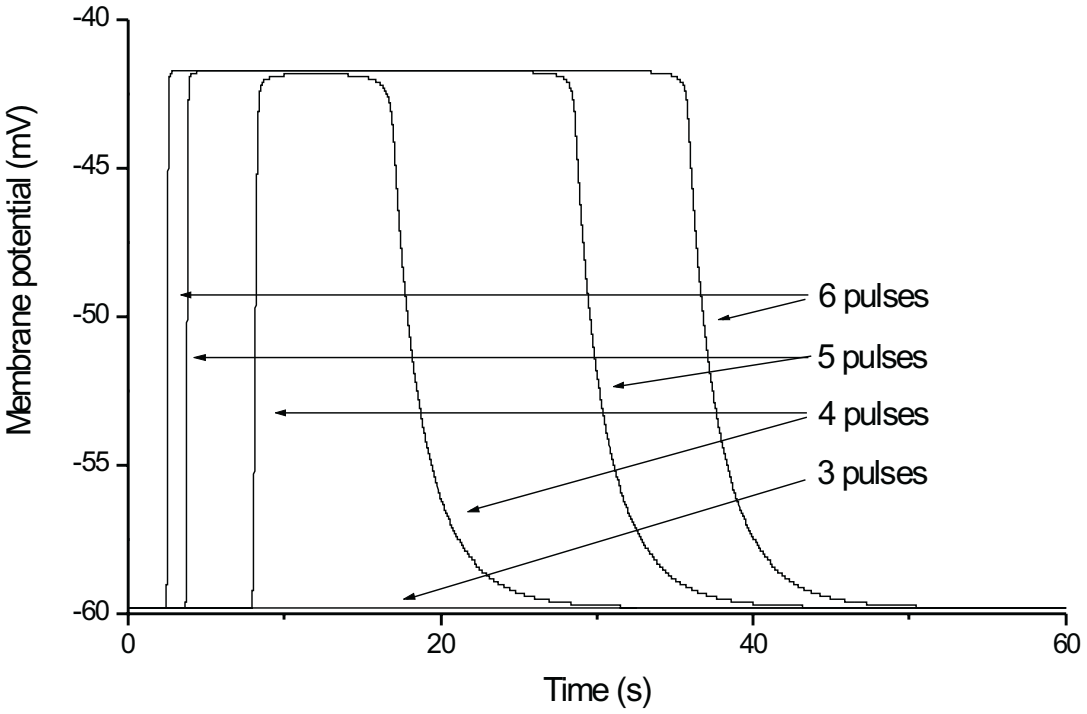

Figure 3.11: These are membrane potential responses for the model described by equations (3.22). Stimuli of 3, 4, 5, or 6 synaptic events have been delivered at 10Hz. The 3 pulse stimulus has not generated a response. The delay becomes shorter and the duration becomes longer as the number of pulses increases. The parameters for the equations have not been derived from data, but chosen for illustrative purposes.

3.4 Discussion

A model has been developed that describes the activation of a G-protein, cAMP/PKA pathway resulting in the phosphorylation of a potassium channel. A major finding is that important features of the signalling cascade can be abstracted out by a process of mathematical simplification, yet still produce a model capable of fitting a wide range of experimental data. Equally important is that more than one, though not all, of the models fit the data well.

Decay phases of stages 1 and 2

There were two assumptions about the decay phases of the first two stages that were incorporated into all of the successful models. Where tested, models based upon alterate assumptions failed to fit the data (not shown).

In the first stage, the decay is due to the hydrolysis of cAMP by a PDE. If this is described by Michaelis-Menton kinetics then there are two simple approximations that can be made. The first is that the rate of decay is proportional to the amount of PDE and hence constant for positive D (cAMP). If this is true, then for large stimuli, the halflife of the first stage will be linearly related to the stimulus size and hence the total halflife of the output will be at least linearly related to the stimulus size. An examination of the Morita and North [1985] data (Figure 3.7) shows that with increasing stimuli, the halflife increases less than linearly. Thus, having the decay proportional to D was chosen.

The decay of the second stage is caused by the rebinding of two catalytic PKA subunits with the single, tightly bound pair of regulatory subunits. The simplest

assumption is that the rate of decay is proportional to the square of the amount of catalytic subunit, C in Equation (3.3) which leads to a $1/C$ decay. However, equations based on this assumption were not able to fit any of the datasets (not shown). An assumption that removal was linear gave the results presented. These data are not known for enteric neurons but can be justified by several known biochemical mechanisms such as an auto-inhibition of the catalytic subunit [Taylor, 1989, Buxbaum and Dudai, 1989, Gray et al., 1998].

Evaluation of the model

A 3 stage model with either 1^{st} order or 2^{nd} order kinetics in the second stage fit the dataset of Morita and North [1985] well, though with some qualitative differences (see figure 3.7) while both models fit the individual trace data with identical results (not shown). A 2 stage or 3 stage model with 2^{nd} order kinetics in the second stage also fit the Morita and North [1985] data well, with the 3 stage model having a minor advantage in the way it fit the slow rise and complex decay phases of the complete waveforms (figure 3.8). A 2 stage model with 1^{st} order kinetics in both stages was unable to fit either dataset (not shown). It may be that this set of equations simply did not have the complexity necessary to fit the wave form of the slow EPSP.

Thus, any of the more complex systems of equations could prove useful in investigating slow EPSPs in large scale simulations. To make stronger conclusions about which set of equations is better, it would be necessary to obtain a series of slow EPSPs (similar to figure 1) from a large sample of cells that are receiving both synchronised and non-synchronised input. This refinement is left for a future study.

The delayed EPSP model

A model was constructed that reproduces an activity dependent delay in the slow EPSP before a response is visible as a membrane potential change. The additional assumptions made were: each channel has two phosphorylation sites; the affinity of the first site is much greater than that of the second; and the channel closes only when both sites are bound. There is very little data available which can be used to evaluate the delayed slow EPSP model. However, this model does make a testable prediction about a relationship between the maximum latency and the rate of decay that can be used to refute the model. Equation (3.26) states that $t_T = \tau/ln(2)$, where t_T is the maximum delay and τ is the halflife of the first two stages. More generally, if there are more stages, or if the stages have different halflives, the decay phase will be a mixture of several exponentials. However, it can be approximately characterised by a single exponential decay rate which will be a combination of the decay rates for the internal processes. The maximum delay, t_T, will be a similar combination of the decay rates of the internal model stages. Thus, $t_T \sim \tau$, or t_T should be within a factor of 2 or less of the decay time constant.

An experiment to test this would apply electrical pulses to internodal strands, using standard techniques [Morita and North, 1985]. The stimuli would be at high frequency, to approximate the simplification of the calculation that the stimulus is brief. A number of measurements would be taken with different numbers of pulses, from 1 pulse up to a stimulus that produces a slow EPSP with maximal depolarisation sufficient to determine the decay for events with different durations. As well as the relationship between t_T and τ the model predicts that τ will be

independent of the stimulus and that the delay will decrease with increasing numbers of pulses.

Other models of G-protein and second messenger signalling

A model similar to that of the present work is that of Nauroschat et al. [1997] which is based on receptor/G-protein interactions with the production of a generic second messenger as the final step. Their aim was to abstract out a system of general equations and determine their mathematical properties. Thus they did not include any reaction rates nor did they fit their model to any data. Their process of abstraction and mathematical simplification is similar to the methodology used in the present study. In contrast, they include receptor/agonist complex desensitisation and receptor sequestration via endocytosis which we chose not to model in order to reduce complexity, in part, because we were modeling several stages past the production of cAMP. There is evidence that receptor internalisation occurs in myenteric neurons [Southwell et al., 1996, Carman and Benovic, 1998], though any effects of this in the current model will have been subsumed by the multiple decay phases.

Quite a different approach was taken in a model by Lamb and Pugh [1992], where the numbers of molecules and the rates for many of the reactions were known and diffusion was modeled as a stochastic process. The system studied was that of light transduction in the salamander rod cell [Lamb and Pugh, 1992, Lamb, 1996]. Light is the agonist and rhodopsin molecules are G-protein coupled receptors which activate a cGMP PDE. While cGMP is present, ion channels are open; when light is present, the PDE is activated and concentrations of cGMP fall causing channels to close. This model matches experimental data very closely for the activation phase

of the pathway, but does not incorporate an inactivation phase.

The model of Lamb and Pugh [1992] includes many real parameters for a tightly coupled system. For many other systems, not all these parameters are known, nor are the pathways involved as well characterised [Lamb and Pugh, 1992]; slow EPSPs in myenteric neurons are a good example. Because the present study aimed to produce a model which would facilitate the investigation of large scale neuronal interactions, we chose to use a more abstract approach [Lamb, 1996]. In addition, the model described here was designed to handle situations where neurons receive complex, ongoing inputs, which last beyond the initial activation of the pathway; thus it was necessary to model the inactivation phase of the second messenger system. The inactivation, or the return to the initial state, includes many more reaction rates that are not available for myenteric neurons, or even for the salamander rod cell [Lamb and Pugh, 1992, Lamb, 1996].

A detailed model of $GABA_B$ receptor activation has been presented by Destexhe and Sejnowski [1995]. Similar to the present study, they fit their model to biophysical data to derive parameters and like Lamb and Pugh [1992], they explicitly modeled the movement of transmitter in the synaptic cleft. However, like the model of Nauroschat et al. [1997], they only consider the pathway one step beyond the G-protein, which in this case is a potassium channel. Their aim was to use their model to differentiate between proposed mechanisms underlying observed differences in $GABA_B$ and $GABA_A$ responses. One of their conclusions is that higher order binding kinetics of G-protein to the potassium channel can account for significant non-linearities in the $GABA_B$ stimulus response relationship [Destexhe and Sejnowski, 1995]. Although the potassium channel modeled in the present study

does not directly interact with G-proteins, it is interesting to note that the gating of the $g_K/g_{K,Ca^{++}}$ by phosphorylation presents a similar argument.

Finally, a quantitative and detailed model of the activation of PKA by cAMP has been presented by Buxbaum and Dudai [1989]. Although limited to one stage of the signalling cascade, their aim was to model the effects that changes in the ratio and in the state of phosphorylation of the catalytic and regulatory subunits have on production of cAMP. Like some of the previous models, extensive reaction data from wild-type and mutant *Drosophila* were used. This allowed them to correlate behavioural differences in mutants with differences in the activation of PKA and conclude that its long term activation is important for memory-like functions. Unlike the model developed in this study, Buxbaum and Dudai [1989] modeled neither the creation of cAMP from synaptic inputs nor the role of activated PKA at the single neuron level. Conversely, the model described in this chapter used much of the same kinetic data as a starting point, but it was abstracted out during development of the model.

Conclusion

This chapter has demonstrated a method by which relatively general biochemical processes can be extracted from a complex system and, by fitting to experimental data, used to model specific pathways. The model created is mathematically simple and computationally efficient in both processor time and memory. The model can reproduce peak response and time to half decay data over a range of fixed frequency stimuli, and so should be able to predict responses for more complex inputs. Future refinements of this system will include exploring the role of intracellular calcium.

improving the multiple phosphorylation site model and comparing it to experimental data.

Chapter 4

The role of the after-hyperpolarisation

4.1 Introduction

This is first of four chapters that attempts to analyse roles of the recurrent network of intrinsic sensory neurons of the intestine and how it performs those roles. The intrinsic sensory neurons are the first point of entry into the enteric nervous system so it is of significant interest to understand how the recurrent connections affect the ability of the network to transduce stimuli? What are the important membrane conductances? What are the properties of these networks as dynamical systems?

Recurrent neural networks with excitatory feedback, and no inhibition, have two stable firing states, the quiescent state and a state in which all neurons are firing at the maximum rate [Beurle, 1956, Ashby et al., 1962]. Any stimulus or spontaneous activity, larger than some threshold, will amplify until the network is firing at its maximum rate and it will not return to a low firing state. Even if some other

mechanism, with a longer time course, came into play to return the network to the basal state, such a network cannot give a graded response to stimuli above the threshold. As discussed in chapter 1, intrinsic sensory neurons form a recurrent network interconnected by synapses at which slow EPSPs are the predominant form of transmission. Inhibitory interneurons, connecting to sensory neurons, appear to be absent, so it seems likely that networks of sensory neuron are also bistable and so have all-or-nothing responses to significant stimuli. In some cases, intestinal reflexes give all-or-nothing responses [Brookes et al., 1999], but most intestinal reflexes are graded [Hukuhara et al., 1959, Smith and Furness, 1988, Yuan et al., 1991, Smith et al., 1990, 1988, Furness et al., 1995a, Tonini et al., 1996] and, in those that are not, electrical responses recorded in the circular muscle are graded with stimulus strength [Brookes et al., 1999]. Thus, because sensory neuron circuits are in the pathway between stimulus and response they must also be producing a graded response.

Intrinsic sensory neurons show a prominent after-hyperpolarisation (AHP) lasting from 2 to 20s following an action potential [Hirst et al., 1974, 1985b]. This is caused by calcium entering the cell during the action potential, leading to the opening of calcium activated potassium channels. (See page 51 for more detail.) The slow excitatory postsynaptic potential (EPSP) closes the same channels so it significantly reduces the AHP [Grafe et al., 1980]. The role of the AHP is usually discussed in terms of its properties in neurons at rest [Nishi and North, 1973, Morita et al., 1982a] where its role is to limit firing of sensory neurons. Because the AHP is suppressed by slow EPSPs and other hormonal messengers, it has been suggested that this allows sensory transduction to be modulated [Wood, 1989]. These ideas are incomplete, but to date, there have been no studies, theoretical or otherwise, to

analyse sensory neuron networks or how slow synaptic transmission and the AHP interact to determine network firing. In this chapter, the role that AHPs may play in network transduction of sensory stimuli was examined, especially in light of the fact that they are diminished during slow EPSPs. The guiding assumption was that sensory neuron networks need to control their firing and that output firing rate is graded with input strength in order to perform biologically useful sensory transduction. This means that in the absence of input the firing rate must be zero or very low, in response to a stimulus the firing must be less than the maximum firing rate and at the cessation of the stimulus the firing rate must return to the basal level.

Two techniques were used to study this question. The mean firing rate model of Wilson and Cowan [1972] was modified to allow the interactions of slow EPSPs and slow AHPs in recurrent networks of intrinsic sensory neurons to be examined analytically. The revised analytical model was only used to test the steady state situation, so numerical simulations were used to test the predictions of the analytical model and to investigate the role of residual AHPs in transduction of time varying inputs.

4.2 Methods

Computer simulations were performed according to the techniques described in chapter 2 and with the slow EPSP model described in chapter 3. In addition, a model of the interaction of the slow EPSP and the AHP was developed. The suppression of the AHP could be modelled by simply making the AHP smaller, but this would only be correct when the slow EPSP is fully active. A better model will allow a

gradation of the AHP size with the degree of slow EPSP activity and so will be applicable over the entire range of network firing rates.

Interactions of the AHP and slow EPSPs

In intrinsic sensory neurons the channel closed by the slow EPSP is also the Ca^{++} dependent K^+ channel opened during the AHP [Grafe et al., 1980], which leads to a marked reduction in the AHP during a slow EPSP. In this study, the relative amount of Ca^{++} bound following a single action potential is modelled by

$$c(t) = r_{\mathrm{Ca}}\ (t/k_{\mathrm{AHP}}) \exp(1 - (t/k_{\mathrm{AHP}})) \tag{4.1}$$

after a delay t_{delay}. The amount of bound Ca^{++} for several action potentials sums linearly up to a maximum value of 1. The degree of summation is determined by the parameter r_{Ca}.

The channel molecule was assumed to be able bind one Ca^{++} ion and to have one phosphorylation site. When neither site is bound, the channel molecule is assumed to have a small opening probability so that these channels have a nonzero conductance at rest. When the phosphorylation site is bound, and Ca^{++} is not bound, the channel is assumed to be closed. This corresponds to a slow EPSP being active, but no AHP. When Ca^{++} is bound, and the channel is not phosphorylated, the channel is assumed to be open, corresponding to an AHP and no slow EPSP. When both sites are bound the channel has a small residual opening probability, so that AHP occurring at the same time as a slow EPSP will produce a small hyperpolarising current. The amount of open g_{KCa} at any time is given by

$$\frac{g_{\mathrm{KCa}}(t)}{\bar{g}_{\mathrm{KCa}}} \quad = \quad r_{\mathrm{basal}}\,(1 - p(t))\,(1 - c(t)) +$$

$$(1 - p(t))\, c(t) +$$

$$\rho\, p(t)\, c(t) \tag{4.2}$$

where $p(t)$ is given in equation (2.6) and $c(t)$ is given in equation (4.1). The three terms, on each of three lines, in this equation are as follows. $r_{\text{basal}}\,(1-p(t))\,(1-c(t))$ is the amount of channel which is neither phosphorylated nor has calcium bound. The parameter r_{basal} provides a resting conductance which also contributes to the resting membrane properties. $(1 - p(t))\, c(t)$ is the amount of channel which is unphosphorylated and has calcium bound. $\rho\, p(t)\, c(t)$ is the amount of channel which is both phosphorylated and has calcium bound. The quantity ρ provides a residual AHP in the presence of a slow EPSP and this parameter was varied as part of the study. Phosphorylated channel with no calcium bound is closed and so does not contribute to the conductance. The value ρ was varied systematically as part of the study. A value of 0.1 gave a reduction in the magnitude of the AHP during a maximal slow EPSP that was slightly larger than that seen experimentally (Johnson & Bornstein, unpublished).

Figure (4.1) shows results from simulation of these sub-models. Panel A shows an AHP following an action potential in a neuron that was initially at rest. Panel B shows a slow EPSP resulting from 10 synaptic events in 1 s and in which the neuron has been prevented from firing action potentials. In panel C, the neuron has fired a single action potential in response to the slow EPSP. The AHP in this case is markedly suppressed. In panel D, the neuron has fired two action potentials in response to the slow EPSP. In this case the AHPs from both action potentials sum.

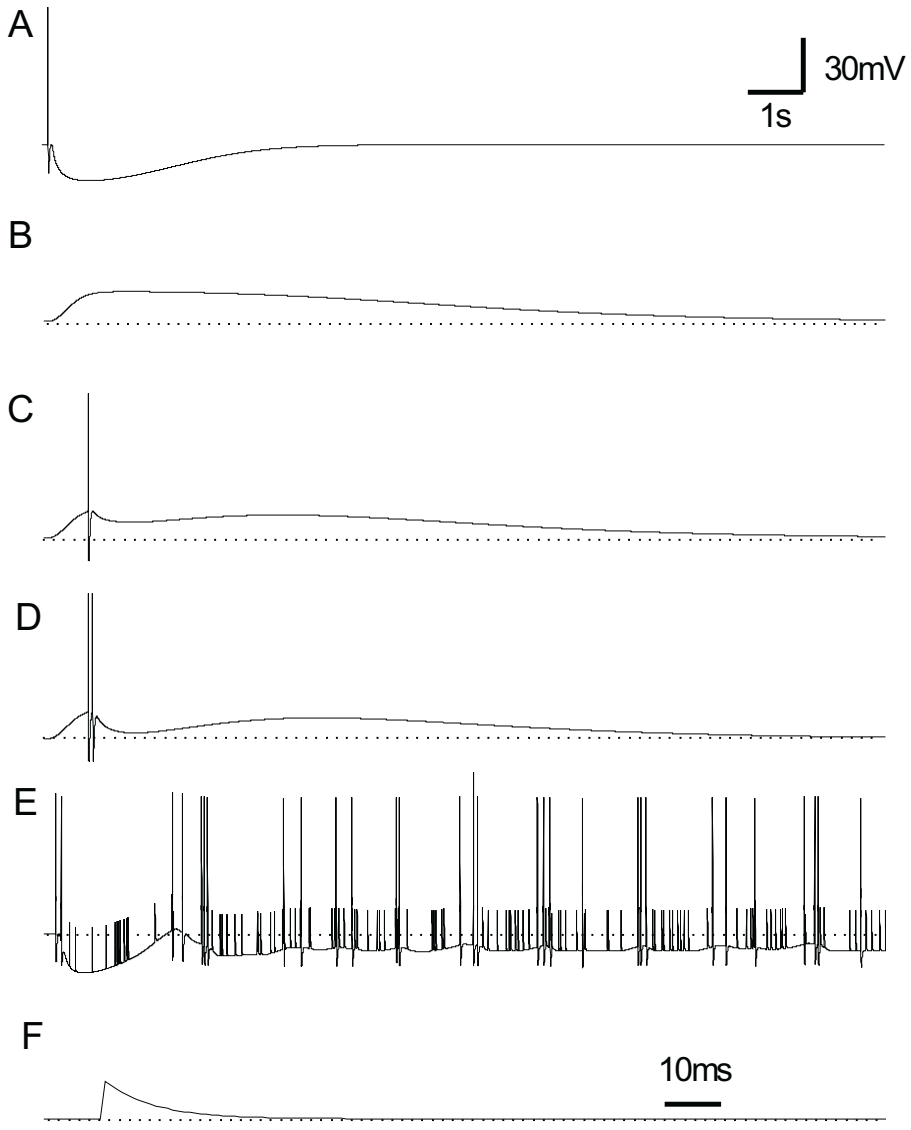

Figure 4.1: The traces are simulated membrane potentials produced from the model described in the text. *A.* An action potential has been induced in a neuron at rest. It is followed by the prolonged AHP. The dotted line in this and subsequent traces indicates the resting membrane potential. Scale bars apply to all panels except for time in panel F. *B.* A slow EPSP has been induced by 10 synaptic events delivered in 1 second. The synaptic events are not visible. The neuron has been prevented from firing action potentials. *C.* A slow EPSP has been induced in the neuron but the neuron has been allowed to fire a single action potential. The AHP following the action potential is significantly reduced compared to panel A. *D.* A slow EPSP, identical to that in panel C, has been induced in the neuron, which neuron has been allowed to fire 2 action potentials, demonstrating the ability of the AHPs to sum. *E.* A neuron in a network is receiving PPP input (short spikes) at 10Hz, on average. Initially, the neuron is at rest so the first PPPs cause action potentials (tall spikes) with large AHPs. The neuron is also receiving slow synaptic input from other neurons, which suppresses the AHP. The AHP still appears large because of summation. *F.* A PPP induced at in a neuron at rest.

Stimuli

Most stimuli were proximal process potentials (PPPs) delivered randomly, but with constant average frequency, over the entire network, or localised in the centre of the network, as indicated in the text. For some stimuli the instantaneous average frequency varied sinusoidally in time. A PPP is illustrated in figure (4.1), panel G. Figure (4.1), panel F shows a membrane potential trace from a neuron in a network receiving 10 Hz PPP per neuron input. Tall spikes are action potentials and small spikes are PPPs that failed to reach threshold. Initially there is a large AHP following the first action potentials. Following this, the slow EPSP becomes active and the size of the AHP is reduced.

Parameter values used in the numerical simulations are given in Table (2.1).

4.3 Results

Theory

A theoretical analysis based on the model of Wilson and Cowan [1972] (WC) of the interaction of slow EPSP and AHPs in recurrent networks of intrinsic sensory neurons was undertaken. The analysis shows that these networks can encode the magnitude of a sustained stimulus, provided the residual AHP is larger than a minimum size, and that increasing the AHP size controls the gain of the response.

The WC model consisted of a population of inhibitory neurons and a population of excitatory neurons and was based on a number of assumptions. These are that neurons are uniformly interconnected, propagation delays can be neglected, the

network dynamics are well captured by the mean firing rate of a population of neurons and the mean firing rate depends only on the mean membrane potential and the statistical distribution of membrane thresholds. To make the problem tractable Wilson and Cowan [1972] also assumed that synaptic inputs were brief and summed linearly.

If $E(t)$ is the firing rate of a population of neurons at time t, then the firing rate at a later time, $t+\tau$, was shown to be [Wilson and Cowan, 1972]

$$E(t+\tau) = \int_{t-r}^{t} S(x(t), \theta(t-s))\ R(t,s)\ ds + \left[1 - \int_{t-r_a}^{t} E(t')\ dt' - \int_{t-r}^{t} R(t,s)\ ds\right] S(x(t), \theta_0) \tag{4.3}$$

The symbols have the following meanings:

- $\theta(t)$ is the threshold for firing. This may vary in time in response to previous firing history. θ_0 is the resting threshold.
- $S(x, \theta)$ is the proportion of neurons that fire given an input of x and a threshold θ.
- $x(t)$ is synaptic input, which in turn depends on E and exogenous input.
- r is the duration of the relatively refractory period
- r_a is the duration of the absolute refractory period.
- $R(t,s)\delta t$ is the number of neurons that fired between times s and $s+\delta t$ and are still relatively refractory at time t. R is not an independent function, but can be derived from E, S and θ.

The model here differs from the WC model in that only a single population of neurons is described and summation of synaptic input is not assumed to be linear or

brief. The latter makes the problem more difficult so only steady state solutions are considered. Small networks, for example 5 mm $\times$ 5 mm, in the presence of spatially uniform inputs, can be considered to be uniformly interconnected. This also means that the propagation delay is around 10 ms (conduction speeds in the axons of sensory neurons are 50 cm/s [Stebbing and Bornstein, 1996]). This delay is small compared to slow EPSP time scales which are hundreds of milliseconds or longer [Morita and North, 1985] and so can be neglected. An assumption of the WC model is that a neuron will fire if it is above threshold and if it is not absolutely refractory. The threshold can vary following the absolute refractory period (a relative refractory period) and this is how the AHP is modelled.

The average firing rate is given by $E(t)$ and the average level of excitation, or increase in membrane potential toward threshold, is defined as $x(t)$. Directly ligand gated synaptic events are usually brief and, for small depolarizations can be assumed to sum linearly at the level of the membrane potential. If each synaptic event has a time course $\alpha(t)$ (the details of which do not matter here) then

$$x(t) = c \int_{-\infty}^{t} \alpha(t-s)\, E(s)\, ds \tag{4.4}$$

where c accounts for the distribution and strength of synaptic connections. The integral arises because at any point in time the contribution to the ongoing synaptic potential includes all inputs that have occurred at all previous times (although very early contributions will have decayed to zero and hence not actually contribute at the current time). The integration with $\alpha(t)$ maps the function $E(t)$ onto the function $x(t)$, and so acts as a *functional*. This functional is linear in E, e.g. input $a\,E(t)$ leads to an output $a\,x(t)$.

More generally, the input waveform $E(t)$ is mapped onto the output waveform, $x(t)$, by a functional, $\mathcal{L}$, which need not be linear in $E(t)$. For example, the slow EPSP model above (equation (2.6)) maps the input firing rate, onto $p(t)$, the relative amount of phosphorylated channel, which in turn leads to a membrane potential change. This is written

$$x(t) = \mathcal{L}_t(E)$$

to indicate the mapped image of E evaluated at time t. To simplify the analysis, it is assumed that if

$$\lim_{t\to\infty} E(t) = \bar{E}$$

then the following limit also exists:

$$\mathcal{L}(\bar{E}) \equiv \lim_{t\to\infty} \mathcal{L}_t(E) \tag{4.5}$$

This defines the quantity $\mathcal{L}(\bar{E})$. In other words, the level of excitation produced by a steady state input is itself steady state. This is true for linear synapses (equation (4.4) and the slow EPSP model (equation (2.6)) used in the network simulations. It is not a restrictive requirement for a population of neurons and, in particular, it does not exclude non-steady state solutions.

Three contributions to the level of excitability are considered; excitatory synaptic inputs (E), inhibitory synaptic inputs (I) and external excitatory inputs (P). (Inhibitory input is considered in more detail in the next chapter.) It is assumed that there is no internal interaction between these mechanisms so that the level of excitation can be written as the sum of each effect.

$$x(t) = \mathcal{L}_t^{(E)}(E) - \mathcal{L}_t^{(I)}(E) + \mathcal{L}_t^{(P)}(P).$$

Unlike the WC model, there is no separate population of inhibitory neurons so inhibitory synaptic inputs are driven by the same neurons as the excitatory input. For simplicity, it is also assumed that external inputs are brief compared to other time scales and sum linearly. This is analogous to the linear synapse model (equation (4.4)). If the function, α, is brief compared to other time scales (of the order of tens of milliseconds compared to seconds) then only contributions near t will matter and $x(t) \approx c\,\delta t\,E(t)$ [Wilson and Cowan, 1972]. By applying the same logic to P and absorbing the constants the last term can simply be written as $P(t)$.

If r_a is the absolute refractory period then any neuron that fired between $t - r_a$ and t is refractory and the total number of neurons at time t that are refractory is then [Wilson and Cowan, 1972]

$$\int_{t-r_a}^{t} E(s)\,ds$$

The population response function $S(x, \theta)$ is the proportion of neurons that can fire given a synaptic input of x [Wilson and Cowan, 1972]. The population response function depends on a number of physical properties of the neurons but the firing threshold, θ, is explicitly mentioned because the relative refractory period means that it is also a function of time. Wilson and Cowan [1972] then show that the contribution of relative refractory neurons to the firing in the next time interval is

$$\int_{t-r}^{t} S(x(t), \theta(t-s))\,R(t,s)\,ds$$

where r is the duration of the relative refractory period. The contribution from neurons that are not refractory is then

$$(1 - \int_{t-r_a}^{t} E(s)\,ds - \int_{t-r}^{t} R(t,s)\,ds)\;\; S(x(t), \theta_0)$$

where θ_0 is the resting threshold. Thus the firing rate at time $t+\tau$ is given by

$$\begin{aligned} E(t+\tau) &= \int_{t-r}^{t} S(x(t), \theta(t-s))\ R(t,s)\ ds + \\ & (1 - \int_{t-r_a}^{t} E(s)\ ds - \int_{t-r}^{t} R(t,s)\ ds)\ \ S(x(t), \theta_0) \end{aligned} \tag{4.6}$$

This problem is simplified as follows. First only the steady state is considered, thus

$$E(t+\tau) = E(t) \equiv \bar{E}$$

In this case, because of the assumption described by equation 4.5, $x(t) = \mathcal{L}_t^{(E)}(\bar{E}) - \mathcal{L}_t^{(I)}(\bar{E}) + P \equiv x(\bar{E})$ is also constant. The regime of interest is where the average interspike interval is less than the AHP duration (2–20 seconds in enteric neurons [Hirst et al., 1985a, Vogalis et al., 2001]). It is also assumed that any delay to the onset of the AHP is small compared to the AHP duration (70 ms compared to 2–20 s [Hirst et al., 1985a]). Thus, nearly all neurons will be refractory to some degree and so the second term in equation (4.6) is zero. Finally, because the system is in steady state, the proportion of neurons firing at s is constant as are the proportion of neurons still refractory at time t, that is $R(t,s)$ is also constant.

The steady state firing rate reduces to

$$\bar{E} = \frac{1}{r} \int_0^r S(x, \theta(s))\ ds \tag{4.7}$$

where, because the integrand no longer depends on t, the range of the integral has been shifted back to the origin.

In intrinsic sensory neurons the AHP is strongly suppressed during slow synaptic transmission. By concentrating on the more interesting regime of marginal stability $\theta(t) - \theta_0$ is small and S can then be approximated by a Taylor's series to the first

power in θ

$$S(x, \theta(t)) \approx S(x, \theta_0) + (\theta(t) - \theta_0) \left. \frac{\partial S}{\partial \theta} \right|_{\theta_0}$$

The only term that has time dependence is $\theta(t)$, because $x(\bar{E})$ is constant and θ_0 is just a parameter, so the integral in equation (4.7) can be evaluated, giving

$$\bar{E} \approx S(x, \theta_0) + \gamma \frac{\partial S(x, \theta_0)}{\partial \theta} \tag{4.8}$$

where

$$\gamma = \frac{1}{r} \int_0^r (\theta(s) - \theta_0)\, ds$$

This is the area under the threshold curve following an action potential, divided by its duration, and so is a measure of the "size" of the relative refractory period. To the first order it is the only quantity that depends on the size of the AHP and it is independent of $\bar{E}$. The quantity $\partial S/\partial \theta$ is a threshold sensitivity function and is a measure of how sensitive the synaptic response is to changes in the resting threshold. As the firing threshold, θ, increases, the population response, S, must decrease so the partial derivative is negative. Furthermore, the solution for $\bar{E}$ depends only on its value at the resting threshold. This is represented diagrammatically in figure (4.2). (This block diagram is analogous to engineering block diagrams, the difference being that engineering diagrams usually describe algebraic relationships in the frequency domain, whereas this diagram describes an algebraic relation in the "$\bar{E}$" domain.)

A geometric analysis (Figure (4.3)) can be used to show how equation (4.8) can lead to a single stable state for each input, P. Equation (4.8) is rewritten as

$$\bar{E} = f(\bar{E}, P) \tag{4.9}$$

where

$$f(\bar{E}, P) = S(x, \theta_0) + \gamma \left. \frac{\partial S(x, \theta)}{\partial \theta} \right|_{\theta = \theta_0} \tag{4.10}$$

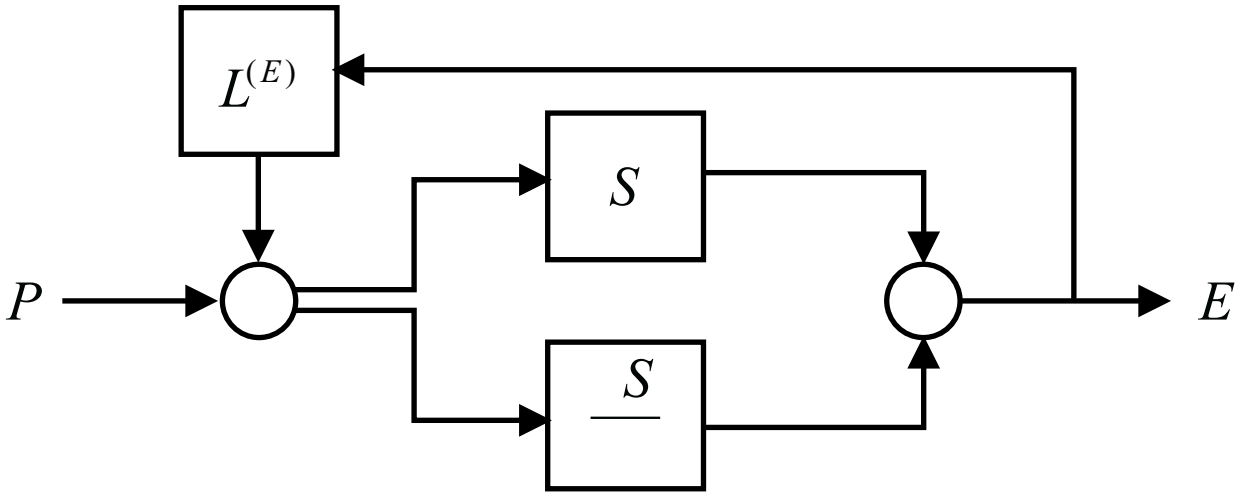

Figure 4.2: Diagrammatic representations of equations (4.9–4.11). Arrows indicate the direction of signal flow, circles indicate addition or subtraction as indicated, blocks represent processing of the signal. P is proximal process potential input and E is output action potential firing rate. The network is recurrent so the output signal, E loops back into the input.

and

$$x = P + \mathcal{L}(\bar{E}) \tag{4.11}$$

Solutions to equation (4.9) occur at the intersections of the two curves $y = \bar{E}$ and $y = f(\bar{E}, P)$. Wilson and Cowan [1972] argue that $S(x)$ is sigmoidal in x for unimodal distributions of synaptic connections and strengths. (Otherwise, it is a sum of sigmoids and the argument still holds.) The quantity x is monotonic in $\bar{E}$, that is, if the synaptic input increases then $\bar{E}$ increases, so $S(x(\bar{E}))$ will also be sigmoidal in $\bar{E}$. (Imagine smoothly distorting the X axis on a sigmoid without changing the order or duplicating any regions of the axis.) Figure (4.3) illustrates three solutions of equation (4.9). Panel A shows the case when there is no AHP and no input ($P = 0$). In this case there are three solutions, one at $\bar{E} = 0$ which corresponds to the quiescent state, one at a high firing state and one at an intermediate firing state. The intermediate firing state is unstable — any perturbation that causes a decrease in firing will cause the network to decay to the quiescent state, while any perturbation that causes an increase in firing will lead to the highest firing state because of the positive feedback. This intermediate state acts as a threshold. Any input that drives the firing rate higher than the threshold will cause the network to move to the high firing rate state and once the input stops the network will stay in this state.

Panel B indicates how the AHP "stabilises" the network by removing the high firing rate state. As the size of the AHP increases γ becomes larger. The quantity $\partial S/\partial\theta$ is negative (see appendix) and so $\gamma\partial S/\partial\theta$ is also negative. If the AHP is large enough the $y = f(\bar{E}, 0)$ curve drops below the $y = \bar{E}$ curve. In this case, the system is only stable in the quiescent state.

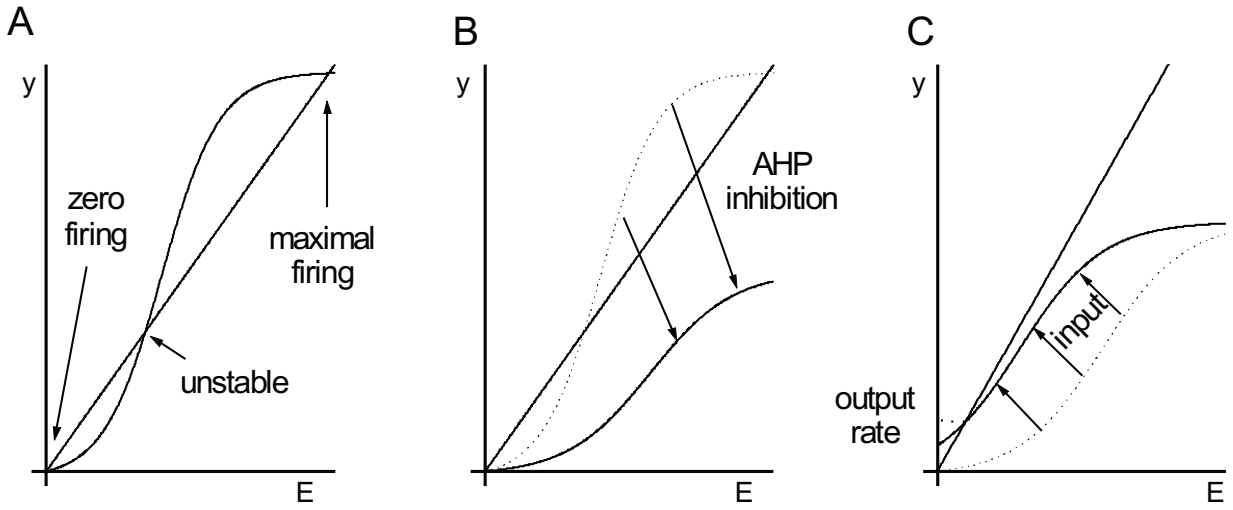

Figure 4.3: A geometric interpretation of equations (4.9–4.11). The solution of equation (4.9) occurs at an intersection of the curves $y = E$ and $y = f(E, 0)$, where E is the output firing rate and f is defined in the text. *A.* In the case of no input and no after-hyperpolarization (AHP) there are three solutions, the quiescent state, an intermediate firing state which is not stable and a high firing state. *B.* The effect of the AHP is to lower the $y = f(E, P)$ curve while still maintaining a sigmoid shape. *C.* The effect of exogeneous input, P, is to shift the curve to the left and flatten it. There is only one solution, which occurs well below the maximum firing rate.

Panel C shows how the network responds to sensory input, that is $P > 0$. In this case the $y = f(\bar{E}, P)$ curve shifts to the left, possible flattening out, but remaining sigmoidal. There is still only one intersection of the $y = \bar{E}$ and $y = f(\bar{E}, P)$ curves and this occurs at a nonzero value of $\bar{E}$ — the output firing rate. The important observations are that this output firing rate is graded with input firing rate and that it is unique. Thus, the output firing rate, $\bar{E}$, is graded with stimulus strength, P, and uniquely codes the magnitude of the stimulus.

Numerical simulation

Networks were tested by playing random, constant mean frequency PPP input into neurons and determining the average action potential rate per neuron after the network reached the equilibrium firing rate. When stimuli greater than 0.1Hz were applied to a network with no AHP, the network always made a transition to a state in which all neurons were firing maximally. This is shown in figure (4.4), panel A, in which average neuron firing rate is plotted against time for a variety of input frequencies. Furthermore, when the input ceased, the network did not return to the quiescent state (not illustrated), but remained in the excited state indefinitely. On the other hand, when a residual 10^{-1} AHP was present (figure (4.4), panel B), the network firing rate was significantly less than the same network with no AHP. The firing rate was roughly proportional to the input frequency, and hence was graded with the size of the input. Furthermore, the network returned to the quiescent state when the input ceased (not illustrated). When the AHP, but no slow EPSP, was present the response was only graded up to an input frequency of 5Hz, for which the corresponding output frequency was 1.2Hz, after which the response did not

increase.

Stimulus response curves were obtained for a range of residual AHPs. These are illustrated in figure (4.5), in which output frequency is plotted against input frequency for various residual AHP sizes. When no AHP was present, no graded response was possible. When a 10^{-3} residual AHP was present, a graded response was only possible for input frequencies less than 1Hz, and for frequencies greater than this the network went into the maximal firing rate state. However, for a 10^{-1} or 10^{-2} residual AHP a graded response was possible for frequencies up to 50Hz.

For the values of synaptic strength used to generate the previous results, the stable networks always returned to a state of total quiescence after the stimulus ceased. However, when synaptic strength was increased some combinations of residual AHP size and synaptic strength created networks which returned to a state with a level of ongoing activity. Values of the synaptic strength tested were 3, 5 and 10 times greater than the value used to generate the previous results. Stable firing rates of 0.3, 0.6 and 1.0Hz were observed for the residual AHP size and synaptic strength pairs $(10^{-1}, 10)$, $(10^{-2}, 5)$ and $(10^{-2}, 10)$, respectively. In these cases the neurons were firing well below their maximum rates and so were still able to produce a graded response to a new stimulus.

Figure (4.6) shows the effect of varying the duration of the AHP from 1, 2, 4 and 8 seconds (defined as the time required for the conductance to return within 10% of its resting value). The AHP duration has also been observed to shorten in the presence of slow EPSPs [Grafe et al., 1980]. The longer the duration the smaller the response range and the smaller the gain for constant stimuli. The maximum conductance available for the AHP was varied between 1 and 4 times the peak conductance of a

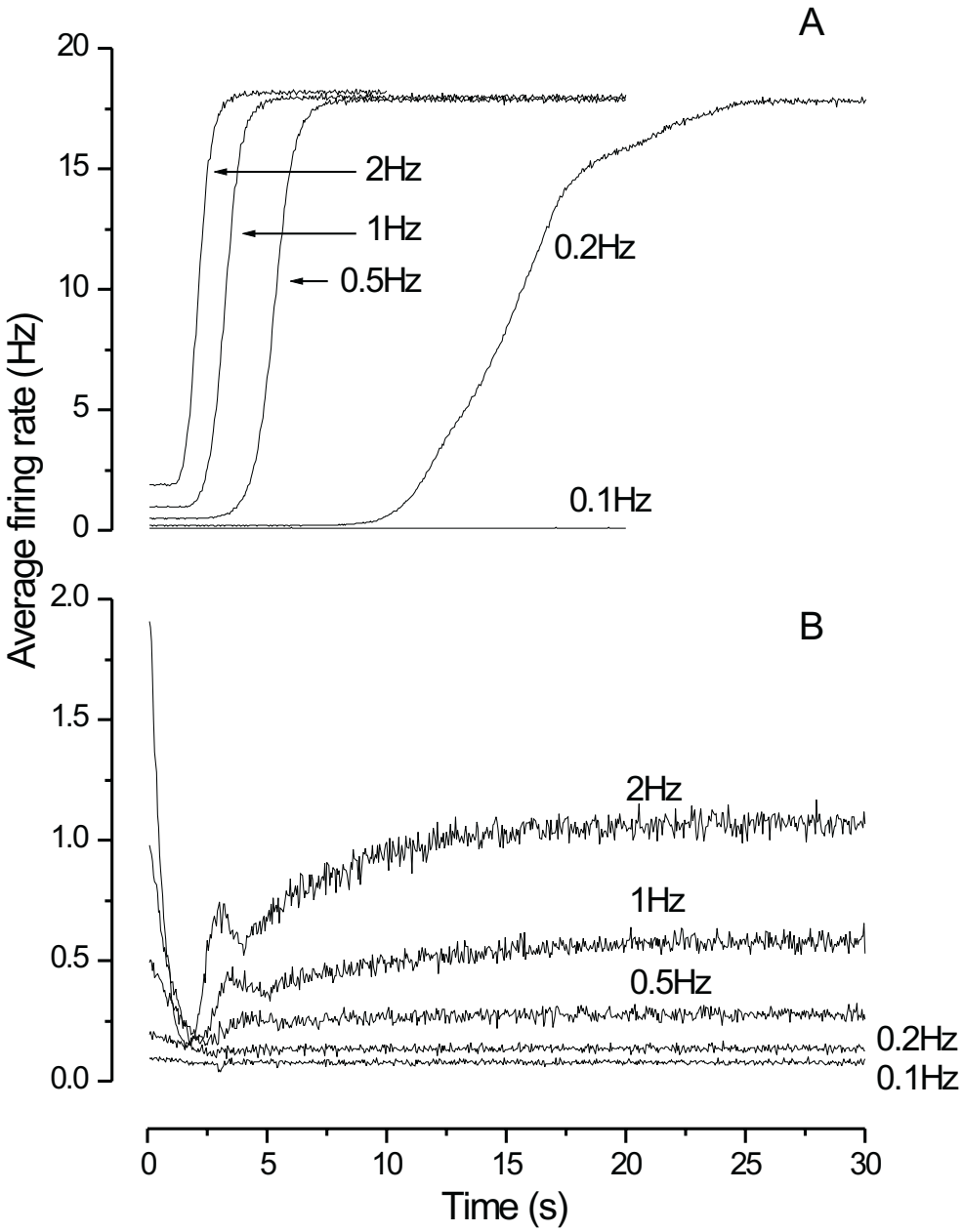

Figure 4.4: Action potential firing rate, averaged over the the network, is plotted against time, for a variety of input frequencies. *A*. No after-hyperpolarization (AHP) was present in the neurons used to generate these data. All curves, other than for the 0.1Hz input, eventually reach the maximum firing rate. *B*. In the network used here, the neurons had a residual AHP, equal to 10^{-1} of its resting value, during the slow EPSP. The final output firing rate depends on the input firing rate. Note that the Y axes on the two graphs are different.

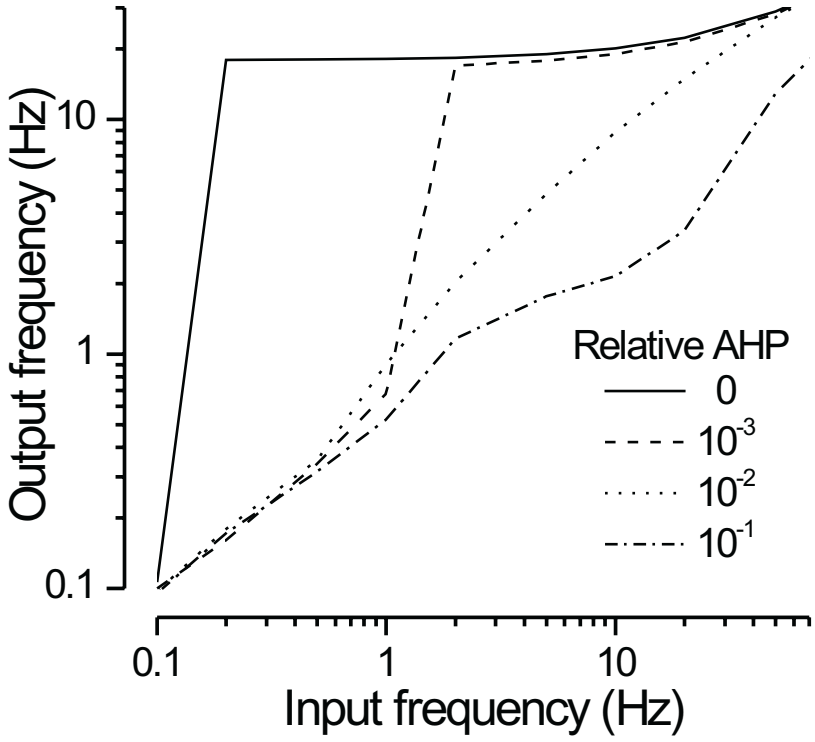

Figure 4.5: Neuron action potential firing rate, averaged over the entire network, is plotted against average input rate, for a variety of residual after-hyperpolarization (AHP) values. Log scales are used for both axes. Networks with no AHP or with a residual AHP of 10^{-3} are bistable for large stimuli, while networks with residual AHPs of 10^{-1} and 10^{-2} have a single, submaximal, firing rate state for all stimuli.

single AHP. All networks responded similarly at low input frequencies, but networks with greater summation, and hence more inhibition, fired at lower rates for higher input frequencies. Greater summation leads to reduced dynamic range and reduced gain for constant stimuli.

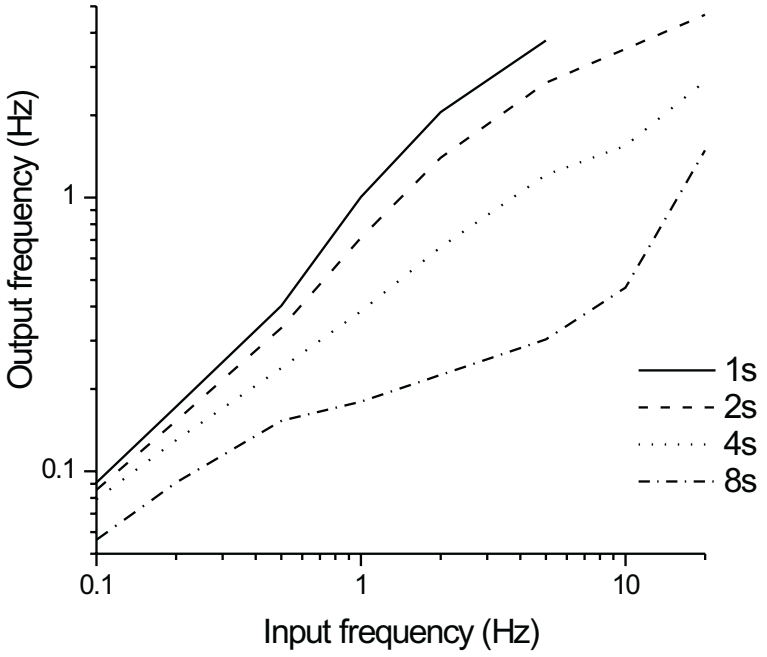

Figure 4.6: Stimulus response curves for networks with AHP based inhibition. Constant frequency exogenous input, in the form of proximal process potentials, is played into the network and the output in action potentials per second, averaged over the network, is determined after the firing rate reaches equilibrium. The time required for an AHP, in a neuron otherwise at rest, to return to within 10% of the resting membrane potential is indicated in the figure legend. Log scales are used for both axes.

Figure 4.7 shows the stimulus response curves for networks in which the maximum conductance available to the AHP is systematically varied. The stimulus is the input rate of PPPs averaged over the network and the response is the AP firing rate averaged over the network. The amount of conductance available was limited

to 1, 2 or 4 times the peak conductance of a single AHP. At low input frequencies all networks responded similarly, but at higher frequencies networks with greater summation, and hence more inhibition, fired at lower rates. Greater summation leads to reduced dynamic range and reduced gain for constant stimuli.

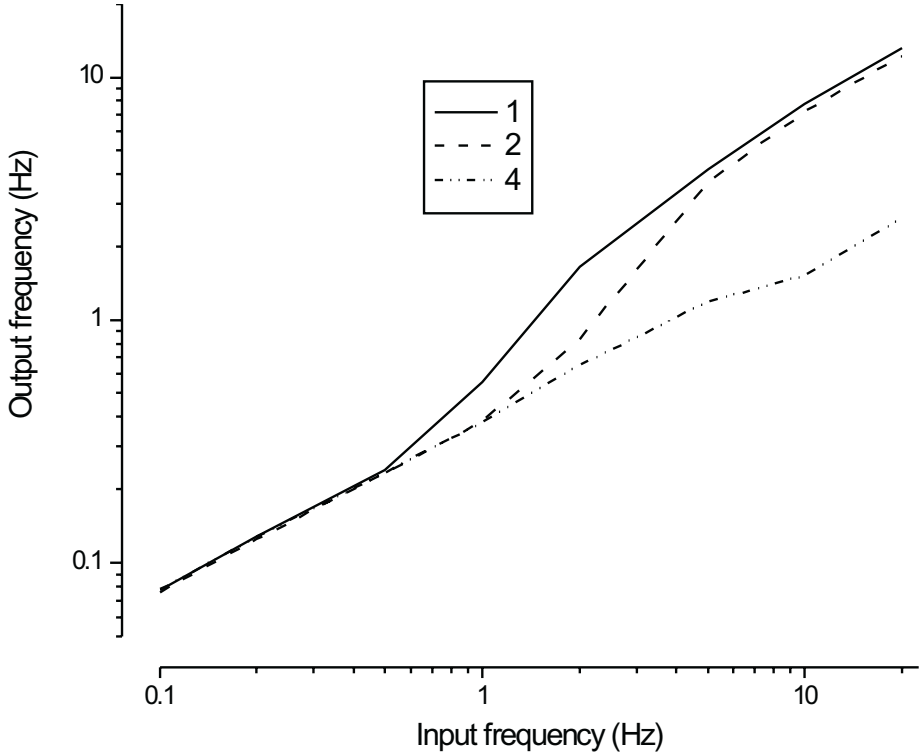

Figure 4.7: Action potential firing rate, averaged over the entire network, is plotted against average input rate, for a variety of values of the maximum number of channels available to bind calcium, which in turn determines the degree of summation possible for the after-hyperpolarization. Log scales are used for both axes.

Response to time varying input

The responses of these networks to time varying signals, also referred to as periodic forcing, were tested for two reasons. Firstly, the theoretical analysis indicates that these networks do not have complex states such as oscillations. Periodic forcing

can potentially uncover complex dynamics; for example, if an oscillatory state exists then forcing the system near the frequency of the oscillation will result in a strong distortion of the signal or unusual gain of the signal. Secondly, sensory input into the gut wall is not constant under physiological conditions, but varies continuously with time. Therefore, sinusoidal inputs were used to give an indication of how the system encodes time varying input.

The networks were tested with input given by

$$r(t) = \frac{1}{2}A(1 + \sin(2\pi f t))$$

where $r(t)$ is the input PPP rate, A is the maximum input frequency and f is the modulation frequency. The PPP rate varied slowly between zero and A with a frequency f. Signals tested were all combinations of A in 0.1, 0.2, 0.5, 1, 2, 5, 10 and 20 Hz and f in 0.01, 0.1, 0.2, 0.5, 1 and 2 Hz. These frequencies encompass physiological time scales from very slow distensions ($f = 0.01$ Hz, rise time of 50 s), slow distensions known to initiate peristalsis ($f = 0.1$ Hz, rise time of 5 s) [Brookes et al., 1999] up to very rapid distensions ($f = 1$ Hz rise time of 500 ms) which are known to excite simple reflexes [Smith et al., 1990].

Data for $A = 20$ Hz are shown in Figure 4.8 for a network in which AHPs were suppressed to 10% of their resting conductance change. The responses show a transient depression in firing shortly after the initial onset of the stimulus, because the initial AHPs are unsuppressed before the onset of slow EPSPs. This is most apparent when the modulation frequency is 1 Hz or larger. Beyond the initial transient period, the network is able to follow the stimulus closely, with only slight distortion of the shape. For low frequencies, there is some harmonic distortion of

the signal, that is the introduction of power at frequencies different from the driving frequency. For high frequencies, there is a strong transient response which lasts nearly 5 cycles at 2 Hz, but decreases in number of cycles for higher frequency input. At frequencies of 2 Hz or 0.5 Hz there is a phase lag of about 0.12 or -0.12 cycles respectively. The system is "mildly" nonlinear in that output is monotonic with input and there is only ever a single stable state.

Signal propagation in networks of sensory neurons

As will be discussed in chapter 7 in more detail, it is interesting to know whether these networks will support signal propagation over appreciable distances, that is can sensory neurons act as interneurons? To test this possibility, networks that were 15 mm $\times$ 15 mm in size were stimulated in the centre 5 mm $\times$ 5 mm with 20 Hz PPP input for 4 s. The peak conductance of the residual AHP was either 10^{-1}, 10^{-2} or 10^{-3} times the resting peak conductance. In addition, the synaptic strength was either 1, 3, 5 or 10 times the synaptic strength of the previous networks. (Increasing the synaptic strength decreases the rise time and increases the duration of the slow EPSP, but does not effect the maximum depolarisation.). The results are summarised in table (4.1). The columns show: the residual AHP size; the relative synaptic strength; the speed of signal propagation in the anal direction; the distance the signal travelled in the anal direction; the firing rate that the network settled into after the signal travelled through the network. Signal propagation over an indefinite distance was only found in networks that continued to fire after the activity front had passed. These are the bistable networks (this point is considered further in the discussion).

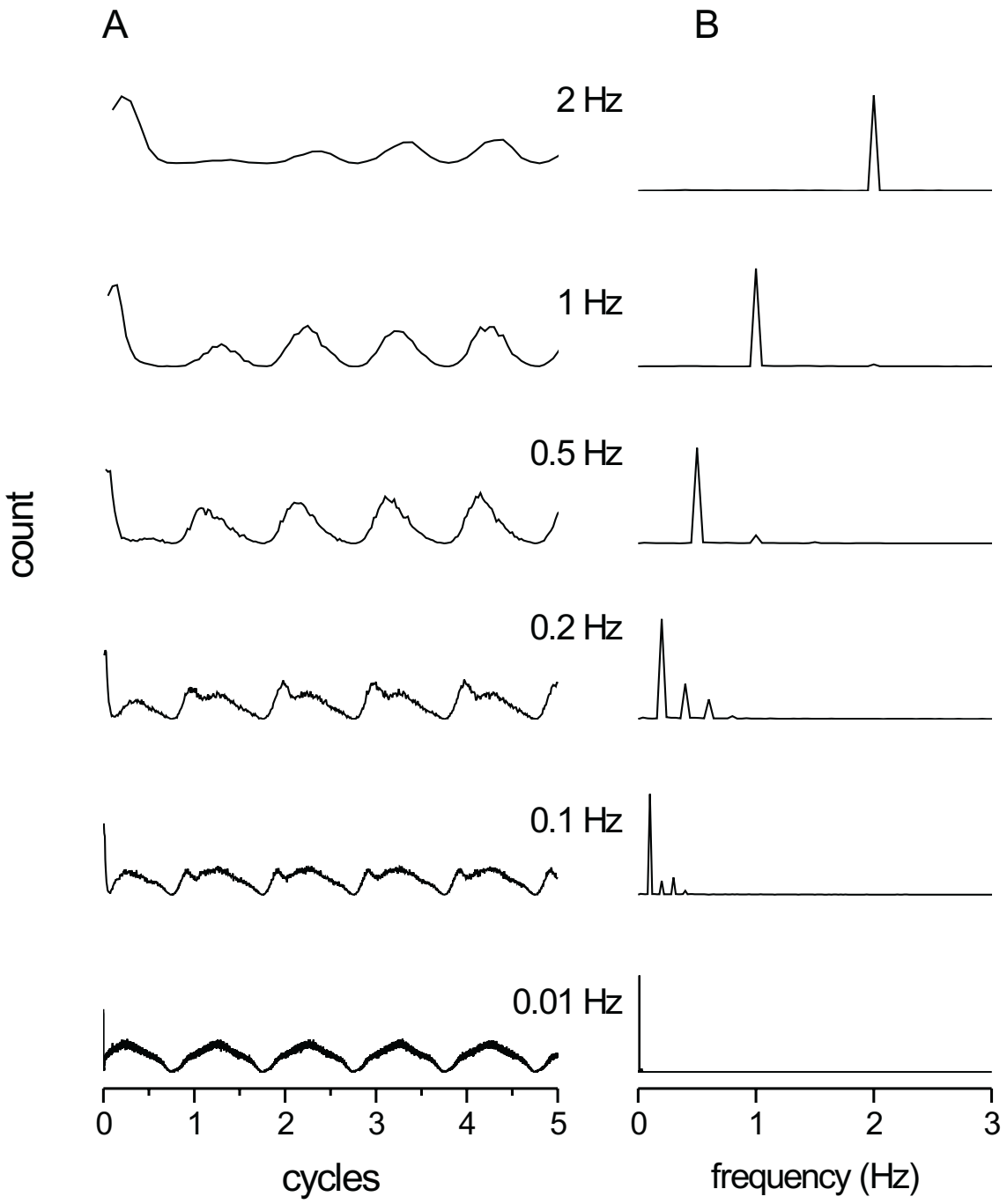

Figure 4.8: Network activity as function of time for networks receiving input of the form $r(t) = \frac{1}{2}A(1 + \sin(2\pi ft))$. In these plots A was 20Hz and f is indicated adjacent to each plot. *A*. Action potential firing rate as a function of phase. *B*. Power spectra for the signals plotted in the left panel. Power spectra were calculated using sufficiently long time series so that the contribution of the initial transient was negligible.

AHP	strength	speed (mm/s)	distance (mm)	rate (Hz)
10^{-1}	1	< 0.1	< 2	0.0
10^{-1}	3	< 0.2	2–4	0.0
10^{-1}	5	1.1	4–6	0.0
10^{-1}	10	2.2	∞	0.3
10^{-2}	1	< 0.1	0–2	0.0
10^{-2}	3	1.5	4–6	0.0
10^{-2}	5	0.8	∞	0.6
10^{-2}	10	2.5	∞	1.0
10^{-3}	1	0.2	∞	23
10^{-3}	3	1.5	∞	25
10^{-3}	5	2.7	∞	25
10^{-3}	10	4.4	∞	25

Table 4.1: This table summarises the ability of networks to transmit a signal over a distance. The size of the residual AHP and synaptic strength have been varied and the speed and distance of propagation in the anal direction are reported. After the activity front passed through an area some networks settled into a nonzero firing rate state and the firing rate of this state is reported in the rightmost column.

4.4 Discussion

Using a modification of the mean firing rate model of Wilson and Cowan [1972], it has been shown that in the absence of inhibition recurrent networks of sensory neurons have two stable firing rate states and are unable to meaningfully transduce input. This is shown by equation (4.9) and figure (4.3). However, if the AHP is larger than a threshold value, then the stable state at high firing rates is removed and the network can give graded responses to constant input. Furthermore, the low firing rate state is always stable and possibility of more complex dynamics, such as oscillations, is low. As long as the AHP is not completely suppressed by the slow EPSP, these qualitative properties of the network are insensitive to the exact values of the parameters making this a robust network architecture.

These predictions were tested numerically. Figure (4.4) shows that the simulated networks are bistable in the absence of input and figure (4.5) shows that the presence of AHPs, even when suppressed, "stabilises" the network by removing the high firing rate state. The prediction that these networks lack complex states, such as periodic solutions was tested by applying time varying input into an anatomically realistic network, which has the potential to uncover complex dynamics such as periodic solutions. For example, if the system had an oscillatory state then this should have been revealed by driving the system at close to its natural frequency. However, while the network was tested with sinusoidal inputs covering a wide range of frequencies and amplitudes it only showed some distortion at low frequency and a transient filtering of high frequency signals. Low frequencies correspond to slowly applied stimuli equivalent to the slow distensions often used to initiate peristalsis in isolated

segments of small intestine [Waterman et al., 1992, 1994a, Brookes et al., 1999]. High frequencies correspond to time courses of rapid distension or mechanical stimuli applied to the mucosa that evoke simple ascending or descending reflexes in isolated preparations of the small and large intestine [Smith and Furness, 1988, Smith et al., 1990, Yuan et al., 1991, Smith and Robertson, 1998, Spencer et al., 1999]. The transient depression in firing seen in the network simulations has a counterpart in physiological experiments. When two or more mechanical stimuli are applied to the mucosa within 1–2 s, then the second and subsequent reflex responses recorded in either neurons or muscle are markedly depressed [Bornstein et al., 1991a, Smith et al., 1991, 1992, Yuan et al., 1991]. This appears to be due to failure in the output of sensory neurons. A similar effect is seen when a distension is applied rapidly and then maintained at a constant volume for several seconds [Smith et al., 1991, 1992]. In each case, the time course of the initial suppression of the reflex is similar to that of the suppression in firing seen in the simulation studies. In the simulation, this transient suppression of firing is due to the full size AHPs that occur at the beginning of the input before the slow EPSPs develop, suggesting that the early decline in responses seen during physiological recordings may come from the same source.

The simulated networks display two types of signal propagation (table 4.1) — propagation where the signal decays within a few millimetres and propagation over an indefinite distance. The distance that the signal will propagate increases with increasing excitability of the network, either stronger synaptic strength or greater suppression of the AHP. The first type of propagation may be important in local reflexes as a form of facilitation. Propagation over indefinite distances only occurs

in bistable networks. In some of these networks, the firing rate of the non-quiescent state is low enough that they still support signal transduction, but propagation only occurs through a quiescent network. In the non-zero firing rate state, the network activity is such that slow EPSPs are fully active and neurons are as depolarised as much as they can be, and so further synaptic input is unable to alter the postsynaptic firing rate. In other words, synaptic transmission is no longer effective and signal propagation is not possible. Once in the non-zero firing rate state, these network will never return to the zero firing rate state. Thus, these networks do not support propagation over indefinite distances under physiological conditions. Propagation in sensory neuron networks is discussed more fully in chapter 7.

These results suggest an important role for the AHP in enteric sensory neurons. When no slow EPSP is present, groups of sensory neurons are similarly unable to transduce input because their firing rate is limited. Slow EPSP excitation and AHP inhibition interact to keep neurons at a high level of excitability while preventing them from firing at high frequency, and hence they are able to convert PPP input to AP output. Interestingly, in some cases the stable network state does have activity, which can be interpreted as spontaneous firing. Experimental preparations in which the mucosa is intact also display spontaneous activity [Kunze et al., 1997], however it is unclear whether this is due to sensory drive or is intrinsic to the network. Simulated networks with small amounts of spontaneous activity are still able to transduce stimuli, other than those of very low frequency. This may be related to the observation that, at least for some brief stimuli, sensory neurons fire a burst of action potentials [Bertrand et al., 1997a]. This would ensure that weak, or highly phasic, stimuli are discernible above spontaneous activity.

There is some evidence that the AHP is completely abolished after long term synaptic activation [Clerc et al., 1999], so the AHP is probably not the only mechanism to control network firing. However, the analytical model shows that any change in firing properties that mimic a relative refractory period will also provide the required inhibition. Such changes might come from an increase in firing threshold due to voltage dependent conductances. Further exploration of this idea requires the construction of realistic conductance models of intrinsic sensory neurons. Other candidates for inhibition are examined in the following chapters.

Chapter 5

The role of IPSPs

5.1 Introduction

In this chapter, the role of inhibitory postsynaptic potentials in the recurrent networks of sensory neurons is examined. Although not prominent, slow IPSPs are also seen in many myenteric neurons, including the intrinsic sensory neurons [Johnson et al., 1980, Christofi and Wood, 1993]. The source of these IPSPs is unknown and no specialised inhibitory interneurons, which make connections to sensory neurons, have been identified in the enteric nervous system [Costa et al., 1996]. However, IPSPs can be evoked by electrical stimulation of circumferentially directed internodal strands (Johnson & Bornstein, unpublished), which largely contain the circumferentially directed axons of intrinsic sensory neurons [Stebbing and Bornstein, 1996]. Thus, it is likely that both slow EPSPs and slow IPSPs seen in intrinsic sensory neurons arise from the recurrent terminals of neurons of the same functional class. Although it has been difficult to prove that a single nerve terminal produces both excitation and inhibition in the postsynaptic neuron, there is now good evidence to

indicate that this can happen, even when only a single transmitter is released [Fiorillo and Williams, 1998]. The role of a mixed excitatory and inhibitory transmission remains an important question in neuroscience.

The mean firing rate model of Wilson and Cowan [1972] was modified to test the possibility that slow IPSPs arising from cotransmission from the terminals of intrinsic sensory neurons may act in place of residual AHPs to *stabilise*, or remove the high firing rate state from, these recurrent networks and, if so, how the qualitative properties of such networks differed from those stabilised by AHPs. The revised analytical model was only used to test steady state input so numerical simulations, based on anatomically realistic models, were used to test the predictions of the analytical model and to investigate transduction of time varying inputs.

5.2 Methods

Computer simulations were performed as described in chapter 3 and chapter 4, section 4.2, with the addition of IPSPs arising from activation of terminals in the intrinsic sensory neurons. The IPSP conductance was described by

$$g_{\mathrm{IPSP}}(t) = \bar{g}_{\mathrm{IPSP}}\, p(t) \tag{5.1}$$

where, $p(t)$, is also described by equation (3.4), but rate constants were different, a conductance was opened (instead of closed), the driving potential was V_{K} and there was no interaction with any other conductances. Parameters were chosen to reflect the experimental observation that myenteric IPSPs are shorter and involve smaller conductance changes than the slow EPSPs [Johnson et al., 1980, Christofi and Wood, 1993]. Unpublished data from our group indicate that, of 67 intrinsic sensory neurons

studied, IPSPs could be observed in 25 neurons in response to repetitive electrical stimulation of internodal strands (10 or 20 pulses in 1 s). Durations ranged from 2–17 s and amplitudes ranged from 0.5–6.7 mV. All had short latencies (< 1 s), which were much shorter than slow EPSP latencies. Simulation parameters were chosen to encompass the observed data and it was assumed that all intrinsic sensory neurons were able to generate IPSPs. An example of a simulated IPSP elicited by 10 synaptic inputs in 1 s is illustrated in Figure 5.1*A* and a real IPSP elicited by 10 internodal strand electrical shocks in 1 s is shown in panel *B*. The simulated IPSP is one of the smaller ones tested.

5.3 Results

Theory

In order to examine how both IPSPs and EPSPs arising from the same terminals can effect the firing rate, an analysis based on the WC model and similar to that in section 4.3 was performed. Again, only steady state firing is analysed.

For networks with IPSPs and no AHP, equation (4.8) becomes:

$$\bar{E} = f(\bar{E}, P) \tag{5.2}$$

$$f(\bar{E}, P) = S(\mathcal{L}^{(E)}(\bar{E}) - \mathcal{L}^{(I)}(\bar{E}) + P). \tag{5.3}$$

where symbols have the same meaning as equations (4.9–4.11), with the addition that $\mathcal{L}^{(I)}$ and $\mathcal{L}^{(E)}$ describe the inhibitory and excitatory synaptic response for a given steady firing rate $\bar{E}$. The minus sign in the argument of S leads to more complex behaviour because the relative strengths of the inhibition and excitation

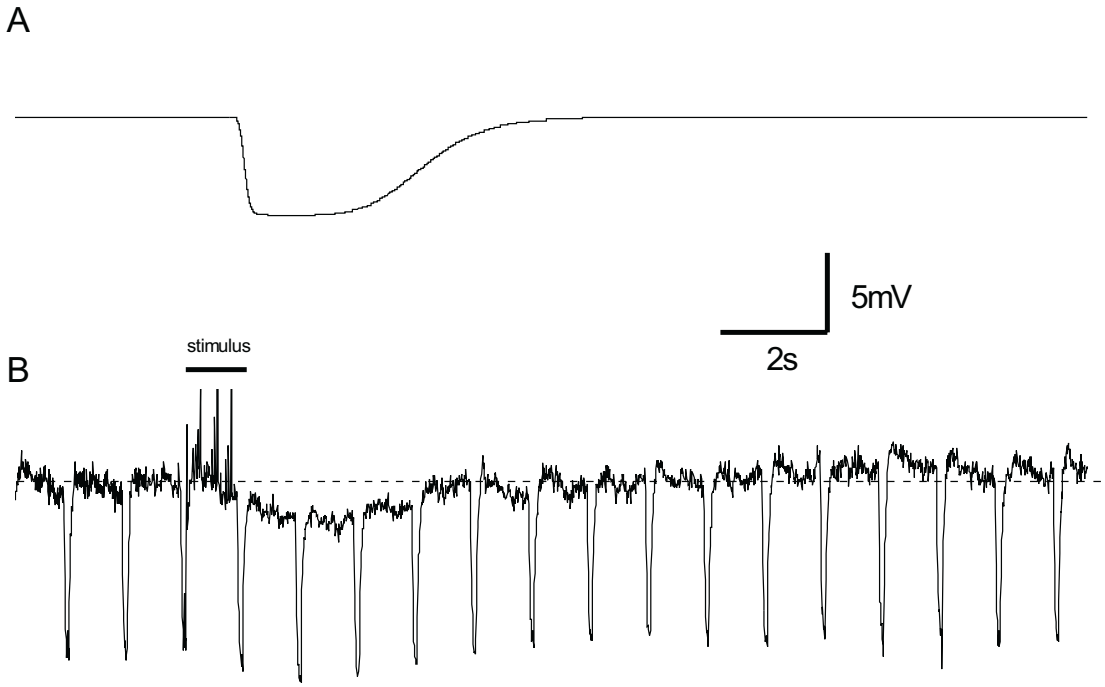

Figure 5.1: Simulated and real IPSPs. *A.* A simulated membrane potential trace produced from the model described in the text. The stimulus was 10 synaptic events in 1 s and the parameters used were $\bar{g}_{\mathrm{IPSP}} = 0.26$, $\alpha = 4$ and $\tau = 0.25$. *B.* A IPSP observed in a sensory neuron by P. J. Johnson. The simulated IPSP was not meant to match the time course of the real IPSP.

can change for different rates of firing.

The algebraic relationship described by equation (5.2) is illustrated diagrammatically in figure 5.2.

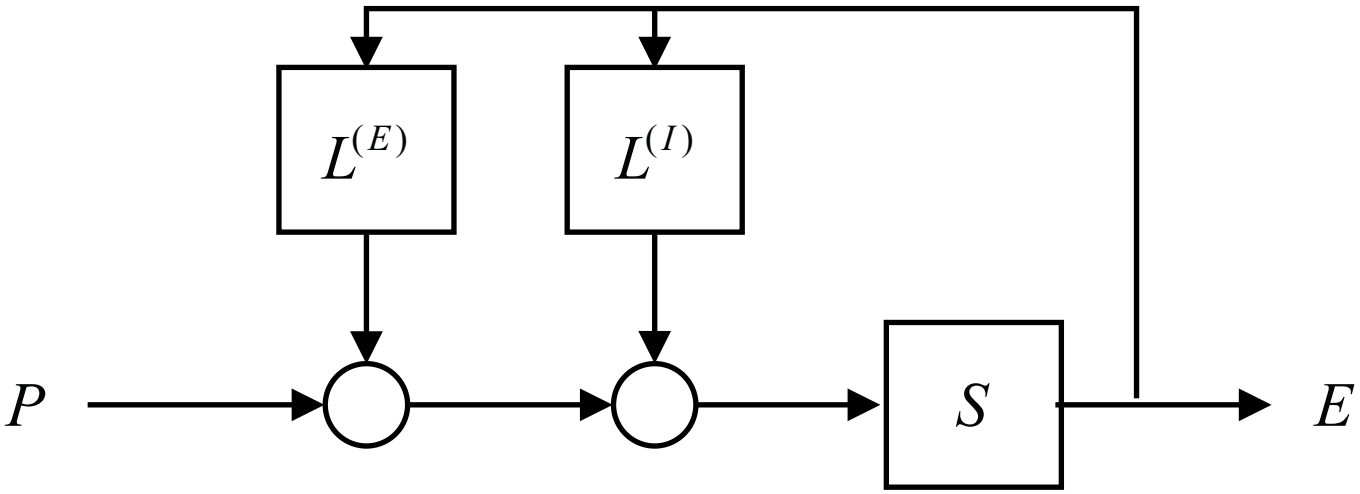

Figure 5.2: Diagrammatic representations of equation (5.2) Arrows indicate the direction of signal flow, circles indicate addition or subtraction as indicated, blocks represent processing of the signal. P is proximal process potential input and E is output action potential firing rate. The network is recurrent so the output signal, E loops back into the input.

The effect of inhibitory cotransmission on network behaviour is illustrated with some examples.

Example 1 — fast transmission For the first example directly ligand gated synaptic currents (fast EPSPs) are considered, these are brief (a few tens of milliseconds at most) and sufficiently small (a few millivolts) that they can be considered to sum linearly. As shown by Wilson and Cowan [1972]

$$\mathcal{L}^{(E,I)}(\bar{E}) = k_{E,I}\,\bar{E} \tag{5.4}$$

and equation 5.2 reduces to the form

$$\bar{E} = S((k_E - k_I)\bar{E} + P).$$

If $k_E - k_I > 0$ then this is equivalent to a purely excitatory network and is bistable. If $k_E - k_I < 0$ the network is equivalent to a network with only inhibitory transmission. An interesting conclusion from this is that for recurrent networks made up of a single type of neuron, synaptic transmission must be nonlinear for the network to perform biologically useful transduction.

Example 2 — bistability If synaptic transmission is neither linear nor brief the network may have more than one stable state. For example, if

$$\mathcal{L}^{(I)}(\bar{E}) = k_I\,\bar{E} \tag{5.5}$$

$$\mathcal{L}^{(E)}(\bar{E}) = 1 - \exp(-k_E\bar{E}) \tag{5.6}$$

and $k_E > k_I$ the excitation will exceed inhibition at low levels of activity, but inhibition will exceed excitation at high levels. The $y = f(\bar{E}, 0)$ (the zero input case) and $y = \bar{E}$ curves for this scenario are shown in Figure 5.3, panel A. There is always a zero firing solution and a second solution for $f(\bar{E}, 0) = \bar{E}$ will be stable if the inhibitory input changes more rapidly with firing than the excitatory input. If firing increases, inhibition increases more rapidly than excitation moving the system back to the equilibrium; and if firing decreases, inhibition will decrease faster than excitation, again pushing the system back to the equilibrium. Bistable states were observed in numerical simulations for an IPSP model in which the conductance summed linearly for multiple events.

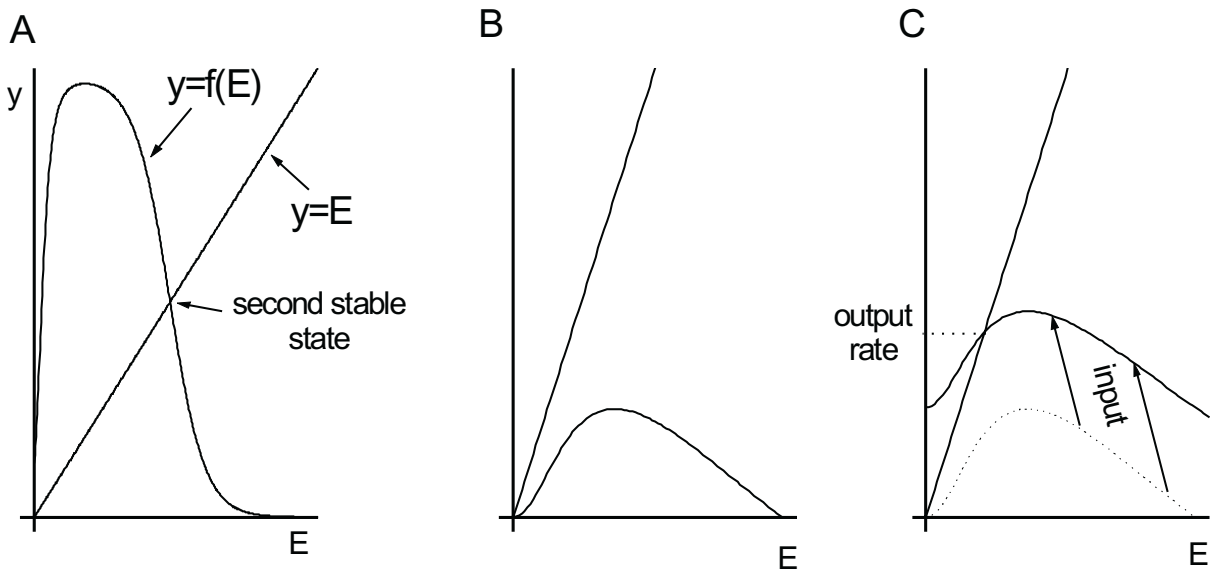

Figure 5.3: A geometric interpretation of equation (5.2). The solution of equation (5.2) occurs at an intersection of the curves $y = E$ and $y = f(E, P)$, where E is the output firing rate, P is the magnitude of the input and f is defined in the text. *A.* With appropriate dynamics for the inhibitory and excitatory synaptic transmission it is possible for the network to have two stable firing rates, in the absence of input. *B.* When the difference between excitatory and inhibitory transmission is small, as described in the text, the $y = f(E, 0)$ curve will drop below the $y = E$ curve, leaving the zero firing state as the only stable state in the absence of input. *C.* The effect of exogenous input on the $y = f(E, P)$ curve is to flatten it and move it to the left. There is still only a single stable firing state, which is graded with the magnitude of the input.

Example 3 — slow transmission If a population of neurons is receiving a constant average input of $\bar{E}$ then the slow EPSP model described by equation (2.6) predicts that the average membrane depolarization is given by

$$\mathcal{L}^{(E)}(\bar{E}) = A\,\frac{\bar{E}^2}{\bar{E}^2 + B}$$

where A and B are constants that depend on the parameters of the model and the amount of conductance closed. There is a similar expression for $\mathcal{L}^{(I)}$. In this case, by appropriate choices of parameters

$$D = \mathcal{L}^{(E)}(\bar{E}) - \mathcal{L}^{(I)}(\bar{E}) \tag{5.7}$$

can be kept small and so $S(D)$ will also be small. Physiologically, these parameters determine the strength of responses to a given input and how quickly the response dies away. These, in turn, determine the average degree of membrane potential change for a constant input. At high firing rates, D will depend only on the difference in maximum synaptic currents. At low firing rates, D will depend on how sensitive synaptic currents are to the firing rate. The sign of D can be the same throughout the range of E corresponding to the case where either inhibition or excitation dominate throughout the firing range. Alternatively, D can change sign at some point, corresponding to the case where one type of synaptic input overtakes the other as E increases. In any case, provided $\max(D)$ is small enough, there will be only a single stable state at rest.

Figure 5.3, panel B illustrates how IPSPs can "stabilise" the network by removing the high firing rate state. In this figure, excitation dominates at low firing rates and inhibition dominates at high firing rates so the $y = f(\bar{E}, 0)$ curve is no longer sigmoidal and is dragged below the $y = \bar{E}$ curve leaving only the zero firing state as

a solution.

Figure 5.3, panel C illustrates the effect of sensory input, $P > 0$. As P increases the $y = f(\bar{E}, P)$ moves left and flattens out. Now, the intersection of the $y = \bar{E}$ and $y = f(\bar{E}, P)$ curves occurs at a nonzero value of E — the output firing rate. As with the AHP networks, the output firing rate is graded with input firing rate and it is unique. Thus, the output firing rate, E, is graded with stimulus strength, P, and uniquely codes the magnitude of the stimulus. This argument holds true no matter what the sign of D since P always lifts the $y = f(\bar{E}, P)$ curve (and possibly flattens it), but because the $y = f(\bar{E}, P)$ curve does not turn back on itself the value of E at the intersection with the $y = E$ curve is never decreasing. These arguments apply in general when both inhibitory and excitatory transmission saturate within physiological firing rate limits, and show that a recurrent network with inhibitory and excitatory cotransmission can uniquely code the magnitude of a steady input.

Numerical simulation of networks with IPSPs

The IPSPs in the intrinsic sensory neurons are typically only seen as a result of repetitive electrical stimulation and have time courses that strongly suggest activation of metabotropic receptors (e.g. they can last up to 10 s) [Johnson et al., 1980, Christofi and Wood, 1993]. There are no quantitative data about stimulus response characteristics, however second messenger mediated events sum nonlinearly at the level of membrane conductance change. In the numerical model, the IPSP equations were the same as those for the second messenger mediated slow EPSP (equations (2.6)) [Bertrand et al., 2000b]. The durations of IPSPs in the myenteric plexus are always shorter than those of slow EPSPs in the same neurons (Johnson & Bornstein,

unpublished), so the slow IPSP halflives were the slow EPSP halflives multiplied by the factor $\tau \in \{0.25, 0.5, 1\}$. Other parameters tested were all combinations of $\bar{g}_{\text{IPSP}} \in \{0.13, 0.26, 0.52, 1.0, 2.1, 4.2\}$, $\alpha \in \{1, 2, 4\}$.

Stimulus response curves were obtained by playing random, constant mean frequency PPP input into neurons and determining the average action potential rate per neuron after the network reached the equilibrium firing rate. All parameter sets listed above, except for one, lead to networks with a single stable firing state for each input, when the input was zero this state was the quiescent state. Figure 5.4 shows stimulus response curves for a selection of these parameters. For low values of $\bar{g}_{\text{IPSP}}$ the IPSP keeps the membrane potential below threshold, but not so low that a single PPP cannot trigger an action potential. Thus, other than during the refractory period, these networks simply converted PPPs into action potentials. At higher values of $\bar{g}_{\text{IPSP}}$, the membrane spends considerable time below resting potential and PPPs are gated. In the case of very large IPSPs ($\bar{g}_{\text{IPSP}} = 4.2$, $\alpha = 4$ and $\tau = 1$, which gives a maximum hyperpolarization of 24mV in response to 10 synaptic events in 1 s) the output does not always increase with increasing input. This is not predicted by the theoretical analysis above. The reasons for this behaviour are unclear, however it may due to a breakdown in the assumption that network behaviour can be predicted from the mean firing rate. These networks show strong erratic bursting (more below) and this network behaviour may depend on higher order moments of the spiking statistics.

The network with $\bar{g}_{\text{IPSP}} = 0.13$, $\alpha = 1$ and $\tau = 0.25$ did not return to the quiescent state when input ceased, if the input was greater than a threshold of around 1 Hz. These networks settled on an average firing rate of 1.1Hz. These

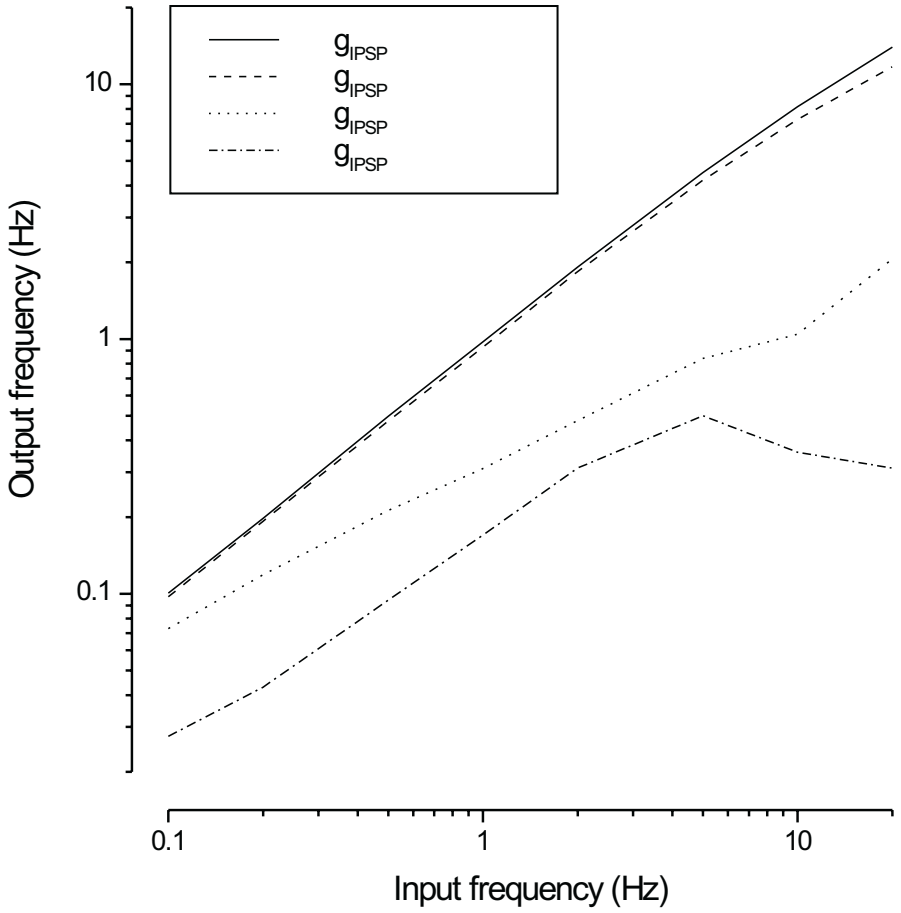

Figure 5.4: Stimulus response curves for networks with IPSP based inhibition. Constant frequency exogenous input, in the form of proximal process potentials, is played into the network and the output in action potentials per second, averaged over the network, is determined after the firing rate reaches equilibrium. Four curves are shown for different IPSP parameter sets, the meaning of the parameters is explained in the text. Log scales are used on both axes.

parameters produce an IPSP with a maximum hyperpolarisation of -3 mV and that returns to within 10% of rest in 3.8 s, in response to 10 synaptic events delivered in 1 s, which closely matches those observed experimentally (P. J. Johnson and J. C. Bornstein, unpublished). Figure 5.5, panel A shows network activity as a function of time for these parameters, in a network that was given a 5 Hz stimulus for 20 s. In the previous chapter, these networks were referred to as spontaneously active, since the quiescent state would not be observable in practice. This network was still able to give graded responses when the input rate was higher than that of the spontaneous activity.

Erratic bursting in IPSP networks

The IPSP networks had two parameter regimes in which individual neurons fired erratic bursts. Bursts are distinct clusters of spikes separated by quiescent periods that are long compared the interval between spikes within a burst. Erratic bursting means that the duration and number of spikes in a burst and the intervals between bursts showed significant variation. Bursting was quantified with the simple measure $\beta = \sigma/\mu$ where μ is the mean of the interspike intervals and σ is the standard deviation of the interspike intervals [Zar, 1984]. The larger the value of β the more clustered are the spikes. For a Poisson distribution $\beta = 1$ and for a perfectly regular spike train $\beta = 0$.

The first parameter regime was around $\bar{g}_{\mathrm{IPSP}} = 0.13$, $\alpha = 1$ and $\tau = 0.25$, which is within the range observed *in vitro*. These networks are spontaneously active and the erratic bursting occurs in the absence of input. Data are illustrated in Figure 5.5 for an experiment in which a stimulus of 5 Hz average PPP input is applied for the

first 20 s. After the stimulus ceases, network firing immediately plummets to zero since the membrane potentials are below threshold. The IPSPs quickly die away and the longer lasting EPSPs drive the membrane potentials above threshold and firing resumes. Panel B of Figure 5 shows spike trains (not membrane potentials) of neurons selected from this network. For the neurons shown β ranged from 6.1–9.3 with a mean of 7.7 indicating a high degree of clustering.

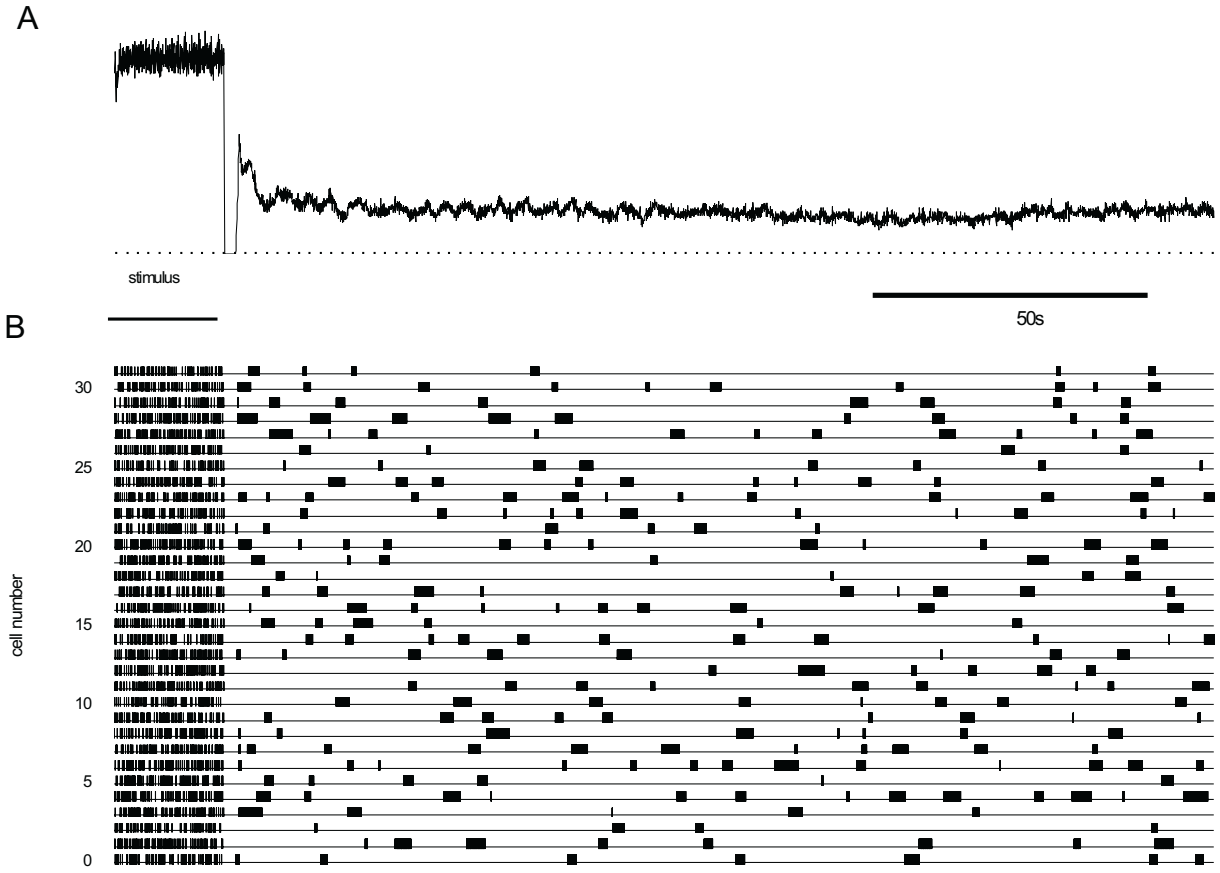

Figure 5.5: For very small, brief IPSPs the network has a second stable firing state. These data are recorded from a network in which a 20 s stimulus of 5Hz proximal process potential input has been applied, as indicated. The network settled into a nonzero firing state. *A.* Network firing rate in action potentials per second, averaged over the network, as a function of time. *B.* Spike trains (not membrane potential traces) for 32 neurons selected from the network. Erratic bursting is clearly apparent once the stimulus has ceased.

In the second regime, the size of the IPSPs was large enough to hyperpolarise the membrane below resting membrane potential. This occurred even in the presence of slow EPSPs, so that a single PPP was no longer able to generate a spike until the IPSP died away and the membrane repolarized. In this parameter regime, erratic bursting was present when networks were exogenously driven. Figure 5.6 shows spike trains selected from a network with $\bar{g}_{\mathrm{IPSP}} = 2.1$, $\alpha = 1$ and $\tau = 0.25$, with the β value indicated on the right of each trace. These parameters produce an IPSP with a maximum hyperpolarization of -23.7 mV and that returns to within 10% of rest in 4.8 s, in response to 10 synaptic events delivered in 1 s. Each neuron received, on average, 5Hz PPP input. The β values for the neurons in the figure ranged from 1.1–5.0 with a mean of 2.6. The range of firing rates varied from zero up to firing an action potential with almost every PPP. In all cases, $\beta > 1$ indicating some clustering of spikes. The average values of β from about 30 neurons increased as the IPSP conductance increased and increased slightly with increasing τ and α.

Time varying inputs

Figure 5.7 shows the response of a network in which AHPs are absent and IPSPs are present. The IPSP parameters for this network were $\bar{g}_{\mathrm{IPSP}} = 0.26$, $\alpha = 1$ and $\tau = 0.25$, which gives an IPSP with a maximum hyperpolarization of 5.6mV and which takes 3.9 s to return to within 10% of rest in response to 10 synaptic events in 1 s. For these parameters, there is little transient response at the onset of the stimulus and little distortion of the signal. Networks with larger and longer IPSPs do display an initial transient depression which can be several seconds if the IPSP is large and lasts several seconds.

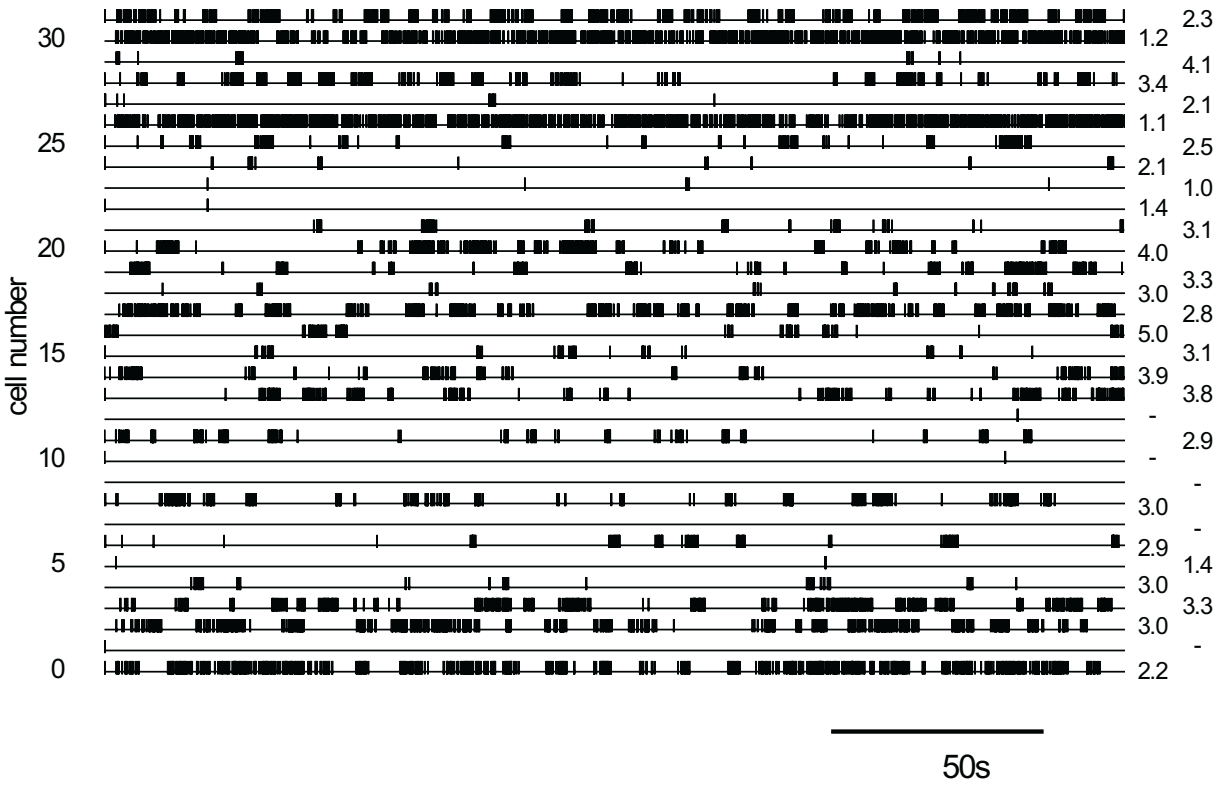

Figure 5.6: Total network activity and spike trains (not membrane potential traces) for 32 neurons. The parameters used were $\bar{g}_{\mathrm{IPSP}} = 4.2$, $\alpha = 1$ and relative halflives of 1. Trace durations are 250 seconds. A variety of patterns are evident, from almost continuous firing to very low apparently random spike rates. The numbers on the right, next to each trace, are the values of β (see text). Not all traces had a sufficient number of spikes to calculate β.

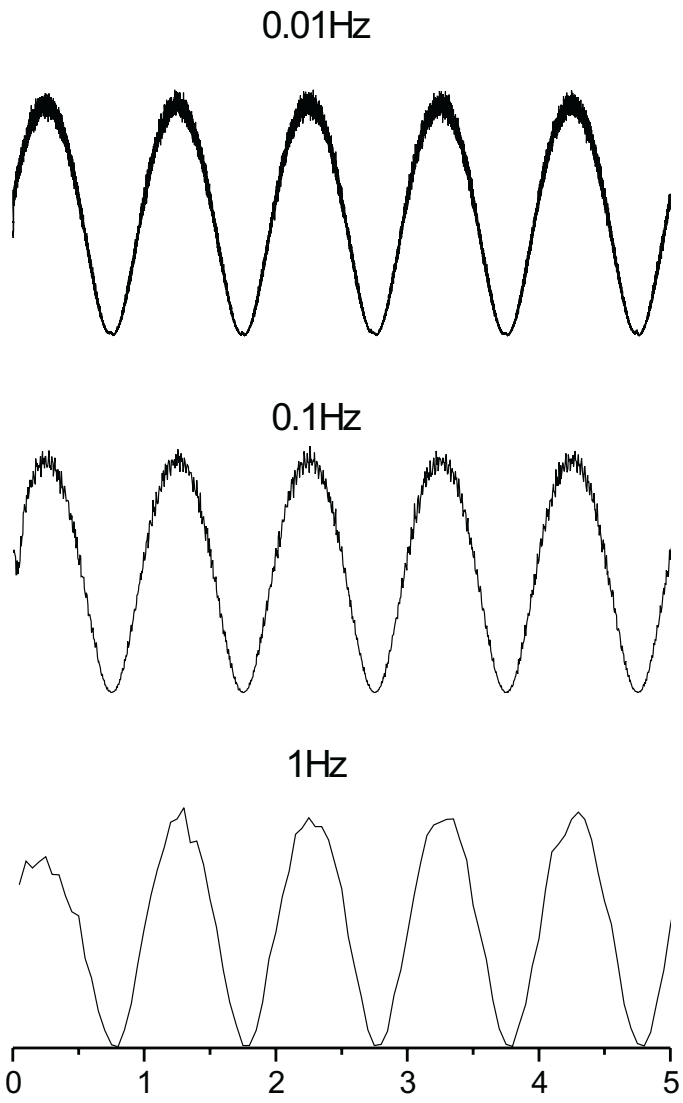

Figure 5.7: Sinusoidally varying inputs were played into networks, initially at rest, as described in the text. The network activity, as action potentials per second averaged over the network, is plotted against the phase of the sine wave. In these plots the peak amplitude was 20Hz and the sine wave frequencies are indicated in the figure, adjacent to each plot. The parameters of the IPSPs were $\bar{g}_{\mathrm{IPSP}} = 0.26$, $\alpha = 1$ and $\tau = 0.25$.

IPSPs and AHPs

Data from electrophysiology suggest that under normal circumstances, both IPSPs and AHPs can be expected to act on the intrinsic sensory neurons. Thus, the behaviour of simulated networks in which both were active, but where the AHP was reduced to 0.1% of its original amplitude during a maximal slow EPSP were examined. The previous analysis indicated that networks with such a small AHP were bistable and unable to code physiological levels of input (see Figure 4.4). It was found that the addition of even the smallest metabotropic IPSPs from the parameter sets listed above allowed networks with such small residual AHPs to have a single stable state and to encode sustained inputs. As with IPSPs or AHPs alone, the gain of the networks could be controlled by the size of either the AHPs or the IPSPs.

Propagation in IPSP networks

These networks were tested for their ability to support signal propagation, in a manner similar to section 4.3. Networks 15 mm in the longitudinal direction and 5 mm in the circumferential direction were stimulated in the oral 5 mm section for 4 s with 20 Hz PPP input. All parameter combinations of IPSPs listed above were tested. None of the parameter combinations supported signal propagation over large distances, including the bistable network discussed above.

5.4 Discussion

This chapter has examined the properties of networks with a single population of recurrently connected neurons. These neurons caused both EPSPs and IPSPs in

their postsynaptic targets by coreleasing both excitatory and inhibitory transmitters from the same terminals. It was shown that if neurons have properties similar to those seen in physiological experiments then these networks can perform sensory transduction in a biologically useful way.

A theoretical analysis was done using a modification of the mean firing rate model of Wilson and Cowan [1972] and is summarised in figure 5.3. It provides a qualitative explanation of how IPSPs and EPSPs induced by the same source neurons, can ensure that recurrent networks encode the magnitude of sustained input. Numerical simulations also indicate that IPSPs alone, or with AHPs, can lead to encoding of the magnitude of sustained input. The ability to do this is robust over a large range of parameters and the gain of the transduction can be varied by varying properties of the inhibitory cotransmission. Furthermore, simulations of the behaviour of intrinsic sensory networks with time varying inputs indicate that these networks can faithfully encode time dependent stimuli.

Although IPSPs have been observed in many myenteric neurons [Johnson et al., 1980, Christofi and Wood, 1993] their origins and the neurotransmitters that mediate them are unknown. No separate population of neurons with projections onto sensory neurons, has been identified in over 20 years of intense immunohistochemical studies [Costa et al., 1996] suggesting that IPSPs arise from neurons that also release excitatory neurotransmitters. The study from which our quantitative data was obtained (Johnson & Bornstein, unpublished) evoked IPSPs by stimulating circumferentially and thus preferentially selecting the axons of sensory neurons [Bornstein et al., 1991b, Stebbing and Bornstein, 1996]. Thus, the possibility that IPSPs are produced by a transmitter released from the terminals of sensory neurons together

with the excitatory transmitters responsible for slow EPSPs has been explored. Both the analytical results and numerical simulations demonstrate that inhibitory cotransmission can stabilise a network by removing the high firing rate state and allowing a unique output firing rate state for each sustained input state.

Numerical simulation uncovered the interesting result that neurons in networks with IPSPs, and without AHPs, display erratic bursting in their spike firing patterns. This was seen under two sets of conditions. Firstly, when IPSPs were small, comparable to those seen in the enteric nervous system, erratic bursting was present when sensory drive was absent. The second set of conditions which lead to erratic bursting was that IPSPs were large, comparable to those seen in central nervous system [Fiorillo and Williams, 1998], and the presence of sensory drive.

Erratic bursting has been observed in the myenteric plexus using extracellular electrodes in unparalysed tissue [Wood, 1970, Ohkawa and Prosser, 1972]. This bursting was uncorrelated with any other measurements, such as the rhythmic electrical or mechanical activity of the muscle. Erratic bursting depends on synaptic drive [Wood, 1975, Athey et al., 1981], which was also a finding of this study. However, bursting is only rarely seen using intracellular recording techniques, perhaps because in these preparations the muscle is paralysed and the mucosa is removed from the area near the impalements [Nishi and North, 1973, Hirst et al., 1974, Bornstein et al., 1994]. Spontaneous firing is seen under conditions where sensory drive is present in the form of mucosal input or spontaneous movements of the muscle [Kunze et al., 1997, 1995].

Thus it can be concluded that transmission of substances with opposite effects from the same group of terminals can allow networks to control their firing and

process stimuli over a wide variety of inputs.

Chapter 6

Synaptic depression introduces complex network dynamics

6.1 Introduction

The gut displays many rhythms [Bayliss and Starling, 1899, Cannon, 1902, Sarna, 1985, Bouchoucha et al., 1999, Andrews et al., 2001, Thuneberg and Peters, 2001] that are, at least in part, neurally mediated, from rhythmic peristaltic contractions which last seconds to migrating motor complexes whose entire cycle lasts hours. Rhythmogenesis requires that the current phase of the cycle is stored in one more state variables. These state variables may reside within neurons or they may be an emergent property of a network. Even if the phase is stored in individual neurons, a mechanism is required to ensure that all neurons are synchronised and this implies recurrent synaptic transmission. Therefore, the intrinsic sensory neurons are ideally placed to coordinate reflex activity over relatively long time scales of tens of seconds or more.

The forms of inhibition tested in recurrent networks thus far in this thesis are the AHP and IPSPs. These both act at the same time, or faster, than excitation, in the intrinsic sensory neurons. The AHP activates within 70 ms of an action potential firing [Hirst et al., 1974]. The time scale of onset of excitation is hundreds of milliseconds for slow EPSPs and the movements of the intestinal wall are also slow compared to the AHP delay. Thus, AHP inhibition activates essentially instantly. Similarly, IPSPs have short delays compared to slow EPSPs (Johnson & Bornstein, unpublished). (IPSPs with long delays may be masked by excitatory transmission.) Furthermore, *in vitro* experiments seem to indicate that both forms of inhibition operate at a marginal level, being just sufficient to remove the high firing rate states. It is therefore unlikely that these networks can display rhythmic behaviour and none were found by numerical simulation (see chapters 4 and 5). (Latham et al. [2000a] predict rhythmic bursting in a system with an AHP like current, however, as can be seen from equations 1.21 and 1.22, their current comes on slowly.) Such rapid onset, marginal inhibition is biologically useful when the task is a relatively simple transduction of a stimulus, but beucase it forces the networks to rapidly come to equilibrium they cannot engage in long term behaviour. Although not a strict requirement, slow, strong negative feedback with the appropriate parameters can lead to oscillations. Therefore, in this chapter activity dependent synaptic depression tested for its ability to generate rhythm in the networks of intrinsic sensory neurons.

Recurrent networks with excitatory transmission and activity dependent synaptic depression are capable of complex behaviours such as oscillations and chaos [Donovan et al., 1998, Senn et al., 1996, Tabak et al., 2000]. (Chaotic dynamics are aperiodic and bounded, but extremely sensitive to initial conditions.) Oscillations

occur when the negative feedback of synaptic depression is sufficiently slow that it is always "chasing the excitation" (see chapter 1 for a more detailed discussion of these networks). Short term synaptic plasticity, including depression, seems to be very common in the nervous system [O'Donovan, 1999, Nadim and Manor, 2000, Zucker, 1999, Fortune and Rose, 2001], and has been implicated in sensory processing and motor pattern generation.

In this chapter, the complex dynamics introduced by activity dependent synaptic depression were examined using both numerical simulation and analysis based on the 2 dimensional, model of Donovan et al. [1998] and Tabak et al. [2000] (also reviewed in chapter 1, section 1.7). The analytical model is a mean firing rate model, similar to the model of Wilson and Cowan [1972], but modified to include only excitatory neurons and including activity dependent synaptic depression. The analytical model provides powerful intuitive insight into oscillatory states displayed by this sort of network. The numerical simulations test the results in the analytical model with fewer constraints. For oscillatory states, the results of both models are presented in parallel.

6.2 Methods

Computer simulation

Numerical simulations were performed as described in chapter 2. Neurons transmitted to each other by slow EPSPs and not IPSPs. Some networks included AHPs as noted in the text. Networks were constructed to simulate a 5 mm $\times$ 5 mm section of guinea-pig ileum. Stimuli were mainly random PPP input with constant mean

frequency. In some cases, networks were tested with feedback, nominally representing the sensory feedback from muscle contraction. The feedback was proportional to the activity in the network and delayed by 50 ms. This delay was for ease of implementation and was not meant to represent the delay between neurons firing and contraction. The feedback was implemented by reading the activity as it was generated and feeding stimuli back via the "external stimulator" facility (see section 2.2). The degree of feedback is quantified as the number of PPPs generated for each action potential. The neurons that receive the PPPs are selected randomly, they are not the necessarily the neurons that issued the action potential. Output was read every 50 ms, for implementation reasons, and feedback played uniformly over the next 50 ms. In addition, $\alpha = 4.0 \times 10^{-3}$ (equation (2.6)), an increase over the value used in the previous chapters.

Activity dependent synaptic depression was modelled using this simple equation

$$\tau_s \frac{ds}{dt} = \Delta \sum_i \delta(t - t_i)\, s + (s_0 - s). \tag{6.1}$$

where $s(t)$ is the synaptic strength (see equation (2.6) on page 109), s_0 is the resting synaptic strength, t_i are the presynaptic spike times, τ_s is the rate of recovery, $\delta(t)$ is the Dirac delta function which describes an idealised pulse and Δ is a parameter. The term $\Delta\, \delta(t - t_i)\, s$ means that at spike time t_i the strength is instantaneously changed to $\Delta\, s$. For example, if $\Delta = 0.9$ the synaptic strength is reduced by 10% at each spike. (Potentiation can be modelled when $\Delta > 1$.) Between spikes the synaptic strength recovers to s_0 exponentially with a time constant τ_s. For long duration spike trains, the synaptic strength will reach an equilibrium value that depends on Δ and τ_s. The parameters Δ and τ_s were varied systematically as part

of the study.

Theoretical model

The equations for the mean firing rate model are [Donovan et al., 1998]

$$\tau_E \frac{dE}{dt} = S(d\,E) - E \tag{6.2}$$

$$\tau_d \frac{dd}{dt} = D(E) - d \tag{6.3}$$

where E is the mean firing rate; d is the synaptic depression. S is a sigmoid shaped population response function, given by

$$S(x) = \frac{1}{1 + \exp(-(x-\theta)/k_E)}. \tag{6.4}$$

D is also a sigmoid given by

$$D(x) = \frac{1}{1 + \exp((x-\theta_d)/k_d)}. \tag{6.5}$$

D is reversed, so it decreases as its argument increases, and τ_d and τ_E are the time constants for the two state variables [Donovan et al., 1998, Tabak et al., 2000]. Parameters were based on those in Tabak et al. [2000] and chosen to demonstrate the qualitative properties of the model. These are given in table 6.1 or noted in the text. Some properties of this model are summarised in the introduction (section 1.7).

Data for phase plane portraits are generated with the pplane6 software package (`http://math.rice.edu/~dfield/`) for Matlab 6.0 and plotted using Origin 6.0 (OriginLab Corporation, Northampton, MA, USA).

Parameter	Value
θ	0.2
k_E	0.05
τ_E	1
θ_d	0.5
k_d	0.2
τ_d	2

Table 6.1: Parameter values used in equations (6.2) and (6.3).

6.3 Results

Spontaneous dynamics

This section discusses the results of classifying the dynamics that these networks can display in the absence of ongoing external input. The numerically simulated networks always have the quiescent state as a stable state. However, this would not be visible under physiological conditions because even small stimuli will knock the network out of the quiescent state. To investigate states with nonzero firing, the networks were stimulated with a 5 Hz stimulus for 10 s to "kick" them into other states that they might have. This procedure is not guaranteed to uncover all possible states.

Because there are no measurements of synaptic depression between sensory neurons, a large space of synaptic parameters was searched. The values tried were $\Delta \in \{0.1, 0.2, 0.5, 0.6, 0.9, 0.99\}$ and $\tau_s \in \{0.5, 1, 2, 4, 8, 12, 16\}$ seconds. In many cases, the network firing returned rapidly to zero firing after the stimulus, evidence

that the network had only a single stable state. In other cases, firing settled at a new steady firing rate state. These networks were probably bistable, having only the quiescent state and a steady nonzero firing state. A small number of synaptic depression values lead to complex periodic or quasi-periodic states. Figure (6.1) shows a scatter plot of τ_s against Δ, with the category of the network indicated by a symbol. The parameter values for monostable and bistable networks form two simple, connected regions. In between these regions are the networks that have more complex firing states.

Figure (6.2) shows the activity of some of these states plotted against time. Note that the Y axis is different on each panel. When $\Delta = 0.8$ and $\tau_s = 8$ s (panel 6.2C) the network settles into a nearly periodic state with a frequency of 0.07 Hz. There appears to be another, small amplitude, modulation of the main oscillation but with a lower frequency. Firing in the two other states is more complex and consists of small fluctations around a mean, with no apparent structure. Figure (6.3) shows activity from network runs that were identical other than the seed of the random number generator, which determines which neurons are selected for receiving PPP input during the stimulus, and for providing minor variations in action potential firing. The activity between traces quickly diverges in time. Extreme sensitivity to initial conditions and perturbations is a characteristic of chaotic dynamics. Senn et al. [1996] observed chaos in excitatory networks with synaptic depression which may explain these states; however, other aspects of chaotic dynamics, such as a large number of period doubling bifurcations, were not observed. Given the moderate amplitude of the fluctuations there is no clear physiological role for these networks, so the question of whether they have a low order determinism, and whether it is

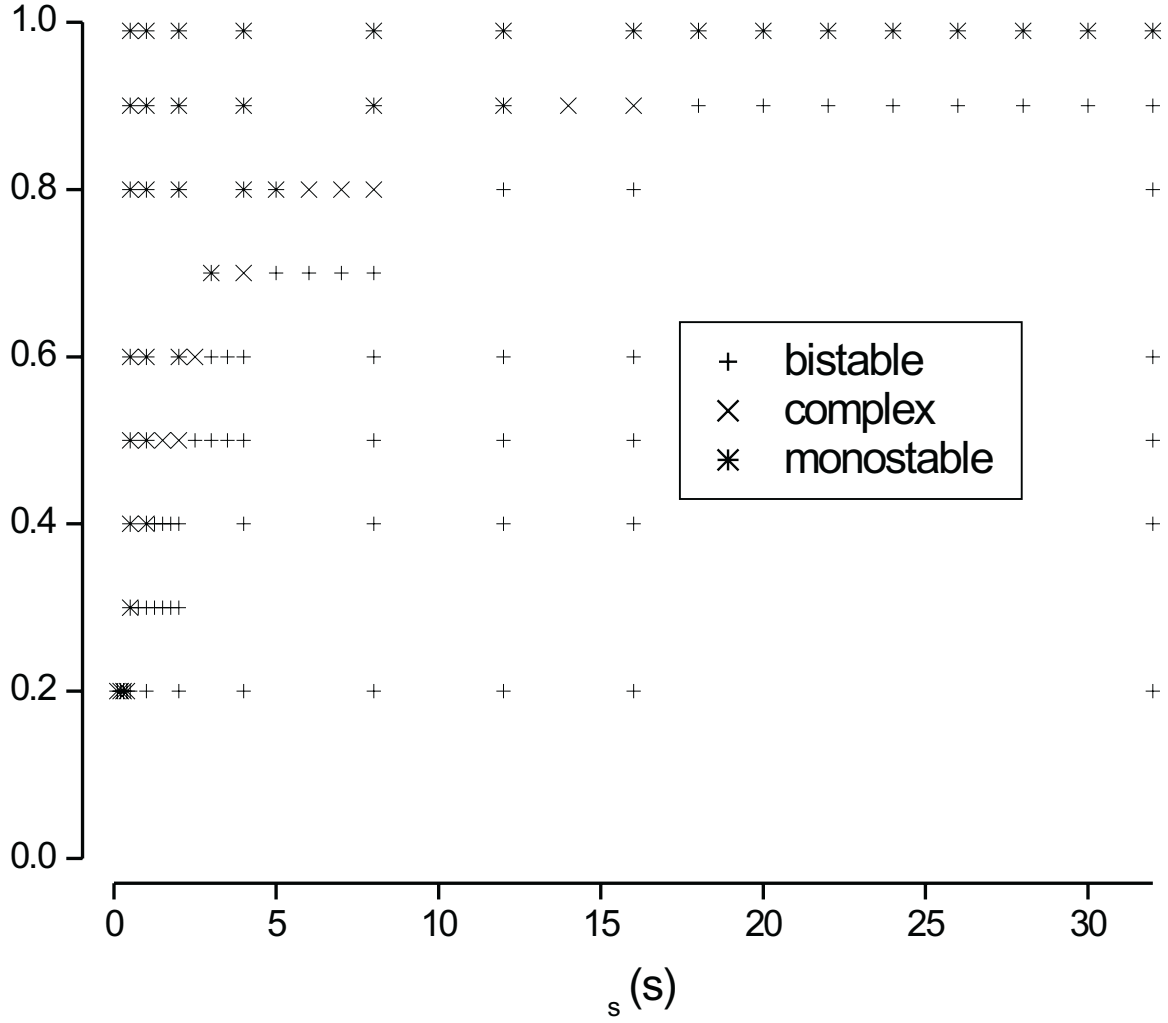

Figure 6.1: The dynamical states that a network can exhibit are dependent on the parameters controlling the synaptic depression. In the absence of exogeneous input the they have been classified into systems that are monostable (only the zero firing rate state is stable), bistable (a zero firing rate state and a high firing rate state are stable) and complex in which oscillatory, quasi-periodic or chaotic solutions are possible. This classification is plotted as a scatter plot for the parameters Δ and τ_s. This classification is approximate only.

chaotic, was not pursued.

Oscillatory states, in the absence of input, are predicted by the analytical model described by equations (6.2 – 6.3) Donovan et al. [1998], Tabak et al. [2000] (see also section 1.7). However, because the analytical model is two dimensional and so does not have chaotic dynamics.

Responses to constant stimuli

As in the previous two chapters, the response of the network to stimuli of constant mean frequency, random input was determined. Monostable networks fired at rates that were graded with input strength. Networks with two constant firing rate states showed responses that were graded below the threshold and went into high firing rate states for inputs above the threshold and when the input ceased they continued firing at high rates. Examples of time courses and stimulus response curves are shown in figure (6.4). These networks showed a strong transient increase in firing at the onset of the stimulus, unlike networks with AHP inhibition which transiently showed decreased firing. This transient increase in firing is consistent with a fade in electrical response recorded in circular muscle during reflex experimenents [Smith et al., 1991]. In Chapters 4 and 5, bistable networks were identified in which the nonzero firing rate state had a very low firing rate. These networks were termed spontaneously active and were still capable of giving graded responses to inputs and so were potentially physiologically useful. Interestingly, spontaneously active networks were not found when the only inhibition was synaptic depression. Instead, all networks with activity in the absence of input showed periodic or aperiodic variations in firing.

In the previous section, it was noted that, for some parameter values, networks had non steady firing states in the absence of input. In the numerical simulations, when constant input was applied to these networks the amplitude of the variations in firing decreased. These results are not specifically illustrated, but the effect is similar to that shown in figure (6.6).

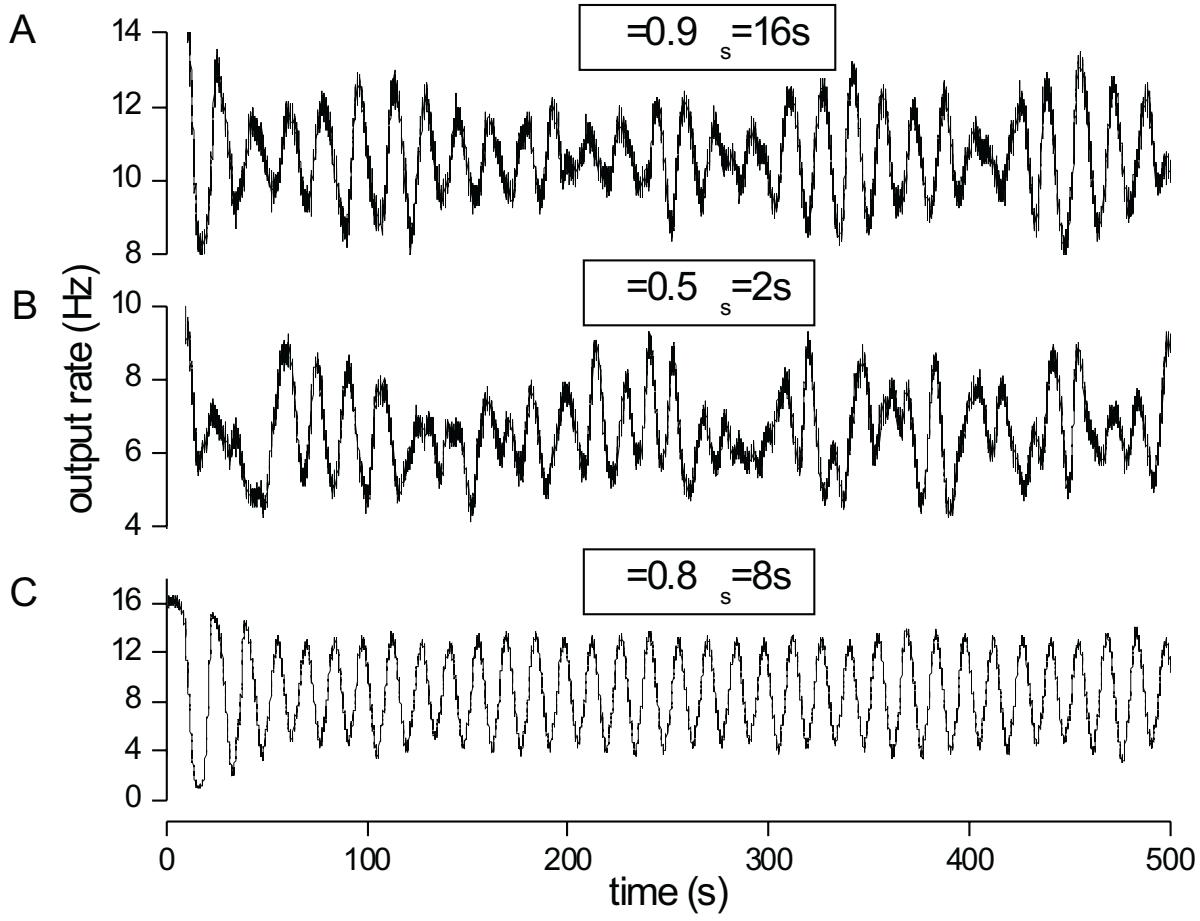

Figure 6.2: These graphs illustrate some of the complex firing patterns exhibited by networks, with activity dependent synaptic depression, for some values of Δ and τ_s. The plots show network activity, as the average firing rate per neuron, plotted against time. The networks have received a constant stimulus for the initial 10 s, as described in the text, after which they received no further exogenous input. The Y axis is not the same on all plots.

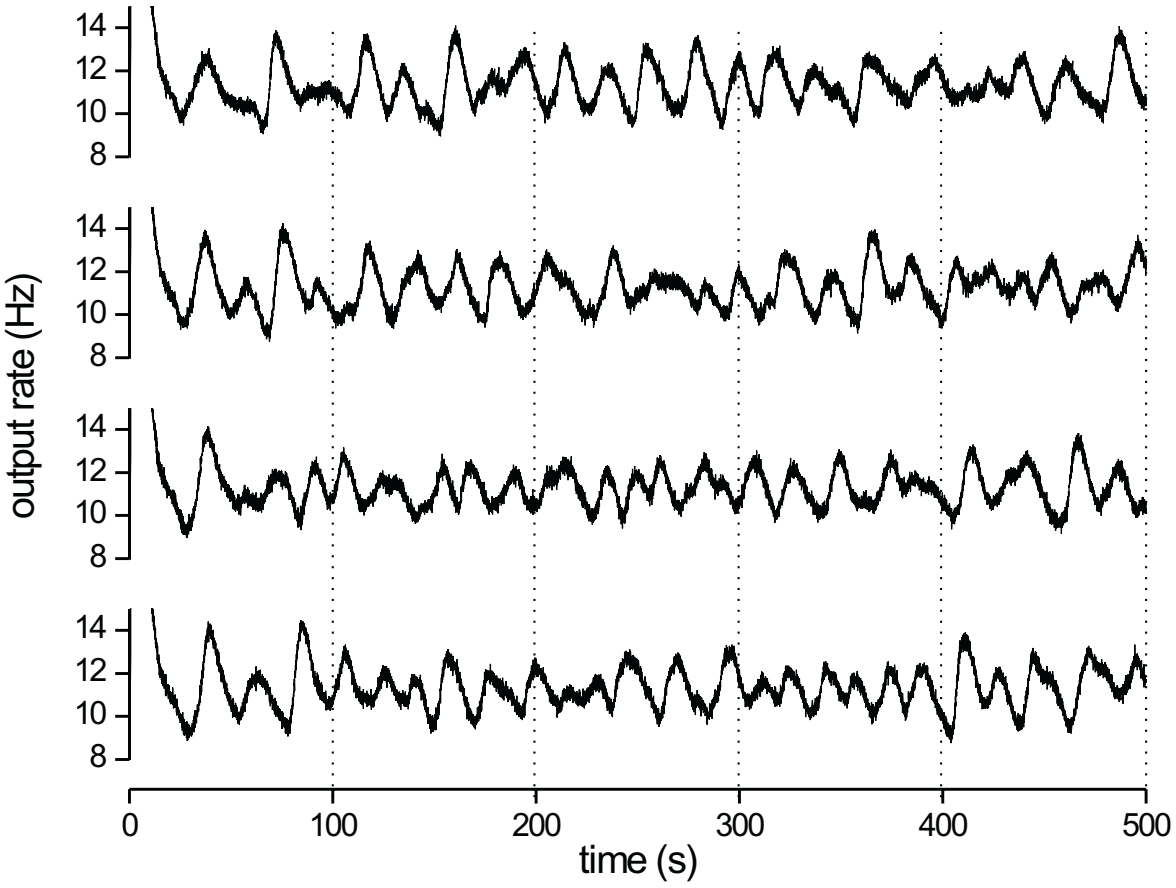

Figure 6.3: Some values of Δ and τ_s yield networks that seem to exhibit chaotic states. These data show network activity as a function of time from the network with $\Delta = 0.9$ and $\tau_s = 14$ s. The only difference between runs is the seed for the pseudo-random number generator, which determines which neurons will receive a proximal process potential input at each time step. The network has received a constant stimulus for the initial 10s, as described in the text, after which it received no exogenous input. The firing rate is initially similar in all runs, but rapidly diverges. At later times the state of the network appears to unpredictable, which can be seen by observing the firing rates at the dotted lines.

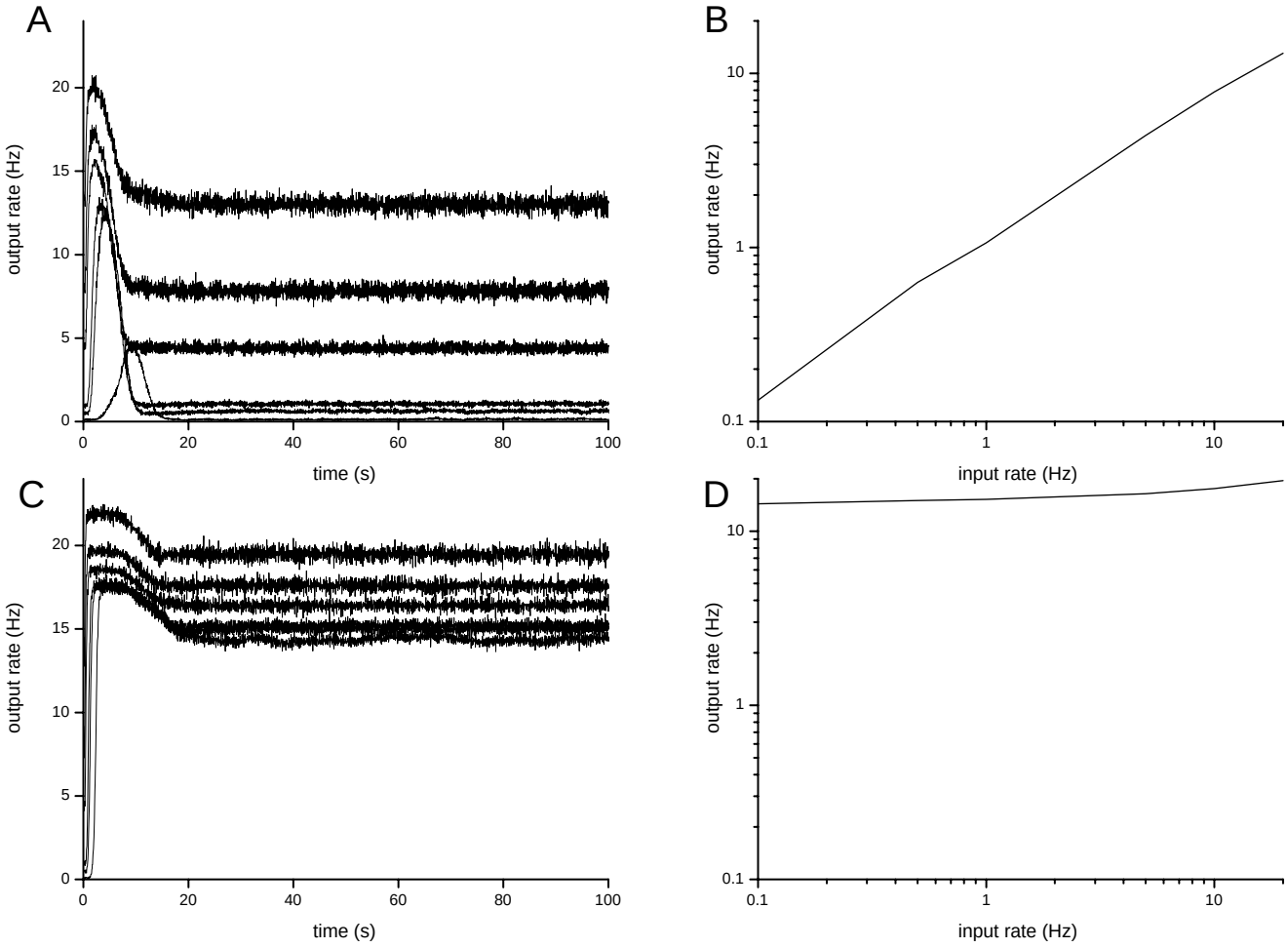

Figure 6.4: These data summarise the responses of two networks, with activity dependent synaptic depression, to constant input. *A.* Network firing rate as a function of time for constant stimuli applied at $t = 0$. The frequencies of these stimuli were 0.1, 0.5, 1, 5, 10, 20 Hz. The parameters of the network were $\tau_s = 12$s and $\Delta = 0.5$. *B.* The stimulus response curve for the equilibrium response shown in the adjacent panel. Log scales are used on both axes. *C.* Similar data to panel *A*, except $\Delta = 0.9$. *D.* Similar data to panel *B*, except $\Delta = 0.9$.

The suppression of complex firing can be understood in terms of the two variable model described by equations (6.2 – 6.3). In the absence of exogenous input, periodic solutions arise as a Hopf bifurcation out of the stable high firing equilibrium. In the presence of a steady exogenous input, P, equation (6.2) becomes

$$\tau_E \frac{dE}{dt} = S(d\,E + P) - E. \tag{6.6}$$

Nullclines and solutions to this equation and equation (6.3) in the phase plane are shown in figure (6.5). Panel A shows the case when there is no exogenous input, $P = 0$. There is a stable solution at zero firing, while the upper solution is unstable and a stable periodic orbit exists around it. This corresponds to the class of periodic solutions uncovered by giving the network a brief stimulus. In the presence of exogenous input, $P > 0$, the $dE/dt = 0$ nullcline moves, removing the quiescent stable point (panel B). In this case, only the periodic solution is available and the amplitude of the orbit is reduced. Increasing P further reduces the size of the oscillation (panel C). Increasing P still further causes the oscillation to completely disappear through another Hopf bifurcation as the remaining equilibrium point regains stability (not illustrated).

Some numerically simulated networks oscillated in the presence of very low frequency (0.1Hz) constant input. The amplitude of the oscillations was very large, varying from almost 0 to 16Hz (the model neurons fire at maximum of around 18–20 Hz). When the stimulus ceased, so did the oscillations. As the stimulus frequency increased the mean response remained approximately constant, however the amplitude of the oscillations decreased. This is illustrated in figure (6.6) which shows 400 seconds of activity for a network with $\tau_s = 12$ s and $\Delta = 0.8$. A sequence of

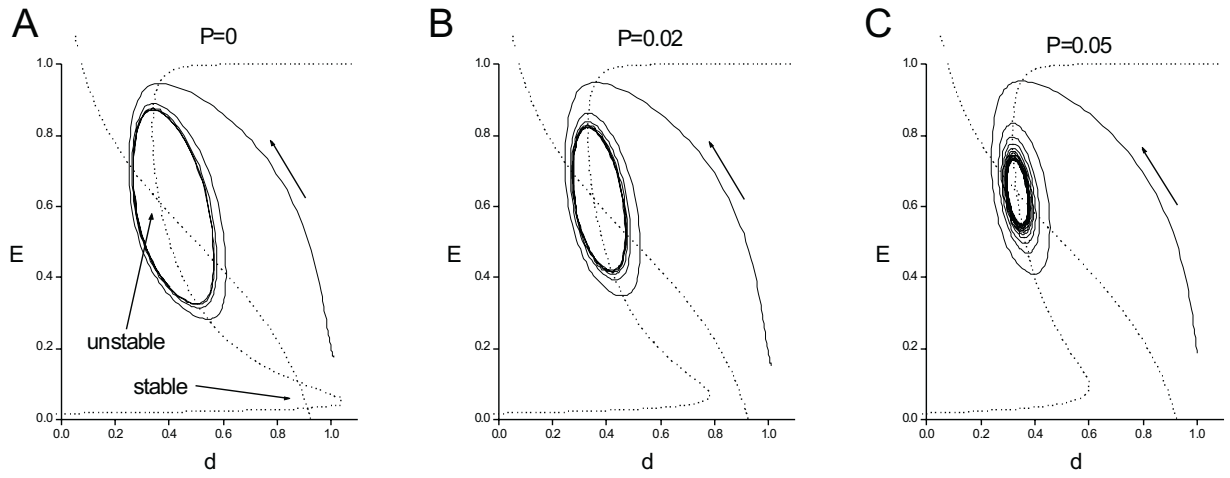

Figure 6.5: The are phase plane diagrams for the model of Donovan et al. [1998], Tabak et al. [2000], modified for the presence of an exogenous input, P, as described by equation (6.6). The dashed curves are the E and d nullclines and solid curves are typical trajectories. The direction of travel along the trajectory can be deduced from the arrows on the nullclines. *A)* In the absence of exogenous input ($P = 0$) the network has a stable limit cycle of moderate amplitude. *B)* When $P = 0.02$ the amplitude of the oscillation is decreased. *C)* $P = 0.05$.

constant frequency inputs of 0.1, 0, 0.5, 2 Hz were played into the network for 100 s each.

The origin of the large amplitude, driven oscillations can be understood by glancing at the phase plane diagram, figure (6.7), which is based on the model of Donovan et al. [1998] and [Tabak et al., 2000], modified to include exogenous input (equations (6.2) and (6.6)). In addition the time constant of synaptic recovery has been increased to $\tau_d = 4$. The case of no exogenous input ($P = 0$) is shown in panel A. There is a stable equilibrium at (or near) zero firing. The upper equilibrium is unstable and in this case is so repulsive that trajectories emerging from it are driven into the stable equilibrium at zero firing. This is because the synaptic strength recovers so slowly that the network falls into the zero firing state before the synapses can recover their strength to support more firing. (When $\tau_d = 2$ a stable limit cycle can coexist with the zero firing state. These are the oscillations in the absence of input discussed above and in section 1.7.) The physiological interpretation of the trajectory shown in panel A is that a small input leads to run away firing. Synaptic depression comes on and the firing decays back toward zero, but the recovery of synaptic strengths is too slow to prevent the network from falling into the zero firing rate state. In the presence of a small constant exogenous input ($P > 0$) the $E = 0$ stable equilibrium disappears and the system must oscillate. This is because the exogenous input is enough to cause run away excitation, once the synaptic strengths have recovered. This also explains why the exogenously driven oscillations have such large amplitude. As the exogenous input increases, the amplitude of oscillation decreases for the same reason as the oscillations that occur in the absence of exogenous input.

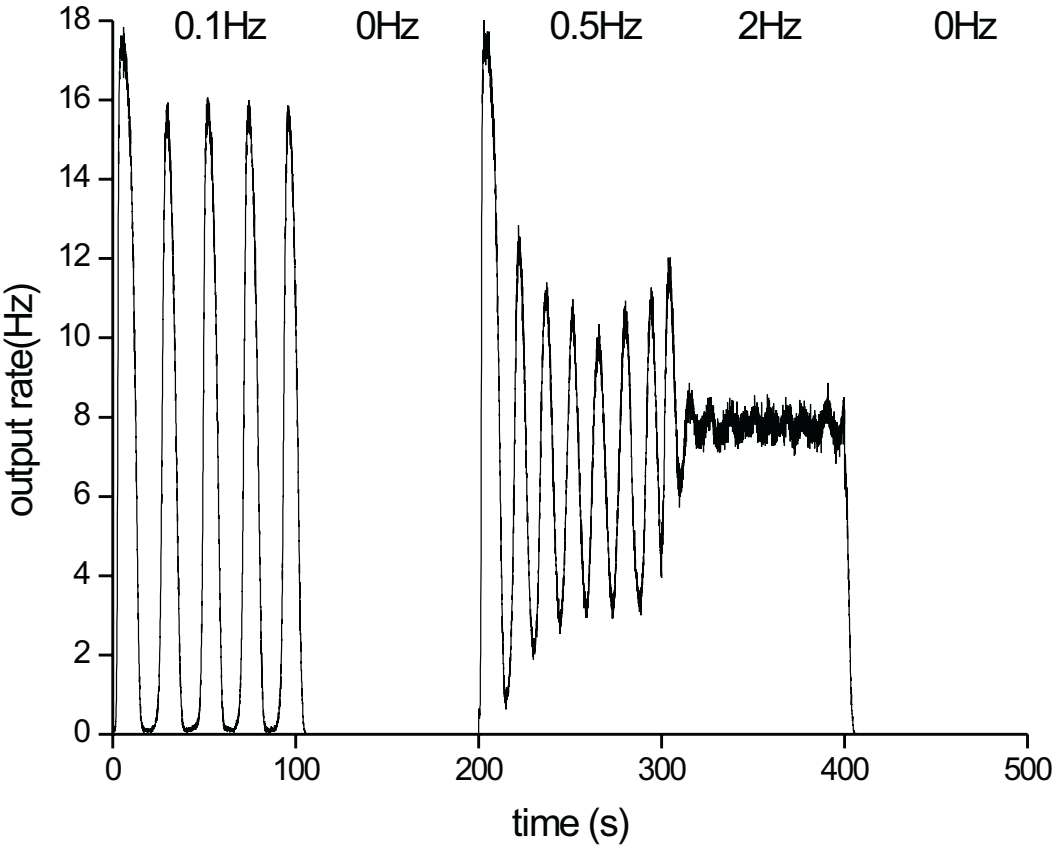

Figure 6.6: The plot shows activity for a network with activity dependent synaptic depression which oscillates in response to exogeneous input. The parameter values are $\Delta = 0.8$ and $\tau_s = 12$ s. The network receives a sequence of constant stimuli, for 100 s each, with average proximal process potential frequency, P, as indicated. When $P = 0.1$Hz the network shows large amplitude oscillations. When the the input ceases, $P = 0$, the network returns to the quiescent state. As P increases the amplitude of the oscillation decreases.

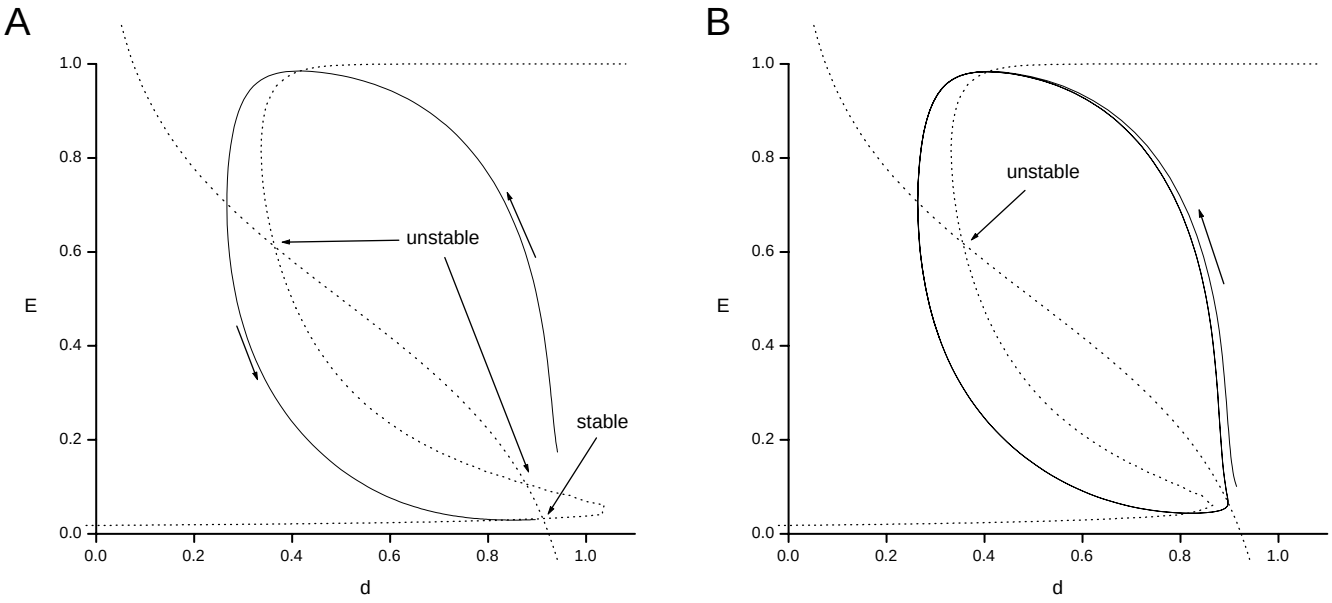

Figure 6.7: The are phase plane diagrams for the model described by equations (6.2) and (6.6). The dotted curves are the E and d nullclines and solid curves are typical trajectories. The direction of travel along the trajectory is indicated by the arrows. In these diagrams $\tau_d = 4$ and other parameters are as in table (6.1). *A)* $P = 0$. The upper equilibrium is unstable and sufficiently repulsive that a limit cycle is not possible. All orbits end in the single stable equilibrium at low or zero firing. *B)* In the presence of small exogenous input, $P = 0.12$ the stable equilibrium disappears and a large amplitude limit cycle is born.

The AHP increases the amplitude of oscillations

As noted in chapter 4 (see table 4.1) networks, without synaptic depression, but with some combinations of residual AHP and synaptic strength were bistable because the AHP was too weak to eliminate the high firing rate state. This introduces the possibility of oscillations if the stability of the high firing rate state can be lost with the inclusion of synaptic depression. Such states were found by numerical experiments as illustrated in figure (6.8). In physiological terms, positive feedback will still drive the network to high firing rates, but at low firing rates the AHP becomes large and causes the trough in the oscillations to occur at lower firing rates. Other states with complex dynamics appear to have been lost.

Feedback driven oscillations

There are also oscillatory states driven by feedback with zero delay, in both the analytical and numerical models. In the analytical model, instead of exogenous input, $P = \alpha E$, where α is the strength of the feedback. Now equation (6.2) becomes

$$\tau_E \frac{dE}{dt} = S(d\,E + \alpha\,E) - E. \tag{6.7}$$

Oscillations arise in this model in an almost identical way to the networks driven by constant exogenous input. In the analytical model, the low firing rate state is not exactly at zero firing, so if α is large enough the low firing rate state disappears. If the high firing rate state is unstable then a large amplitude oscillation will occur around the unstable state. The numerical model differs from the analytical model in that the zero firing rate state is still stable, even in the presence of feedback. However, there

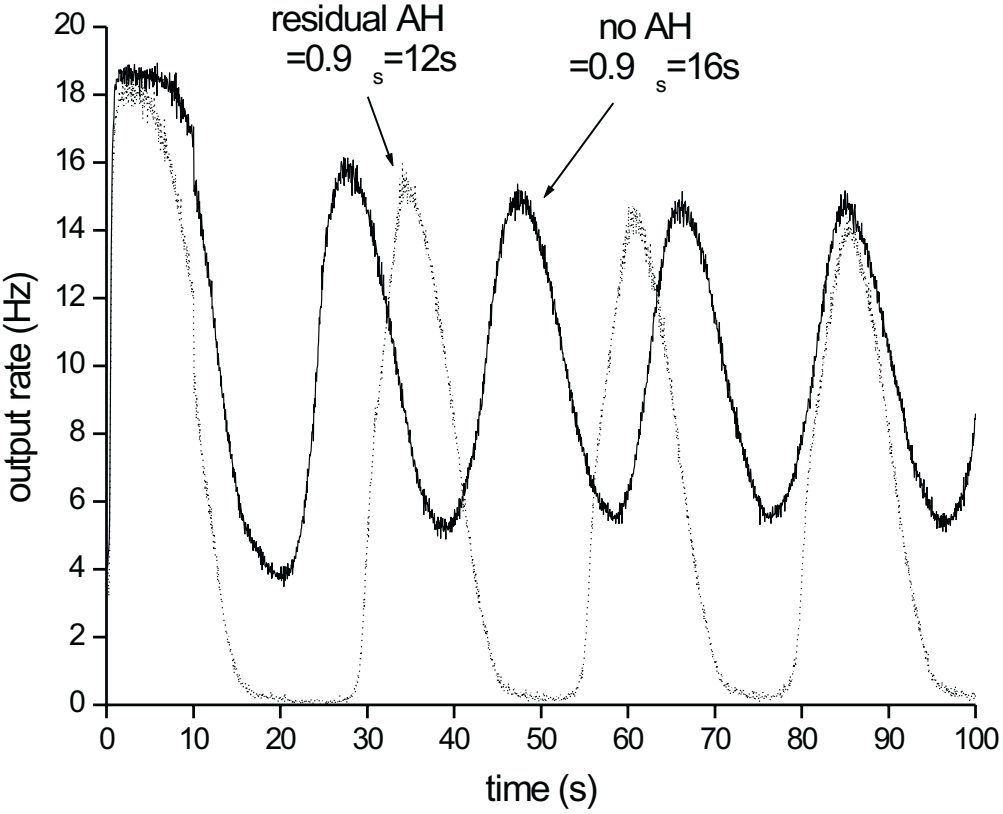

Figure 6.8: The inclusion of an AHP dramatically increases the amplitude of oscillations in networks that oscillate in the absence of input. The dashed curves shows activity (as average neuron firing rate) for a network in which the neurons do not have an AHP. The neurons in the network that displayed the activity shown in solid had an AHP which was almost completely suppressed in the presence of a slow EPSP. These networks received constant stimuli for the initial 10s, as described in the text, after which they received no exogenous input.

are parameter regions in which an oscillation exists around an unstable high firing rate state, but because the stable state still exists, these oscillations are not of large amplitude. The only parameter combination in which feedback driven oscillations were found was $\Delta = 0.8$ and $\tau_s = 8$ s, corresponding to a 20% reduction in synaptic strength per action potential and a halflife of recovery of 8 s. The network firing rate varied between 10% and 80% of the maximum firing rate.

6.4 Discussion

In this chapter, activity dependent synaptic depression has been investigated for synapses connecting sensory neurons to each other. As with other studies [Senn et al., 1996, Donovan et al., 1998, Tabak et al., 2000] oscillations and possibly chaotic states were found. Oscillations were found in both the analytical and numerical models and occurred under a variety of conditions depending on the parameter regime. Oscillations can occur intrinsically, that is in the absence of input, and these oscillations are quenched in the presence of exogenous input. Other oscillatory states are driven by small constant exogenous input, but again, as the input increases these oscillations are also quenched. Finally, oscillations can be driven by feedback, representing sensory feedback from smooth muscle contractions. The numerical model displays states that are driven by exogenous input and which have aperiodic firing. The precise time course of firing is highly sensitive to which neurons are chosen to receive the random inputs, which in turn, depends on the seed of the random number generator. These states were called chaotic by analogy with chaos exhibited by some dynamical systems. It would be technically interesting to know

whether these states are truly chaotic and what the important variables are that lead to this chaos.

Activity dependent synaptic plasticity in the enteric nervous system (ENS) has not received a great deal of attention. Synapses mediating fast transmission have at least two time scales of run down. When stimuli are applied at frequencies of 0.1Hz or higher, fast EPSPs run down significantly within a 10 pulses [Nishi and North, 1973]. This appears to be due to inhibition at muscarinic receptors on the presynaptic membrane [Morita et al., 1982b]. At 40Hz, fast EPSPs are reduced to 30% of their initial size. Assuming no recovery this corresponds to a decrease of about 10% per event. On a longer time scale, receptors mediating fast transmission desensitise [Galligan et al., 2000]. Nicotinic acetylcholine receptors in the ENS desensitise in less than 0.3 s to high concentrations of acetylcholine [Galligan et al., 2000], the P2X receptor desensitises in 7 s [Zhou and Galligan, 1996] and the 5-HT_3 receptor desensitises in 2 s [Zhou and Galligan, 1999].

Receptors mediating slow EPSPs have a number of desensitisation mechanisms. NK1 receptors desensitise by phosphorylation and require internalisation to resensitise [Garland et al., 1996]. NK1 internalisation has been observed in guinea-pig myenteric neurons [Southwell et al., 1998] and there is evidence that it occurs under physiological conditions in rat [Mann et al., 1999]. NK3 receptors desensitise in response to prolonged exposure to the agonist senktide [Johnson et al., 1996]. Slow EPSPs in myenteric neurons may be mediated through the 5-HT_{1P} receptors which also desensitise "rapidly" [Michel et al., 1997]. There appears to be no quantitative data on time courses of desensitisation and resensitisation.

Presynaptic inhibition mediated by muscarinic receptors occurs at terminals re-

leasing acetylcholine [Morita et al., 1982b, North et al., 1985], and this mechanism may also inhibit slow EPSPs. Again, no quantitative data on time courses have been reported.

For the parameters of synaptic transmission and synaptic depression used in this study the networks oscillated with frequencies around 4.2 cycles per minute (cpm). These oscillations may be the explanation for segmentation and phase II contractions. Segmentation consists of rhythmic contractions occurring at about 30 cpm in cat [Cannon, 1912] and 15–20 cpm in mouse [Thuneberg and Peters, 2001]. Adjacent sections of intestine oscillate 180 degrees out of phase and do not propagate, which indicates that they are probably not generated by muscle slow waves. Furthermore, genetically modified mice that lack Interstitial cells of Cajal, and hence lack slow waves, are still capable of segmentation [Thuneberg and Peters, 2001]. Thus, the segmentation rhythm appears to be neurally generated. One problem with identifying the oscillations observed in this study with segmentation is that activity in the simulated networks tends to be synchronised spatially, as will be shown in the next chapter, in contradiction to the fact the adjacent sections of intestine oscillate out of phase during segmentation. This issue might be addressable in a more sophisticated model that includes feedback from both excitatory and inhibitory local reflexes or reflexes mediated through interneurons.

Phase II contractions of the interdigestive cycle of motor patterns occur as random, irregular short burst of activity that usually do not propagate [Kellow et al., 1986]. This may be the result of interaction between oscillations in the sensory neuron network interacting with slow waves. If the sensory neuron network enters a relatively short lived oscillatory period then the interactions between periodic neural

drive and slow wave depolarisations will give the appearance of a series of irregular contractions.

Chapter 7

Propagation in sensory neuron networks as a model of migrating motor complexes

7.1 Introduction

The intestine shows a remarkable temporal and spatial complex of motor patterns in the fasted state (see section 1.2), known as the migrating motor complex (MMC). This is organised spatially from the stomach to the terminal ileum and has a cycle time of the order of 1–2 hours depending on the species [Code and Marlett, 1975, Kellow et al., 1986, Galligan et al., 1985] (see also table 1.1). It is made of three main phases. Phase I is marked by relative quiescence, with only occasional contractions. Phase II shows more frequent irregular and apparently random contractions, which can occur in clusters at the slow wave frequency or they can appear to propagate rapidly in the anal direction. The frequency of contractions increases gradually over

the course of phase I and II and the boundary between these two phases is arbitrary. Phase III is clearly delineated as period of strong contractions occurring at slow wave frequency. The site of initiation of the phase III is highly variable in humans, even within subjects, varying from the esophagus to the proximal ileum [Kellow et al., 1986]. In dogs there is also some variability, but it appears to much less, with most phase IIIs starting in the stomach and terminating in the terminal ileum [Code and Marlett, 1975]. In guinea-pig phase III contractions were always observed at the first recording electrode in the duodenum [Galligan et al., 1985]. The speed of the complex decreases as it moves anal, but is of the order of mm/s. The bulk of the cycle time is spent in phases I and II with phase III lasting only a few minutes. The enteric nervous system (ENS) initiates and coordinates this cycle, although extrinsic innervation plays a modulatory role [Itoh et al., 1981, Sarna et al., 1981, 1983, 1993]. Furthermore, blocking neuromuscular transmission blocks passage of phase III contractions indicating that feedback from the muscle is probably required.

This chapter examines the hypothesis that the MMC cycle is governed by the intrinsic sensory neurons of the gut and the synapses that connect them together. Phase III is a wave of maximal firing that propagates within this network, which reduces synaptic efficacy. Phase I and II is the result of synapese recovering, culminating in a highly excitable network. When the network is the highly excitable state another phase III wave is possible. It was shown by numerical simulation in chapters 4 and 5 that networks with after hyperpolarising potentials (AHPs) or inhibitory postsynaptic potentials (IPSPs) cannot support signal propagation in the longitudinal direction over long distances. As with oscillatory states (chapter 6), this is because these forms of inhibition "track" excitation too closely (more below),

thus the crucial element to support propagation in these networks may be activity dependent synaptic depression.

7.2 Methods

The methods for numerical simulations were as in the chapter 6, except that networks were 25 mm long in the longitudinal direction and 5 mm in the circumferential direction. Stimuli were applied in the centre 5 mm $\times$ 5 mm section of the strip, with protocols as described in the text. This allowed propagation out of the stimulus area in either the oral or the anal directions to be observed. In some experiments feedback was present. Activity from 1 mm circumferential strips was feed back into the same strip. Other details of the feedback algorithm are as in sections 6.2 and 2.2.

7.3 Results

Signal propagation in sensory neuron networks

The networks with AHP or IPSP inhibition cannot support *stable* signal propagation, where stable means that the signal can propagate with constant amplitude over indefinite distances. Imagine a one dimensional network with recurrent connections that are equal in either directions. Imagine also, activity in a small section of the network. If the signal is to propagate over long distances then the activity in one section must drive the activity in the adjacent section to the same level. But because of the reciprocal connections the activity in the second segment will drive the first

segment with the same strength, so the activity will never die away and the network will enter a high firing rate state. In other words, for stable signal propagation the network must be bistable. However, as pointed out in chapter 4, these networks only support propagation in the quiescent state. Once they enter the high firing rate state they never return to the quiescent state and stable propagation is not realisable in a biologically useful way. Returning to the example network, if there is a bias in the connections, for example, in the anal direction, then stable signal propagation might be possible in that direction. In this case, the feedback into the original segment is less than the feedforward signal and so activity can die away in the original segment. The networks of sensory neurons have a bias in the anal direction, but the networks are two dimensional and the circumferential connections do not have a bias. This will cause activity to remain "trapped" within the circumferential connections and so stable propagation is still not possible. These conclusions are supported by the numerical simulations for networks with AHP inhibition in chapters 4 page 181 and for networks with IPSP inhibition chapter 5 page 205.

This argument breaks down if inhibition is much more slowly acting than excitation. The network is not bistable, but it can enter a high firing rate state for long enough to generate sufficient activity in an adjacent section to maintain propagation. Inhibition comes on more slowly and returns the network to the quiescent state. Delayed negative feedback is also the key to oscillations and so oscillations and propagation are closely related.

This possibility was studied, with synaptic depression as the candidate for slow negative feedback, as follows. Networks 5 mm in the circumferential direction and 25 mm in the oral direction were constructed using patterns of connections as de-

scribed in chapter 2 section 2.2. These patterns included the slight anal bias of the longitudinal component of the projections [Bornstein et al., 1991b]. The neurons in this network also had an AHP following the action potential, however it was suppressed in the presence of a slow EPSP to such an extent that the network would be bistable without synaptic depression. A stimulus of constant frequency, f, was played into 5 mm region in the centre of the preparation. All combinations of $f \in 1, 2, 5$, $\Delta \in 0.7, 0.8, 0.9, 0.95$ and $\tau_s \in 10, 12, 14$ were used. These values were chosen because they are in the vicinity of the low frequency, high amplitude oscillatory state described in the previous chapter.

Network responses fell into two broad categories. The simplest and least interesting case is when activity propagated out from the stimulus region and the invaded regions remained in a high firing rate state, i.e. these networks were bistable.

Network responses in the second category consisted of *waves* of activity propagating in the oral and anal directions out of the stimulus area. A wave is defined as a region of activity that propagates without loss of amplitude over an indefinite distance and in the the activity in the network returns to zero or near zero. An example of a response from this category is shown in figure 7.1. The X axis is the longitudinal position within the simulated network, the Y axis is time in seconds and the Z axis proportional to the number of action potentials fired per 50 ms time bin in the entire 1 mm circumferential strip. The stimulus is visible in the center of the strip and running the entire duration of the graph. Two waves of activity propagate out of the stimulus region in the oral and anal directions. Once the wave had propagated through a region, the firing rate returned to zero. The uneveness in activity at the peak of the wave is due to the uneven density of neurons within

the network. Waves continue to roll out of the stimulus region, in figure 7.1 the frequency was so low that after the initial waves no further activity was apparent in that run. However, for different parameters, waves at much higher frequency are possible, as illustrated in figure 7.2. In this case, anally propagating waves of activity flowed out of the stimulus region at relatively high frequency.

The two categories were not distinct, some networks, with parameters that made them highly excitable, showed behaviour that was intermediate between the two. In these networks the few millimetres either side of the stimulus fired at a constant rate shortly after the stimulus started. Further away from the stimulus region waves developed. These parameter regimes did not seem to correspond to known physiology and were not studied further.

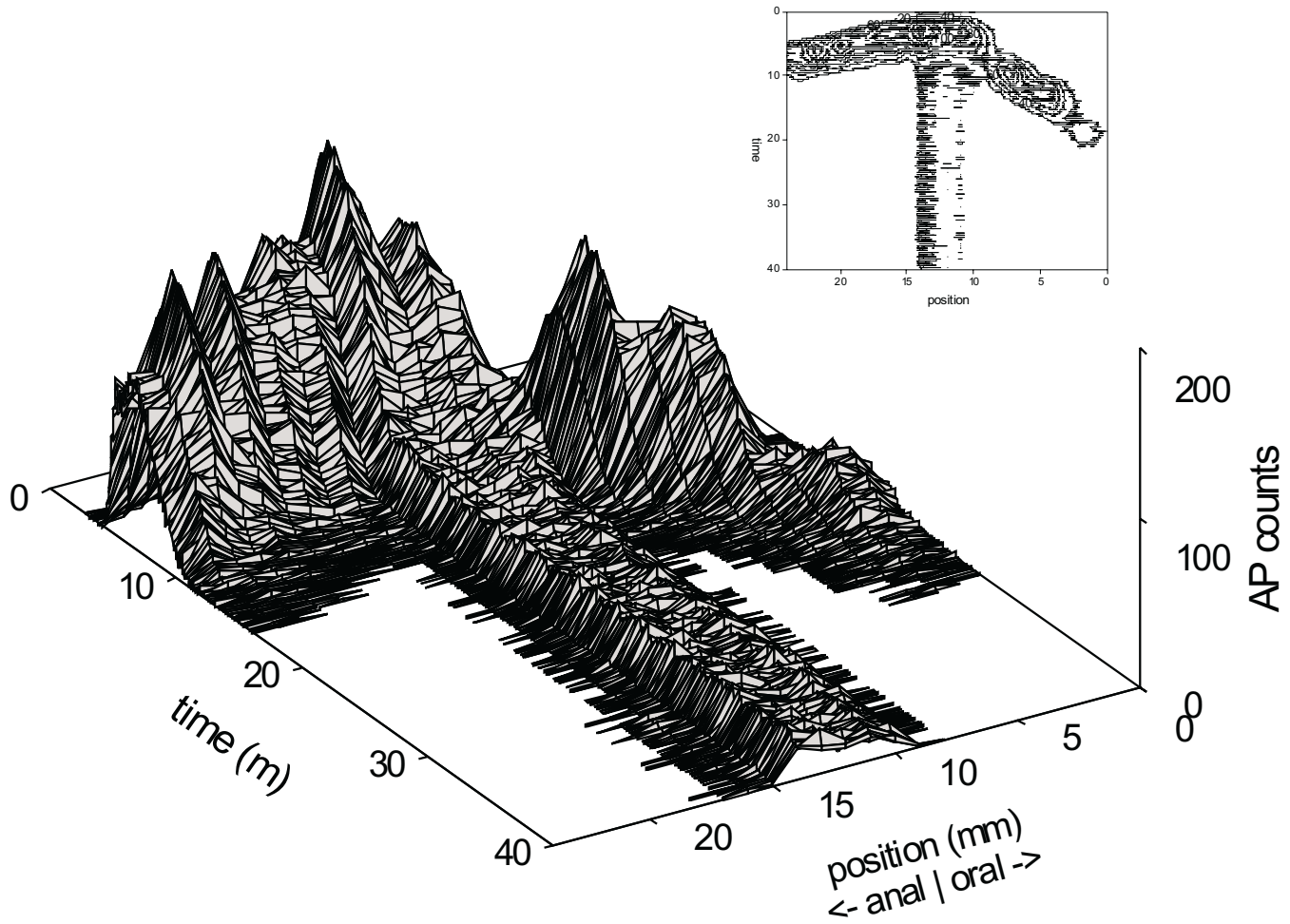

Figure 7.1: The graph plots action potential count per 50ms time bin and 1mm spatial bin in the longitudinal direction against time for a network 25mm long in the longitudinal direction. A constant stimulus of 2 Hz has been applied to the central 5mm. A single wave of activity propagates out of the stimulus region in both the oral and the anal direction. The propagation in the anal direction is faster due to the bias of connections in the anal direction. In this network $\Delta = 0.8$ and $\tau_s = 14$ s. The inset shows the same data, viewed from above, as contours.

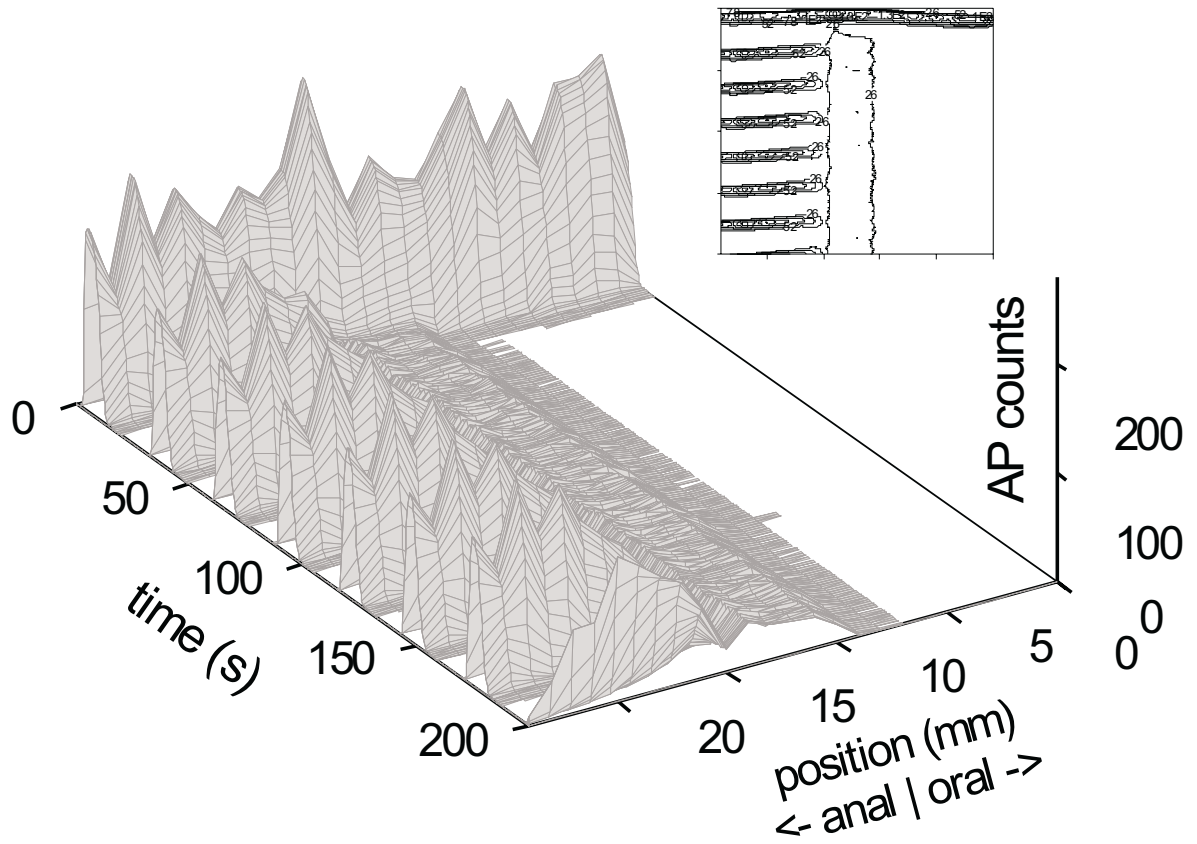

Figure 7.2: The graph plots action potential count per 50ms time bin and 1mm spatial bin in the longitudinal direction against time for a network 25mm long in the longitudinal direction. A constant stimulus of 2 Hz has been applied to the central 5mm. A single wave of activity propagates out of the stimulus region in the oral direction. Multiple waves, approximately evenly spaced, propagate in the anal direction. In this network $\Delta = 0.9$ and $\tau_s = 14$s. The inset shows the same data, viewed from above, as contours.

When wave propagation was stable (i.e. the wave propagated to the end of the preparation), the peak amplitudes of the waves were at, or near, the peak firing rate of the networks, making them all-or-nothing events. Some quantitative properties of the waves, and their dependence on Δ and τ_s, are summarised in table 7.1. In general, waves propagating in the anal direction were faster and more frequent than in the oral direction. The only asymmetry in the network is the bias of connections towards the anal end, so this must be the cause of the preference for anally propagating waves. Increasing the stimulus strength decreased the frequency of waves in some cases, and increased it in others. Where it is possible to compare, increasing the halflife of synaptic recovery decreased the frequency of waves, but did not substantially effect the speed of propagation. The duration of most runs was 200 s and so it was not possible to determine the frequency of waves in many cases. Increasing Δ increases the speed of propagation and the number of waves. For most parameter values, only a single wave propagated in the oral direction in the 200 s run. Of particular interest is the speed of anal propagation in simulations which is in the range 1.6–4.9 mm/s. The speed of propagation of phase III migrating motor complexes is the range 0.7–2.9 mm/s in guinea-pigs [Galligan et al., 1985].

τ_s	Δ	stimulus (Hz)	V_{oral} (mm/s)	F_{oral} (Hz)	V_{anal} (mm/s)	F_{anal} (Hz)
10	0.7	1	-	$< 5^{-3}$	1.6	$< 5^{-3}$
10	0.7	2	-	$< 5^{-3}$	1.6	$< 5^{-3}$
10	0.7	5	-	$< 5^{-3}$	1.4	$< 5^{-3}$
10	0.8	1	1.0	$< 5^{-3}$	2.5	0.021
10	0.8	2	1.1	$< 5^{-3}$	2.5	0.021
10	0.8	5	1.0	$< 5^{-3}$	3.3	0.022
10	0.9	1	3.3	0.017	4.9	0.050
10	0.9	2	3.3	0.016	4.9	0.045
10	0.9	5	3.3	0.007	3.3	0.045
12	0.7	1	-	$< 5^{-3}$	1.4	$< 5^{-3}$
12	0.7	2	-	$< 5^{-3}$	1.6	$< 5^{-3}$
12	0.7	5	-	$< 5^{-3}$	1.6	$< 5^{-3}$
12	0.8	1	0.8	$< 5^{-3}$	3.3	0.007
12	0.8	2	1.0	$< 5^{-3}$	3.3	$< 5^{-3}$
12	0.8	5	0.9	$< 5^{-3}$	3.3	$< 5^{-3}$
12	0.9	1	3.3	$< 5^{-3}$	4.9	0.039
12	0.9	2	2.5	0.009	4.9	0.039
12	0.9	5	2.6	$< 5^{-3}$	3.3	0.060
14	0.7	1	-	$< 5^{-3}$	1.4	$< 5^{-3}$
14	0.7	2	-	$< 5^{-3}$	1.6	$< 5^{-3}$
14	0.7	5	-	$< 5^{-3}$	1.6	$< 5^{-3}$
14	0.8	1	0.8	$< 5^{-3}$	3.3	$< 5^{-3}$
14	0.8	2	0.8	$< 5^{-3}$	3.3	$< 5^{-3}$
14	0.8	5	0.8	$< 5^{-3}$	3.3	$< 5^{-3}$
14	0.9	1	4.9	$< 5^{-3}$	3.3	0.040
14	0.9	2	3.3	$< 5^{-3}$	4.9	0.034
14	0.9	5	3.3	$< 5^{-3}$	4.9	0.034
20	0.9	2	1.9	0.009	2.8	0.011
30	0.9	2	1.9	$< 5^{-4}$	2.9	0.004
40	0.9	2	1.9	$< 5^{-4}$	2.8	0.0006

Table 7.1: This table summarises some properties of waves to emerge from a region receiving a constant stimulus. The first three columns represent the independent variables τ_s, Δ and the strength of the stimulus. The dependent variables are the speeds of the first waves to emerge, if one does, and the frequency of the waves. Inequalites indicate that there was less than 2 waves in the simulation run.

Effect of slow EPSP duration on propagation

For reasons of computational efficiency, the durations of slow EPSPs in most of the analysis reported in this thesis were kept fairly short. However, the goal of this chapter is to develop the hypothesis that the phase III of the migrating motor complex is caused by slowly moving waves of activity in the sensory neuron network. Therefore, some runs were done in which the halflives of the three stages of the slow EPSP were increased by a factor of 4. The other time scale, τ_s, in the model also needs to be scaled by a similar amount so that it retains the same relationship with the slow EPSP time scale and system retains qualitatively similar dynamical behaviour. Values tested were $\tau_s \in \{40, 48, 56\}$ s. The same two classes of behaviour were observed as for short EPSPs. An example of repeated waves is shown in figure 7.3. The most obvious effect of increasing the slow EPSP duration is that the duration of each wave has increased. For the parameters used to generate the figure the wave duration was 60 seconds. The speed of propagation was 3 mm/s. Other parameters generated waves of similar duration.

Effect of long anal projections

A subset of sensory neurons in the guinea-pig ileum have long anally directed processes, without side branches, which can be up to 10cm long [Brookes et al., 1995]. It is not known what these processes connect to, so they may connect to other sensory neurons. To test a possible role of these processes in sensory neuron networks, long anal projections were included in a series of runs. Networks were kept at 25 mm, as before and additional projections were added within a region 0.2 ± 0.1 (mean $\pm$ standard deviation, Gaussian distribution) in the circumferential direction and

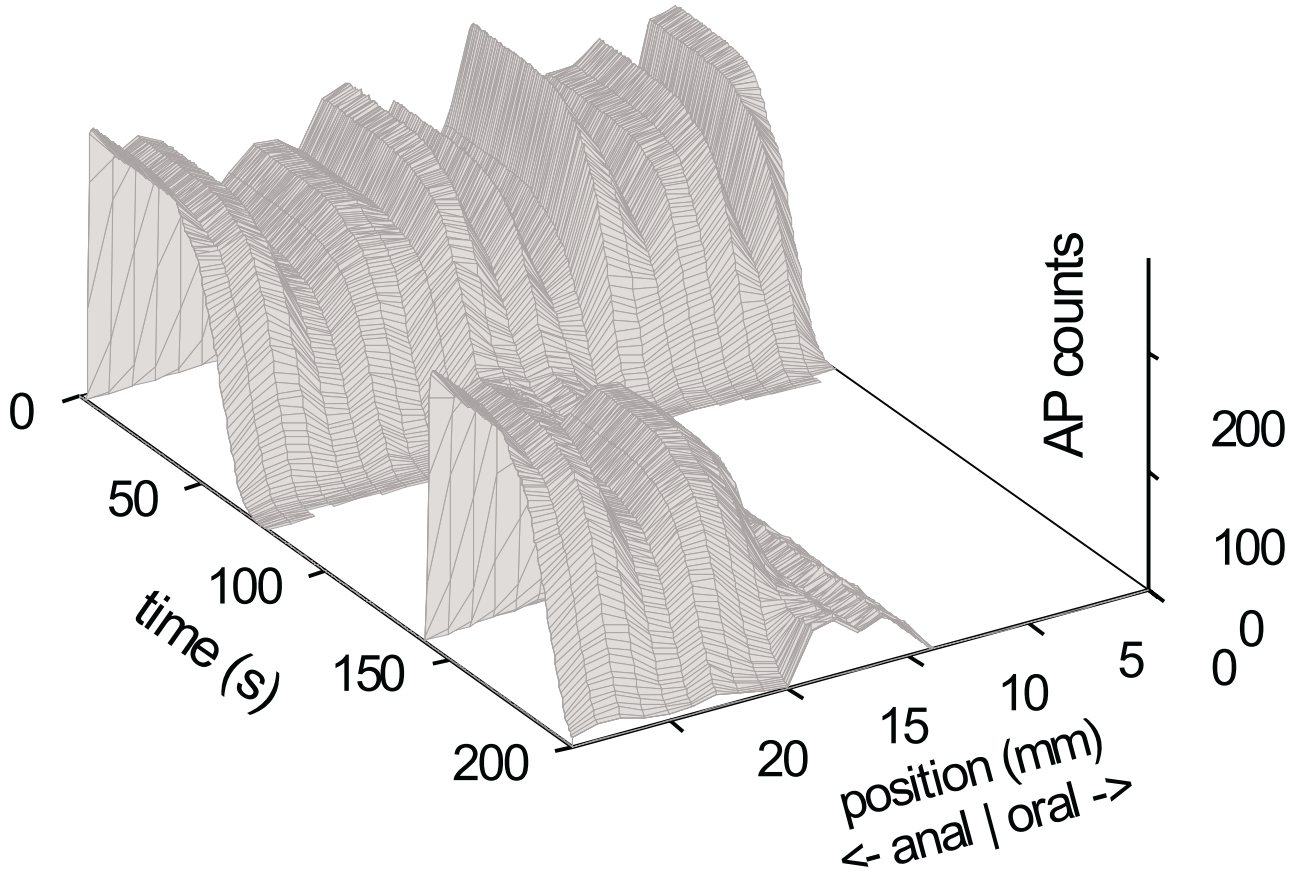

Figure 7.3: The graph plots action potential count per 50ms time bin and 1mm spatial bin in the longitudinal direction against time for a network 25mm long in the longitudinal direction. A constant stimulus of 5 Hz has been applied to the central 5mm. Multiple waves, approximately evenly spaced, propagate in the anal direction. In this network $\Delta = 0.8$ and $\tau_s = 48$s. In addition the parameters controlling the duration of the slow EPSPs have been increased by a factor of 4 and this has lead to an increase in the duration of the waves.

1.5 ± 0.5mm in the anal direction. These additional projections were shorter than those observed in the guinea-pig ileum so that the network size did not have to be increased and run times were kept manageable. The average number of contacts within this region was either 0, 1, 2, 4 or 8 with a standard deviation of 50% of the mean. The physiological numbers of contacts is not known, but given that only around 10% of neurons have a long projection and the projection does not branch, the average number of these connections is probably less than one. Parameter values tested were $\tau_s = 14$ s and $\Delta = 0.8$ or $\Delta = 0.9$ with stimulus of 2 Hz.

Data from runs with $\Delta = 0.9$ and with 0, 1, 4 and 8 additional contacts is illustrated in figure 7.4. The parameters that generated these data are the same as those used to generate figure 7.2, other than the additional contacts. When the average number of additional contacts was 1, the effect was a slight increase in the frequency of waves in both the oral and anal directions (panel B compared to panel A). As the number of additional contacts was increased, activity on the anal side of the stimulus increased, resulting in a region of constant firing near the stimulus area that moved further out as the number of additional contacts increased. Anally directed wave frequency also increased as the number of additional contacts increased. On the oral side, wave frequency fluctuated with increasing numbers of contacts. These results indicate that if the long projections play a role in generating these waves, then it is simply to raise the overall level of excitation in the network. For these waves to exist, the network needs to be at a level of moderate excitation and the long contacts in the physiological range simply increase the excitability of the network slightly.

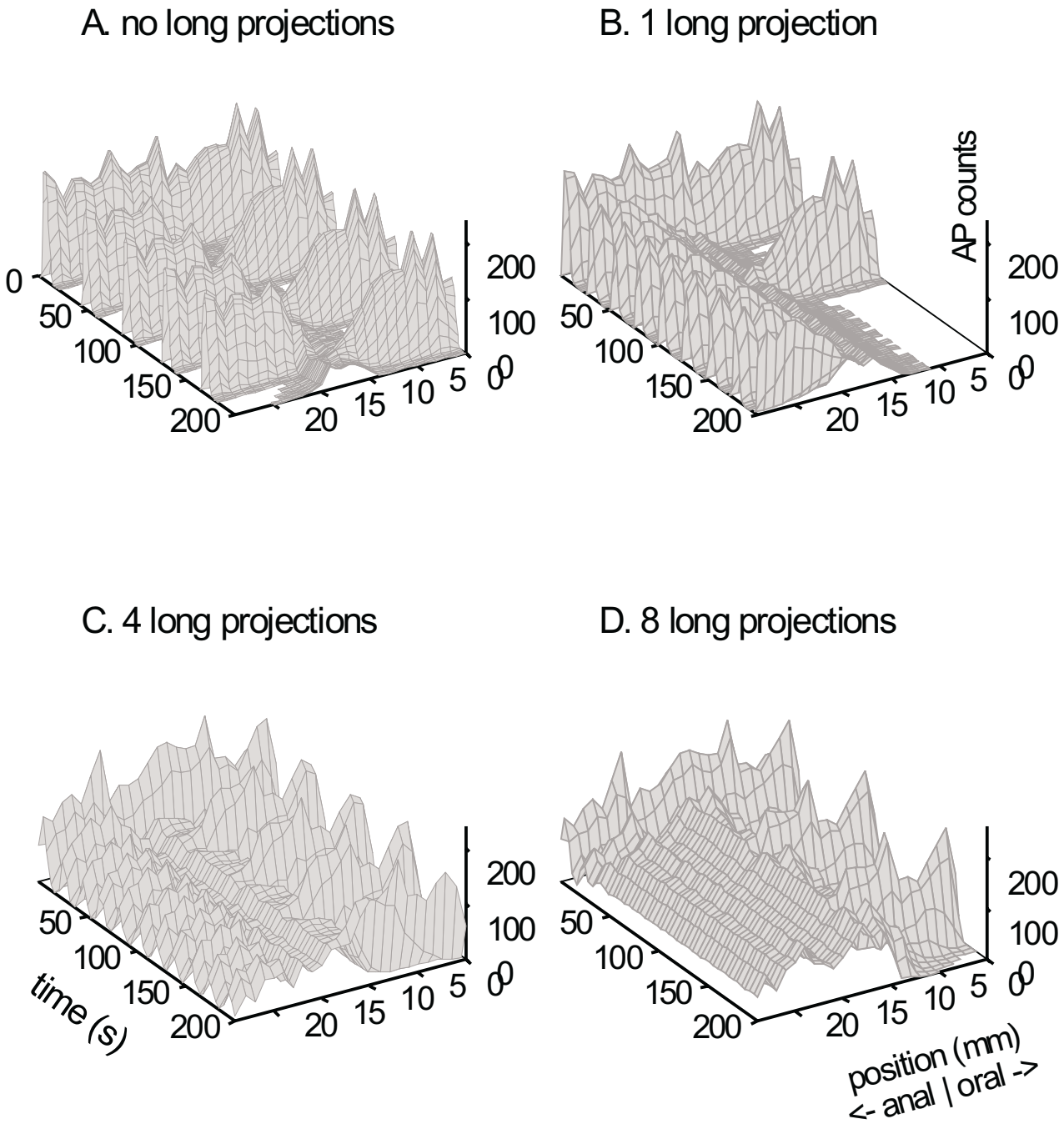

Figure 7.4: These data were generated in networks similar to those used to generate figure 7.2 except that neurons made additional anally projecting contacts within a region 1–2 mm from the cell body. *A.* No additional contacts. *B.* 1 additional contact, on average. *D.* 4 additional contacts *D.* 8 additional contacts.

Feedback driven waves

As with oscillations (page 227), there are parameter regions in which waves only exist with the presence of feedback, an example of which is shown in figure 7.5. To generate these data, the per action potential change in synaptic efficacy was $\Delta = 0.5$ and the recovery halflife was $\tau_s = 16$ s. A stimulus of 2 Hz was applied to the central 5 mm of the network for 10 s. The amount of feedback is indicated above each graph. In the absence of feedback neurons in the stimulus region respond, however very little activity leaves the stimulus region, either in time or space. With a feedback level of 0.1 PPP input per action potential, a single wave propagates in the anal direction. When feedback is 0.2 or 0.4 PPPs per action potential a wave also propagates in the oral direction. The larger the feedback the faster the waves propagate. Feedback dependent waves only existed for $\Delta = 0.5$, but their properties were almost completely independent of τ_s. This parameter regime is adjacent to the regime in which waves propagate without feedback ($\Delta >= 0.6$).

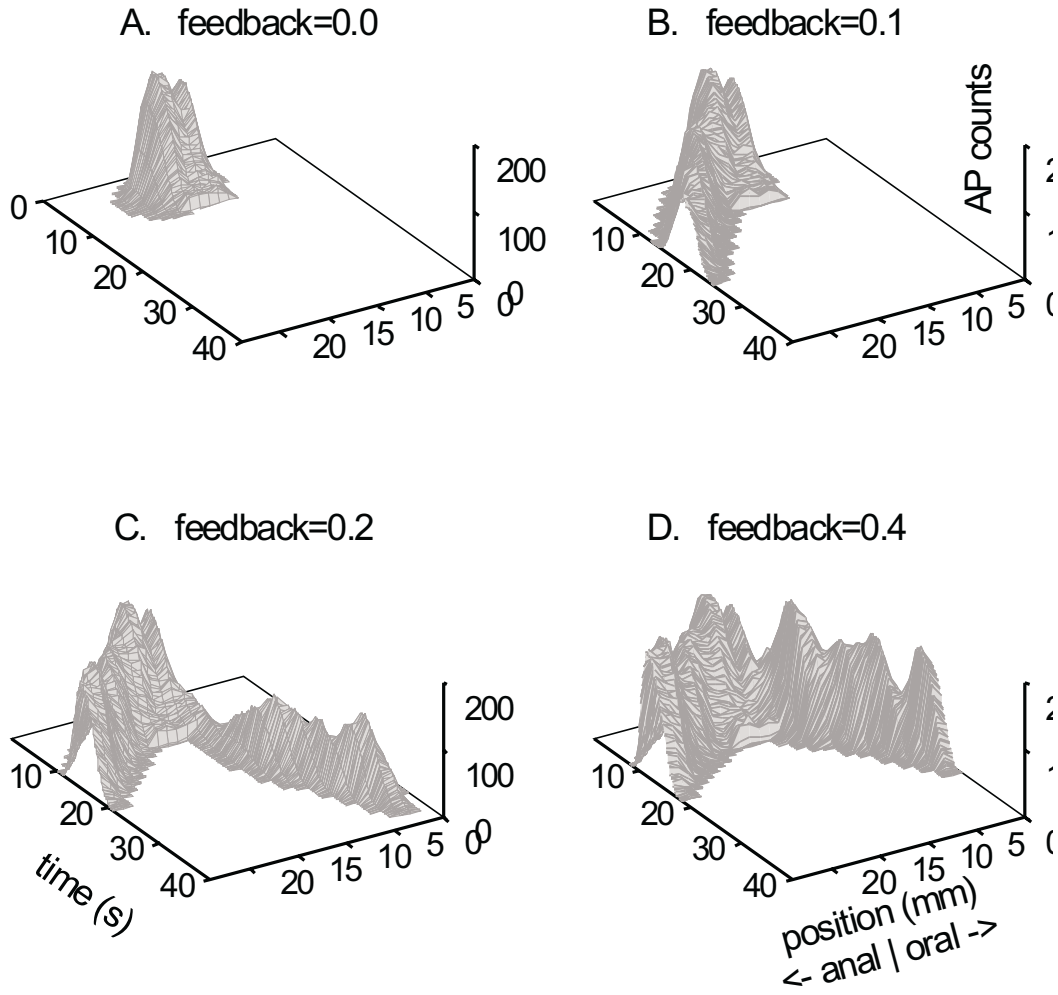

Figure 7.5: The graph plots action potential counts per 50ms time bin and 1mm circumferential bin for 25 mm long networks. A 2 Hz, 10 s stimulus was applied to the central 5 mm. Sensory neurons received feedback as PPP inputs proportional to the number of action potentials in each 1 mm circumferential strip. *A.* No feedback. *B.* 0.1 PPPs for each action potenial (AP). *C.* 0.2 PPPs for each AP. *D.* 0.4 PPPs for each AP.

7.4 Discussion

In this chapter, it has been shown that networks with activity dependent synaptic depression can support the stable propagation of all-or-nothing waves of activity. Although theoretical and numerical simulation of wave propagation in neural tissue is now being explored [Golomb and Amitai, 1997, Ermentrout and Kleinfeld, 2001, Chen et al., 1998, Rinzel and Ermentrout, 1998], this is the first report of wave propagation in networks with activity dependent synaptic depression. The effects of varying the synaptic depression parameters, Δ (the change in synaptic efficacy per action potential) and τ_s (the halflife of synaptic recovery), were studied as well as the EPSP duration, the nature of feedback and some aspects of network architecture. The smaller the decrease in synaptic efficacy per action potential, the more excitable the network and waves travel faster and are more frequent in response to constant stimuli. But if the depression is too small the network is too excitable and does not return to rest after the activity front passes through a region. If the depression is too large, activity does not propagate. The synaptic recovery halflife controls the spacing between waves and the duration of each wave can be controlled by the duration of the slow EPSP.

Migrating complexes

MMC phase III initiation and propagation are known to be neurally mediated [Sarna et al., 1983, 1981, Itoh et al., 1981]. Feedback from the muscle may also be required since phase III passage is blocked by locally perfused hexamethonium and atropine [Sarna et al., 1983]. Blockade by hexamethonium can understood because transmis-

sion from sensory neurons has a large cholinergic component [Johnson et al., 1996]. Atropine blocks receptors that mediate excitatory transmission onto circular muscle [Kosterlitz and Lees, 1964, Hirst et al., 1975]. However, atropine also blocks receptors responsible for presynaptic inhibition [North et al., 1985] and this may disrupt synaptic transmission, or recovery from depression, sufficiently to prevent the phase III activity from propagating.

The simulated waves propagate at a speed of the order of millimetres per second, suggestive of MMC phase III [Szurszewski, 1969, Code and Marlett, 1975]. The only circuit within the ENS that can support signal propagation at such low speeds is the network of intrinsic sensory neurons, which can be seen as follows. The speed of propagation of a wave through a neural network is approximately

$$\frac{1}{V} = \frac{1}{v_a} + \frac{\tau_\theta}{L} \tag{7.1}$$

where v_a is the axonal propagation speed, τ_θ is average time for the synaptic input to drive the membrane potential to threshold (irrespective of the type of EPSP) and L is the average projection length. The descending interneurons will transmit a signal too quickly — axonal propagation speeds are observed to be greater than 200 mm/s [Stebbing and Bornstein, 1996] and the average projection length of descending interneurons (in guinea-pig) is 60–70mm for somatostatin positive neurons [Song et al., 1997, Meedeniya et al., 1998] and 5–10mm for neurons positive for nitric oxide synthase [Costa et al., 1992]. Conservatively, using $L = 5$mm gives $\tau_\theta = 5$ s. This is a long rise time which requires previously unobserved synaptic dynamics. On the other hand, the average oral-anal projection distance of sensory neurons is about 0.2 mm, on average [Bornstein et al., 1991b] and thus $\tau_\theta = 200$ms, well within

the observed range [Morita and North, 1985]. Thus, propagation within the sensory neuron network is a plausible mechanism consistent with current knowledge.

These data suggest the following model. The interdigestive cycle starts after a period of fasting (in some species) [Sarna et al., 1993, Kellow et al., 1986] by altering the properties of intrinsic sensory neurons in a number of possible ways. Either the inhibitory mechanisms discussed in chapters 4 and 5 are down regulated or the efficacy of synaptic transmission is up regulated. Increased synaptic efficacy has been suggested as the mechanism for qualitatively altering rhythmogenesis resulting from synaptic depression [Nadim et al., 1999]. These changes move the sensory neuron network into the parameter regime where wave propagation is possible within the network. This wave of activity is phase III, which drives individual contractions by generating muscle action potentials on top of the underlying muscle slow waves. The drop in speed of the wave as it propagates down the intestine is due to variations in the properties of sensory neurons along the intestine (see more below). Following the phase III period, there is a refractory period due to strong depression of the synapses between sensory neurons. The time period of recovery of synaptic efficacy determines the time until the next phase III. During recovery, the excitability of the network increases and this suggests that contractions during phase II are either spontaneous events due to local fluctuations in excitability and sensory input or, more speculatively, the system may move through a chaotic parameter region (see chapter 6), which may account for the highly irregular small contractions that make up the late phase of MMC phase II [Code and Marlett, 1975, Kellow et al., 1986]. This is also consistent with the fact that phase II does not migrate [Lang et al., 1986]. The next phase III starts when synapses have recovered to the point where

the network is excitable enough to support another wave of activity. The phase III is triggered by spontaneous sensory input, such as a spontaneous contraction or other mechanical event, similarly to phase II contractions. Because it depends on recovery of synaptic efficacy, it is most likely to be triggered near the region where the last phase III started. This is consistent with the notorious variability of phase III, even within individuals [Husebye, 1999]. It is also consistent with the variability in the site of initiation of the phase III in humans [Kellow et al., 1986]. Finally, it also explains how isolated segments of intestine can maintain their own independent MMC cycle [Itoh et al., 1981]. Alternatively, there may be one or more "trigger regions", in the duodenum or stomach for example, where a phase III is more likely to start. The anal bias of sensory neuron projections naturally explains the propensity of phase IIIs to propagate anally. However, numerical simulations show oral waves are also possible. Normally these will not be seen because anal waves are much more likely, but if the network is hyperexcitable, a phase III like event can propagate orally and this is seen in some pathological conditions [Jebbink et al., 1996] and, on rare occasions, in apparently healthy humans [Castedal and Abrahamsson, 2001].

Model shortcomings

The model is in good qualitative agreement with observed phase III propagation speeds; however, it is in poor agreement with phase III durations and overall MMC duration. This may be due to poor data on the slow EPSP and synaptic depression. The duration of the simulated phase III is graded with slow EPSP duration (figure 7.3), but the duration of simulated slow EPSPs was also only a few seconds in

response to a typical experimental stimulus (figure 4.1, panel B), however slow EPSPs in intrinsic sensory neurons of the guinea-pig ileum can last minutes in response to similar stimuli (P. J. Johnson, unpublished observations). The time between phase III episodes depends the synaptic recovery halflife (table 7.1) and there are no quantitative data on the dynamics of synaptic depression in the ENS. It is possible that with better data for synaptic dynamics, the model will be in better agreement with observed MMC properties.

Transit of phase III is blocked by hexamethonium or atropine perfused into arteries close to the intestine [Sarna et al., 1983]. In the case of hexamethonium, this is probably due to blockade of cholinergic transmission onto excitatory motor neurons [Johnson et al., 1996]. In the case of atropine, the simplest interpretation of these data is that muscarinic transmission to the muscle is blocked [Kosterlitz and Lees, 1964, Hirst et al., 1975] and therefore feedback from the muscle, required to maintain propagation, is blocked. Feedback driven waves were observed in the numerical simulations; however, they occur in a comparatively small parameter regime compared to non-feedback driven waves and this parameter regime is adjacent to the parameter regime for non-feedback drive waves. In other words, feedback driven waves are less robust than non-feedback driven waves. Of course, this may be dependent on details of the model. An alternative explanation of blockade of phase III transit by atropine is that it may reduce or block synaptic depression by blocking the muscarinic component of presynaptic inhibition [North et al., 1985]. In this argument, atropine is blocking inhibition in the system which may be able to disrupt the MMC. Blocking inhibitory neuromuscular transmission disrupts the MMC [Sarna et al., 1993]. However, the model in its current form does not offer an

explanation for this.

The requirement for feedback has lead Sarna et al. [1981] to propose that propagation works by muscle contraction exciting the next section of the sensory neuron network, but this model fails to explain why propagation should be in the anal direction, especially given the usual expectation of descending inhibition.

Experimental tests

The models described in chapters 3–5 are based closely on data and make predictions about aspects of the circuits that are difficult to isolate experimentally from larger scale phenomena. The model presented in this chapter, by contrast, makes a number of assumptions and is a complete model of a motor pattern and this makes it easier to test.

An assumption of the model is that inhibition in sensory neurons is down regulated during the interdigestive period for species in which feeding disrupts the MMC cycle. This may be possible to detect by comparing the properties of sensory neuron, and sensory neuron synaptic transmission, between neurons in fed and fasted animals. This should manifest itself as one or more of the following; a decrease in the AHP, possibly at rest, but specifically during a slow EPSP; a decrease in IPSP properties; a reduction in the size or duration of slow EPSPs. A possible confounding issue with this test is that the interdigestive motor patterns are easily disrupted, for example by feeding, some anaesthetics, laparotomy, barbiturates and possibly death and they have never been observed *in vitro*. Thus, *in vitro* recording may not reveal differences between the fed and fasted state neuron properties.

The basic prediction of the model is that the intrinsic sensory neurons are re-

sponsible for coordinating the MMC. There is a decreasing gradient of phase III propagation speed along the intestine; therefore, there must be a gradient in the properties of the sensory neuron along the intestine. Propagation is always faster in the anal direction, because of the anal bias in the pattern of sensory neuron projections (see table 7.1). Thus, the model predicts that a systematic reduction in the bias of projections will lead to a systematic reduction in the propagation speed. This is straight forward to test using standard immunohistochemical techniques [Bornstein et al., 1991b]. Increasing synaptic efficacy, by increasing Δ, also increases propagation speed. Determining the properties (or existence) of synaptic depression in the synapses connecting sensory neurons is technically difficult, however changes in the dynamics of short term synaptic depression should be apparent as changes in response to internodal strand stimuli of 10–40 pulses in 1–2 s. Again, this is straight forward to test experimentally.

It may be possible to detect propagation in the intrinsic sensory network using standard *in vitro* electrophysiology preparations. Typically, no response is seen in sensory neurons away from the stimulus area [Bornstein et al., 1991a, Smith et al., 1992], which is consistent with the absence of propagation in networks with a relatively large AHP (chapter 4). However, it may be possible to manipulate the preparation so that the sensory neuron network switches into a state in which propagation is possible. There is evidence that the AHP may be almost completely suppressed in the presence of tonic input [Clerc et al., 1999] and so by stimulating the tissue to drive activity in the sensory neurons it may be possible to suppress the AHP sufficiently that propagation is possible. This can be tested using standard electrophysiological techniques and preparations [Bornstein et al., 1991a, Smith

et al., 1992], by stimulating a region of the tissue and impaling sensory neurons some distance away.

Chapter 8

Conclusions and further work

8.1 Conclusions

The sensory neurons of the gut must play a crucial role in the initiation, organisation and control of intrinsic reflexes. Yet precisely what this role is, and how it is achieved, is largely unknown. This work has taken the tentative first steps in addressing this question. Basic facts about the networks of sensory neurons have dictated what these steps should be. Because sensory neurons are recurrently interconnected, understanding synaptic transmission between neurons and its effect on emergent network properties are prerequisites to understanding the network's role. This in turn requires a model of slow synaptic transmission that reproduces the complex nature of interactions between sensory neurons. In chapter 3, it was shown how such models can be constructed, using a combination of physical insight and experimental data. This model reproduces the experimental data, such as it is, and this demonstrates the value of gray box modelling. This has lead to predictions, specifically in the case of the delay seen in the onset of some slow EPSPs. However,

it is most valuable in building models of key processes that are to be combined together in a model that address a larger construct. In this case, the model of synaptic transmission has been a key element in the network models studied in this thesis.

Chapters 4–7 have dealt with the properties and behaviours of these recurrent networks. The first prediction was that networks with only excitation are not biologically useful — there must be some mechanism to control firing. Such a mechanism has been generically termed inhibition and three candidates for inhibition were examined. The first two candidates were AHPs and IPSPs and these were examined from the point of view of having the network produce a graded response to graded input, as would be required for sensory transduction. Both mechanisms can provide the necessary inhibition to achieve this, but do so in different ways and they both provide explanations for different phenomena. AHP inhibition gives the network strong transient filtering properties when in the quiescent state and this may provide an explanation for the depression seen in response to rapidly applied stimuli. Networks with IPSP inhibition, where IPSPs are small, provide almost no filtering of inputs over the physiological range. Interestingly though, IPSP based networks provide an explanation for erratic bursting, a phenomenon observed in enteric neurons (of unknown class) in unparalysed tissue (section 5.3).

Since both currents are present in enteric sensory neurons and both currents in combination provide a satisfactory inhibition mechanism, this leads to the question of what is the interaction between the two. The AHP is almost unavoidable in normal *in vitro* preparations [Bornstein et al., 1991a], so it is undoubtedly present during electrophysiological recordings of reflex experiments [Bornstein et al., 1991a, Smith et al., 1992]. On the other hand, the AHP may be completely, or almost

completely, suppressed under physiological conditions in which neurons receive long term synaptic drive [Clerc et al., 1999]. This suggests that under quiescent conditions the AHP provides a portion of inhibition, but when there is a lot of sensory input into the network the predominant form of inhibition are IPSPs. Thus, under experimental conditions where the tissue is unparalysed, the predominant form of inhibition is IPSPs and erratic bursting is possible. In paralysed preparations sensory drive is significantly less and the AHP plays the major inhibitory role. Numerical simulations then predict that there is a transient depression of closely spaced stimuli, again consistent with observations in unparalysed tissue [Bornstein et al., 1991a, Smith et al., 1991, 1992, Yuan et al., 1991] (see section 4.4). Irritable bowel syndrome involves hypersensitivity [Mayer and Raybould, 1990] and it has been suggested that is caused by complete suppression of the AHP [Furness et al., 2000a], however if the theory expounded here is correct hypersensitivity is actually the result of suppression myenteric IPSPs.

AHP and IPSP inhibition come on quickly — AHPs initiate within a few tens of milliseconds of action potential firing [Hirst et al., 1974, Hillsley et al., 2000] and IPSPs seem to have a shorter delay than EPSPs in sensory neurons (P. J. Johnson and J. C. Bornstein, unpublished). Furthermore, both operate at a level that provides just enough inhibition to allow the networks to function as simple stimulus encoders and therefore inhibition also turns off quickly as the level of drive decreases. Although not a mathematical rigorous argument, this implies that periodic firing is not possible when the network operates in this regime. (Latham et al. [2000a] predict rhythmic bursting in a network with both inhibitory and excitatory neurons and firing adaptation based on an AHP, however the AHP in this case is much larger

and continues to provide strong inhibition for some time after firing ceases.) Activity dependent synaptic depression, on the other hand, does inhibit firing more slowly and causes reduced excitability for some time after firing has been suppressed. This creates the possibility of more complex dynamics which were presented in chapters 6 and 7.

This again leads to the question of when and how does the intestine switch from one mode of operation to another? The ENS drives a number of intrinsic reflexes or motor patterns (peristalsis, segmentation, the interdigestive motor patterns) and so there must be one or more "switches" that change it from one behaviour to another. In this thesis, it is proposed that the switch between digestive and interdigestive motor patterns resides, in large part, in the intrinsic sensory neurons. In the digestive state, inhibition is strong and synaptic transmission is weak. In the interdigestive state, inhibition is weak and synaptic transmission is strong and subject to depression. Thus, the Dogiel type II neurons reconfigure themselves from being primarily sensory neurons to being a combination of interneuron and rhythm generator. There is growing evidence that both invertebrate [Marder, 2000, Nadim et al., 1999] and central vertebrate [Lieske et al., 2000] neurons and networks "reconfigure" themselves to perform different functions. Furthermore, in some cases this achieved by changing the strength and activity dependent plasticity of key synapses [Nadim and Manor, 2000, Lieske et al., 2000].

8.2 Wider implications

This study has examined the interactions of metabotropic slow EPSPs with AHPs, slow IPSPs or synaptic depression in recurrent networks with a single class of neuron. These mechanisms exist throughout the central nervous system (CNS) and the periphery in various combinations. Metabotropic transmission is common in the CNS (see section 1.6) yet its role in single neuron dynamics has only recently been examined [Batchelor and Garthwaite, 1997] and there are virtually no studies into it effects on network behaviour. Similarly, AHPs are seen in many other neurons [Davies et al., 1996, Kelly et al., 1991, Sah and Isaacson, 1995], often they are seen in conjunction with metabotropic transmission and are the targets of neuromodulation [Kelly et al., 1991, Sah and Isaacson, 1995]. Similarly, excitatory and inhibitory cotransmission is seen at other central synapses [Fiorillo and Williams, 1998], sometimes mediated by the same transmitter. The finding that stability can be conferred on a recurrent network by inhibitory cotransmission suggests an explanation for the paradox of both excitatory and inhibitory substances being present in the one nerve terminal. This is seen in many parts of the central nervous system, for example, the projection neurons in the *corpus striatum* contain both GABA and substance P [Bolam and Smith, 1990]. If both are released, but with different dynamics, the system is more adequately able to regulate its firing in response to external stimuli.

8.3 Modelling as a means of understanding

It is still necessary to defend modelling of biological processes as a way to manage the complexity living things and gain a deeper understanding of how they operate.

This may be because expectations of models are greater than what they are currently able to do. The complexity of living things means that initial models will be limited in their predictive and explanatory ability, and what is more, these models may highly technical and only understandable by *aficionados*. This is exemplified in chapters 4 and 5 where basic questions about the nature of homogeneous recurrent networks were addressed. As with experimental studies, progress will be incremental and slow and evaluating the merit of individual studies will mean understanding the limitations of the techniques used in those studies. Nevertheless, simple mathematical models, like the ones used in chapters 4–6, provide rigorous insight into the relationships between properties of the system, despite being difficult to follow. Numerical models can test analytical models and extend them by relaxing assumptions necessary for building analytical models. In addition, they provide the ideal preparation in that every aspect of the preparation can be varied.

The techniques used in this study are not the only ones. Others include system identification approaches [Ljung, 1999], which are used to construct mathematical models from directly from data. These models have no explanatory power themselves but can be used as parts of larger models. Construction of the slow EPSP model of chapter 3 can be considered an exercise in system identification. In principle, it is also possible construct these types of models for different components of the system, from different types of experiment, and combine them to test the consistency and completeness of the experimental data.

8.4 Further work

Theory

The model of neuron firing used in this study is very simple (see section 2.2) and assumes that sensory neurons will fire tonically at nearly constant frequency when the membrane potential is depolarised beyond a fixed threshold. At rest, sensory neurons are highly phasic due to the large AHP, and will not fire during an AHP even when depolarised the resting potential [Hirst et al., 1974]. Even though the firing properties have not been extensively studied when the AHP is suppressed by slow EPSPs, sensory neuron firing does not conform to the simple model used in this thesis. There is now a great deal of high quality data that can be used to construct realistic conductance models of sensory neurons (section 1.5), and more studies underway. There are many interesting questions that can be answered by single neuron models. For example, what is the origin of the sensory gating phenomenon in which PPPs fail to generate action potentials despite neurons being in a highly excited state [Clerc et al., 1999]? Can sensory neurons exhibit rhythmic bursting seen in extracellular recordings [Wood, 1989]? Is the morphology of enteric neurons important for the way they behave as it is in the central nervous system [Koch and Segev, 2000]? Construction of realistic conductance models will also reveal where experimental data are lacking or inconsistent.

The sensory neurons are part of a network so realistic conductance models should be incorporated in a network simulation. At the very least, the more realistic model can add credibility to the results already obtained and connect macroscopic network behaviour to the molecular level of receptors and channels. It is likely, however, that

voltage and Ca^{++} dependent conductances will play an important role in determining firing patterns and hence in overall network behaviour.

In chapters 4 and 5 the modified Wilson and Cowan (WC) model [Wilson and Cowan, 1972] model was only solved in the steady state case. It has been argued in this and other chapters that complex behaviour is not likely from the recurrent networks of enteric sensory neurons and so the interesting qualitative behaviour is captured by the steady state solutions. However, the concentrations of intracellular substances mediating metabotropic transmission act as degrees of freedom or state variables and it would be interesting to know the implications of this more generally, especially in the more complex circuits of the CNS.

The results of chapter seven 7 derived entirely from numerical simulation, no analytical model was used. As discussed innumerable times above, analytical models serve a valuable role in determining what types of qualitative behaviour a system is capable of and how the parameters of the model are related for each type of parameter. In the case of waves in networks of intrinsic sensory neurons, the parameters of interest are those of the slow EPSPs and the pattern of projections and possible the strength of feedback from the muscle. The two dimensional model of Donovan et al. [1998], Tabak et al. [2000] was highly successful in predicting and explaining the outcome of simulations of local networks, or the "zero dimensional" case (chapter 6). It is therefore natural to simply generalise this model to include spatial interactions. An obvious generalisation is

$$\begin{aligned} \tau_E \frac{dE(x,t)}{dt} &= S\left[d(x,t)\int_{-\infty}^{\infty} E(s,t)\,\kappa(x,s)\,ds\right] - E(x,t) \\ \tau_d \frac{dd(x,t)}{dt} &= D(E(x,t)) - d(x,t) \end{aligned}$$

where $E(x,t)$ and $d(x,t)$ are the firing rate and synaptic depression respectively, at time t and position x. The projection pattern, $\kappa(x,y)$, describes the density of projections from position y onto position x. The integral in the first equation describes the input at x from all other regions of the gut that project into this area. Analysis of this model will describe the qualitative behaviours that are possible in a one dimensional network and relate the properties of waves, such as speed and duration, to parameters of the model, such as rate of synaptic depression, time course of synaptic events and synaptic recovery and parameters characterising the pattern of projections.

The circuit used in this study is highly simplified, consisting of only a single class of sensory neurons. There is certainly more than one sensory modality and probably more than one type of sensory neurons. It is natural to wonder how two (or more) networks of sensory neurons coupled together will intereact to stimuli of different modailites and what motor patterns they can generate [Senn et al., 1998]. Of even more interest is role of the rest of the circuit, that is interneurons and motor neurons. Sensory neurons connect to both inhibitory and excitatory motor neurons and so directly directly drive inhibitory and excitatory input to the muscle and presumably mediate local reflexes. How does this effect the MMC model of chapter 7? How do interneurons effect reflexes? Peristalsis undoubtedly involves interneurons and is the most extensively studied reflex because this, or a close counterpart, is readily seen *in vitro*. A model of peristalsis has been the goal of our laboratory, because of the amount of data available and because predictions can be easily tested. Progress has been slow because of the complexity of the circuit which, in addition to sensory

neurons, involves at least three classes of interneuron.

Experimental data

The patterns of connections of neurons within the guinea-pig ileum have been studied extensively for many years and there is a great deal of qualitative data (section 1.4) that can be used to construct anatomically realistic models. As noted above, electrophysiological studies are now producing data good enough for models (section 1.5). However, there are almost no qualitative data on the dynamics of synaptic transmission. This is in part because the need has not been recognised for this type of data, most studies have focused on determining the pharmacology of synaptic transmission. In fact, it will be not possible to elucidate the dynamics of synaptic transmission at the biophysical level until the pharmacological tools are available to isolate the many different pathways. However, to understand how synaptic transmission operates in a network it may not be necessary to know all the biophysical and pharmacological details. System identification techniques can used to build mathematical models of the dynamics directly from experimentally observed input output relationships. This is a generalisation of the work that made up chapter 3. In that study only brief fixed frequency pulses were used as inputs [Morita and North, 1985] and it cannot be guaranteed that this will uncover all the dynamics that the system is capable of.

The last word

Intrinsic sensory neurons of the intestine form a deceptively simple network. Using physiological data as the basis of the network and its dynamics, modelling has shown

that their is a balance of excitatory and inhibitory influences that control network firing and allow the network to perform biologically useful functions. Modelling is the only way to put together these kind of experimental data in a way that leads to an understanding of how biological systems work.

Bibliography

S. F. Acton. *Numerical methods that work*. Harper & Row, New York, Evanston and London, 1970.

T. Akasu and T. Tokimasa. Potassium currents in submucous neurones of guinea-pig caecum and their synaptic modification. *J Physiol*, 416:571–588, 1989.

G. Alex, W. A. Kunze, J. B. Furness, and N. Clerc. Comparison of the effects of neurokinin-3 receptor blockade on two forms of slow synaptic transmission in myenteric AH neurons. *Neuroscience*, 104(1):263–269, 2001.

W. C. Alvarez and M. F. Bennett. Inquiries into the structure and function of the myenteric plexus. *Am J Physiol*, 99:179–198, 1931.

W. C. Alvarez and E. Starkweather. Conduction in the small intestine. *Am J Physiol*, 50:252–265, 1919.

N. Ambache and M. A. Freeman. Atropine-resistant longitudinal muscle spasms due to excitation of non-cholinergic neurones in auerbach's plexus. *J Physiol*, 199(3): 705–727, 1968.

J. M. Andrews, S. M. Doran, G. S. Hebbard, C. H. Malbert, M. Horowitz, and

J. Dent. Nutrient-induced spatial patterning of human duodenal motor function. *Am J Physiol Gastrointest Liver Physiol*, 280(3):G501–G509, 2001.

W. R. Ashby, H. von Foerster, and C. C. Walker. Instability of pulse activity in a net with threshold. *Nature*, 196:561–562, 1962.

G. R. Athey, A. R. Cooke, and J. D. Wood. Synaptic activation of erratic burst-type myenteric neurons in cat small intestine. *Am J Physiol*, 240(6):G437–G441, 1981.

L. V. Baidan, R. H. Fertel, and J. D. Wood. Effects of brain-gut related peptides on camp levels in myenteric ganglia of guinea-pig small intestine. *Eur J Pharmacol*, 225(1):21–27, 1992.

C. Barajas-Lopez, R. Espinosa-Luna, and V. Gerzanich. ATP closes a potassium and opens a cationic conductance through different receptors in neurons of guinea pig submucous plexus. *J Pharmacol Exp Ther*, 268(3):1397–1402, 1994.

N. M. Barnes and T. Sharp. A review of central 5-ht receptors and their function. *Neuropharmacology*, 38(8):1083–1152, 1999.

L. Barthó and P. Holzer. Search for a physiological role of substance P in gastrointestinal motility. *Neuroscience*, 16(1):1–32, 1985.

L. Barthó, P. Holzer, S. Leander, and F. Lembeck. Evidence for an involvement of substance P, but not cholecystokinin-like peptides, in hexamethonium-resistant intestinal peristalsis. *Neuroscience*, 28(1):211–217, 1989.

A. M. Batchelor and J. Garthwaite. Frequency detection and temporally dispersed synaptic signal association through a metabotropic glutamate receptor pathway. *Nature*, 385(6611):74–77, 1997.

A. M. Batchelor, D. J. Madge, and J. Garthwaite. Synaptic activation of metabotropic glutamate receptors in the parallel fibre-purkinje cell pathway in rat cerebellar slices. *Neuroscience*, 63(4):911–915, 1994.

V. Bauer and H. Kuriyama. Evidence for non-cholinergic, non-adrenergic transmission in the guinea-pig ileum. *J Physiol*, 330:95–110, 1982.

W. M. Bayliss and E. H. Starling. The movements and innervation of the small intestine. *J Physiol (Lond)*, 24:99–143, 1899.

M. R. Bennett and W. G. Gibson. On the contribution of quantal secretion from close-coupled and loose-coupled varicosities to the synaptic potentials in the vas deferens. *Philos. Trans. R. Soc. Lond. B Biol. Sci.*, 347B:187–204, 1995.

K. A. Berg, S. Maayani, and W. P. Clarke. Interactions between effectors linked to serotonin receptors. *Ann N Y Acad Sci*, 861:111–120, 1998.

P. P. Bertrand and J. J. Galligan. Contribution of chloride conductance increase to slow EPSC and tachykinin current in guinea-pig myenteric neurones. *J Physiol (Lond)*, 481(Pt 1):47–60, 1994.

P. P. Bertrand and J. J. Galligan. Signal-transduction pathways causing slow synaptic excitation in guinea pig myenteric AH neurons. *Am J Physiol*, 269(5 Pt 1): G710–720, 1995.

P. P. Bertrand, W. A. Kunze, J. C. Bornstein, and J. B. Furness. Electrical mapping of the projections of intrinsic primary afferent neurons to the mucosa of the guinea-pig small intestine. *Neurogastroenterol. Motil.*, 10:533–541, 1998.

P. P. Bertrand, W. A. Kunze, J. C. Bornstein, J. B. Furness, and M. L. Smith. Analysis of the responses of myenteric neurons in the small intestine to chemical stimulation of the mucosa. *Am. J. Physiol.*, 273:G422–G435, 1997a.

P. P. Bertrand, W. A. Kunze, J. C Bornstein, J. B. Furness, and M. L. Smith. Analysis of the responses of myenteric neurons in the small intestine to chemical stimulation of the mucosa. *Am J Physiol*, 273(2 Pt 1):G422–435, 1997b.

P. P. Bertrand, W. A. Kunze, J. B. Furness, and J. C. Bornstein. The terminals of myenteric intrinsic primary afferent neurons of the guinea-pig ileum are excited by 5-hydroxytryptamine acting at 5-hydroxytryptamine-3 receptors. *Neuroscience*, 101(2):459–469, 2000a.

P. P. Bertrand, E. A. Thomas, W. A. A. Kunze, and J. C. Bornstein. A simple mathematical model of second messenger mediated slow excitatory post-synaptic potentials. *J. Comput. Neurosci.*, 8(2):127–142, 2000b.

R. L. Beurle. Pproperties of a mass of cells capable of regenerating pulses. *Philos Trans R Soc Lond B Biol Sci*, 240:55–94, 1956.

J. P. Bolam and Y. Smith. The GABA and substance P input to dopaminergic neurones in the substantia nigra of the rat. *Brain Res*, 529(1-2):57–78, 1990.

E. Bolzer. Myenteric reflex. *Am J Physiol*, 157:329–337, 1949.

V. Bormans, T. L. Peeters, J. Janssens, D. Pearce, M. Vandeweerd, and G. Vantrappen. In man, only activity fronts that originate in the stomach correlate with motilin peaks. *Scand J Gastroenterol*, 22(7):781–784, 1987.

J. C. Bornstein, M. Costa, J. B. Furness, and R. J. Lang. Electrophysiological analysis of projections of enteric inhibitory motoneurones in the guinea-pig small intestine. *J. Physiol. (Lond)*, 370:61–74, 1986.

J. C. Bornstein, M. Costa, J. B. Furness, and G. M. Lees. Electrophysiology and enkephalin immunoreactivity of identified myenteric plexus neurones of guinea-pig small intestine. *J Physiol*, 351:313–325, 1984a.

J. C. Bornstein, J. B. Furness, H. F. Kelly, R. A. R. Bywater, T. O. Neild, and P. P. Bertrand. A computer simulation of the enteric nervous system. *J. Auton. Nerv. Syst.*, 64:143–157, 1997.

J. C. Bornstein, J. B. Furness, and W. A. Kunze. Electrophysiological characterization of myenteric neurons: how do classification schemes relate? *J Auton Nerv Syst*, 48(1):1–15, 1994.

J. C. Bornstein, J. B. Furness, T. K. Smith, and D. C. Trussell. Synaptic responses evoked by mechanical stimulation of the mucosa in morphologically characterized myenteric neurons of the guinea-pig ileum. *J. Neurosci.*, 11:505–518, 1991a.

J. C. Bornstein, R. Hendriks, J. B. Furness, and D. C. Trussell. Ramifications of the axons of AH-neurons injected with the intracellular marker biocytin in the myenteric plexus of the guinea pig small intestine. *J Comp Neurol*, 314(3):437–452, 1991b.

J. C. Bornstein, R. A. North, M. Costa, and J. B. Furness. Excitatory synaptic potentials due to activation of neurons with short projections in the myenteric plexus. *Neuroscience*, 11(3):723–731, 1984b.

M. Bouchoucha, T. Benard, and M. Dupres. Temporal and spatial rhythmicity of jejunal wall motion in rats. *Neurogastroenterol Motil*, 11(5):339–346, 1999.

B. S. Brewster and P. N. Strong. Naturally occuring potassium channel blockers. In A. H. Weston and T. C. Hamilton, editors, *Potassium channel modulators*, pages 272–403. Blackwell, Oxford, 1992.

S. J. Brookes, B. N. Chen, M. Costa, and C. M. Humphreys. Initiation of peristalsis by circumferential stretch of flat sheets of guinea-pig ileum. *J Physiol (Lond)*, 516 (Pt 2):525–538, 1999.

S. J. Brookes, A. C. Meedeniya, P. Jobling, and M. Costa. Orally projecting interneurones in the guinea-pig small intestine. *J. Physiol. (Lond)*, 505:473–491, 1997.

S. J. Brookes, Z. M. Song, G. A. Ramsay, and M. Costa M. Long aboral projections of Dogiel type II, AH neurons within the myenteric plexus of the guinea pig small intestine. *J Neurosci*, 15(5 Pt 2):4013–4022, 1995.

S. J. Brookes, Z. M. Song, P. A. Steele, and M. Costa. Identification of motor neurons to the longitudinal muscle of the guinea pig ileum. *Gastroenterology*, 103 (3):961–973, 1992.

S. J. Brookes, P. A. Steele, and M. Costa. Calretinin immunoreactivity in cholinergic motor neurones, interneurones and vasomotor neurones in the guinea-pig small intestine. *Cell Tissue Res*, 263(3):471–481, 1991a.

S. J. Brookes, P. A. Steele, and M. Costa. Identification and immunohistochemistry

of cholinergic and non-cholinergic circular muscle motor neurons in the guinea-pig small intestine. *Neuroscience*, 42(3):863–878, 1991b.

S. J. H. Brookes and M. Costa. Identification of enteric motor neurones which innervate the circular muscle of the guinea pig small intestine. *Neurosci. Lett.*, 118:227–230, 1990.

S. E. Builder, J. A. Beavo, and E. G. Krebs. Stoichiometry of camp and 1,n6-etheno-camp binding to protein kinase. *J Biol Chem*, 255(6):2350–2354, 1980.

E. A. Bülbring, A. Crema, and B. Saxby. A method for recording peristalsis in isolated intestine. *Br J Pharmacol*, 13:440–441, 1958.

J. D. Buxbaum and Y. Dudai. A quantitative model for the kinetics of cAMP-dependent protein kinase (type II) activity. long-term activation of the kinase and its possible relevance to learning and memory. *J Biol Chem*, 264(16):9344–9351, 1989.

R. A. Bywater, M. E. Holman, and G. S. Taylor. Atropine-resistant depolarization in the guinea-pig small intestine. *J Physiol*, 316:369–378, 1981.

W. B. Cannon. The movements of the stomach studied by means of the roentgen rays. *Am. J. Physiol.*, 1:359–382, 1898.

W. B. Cannon. The movements of the intestines studied by means of the röntgen rays. *Am. J. Physiol.*, 6:251–277, 1902.

W. B. Cannon. Peristalsis, segmentation and the myenteric reflex. *Am. J. Physiol.*, 30:114–128, 1912.

M. Carandini and D. J. Heeger. Summation and division by neurons in primate visual cortex. *Science*, 264(5163):1333–1336, 1994.

C. V. Carman and J. L. Benovic. G-protein-coupled receptors: turn-ons and turn-offs. *Curr Opin Neurobiol*, 8(3):335–344, 1998.

M. Castedal and H. Abrahamsson. High-resolution analysis of the duodenal interdigestive phase III in humans. *Neurogastroenterol Motil*, 13(5):473–481, 2001.

N. A. Castle, D. G. Haylett, and D. H. Jenkinson. Toxins in the characterization of potassium channels. *Trends Neurosci*, 12(2):59–65, 1989.

K. B. Castleton. An experimental study of the movements of the small intestine. *Am. J. Physiol.*, 107:641–646, 1934.

Z. Chen, B. Ermentrout, and X. J. Wang. Wave propagation mediated by $GABA_B$ synapse and rebound excitation in an inhibitory network: a reduced model approach. *J Comput Neurosci*, 5(1):53–69, 1998.

F. L. Christofi and J. D. Wood. Presynaptic inhibition by adenosine a1 receptors on guinea pig small intestinal myenteric neurons. *Gastroenterology*, 104(5):1420–1429, 1993.

N. Chub and M. J. Donovan. Blockade and recovery of spontaneous rhythmic activity after application of neurotransmitter antagonists to spinal networks of the chick embryo. *J Neurosci*, 18(1):294–306, 1998.

D. E. Clapham and E. J. Neer. G protein beta gamma subunits. *Annu Rev Pharmacol Toxicol*, 37:167–203, 1997.

N. Clerc, J. B. Furness, W. A. A. Kunze, E. A. Thomas, and P. P. Bertrand. Long term effects of synaptic activation at low frequency on enteric neurons. *Neuroscience*, 90(1):279–289, 1999.

C. F. Code and J. A. Marlett. The interdigestive myo-electric complex of the stomach and small bowel of dogs. *J Physiol*, 246(2):289–309, 1975.

M Costa, S. J. Brookes, P. A. Steele, I Gibbins, E. Burcher, and C. J. Kandiah. Neurochemical classification of myenteric neurons in the guinea-pig ileum. *Neuroscience*, 75(3):949–967, 1996.

M. Costa, J. B. Furness, and C. M. Humphreys. Apamin distinguishes two types of relaxation mediated by enteric nerves in the guinea-pig gastrointestinal tract. *Naunyn Schmiedebergs Arch Pharmacol*, 332(1):79–88, 1986.

M. Costa, J. B. Furness, S. Pompolo, S. J. Brookes, J. C. Bornstein, D. S. Bredt, and S. H. Synder. Projections and chemical coding of neurons with immunoreactivity for nitric oxide synthase in the guinea-pig small intestine. *Neurosci Lett*, 148(1–2): 121–125, 1992.

M. Costa, J. B. Furness, C. O. Pullin, and J. Bornstein. Substance P enteric neurons mediate non-cholinergic transmission to the circular muscle of the guinea-pig intestine. *Naunyn Schmiedebergs Arch Pharmacol*, 328(4):446–453, 1985.

J. R. Crist, X. D. He, and R. K. Goyal. Both ATP and the peptide VIP are inhibitory neurotransmitters in guinea-pig ileum circular muscle. *J Physiol*, 447: 119–131, 1992.

P. J. Davies, D. R. Ireland, and E. M. McLachlan. Sources of Ca^{++} for different Ca^{++}-activated K^+ conductances in neurons if the rat superior cervical ganglion. *J Physiol (Lond)*, 495:353–366, 1996.

V. Derkach, A. Surprenant, and R. A. North. 5-HT_3 receptors are membrane ion channels. *Nature*, 339(6227):706–709, 1989.

A. Destexhe, Z. F. Mainen, and T. J. Sejnowski. Synthesis of models for excitable membranes, synaptic transmission and neuromodulation using a common kinetic formalism. *J Comput Neurosci*, 1(3):195–230, 1994.

A. Destexhe and T. J. Sejnowski. G protein activation kinetics and spillover of gamma-aminobutyric acid may account for differences between inhibitory responses in the hippocampus and thalamus. *Proc Natl Acad Sci U S A*, 92(21): 9515–9519, 1995.

A. S. Dogiel. Über den bau der ganglien in den geflechten des darmes und der gallenblase des menschen und der sugetiere. *Arch. Anat. Physiol. (Leipzig)*, pages 130–158, 1899. Translated by J. B. Furness.

M. J. Donovan, P. Wenner, N. Chub, J. Tabak, and J. Rinzel. Mechanisms of spontaneous activity in the developing spinal cord and their relevance to locomotion. *Ann N Y Acad Sci*, 860:130–141, 1998.

A. Einstein. Zur allegemeine Relativitätstheorie. In A. J. Kox, M. J. Klein, and R. Schulmann, editors, *The collected papers of Albert Einstein*, volume 6, chapter 21, pages 214–224. Princeton University Press, 1996.

G. B. Ermentrout and D. Kleinfeld. Traveling electrical waves in cortex: insights from phase dynamics and speculation on a computational role. *Neuron*, 29(1): 33–44, 2001.

R. J. Evans, C. Lewis, C. Virginio, K. Lundstrom, G. Buell, A. Surprenant, and R. A. North. Ionic permeability of, and divalent cation effects on, two ATP-gated cation channels ($P2_X$ receptors) expressed in mammalian cells. *J Physiol*, 497(Pt 2):413–422, 1996.

B. Fedirchuk, P. Wenner, P. J. Whelan, S. Ho, J. Tabak, and M. J. Donovan. Spontaneous network activity transiently depresses synaptic transmission in the embryonic chick spinal cord. *J Neurosci*, 19(6):2102–2112, 1999.

M. B. Feller, D. A. Butts, H. L. Aaron, D. S. Rokhsar, and C. J. Shatz. Dynamic processes shape spatiotemporal properties of retinal waves. *Neuron*, 19(2):293–306, 1997.

M. B. Feller, D. P. Wellis, D. Stellwagen, F. S. Werblin, and C. J. Shatz. Requirement for cholinergic synaptic transmission in the propagation of spontaneous retinal waves. *Science*, 272(5265):1182–1187, 1996.

L. A. Fieber and D. J. Adams. Adenosine triphosphate-evoked currents in cultured neurones dissociated from rat parasympathetic cardiac ganglia. *J Physiol*, 434: 239–256, 1991.

C. D. Fiorillo and J. T. Williams. Glutamate mediates an inhibitory postsynaptic potential in dopamine neurons. *Nature*, 394(6688):78–82, 1998.

E. S. Fortune and G. J. Rose. Short-term synaptic plasticity as a temporal filter. *Trends Neurosci*, 24(7):381–385, 2001.

R. Franco, M. Costa, and J. B. Furness. Evidence for the release of endogenous substance P from intestinal nerves. *Naunyn Schmiedebergs Arch Pharmacol*, 306 (3):195–201, 1979.

J. L. Franklin and A. L. Willard. Voltage-dependent sodium and calcium currents of rat myenteric neurons in cell culture. *J Neurophysiol*, 69(4):1264–1275, 1993.

J. B. Furness. Types of neurons in the enteric nervous system. *J Auton Nerv Syst*, 81(1–3):87–96, 2000.

J. B. Furness, J. C. Bornstein, W. A. A. Kunze, P. P. Bertrand, H. Kelly, and E. A. Thomas. Experimental basis for realistic large scale computer simulation of the enteric nervous system. *Clin. Exp. Pharm. Physiol.*, 23:786–792, 1996.

J. B. Furness, J. C. Bornstein, and D. C. Trussell. Shapes of nerve cells in the myenteric plexus of the guinea-pig small intestine revealed by the intracellular injection of dye. *Cell Tissue Res*, 254(3):561–571, 1988a.

J. B. Furness, N. Clerc, and W. A. Kunze. Memory in the enteric nervous system. *Gut*, 47:iv60–iv62, 2000a.

J. B. Furness, N. Clerc, A. E. Lomax, J. C. Bornstein, and W. A. Kunze. Shapes and projections of tertiary plexus neurons of the guinea-pig small intestine. *Cell Tissue Res*, 300(3):383–387, 2000b.

J. B. Furness and M. Costa. Types of nerves in the enteric nervous system. *Neuroscience*, 5(1):1–20, 1980.

J. B. Furness and M. Costa. *The Enteric Nervous System*. Churchill Livingstone, Edinburgh, 1987.

J. B. Furness, P. J. Johnson, S. Pompolo, and J. C. Bornstein. Evidence that enteric motility reflexes can be initiated through entirely intrinsic mechanisms in the guinea-pig small intestine. *Neurogastroenterol Motil*, 7(2):89–96, 1995a.

J. B. Furness, J. R. Keast, S. Pompolo, J. C. Bornstein, M. Costa, P. C. Emson, and D. E. Lawson. Immunohistochemical evidence for the presence of calcium-binding proteins in enteric neuron. *Cell Tissue Res*, 252(1):79–87, 1988b.

J. B. Furness, W. A. Kunze, P. P. Bertrand, N. Clerc, and J. C. Bornstein. Intrinsic primary afferent neurons of the intestine. *Prog Neurobiol*, 54(1):1–18, 1998.

J. B. Furness, D. C. Trussell, S. Pompolo, J. C. Bornstein, and T. K. Smith. Calbindin neurons of the guinea-pig small intestine: quantitative analysis of their numbers and projections. *Cell Tissue Res*, 260(2):261–272, 1990.

J. B. Furness, H. M. Young, S. Pompolo, J. C. Bornstein, W. A. Kunze, and K. McConalogue. Plurichemical transmission and chemical coding of neurons in the digestive tract. *Gastroenterology*, 108(2):554–563, 1995b.

Fabrizio Gabbiani and Christof Koch. Principles of spike train analysis. In Christof Koch and Idan Segev, editors, *Methods in Neuronal Modeling: from ions to neworks*. The MIT Press, second edition, 1998.

G. Gabella. Innervation of the intestinal muscular coat. *J. Neurocytol.*, 1:341–362, 1972.

J. J. Galligan and P. P. Bertrand. ATP mediates fast synaptic potentials in enteric neurons. *J Neurosci*, 14(12):7563–7571, 1994.

J. J. Galligan, M. Costa, and J. B. Furness. Gastrointestinal myoelectric activity in conscious guinea pigs. *Am J Physiol*, 249(1 Pt 1):G92–G99, 1985.

J. J. Galligan, J. B. Furness, and M. Costa. Effects of cholinergic blockade, adrenergic blockade and sympathetic denervation on gastrointestinal myoelectric activity in guinea pig. *J Pharmacol Exp Ther*, 238(3):1114–1125, 1986.

J. J. Galligan, K. J. Lepard, D. A. Schneider, and X. Zhou. Multiple mechanisms of fast excitatory synaptic transmission in the enteric nervous system. *J Auton Nerv Syst*, 81(1-3):97–103, 2000.

J. J. Galligan, H. Tatsumi, K. Z. Shen, A. Surprenant, and R. A. North. Cation current activated by hyperpolarization (I_h) in guinea pig enteric neurons. *Am J Physiol*, 259(6 Pt 1):G966–G972, 1990.

J. J. Galligan, T. Tokimasa, and R. A. North. Effects of three mammalian tachykinins on single enteric neurons. *Neurosci Lett*, 82(2):167–171, 1987.

A. M. Garland, E. F. Grady, M. Lovett, S. R. Vigna, M. M. Frucht, J. E. Krause, and N. W. Bunnett. Mechanisms of desensitization and resensitization of g protein-coupled neurokinin1 and neurokinin2 receptors. *Mol Pharmacol*, 49(3):438–446, 1996.

D. Golomb and Y. Amitai. Propagating neuronal discharges in neocortical slices: computational and experimental study. *J Neurophysiol*, 78(3):1199–1211, 1997.

P. Grafe, C. J. Mayer, and J. D. Wood. Synaptic modulation of calcium-dependent potassium conductance in myenteric neurones in the guinea-pig. *J Physiol*, 305: 235–248, 1980.

P. C. Gray, J. D. Scott, and W. A. Catterall. Regulation of ion channels by camp-dependent protein kinase and a-kinase anchoring proteins. *Curr Opin Neurobiol*, 8(3):330–334, 1998.

J. R. Grider and J. G. Jin. Distinct populations of sensory neurons mediate the peristaltic reflex elicited by muscle stretch and mucosal stimulation. *J Neurosci*, 14(5 Pt 1):2854–2860, 1994.

J. S. Griffith. On the stability of brain like structures. *Biophys. J.*, 3:299–308, 1963.

S. Guard, K. J. Watling, and S. P. Watson. Neurokinin3-receptors are linked to inositol phospholipid hydrolysis in the guinea-pig ileum longitudinal muscle-myenteric plexus preparation. *Br J Pharmacol*, 94(1):148–154, 1988.

D. G. Haylett and D. H. Jenkisnon. Calcium activated potassium channels. In N. A. Cook, editor, *Potassium Channels: Structure, Classification, Function and Therapeutic Potential*. John Wiley and Sons, London, 1990.

X. D. He and R. K. Goyal. Nitric oxide involvement in the peptide VIP-associated inhibitory junction potential in the guinea-pig ileum. *J Physiol*, 461:485–499, 1993.

C. M. Hempel, P. Vincent, S. R. Adams, R. Y. Tsien, and A. I. Selverston. Spatio-temporal dynamics of cyclic amp signals in an intact neural circuitm. *Nature*, 384 (6605):166–169, 1996.

B. Hille. *Ionic Channels of Excitable Membranes*. Sinauer, Sunderland, Massachusetts, second edition, 1992.

K. Hillsley, J. L. Kenyon, and T. K. Smith. Ryanodine-sensitive stores regulate the excitibility of AH neurons in the myenteric plexus of the guinea-pig ilieum. *J Neurophysiol*, 84:2777–2785, 2000.

G. D. Hirst, M. E. Holam, and H. C. McKirdy. Two descending nerve pathways activated by distension of guinea-pig small intestine. *J Physiol*, 244:113–127, 1975.

G. D. Hirst, M. E. Holman, C. L. Prosser, and I. Spence. Some properties of the neurones of Auerbach's plexus. *J Physiol (Lond)*, 225(2):60–61, 1972.

G. D. Hirst, M. E. Holman, and I. Spence. Two types of neurones in the myenteric plexus of the duodenum in the guinea-pig. *J Physiol (Lond)*, 236:303–326, 1974.

G. D. Hirst, S. M. Johnson, and D. F. van Helden. The calcium current in a myenteric neurone of the guinea-pig ileum. *J Physiol (Lond)*, 361:297–314, 1985a.

G. D. Hirst, S. M. Johnson, and D. F. van Helden. The slow calcium-dependent potassium current in a myenteric neurone of the guinea-pig ileum. *J Physiol*, 361: 315–337, 1985b.

G. D. Hirst and H. C. McKirdy. A nervous mechanism for descending inhibition in guinea-pig small intestine. *J Physiol*, 238:129–143, 1974.

G. D. Hirst and I. Spence. Calcium action potentials in mammalian peripheral neurones. *Nature*, 243:54–56, 1973.

A. L. Hodgkin and A. F. Huxley. A quantitative description of membrane current and its application to conduction and excitation in nerve. *J. Physiol. (Lond.)*, 117:500–544, 1952.

J. P. Hodgkiss and G. M. Lees. Morphological studies of electrophysiologically-identified myenteric plexus neurons of the guinea-pig ileum. *Neuroscience*, 8(3): 593–608, 1983.

T. Hukuhara, S. Nakayama, and R. Nanba. Locality of receptors concerned with the intestino-intestinal extrinsic and intestinal muscular intrinsic reflexes. *Jap J Physiol*, 8:9–20, 1960.

T. Hukuhara, S. Nakayama, and T. Sumi. The role of the intrinsic mucosal reflex in the fluid transport through the denervated loop. *Jap J Physiol*, 9:406–418, 1959.

T. Hukuhara, M. Yamagami, and S. Nakayama. On the intestinal intrinsic reflexes. *Jap J Physiol*, 8:9–20, 1958.

E. Husebye. The patterns of small bowel motility: physiology and implications in organic disease and functional disorders. *Neurogastroenterol Motil*, 11(3):141–161, 1999.

Z. Itoh, I. Aizawa, and S. Takeuchi. Neural regulation of interdigestive motor activity in canine jejunum. *Am J Physiol*, 240(4):G324–G330, 1981.

Z. Itoh, S. Takeuchi, I. Aizawa, K. Mori, T. Taminato, Y. Seino, H. Imura, and N. Yanaihara. Changes in plasma motilin concentration and gastrointestinal contractile activity in conscious dogs. *Am J Dig Dis*, 23(10):929–935, 1978.

V. Iyer, J. C. Bornstein, M. Costa, J. B. Furness, Y. Takahashi, and T. Iwanaga. Electrophysiology of guinea-pig myenteric neurons correlated with immunoreactivity for calcium binding proteins. *J Auton Nerv Syst*, 22(2):141–150, 1988.

H. J. Jebbink, G. P. vanberge henegouwen, L. M. Akkermans, and A. J. Smout. Small intestinal motor abnormalities in patients with functional dyspepsia demonstrated by ambulatory manometry. *Gut*, 38(5):694–700, 1996.

P. J. Johnson, J. C. Bornstein, and E. Burcher. Roles of neuronal NK1 and NK3 receptors in synaptic transmission during motility reflexes in the guinea-pig ileum. *Br J Pharmacol*, 124(7):1375–1384, 1998.

P. J. Johnson, J. C. Bornstein, S. Y. Yuan, and J. B. Furness. Analysis of contributions of acetylcholine and tachykinins to neuro-neuronal transmission in motility reflexes in the guinea-pig ileum. *Br J Pharmacol*, 118(4):973–983, 1996.

P. J. Johnson, O. R. Shum, P. D. Thornton, and J. C. Bornstein. Evidence that inhibitory motor neurons of the guinea-pig small intestine exhibit fast excitatory synaptic potentials mediated via $P2_X$ receptors. *Neurosci Lett*, 266(3):169–172, 1999.

S. M. Johnson, Y. Katayama, and R. A. North. Slow synaptic potentials in neurones of the myenteric plexus. *J Physiol (Lond)*, 301:505–516, 1980.

Y. Katayama, G. M. Lees, and G. T. Pearson. Electrophysiology and morphology of vasoactive-intestinal-peptide-immunoreactive neurones of the guinea-pig ileum. *J Physiol*, 378:1–11, 1986.

Y. Katayama and R. A. North. Does substance P mediate slow synaptic excitation within the myenteric plexus. *Nature*, 274(5669):387–388, 1978.

J. E. Kellow, T. J. Borody, S. F. Phillips, R. L. Tucker, and A. C. Haddad. Human interdigestive motility: variations in patterns from esophagus to colon. *Gastroenterology*, 91(2):386–395, 1986.

J. S. Kelly, P. Larkman, N. J. Penington, D. G. Rainnie, H. Mcallister-williams, and J. Hodgkiss. Serotonin receptor heterogeneity and the role of potassium channels in neuronal excitability. *Adv Exp Med Biol*, 287:177–191, 1991.

H. K. Khalil. *Nonlinear systems*. Prentice Hall, Upper Saddle River, NJ 07458, 1996.

A. L. Kirchgessner, H. Tamir, and M. D. Gershon. Identification and stimulation by serotonin of intrinsic sensory neurons of the submucosal plexus of the guinea pig gut: activity-induced expression of fos immunoreactivity. *J. Neurosci.*, 12: 235–248, 1992.

M. F. Klemm. Neuromuscular junctions made by nerve fibres supplying the longitudinal muscle of the guinea-pig ileum. *J. Auton. Nerv. Syst.*, 55:155–164, 1995.

C. Koch and I. Segev. The role of single neurons in information processing. *Nat Neurosci*, 3 Suppl:1171–1177, 2000.

H. W. Kosterlitz and G. M. Lees. Pharmacological analysis of intrinsic intestinal reflexes. *Pharmacol Rev*, 16:301–339, 1964.

W. A. Kunze, P. P. Bertrand, J. B. Furness, and J. C. Bornstein. Influence of the

mucosa on the excitability of myenteric neurons. *Neuroscience*, 76(2):619–634, 1997.

W. A. Kunze, J. C. Bornstein, and J. B. Furness. Identification of sensory nerve cells in a peripheral organ (the intestine) of a mammal. *Neuroscience*, 66:1–4, 1995.

W. A. Kunze, J.C. Bornstein, J. B. Furness, R. Hendriks, and D. S. Stephenson. Charybdotoxin and iberiotoxin but not apamin abolish the slow afterhyperpolarization in myenteric plexus neurons. *Pflugers Arch*, 428(3–4):300–306, 1994.

W. A. Kunze, N. Clerc, P. P. Bertrand, and J. B. Furness. Contractile activity in intestinal muscle evokes action potential discharge in guinea-pig myenteric neurons. *J Physiol (Lond)*, 517 (Pt 2):547–561, 1999.

W. A. Kunze, N. Clerc, J. B. Furness, and M. Gola. The soma and neurites of primary afferent neurons in the guinea-pig intestine respond differentially to deformation. *J Physiol (Lond)*, 526 Pt 2:375–385, 2000.

W. A. Kunze and J. B. Furness. The enteric nervous system and regulation of intestinal motility. *Annu. Rev. Physiol.*, 61:117–42, 1999.

W. A. Kunze, J. B. Furness, P. P. Bertrand, and J. C. Bertrand. Intracellular recording from myenteric neurons of the guinea-pig ileum that respond to stretch. *J. Physiol. (Lond)*, 506:827–842, 1998.

W. A. Kunze, J. B. Furness, and J. C. Bornstein. Simultaneous intracellular record-

ings from enteric neurons reveal that myenteric AH neurons transmit via slow excitatory postsynaptic potentials. *Neuroscience*, 55:685–694, 1993.

T. D. Lamb. Gain and kinetics of activation in the g-protein cascade of phototransduction. *Proc Natl Acad Sci U S A*, 93(2):566–570, 1996.

T. D. Lamb and E. N. Pugh. A quantitative account of the activation steps involved in phototransduction in amphibian photoreceptors. *J Physiol*, 449:719–758, 1992.

I. M. Lang, S. K. Sarna, and R. E. Condon. Generation of phases I and II of migrating myoelectric complex in the dog. *Am J Physiol*, 251(2 Pt 1):G201–G207, 1986.

P. E. Latham, B. J. Richmond, P. G. Nelson, and S. Nirenberg. Intrinsic dynamics in neuronal networks. I. Theory. *J Neurophysiol*, 83(2):808–827, 2000a.

P. E. Latham, B. J. Richmond, S. Nirenberg, and P. G. Nelson. Intrinsic dynamics in neuronal networks. II. Experiment. *J Neurophysiol*, 83(2):828–835, 2000b.

K. J. Lepard and J. J. Galligan. Analysis of fast synaptic pathways in myenteric plexus of guinea pig ileum. *Am J Physiol*, 276(2 Pt 1):G529–G538, 1999.

S. P. Lieske, M. Thoby-brisson, P. Telgkamp, and J. M. Ramirez. Reconfiguration of the neural network controlling multiple breathing patterns: eupnea, sighs and gasps. *Nat Neurosci*, 3(6):600–607, 2000.

L. Ljung. *System identification. Theory for the user.* Prentice Hall, second edition, 1999.

I. J. Llewellyn-Smith, J. B. Furness, I. L. Gibbins, and M. Costa. Quantitative ultrastructural analysis of enkephalin-, substance P-, and VIP-immunoreactive

nerve fibers in the circular muscle of the guinea pig small intestine. *J Comp Neurol*, 272(1):139–148, 1988.

A. E. Lomax and J. B. Furness. Neurochemical classification of enteric neurons in the guinea-pig distal colon. *Cell Tissue Res*, 302(1):59–72, 2000.

G. M Makhlouf. Smooth muscle of the gut. In T. Yamada, D. H. Alpers, L. Laine, C. Owyang, and D. W. Powell, editors, *Textbook of gastroenterology*, volume 1. Lippincott, Williams and Wilkins, third edition, 1999.

P. T. Mann, B. R. Southwell, and J. B. Furness. Internalization of the neurokinin 1 receptor in rat myenteric neurons. *Neuroscience*, 91(1):353–362, 1999.

P. T. Mann, B. R. Southwell, H. M. Young, and J. B. Furness. Appositions made by axons of descending interneurons in the guinea-pig small intestine, investigated by confocal microscopy. *J Chem Neuroanat*, 12(3):151–164, 1997.

E. Marder. Motor pattern generation. *Curr Opin Neurobiol*, 10(6):691–698, 2000.

E. Marder and R. L. Calabrese. Principles of rhythmic motor pattern generation. *Physiol Rev*, 76(3):687–717, 1996.

A. Marty. The physiological role of calcium-dependent channels. *Trends Neurosci*, 12(11):420–424, 1989.

G. M. Mawe, T. A. Branchek, and M. D. Gershon. Peripheral neural serotonin receptors: identification and characterization with specific antagonists and agonists. *Proc Natl Acad Sci U S A*, 83(24):9799–9803, 1986.

E. A. Mayer and H. E. Raybould. Role of visceral afferent mechanisms in functional bowel disorders. *Gastroenterology*, 99(6):1688–1704, 1990.

K. McConalogue, D. J. Lyster, and J. B. Furness. Electrophysiological analysis of the actions of pituitary adenylyl cyclase activating peptide in the taenia of the guinea-pig caecum. *Naunyn Schmiedebergs Arch Pharmacol*, 352(5):538–544, 1995.

A. C. Meedeniya, S. J. Brookes, G. W. Hennig, and M. Costa. The projections of 5-hydroxytryptamine-accumulating neurones in the myenteric plexus of the small intestine of the guinea-pig. *Cell Tissue Res*, 291(3):375–384, 1998.

K. Michel, H. Sann, C. Schaaf, and M. Schemann. Subpopulations of gastric myenteric neurons are differentially activated via distinct serotonin receptors: projection, neurochemical coding, and functional implications. *J Neurosci*, 17(20): 8009–8017, 1997.

R. N. Miftakhov and G. R. Abdusheva. Effects of selective K^+-channel agonists and antagonists on myoelectrical activity of a locus of the small bowel. *Biol Cybern*, 75(4):331–338, 1996a.

R. N. Miftakhov and G. R. Abdusheva. Numerical simulation of excitation-contraction coupling in a locus of the small bowel. *Biol Cybern*, 74(5):455–467, 1996b.

R. N. Miftakhov, G. R. Abdusheva, and J. Christensen. Numerical simulation of motility patterns of the small bowel. 1. Formulation of a mathematical model. *J Theor Biol*, 197(1):89–112, 1999a.

R. N. Miftakhov, G. R. Abdusheva, and J. Christensen. Numerical simulation of motility patterns of the small bowel. II. Comparative pharmacological validation of a mathematical model. *J Theor Biol*, 200(3):261–290, 1999b.

R. N. Miftakhov, G. R. Abdusheva, and D. L. Wingate. Model predictions of myoelectrical activity of the small bowel. *Biol Cybern*, 74(2):167–179, 1996.

R. N. Miftakhov and D. L. Wingate. Mathematical modelling of the enteric nervous network. II: Facilitation and inhibition of the cholinergic transmission. *J Biomed Eng*, 15(4):311–318, 1993.

R. N. Miftakhov and D. L. Wingate. Biomechanics of small bowel motility. *Med Eng Phys*, 16(5):406–415, 1994a.

R. N. Miftakhov and D. L. Wingate. Mathematical modelling of the enteric nervous network. 1: Cholinergic neuron. *Med Eng Phys*, 16(1):67–73, 1994b.

R. N. Miftakhov and D. L. Wingate. Modelling of the enteric nervous network: 3. Adrenergic neuron. *Med Eng Phys*, 16(6):450–457, 1994c.

R. N. Miftakhov and D. L. Wingate. Mathematic modelling of the enteric nervous network. 5. Excitation propagation in a planar neural network. *Med Eng Phys*, 17(1):11–19, 1995a.

R. N. Miftakhov and D. L. Wingate. Mathematical modelling of the enteric nervous network. 4. Analysis of adrenergic transmission. *Med Eng Phys*, 17(1):3–10, 1995b.

R. N. Miftakhov and D. L. Wingate. Electrical activity of the sensory afferent pathway in the enteric nervous system. *Biol Cybern*, 75(6):471–483, 1996.

S. Mihara, K. Hirai, Y. Katayama, and S. Nishi. Mechanisms underlying intracellular signal transduction of the slow IPSP in submucous neurones of the guinea-pig caecum. *J Physiol*, 436(436):621–641, 1991.

M. C. Miniaci, P. Bonsi, F. Tempia, P. Strata, and A. Pisani. Presynaptic modulation by group III metabotropic glutamate receptors (mGluRs) of the excitatory postsynaptic potential mediated by mGluR1 in rat cerebellar purkinje cells. *Neurosci Lett*, 310(1):61–65, 2001.

K. Morita and Y. Katayama. Substance P inhibits activation of calcium-dependent potassium conductances in guinea-pig myenteric neurones. *J Physiol*, 447:293–308, 1992.

K. Morita and R. A. North. Significance of slow synaptic potentials for transmission of excitation in guinea-pig myenteric plexus. *Neuroscience*, 14(2):661–672, 1985.

K. Morita, R. A. North, and T. Tokimasa. The calcium-activated potassium conductance in guinea-pig myenteric neurons. *J Physiol (Lond)*, 329:341–345, 1982a.

K. Morita, R. A. North, and T. Tokimasa. Muscarinic presynaptic inhibition of synaptic transmission in myenteric plexus of guinea-pig ileum. *J Physiol*, 333: 141–149, 1982b.

C. Morris and H. Lecar. Voltage oscillations in the barnacle giant muscle fiber. *Biophys J*, 35(1):193–213, 1981.

D. D. Mott and D. V. Lewis. The pharmacology and function of central gabab receptors. *Int Rev Neurobiol*, 36:97–223, 1994.

F. Nadim and Y. Manor. The role of short-term synaptic dynamics in motor control. *Curr Opin Neurobiol*, 10(6):683–690, 2000.

F. Nadim, Y. Manor, N. Kopell, and E. Marder. Synaptic depression creates a switch that controls the frequency of an oscillatory circuit. *Proc Natl Acad Sci U S A*, 96(14):8206–8211, 1999.

J. Nauroschat, d. e. r. an, and U. Heiden. A theoretical approach to g-protein modulation of cellular responsiveness. *J Math Biol*, 35(5):609–627, 1997.

M. E. Nelson. A mechanism for neuronal gain control by descending pathways. *Neural Comput*, 6:242–254, 1994.

P. R. Nemeth, J. M. Palmer, J. D. Wood, and D. H. Zafirov. Effects of forskolin on electrical behaviour of myenteric neurones in guinea-pig small intestine. *J Physiol*, 376:439–450, 1986.

S. Nishi and R. A. North. Intracellular recording from the myenteric plexus of the guinea-pig ileum. *J Physiol (Lond)*, 231:471–491, 1973.

R. A. North. The calcium-dependent slow after-hyperpolarization in myenteric plexus neurones with tetrodotoxin-resistant action potentials. *Br J Pharmacol*, 49(4):709–711, 1973.

R. A. North, B. E. Slack, and A. Surprenant. Muscarinic m1 and m2 receptors mediate depolarization and presynaptic inhibition in guinea-pig enteric nervous system. *J Physiol*, 368:435–452, 1985.

M. J. O'Donovan. The origin of spontaneous activity in developing networks of the vertebrate nervous system. *Curr Opin Neurobiol*, 9(1):94–104, 1999.

M. J. O'Donovan, N. Chub, and P. Wenner. Mechanisms of spontaneous activity in developing spinal networks. *J Neurobiol*, 37(1):131–145, 1998.

H. Ohkawa and C. L. Prosser. Electrical activity in myenteric and submucous plexuses of cat intestine. *Am J Physiol*, 222(6):1412–1419, 1972.

H. Pan, H. Y. Wang, E. Friedman, and M. D. Gershon. Mediation by protein kinases C and A of G_0 linked slow responses of enteric neurons to 5-HT. *J Neurosci*, 17 (3):1011–1024, 1997.

S. Pinker. *The language instinct*. Harper Perennial, 1995.

S. Pompolo and J. B. Furness. Ultrastructure and synaptic relationships of calbindin-reactive, dogiel type II neurons, in myenteric ganglia of guinea-pig small intestine. *J Neurocytol*, 17(6):771–782, 1988.

S. Pompolo and J. B. Furness. Origins of synaptic inputs to calretinin immunoreactive neurons in the guinea-pig small intestine. *J Neurocytol*, 22(7):531–546, 1993.

S. Pompolo and J. B. Furness. Sources of inputs to longitudinal muscle motor neurons and ascending interneurons in the guinea-pig small intestine. *Cell Tissue Res.*, 280:549–560, 1995.

S. Pompolo and J. B. Furness. Quantitative analysis of inputs to somatostatin-immunoreactive descending interneurons in the myenteric plexus of the guinea-pig small intestine. *Cell Tissue Res*, 294(2):219–226, 1998.

A. L. Portbury, S. Pompolo, J. B. Furness, M. J. Stebbing, W. A. Kunze, J. C. Bornstein, and S. Hughes. Cholinergic, somatostatin-immunoreactive interneurons in

the guinea pig intestine: morphology, ultrastructure, connections and projections. *J Anat*, 187 (Pt 2):303–321, 1995.

W. H. Press, B. P. Flannery, S. A. Teukolsky, and W. T. Vetterling. *Numerical Recipes in C: The Art of Scientific Computing*. Cambridge University Press, second edition, 1992.

N. G. Publicover, E. M. Hammond, and K. M. Sanders. Amplification of nitric oxide signaling by interstitial cells isolated from canine colon. *Proc Natl Acad Sci U S A*, 90(5):2087–2091, 1993.

V. Rayner, T. E. Weekes, and J. B. Bruce. Insulin and myoelectric activity of the small intestine of the pig. *Dig Dis Sci*, 26(1):33–41, 1981.

H. J. Reis, A. R. Massensini, M. A. Prado, R. S. Gomez, M. V. Gomez, and M. A. Romano-Silva. Calcium channels coupled to depolarization-evoked glutamate release in the myenteric plexus of guinea-pig ileum. *Neuroscience*, 101(1):237–242, 2000.

K. C. Richardson and R. S. Wyburn. Electromyographic events in the stomach and small intestine of a small kangaroo, the tammar wallaby (macropus eugenii). *J Physiol*, 342:453–463, 1983.

J. Rinzel and G. B. Ermentrout. Analysis of neural excitability. In Christof Koch and Idan Segev, editors, *Methods in Neuronal Modeling: from ions to neworks*. The MIT Press, second edition, 1998.

E. M. Ross. Signal sorting and amplification through g protein-coupled receptors. *Neuron*, 3(2):141–152, 1989.

Y. Ruckebusch and L. Bueno. Origin of migrating myoelectric complex in sheep. *Am J Physiol*, 233(6):E483–E487, 1977.

Y. Ruckebusch, M. Pairet, and J. L. Becht. Origin and characterization of migrating myoelectric complex in rabbits. *Dig Dis Sci*, 30(8):742–748, 1985.

D. E. Rummelhart and J. L. McClelland. *Parallel distributed processing: explorations in the microstructure of cognition*. MIT Press, Cambridge, Mass., 1986.

P. Sah and P. Davies. Calcium-activated potassium currents in mammalian neurons. *Clin Exp Pharmacol Physiol*, 27(9):657–663, 2000.

P. Sah and J. S. Isaacson. Channels underlying the slow afterhyperpolarization in hippocampal pyramidal neurons: neurotransmitters modulate the open probability. *Neuron*, 15(2):435–441, 1995.

K. M. Sanders, T. Ordog, S. D. Koh, and S. M. Ward. A novel pacemaker mechanism drives gastrointestinal rhythmicity. *News Physiol Sci*, 15:291–298, 2000.

P. A. Sargent, K. H. Kjaer, C. J. Bench, E. A. Rabiner, C. Messa, J. Meyer, R. N. Gunn, P. M. Grasby, and P. J. Cowen. Brain serotonin1a receptor binding measured by positron emission tomography with [11c]way-100635: effects of depression and antidepressant treatment. *Arch Gen Psychiatry*, 57(2):174–180, 2000.

A. Saria. The tachykinin nk1 receptor in the brain: pharmacology and putative functions. *Eur J Pharmacol*, 375(1-3):51–60, 1999.

S. Sarna, R. E. Condon, and V. Cowles. Enteric mechanisms of initiation of migrating myoelectric complexes in dogs. *Gastroenterology*, 84(4):814–822, 1983.

S. Sarna, C. Stoddard, L. Belbeck, and D. Mcwade. Intrinsic nervous control of migrating myoelectric complexes. *Am J Physiol*, 241(1):G16–G23, 1981.

S. K. Sarna. Cyclic motor activity; migrating motor complex: 1985. *Gastroenterology*, 89(4):894–913, 1985.

S. K. Sarna, M. F. Otterson, R. P. Ryan, and V. E. Cowles. Nitric oxide regulates migrating motor complex cycling and its postprandial disruption. *Am J Physiol*, 265(4 Pt 1):G749–G766, 1993.

M. G. Sarr and K. A. Kelly. Myoelectric activity of the autotransplanted canine jejunoileum. *Gastroenterology*, 81(2):303–310, 1981.

W. Senn, T. Wannier, J. Kleinle, H. R. Luscher, L. Muller, J. Streit, and K. Wyler. Pattern generation by two coupled time-discrete neural networks with synaptic depression. *Neural Comput*, 10(5):1251–1275, 1998.

W. Senn, K. Wyler, J. Streit, M. Larkum, H. R. Lüscher, H. Mey, L. Müller, D. Stainhauser, K. Vogt, and T. Wannier. Dynamics of a random neural network with synaptic depression. *Neural Networks*, 9(4):575–588, 1996.

E. Sernagor, N. Chub, A. Ritter, and M. J. Donovan. Pharmacological characterization of the rhythmic synaptic drive onto lumbosacral motoneurons in the chick embryo spinal cord. *J Neurosci*, 15(11):7452–7464, 1995.

K. Z. Shen and S. W. Johnson. A slow excitatory postsynaptic current mediated by g-protein-coupled metabotropic glutamate receptors in rat ventral tegmental dopamine neurons. *Eur J Neurosci*, 9(1):48–54, 1997.

C. W. Shuttleworth, R. Murphy, and J. B. Furness. Evidence that nitric oxide participates in non-adrenergic inhibitory transmission to intestinal muscle in the guinea-pig. *Neurosci Lett*, 130(1):77–80, 1991.

C. W. Shuttleworth and K. M. Sanders. Involvement of nitric oxide in neuromuscular transmission in canine proximal colon. *Proc Soc Exp Biol Med*, 211(1):16–23, 1996.

C. W. Shuttleworth and T. K. Smith. Action potential-dependent calcium transients in myenteric s neurons of the guinea-pig ileum. *Neuroscience*, 92(2):751–762, 1999.

T. K. Smith, J. C. Bornstein, and J. B. Furness. An electrophysiological study of the projections of motor neurones that mediate non-cholinergic excitation in the circular muscle of the guinea-pig small intestine. *J Auton Nerv Syst*, 22(2): 115–128, 1988.

T. K. Smith, J. C. Bornstein, and J. B. Furness. Distension-evoked ascending and descending reflexes in the circular muscle of guinea-pig ileum: an intracellular study. *J Auton Nerv Syst*, 29(3):203–217, 1990.

T. K. Smith, J. C. Bornstein, and J. B. Furness. Interactions between reflexes evoked by distension and mucosal stimulation: electrophysiological studies of guinea-pig ileum. *J Auton Nerv Syst*, 34(1):69–75, 1991.

T. K. Smith, J. C. Bornstein, and J. B. Furness. Convergence of reflex pathways excited by distension and mechanical stimulation of the mucosa onto the same myenteric neurons of the guinea pig small intestine. *J. Neurosci.*, 12:1502–1510, 1992.

T. K. Smith, E. P. Burke, and C. W. Shutttleworth. Topographical and electrophysiological characteristics of highly excitable S neurones in the myenteric plexus of the guinea-pig ileum. *J. Physiol. (Lond)*, 517.3:817–830, 1999.

T. K. Smith and J. B. Furness. Reflex changes in circular muscle activity elicited by stroking the mucosa: an electrophysiological analysis in the isolated guinea-pig ileum. *J Auton Nerv Syst*, 25(2–3):205–218, 1988.

T. K. Smith and W. J. Robertson. Synchronous movements of the longitudinal and circular muscle during peristalsis in the isolated guinea-pig distal colon. *J Physiol*, 506(Pt 2):563–577, 1998.

Z. M. Song, S. J. Brookes, and M.Costa. All calbindin-immunoreactive myenteric neurons project to the mucosa of the guinea-pig small intestine. *Neurosci Lett*, 180(2):219–222, 1995.

Z. M. Song, S. J. Brookes, G. A. Ramsay, and M. Costa. Characterization of myenteric interneurons with somatostatin immunoreactivity in the guinea-pig small intestine. *Neuroscience*, 80(3):907–923, 1997.

Z. M. Song, S. J. Brookes, P. A. Steele, and M. Costa. Projections and pathways of submucous neurons to the mucosa of the guinea-pig small intestine. *Cell Tissue Res*, 269(1):87–98, 1992.

B. R. Southwell and J. B. Furness. Immunohistochemical demonstration of the nk(1) tachykinin receptor on muscle and epithelia in guinea pig intestine. *Gastroenterology*, 120(5):1140–1151, 2001.

B. R. Southwell, V. S. Seybold, H. L. Woodman, K. M. Jenkinson, and J. B. Furness. Quantitation of neurokinin 1 receptor internalization and recycling in guinea-pig myenteric neurons. *Neuroscience*, 87(4):925–931, 1998.

B. R. Southwell, H. L. Woodman, R. Murphy, S. J. Royal, and J. B. Furness. Characterisation of substance P-induced endocytosis of NK1 receptors on enteric neurons. *Histochem Cell Biol*, 106(6):563–571, 1996.

N. Spencer, M. Walsh, and T. K. Smith. Does the guinea-pig ileum obey the 'law of the intestine'? *J Physiol*, 517 (Pt 3):889–898, 1999.

A. M. Starodub and J. D. Wood. Selectivity of ω-CgTx-MVIIC toxin from *Conus magus* on calcium currents in enteric neurons. *Life Sci*, 64(26):PL305–310, 1999.

A. M. Starodub and J. D. Wood. A-type potassium current in myenteric neurons from guinea-pig small intestine. *Neuroscience*, 99(2):389–396, 2000.

M. J. Stebbing and J. C. Bornstein. Electrophysiological mapping of fast excitatory synaptic inputs to morphologically and chemically characterized myenteric neurons of guinea-pig small intestine. *Neuroscience*, 73(4):1017–1028, 1996.

R. W. Summers, S. Anuras, and J. Green. Jejunal manometry patterns in health, partial intestinal obstruction, and pseudoobstruction. *Gastroenterology*, 85(6): 1290–1300, 1983.

A. Surprenant, G. Buell, and R. A. North. $P2_X$ receptors bring new structure to ligand-gated ion channels. *Trends Neurosci*, 18(5):224–229, 1995.

A. Surprenant and R. A. North. Mechanism of synaptic inhibition by noradrenaline

acting at alpha 2-adrenoceptors. *Proc R Soc Lond B Biol Sci*, 234(1274):85–114, 1988.

J. H. Szurszewski. A migrating electric complex of canine small intestine. *Am J Physiol*, 217(6):1757–1763, 1969.

J. Tabak, W. Senn, M. J. Donovan, and J. Rinzel. Modeling of spontaneous activity in developing spinal cord using activity-dependent depression in an excitatory network. *J Neurosci*, 20(8):3041–3056, 2000.

H. Tatsumi, K. Hirai, and Y. Katayama. Measurement of the intracellular calcium concentration in guinea-pig myenteric neurons by using fura-2. *Brain Res*, 451 (1–2):371–375, 1988.

G. S. Taylor and R. A. Bywater. Antagonism of non-cholinergic excitatory junction potentials in the guinea-pig ileum by a substance P analogue antagonist. *Neurosci Lett*, 63(1):23–26, 1986.

S. S. Taylor. camp-dependent protein kinase. model for an enzyme family. *J Biol Chem*, 264(15):8443–8446, 1989.

E. A. Thomas, P. P. Bertrand, and J. C. Bornstein. Genesis and role of coordinated firing in a feed forward network — a model study of the enteric nervous system. *Neuroscience*, 93(4):1525–1537, 1999.

L. Thuneberg and S. Peters. Toward a concept of stretch-coupling in smooth muscle. i. anatomy of intestinal segmentation and sleeve contractions. *Anat Rec*, 262(1): 110–124, 2001.

M. Tonini, M. Costa, S. J. Brookes, and C. M. Humphreys. Dissociation of the ascending excitatory reflex from peristalsis in the guinea-pig small intestine. *Neuroscience*, 73(1):287–297, 1996.

M. Tonini, G. Frigo, S. Lecchini, L. Angelo, and A. Crema. Hyoscine-resistant peristalsis in guinea-pig ileum. *Eur J Pharmacol*, 71(4):375–381, 1981.

V. Torre, J. F. Ashmore, T. D. Lamb, and A. Menini. Transduction and adaptation in sensory receptor cells. *J Neurosci*, 15(12):7757–7768, 1995.

C. Tournois, V. Mutel, P. Manivet, J. M. Launay, and O. Kellermann. Cross-talk between 5-hydroxytryptamine receptors in a serotonergic cell line. Involvement of arachidonic acid metabolism. *J Biol Chem*, 273(28):17498–17503, 1998.

R. D. Traub, J. G. Jefferys, and M. A. Whittington. Enhanced NMDA conductance can account for epileptiform activity induced by low Mg^{2+} in the rat hippocampal slice. *J Physiol*, 478 Pt 3:379–393, 1994.

J. Trouslard, S. J. Marsh, and D. A. Brown. Calcium entry through nicotinic receptor channels and calcium channels in cultured rat superior cervical ganglion cells. *J Physiol*, 468:53–71, 1993.

G. Vantrappen, J. Janssens, T. L. Peeters, S. R. Bloom, N. D. Christofides, and J. Hellemans. Motilin and the interdigestive migrating motor complex in man. *Dig Dis Sci*, 24(7):497–500, 1979.

F. Vogalis, J. B. Furness, and W. A. Kunze. Afterhyperpolarization current in myenteric neurons of the guinea pig duodenum. *J Neurophysiol*, 85(5):1941–1951, 2001.

F. Vogalis, K. Hillsley, and T. K. Smith. Diverse ionic currents and electrical activity of cultured myenteric neurons from the guinea pig proximal colon. *J Neurophysiol*, 83(3):1253–1263, 2000.

W. C. De Vos. Migrating spike complex in the small intestine of the fasting cat. *Am J Physiol*, 265(4 Pt 1):G619–G627, 1993.

S. A. Waterman and M. Costa. The role of enteric inhibitory motoneurons in peristalsis in the isolated guinea-pig small intestine. *J Physiol*, 477(Pt 3):459–468, 1994.

S. A. Waterman, M. Costa, and M. Tonini. Modulation of peristalsis in the guinea-pig isolated small intestine by exogenous and endogenous opioids. *Br J Pharmacol*, 106(4):1004–1010, 1992.

S. A. Waterman, M. Costa, and M. Tonini. Accommodation mediated by enteric inhibitory reflexes in the isolated guinea-pig small intestine. *J Physiol*, 474(3): 539–546, 1994a.

S. A. Waterman, M. Tonini, and M. Costa. The role of ascending excitatory and descending inhibitory pathways in peristalsis in the isolated guinea-pig small intestine. *J Physiol*, 481(Pt 1):223–232, 1994b.

S. Wiggins. *Introduction to applied dynamical nonlinear dynamical systems and chaos*. Springer-Verlag, 1990.

S. Williamson, S. Pompolo, and J. B. Furness. GABA and nitric oxide synthase immunoreactivities are colocalized in a subset of inhibitory motor neurons of the guinea-pig small intestine. *Cell Tissue Res*, 284(1):29–37, 1996.

H. R. Wilson and J. D. Cowan. Excitatory and inhibitory interactions in localized populations of model neurons. *Biophys. J.*, 12:1–24, 1972.

D. M. Wolpert and Z. Ghahramani. Computational principles of movement neuroscience. *Nat Neurosci*, 3 Suppl:1212–1217, 2000.

J. D. Wood. Electrical activity from single neurons in auerbach's plexus. *Am J Physiol*, 219(1):159–169, 1970.

J. D. Wood. Effects of elevated magnesium on discharge of myenteric neurons of cat small bowel. *Am J Physiol*, 229(3):657–662, 1975.

J. D. Wood. Electrical and synaptic behaviour of enteric neurons. In J. D. Wood, editor, *Handbook of physiology*, volume I, pages 465–517. The American Physiological Society, 1989.

J. D. Wood and C. J. Mayer. Slow synaptic excitation mediated sy serotonin in Auerbachs's. *Nature*, 276:836–837, 1978.

J. D. Wood, C. J. Mayer, T. Ninchoji, and D. N. Erwin. Effects of depleted calcium on electrical activity of neurons in auerbach's plexus. *Am J Physiol*, 236(1):C78–C86, 1979.

C. H. You, W. Y. Chey, and K. Y. Lee. Studies on plasma motilin concentration and interdigestive motility of the duodenum in humans. *Gastroenterology*, 79(1): 62–66, 1980.

H. M. Young and J. B. Furness. Ultrastructural examination of the targets of serotonin-immunoreactive descending interneurons in the guinea pig small intestine. *J Comp Neurol*, 356(22):101–114, 1995.

H. M. Young, J. B. Furness, and J. M. Povey. Analysis of connections between nitric oxide synthase neurons in the myenteric plexus of the guinea-pig small intestine. *J Neurocytol*, 24(4):257–263, 1995.

S. Y. Yuan, J. B. Furness, and J. C. Bornstein. Post-stimulus depression of reflex changes in circular muscle activity in the guinea pig small intestine. *J Auton Nerv Syst*, 40(3):171–180, 1992.

S. Y. Yuan, J. B. Furness, J. C. Bornstein, and T. K. Smith. Mucosal distortion by compression elicits polarized reflexes and enhances responses of the circular muscle to distension in the small intestine. *J Auton Nerv Syst*, 35(3):219–226, 1991.

A. M. Yunker and J. J. Galligan. Extrinsic denervation increases myenteric nitric oxide synthase-containing neurons and inhibitory neuromuscular transmission in guinea pig. *J Auton Nerv Syst*, 71(2-3):148–158, 1998.

J. H. Zar. *Biostatistical Analysis*. Prentice Hall, Englewood Cliffs, New Jersey, USA, second edition, 1984.

A. V. Zholos, L. V. Baidan, A. M. Starodub, and J. D. Wood. Potassium channels of myenteric neurons in guinea-pig small intestine. *Neuroscience*, 89(2):603–618, 1999.

X. Zhou and J. J. Galligan. $P2_X$ purinoceptors in cultured myenteric neurons of guinea-pig small intestine. *J Physiol*, 496(Pt 3):719–729, 1996.

X. Zhou and J. J. Galligan. Synaptic activation and properties of 5-

hydroxytryptamine(3) receptors in myenteric neurons of guinea pig intestine. *J Pharmacol Exp Ther*, 290(2):803–810, 1999.

R. S. Zucker. Calcium- and activity-dependent synaptic plasticity. *Curr Opin Neurobiol*, 9(3):305–313, 1999.

Author/s:
Thomas, Evan Alexander

Title:
Mathematical and computer modelling of the enteric nervous system

Date:
2001

Citation:
Thomas, E. A. (2001). Mathematical and computer modelling of the enteric nervous system. PhD thesis, Department of Physiology, The University of Melbourne.

Publication Status:
Unpublished

Persistent Link:
http://hdl.handle.net/11343/39536